Synergistic Sustainable Biorefinery Approach for Corncob Biomass: Optimization, Production, and Assessment of Bioethanol, Glycerol, and Xylooligosaccharides

Submitted in partial fulfilment of the requirements for the award of the degree of

DOCTOR OF PHILOSOPHY

in

BIOTECHNOLOGY

by

Pradeep Kumar Gandam

(Roll No. 716181)

Research Supervisor

Prof. Rama Raju. B

Associate Professor

DEPARTMENT OF BIOTECHNOLOGY

NATIONAL INSTITUTE OF TECHNOLOGY WARANGAL

TELANGANA, INDIA

December 2023

To my parents, grandparents, and wife

NATIONAL INSTITUTE OF TECHNOLOGY- WARANGAL

DEPARTMENT OF BIOTECHNOLOGY

Thesis approval for Ph.D.

This thesis entitled "**Synergistic Sustainable Biorefinery Approach for Corncob Biomass: Optimization, Production, and Assessment of Bioethanol, Glycerol, and Xylooligosaccharides**" by Mr Pradeep Kumar Gandam (Roll No.716181) is approved for the degree of Doctor of Philosophy

Examiners

Supervisor

Prof. Rama Raju. B
Assistant Professor
Department of Biotechnology
NIT-Warangal

Chairman

Prof. Prakash Saudagar
Head
Department of Biotechnology
NIT-Warangal

NATIONAL INSTITUTE OF TECHNOLOGY- WARANGAL

DEPARTMENT OF BIOTECHNOLOGY

Declaration

This is to declare that the work presented in the thesis entitled "**Synergistic Sustainable Biorefinery Approach for Corncob Biomass: Optimization, Production, and Assessment of Bioethanol, Glycerol, and Xylooligosaccharides**", is a bonafide work done by me under the supervision of **Prof. Rama Raju. B,** and has not been submitted elsewhere for the award of any degree.

I declare that this written submission represents my idea in my own words and where other's ideas or words have been included, I have adequately cited and referenced the sources. I also declare that I have adhered to all principles of academic honesty and integrity and have not misinterpreted, fabricated or falsified any idea/data/fact/source in my submission. I understand that any violation of the above will be a cause for disciplinary action by the Institute and can also evoke penal action from the sources which have thus not been properly cited or from whom proper permission has not been taken when needed.

Date:

Place: Warangal

Mr. Pradeep Kumar Gandam
Roll No 716181
Research scholar
Department of Biotechnology
NIT-Warangal

Acknowledgements

Reflecting on my completed doctoral journey, I want to express deep gratitude to Prof. Rama Raju Baadhe, my esteemed research supervisor. His mentorship was pivotal, guiding me through the intricacies of research and fostering an environment of intellectual curiosity. His openness to unconventional perspectives allowed for a richer exploration of the subject matter, and his encouragement served as a constant source of inspiration. I particularly appreciate his insightful suggestions, which significantly elevated the quality and depth of my research. His constructive feedback, provided at crucial junctures, played a crucial role in refining the conceptual framework and methodology. Beyond the academic realm, his immediate assistance in practical aspects, such as procuring necessary consumables, showcased his proactive commitment to the success of the project.

What sets Prof. Baadhe apart is not just his professional guidance but also the genuine friendship and familial atmosphere he cultivated. His understanding, camaraderie, and genuine interest in my well-being made this academic journey intellectually stimulating and emotionally fulfilling.

Apart from my supervisor, it has been my Doctoral Scrutiny Committee whose timely suggestions and critical assessments helped shape this study. I am grateful, therefore, to my DSC members: Prof. Parcha Sreenivasa Rao, and Prof. R. Satish Babu, Department of Biotechnology, NIT Warangal, and Prof. Shirish H Sonawane, Department of Chemical Engineering, NIT Warangal.

I wish to sincerely thank our director Prof. Bidyadhar Subudhi, and the former director Prof. N. Ramana Rao, National Institute of Technology, Warangal, past and present Deans, and other administration officials who allowed me to carry out my research work successfully.

I am deeply grateful to our Head of the Department, Prof. Prakash Saudagar, Department of Biotechnology, National Institute of Technology, Warangal and the previous HODs of the Department for providing me with the necessary facilities, continuous encouragement, and moral support for the research work. I am also thankful to all the faculty members in the Department of Biotechnology for their valuable suggestions and for extending their help whenever required.

We sincerely express our gratitude to Prof. Vijai Kumar Gupta, Senior Challenge Research Fellow in Agriculture & Business Management at the Biorefining and Advanced Materials Research Centre, Scotland's Rural College. Prof. Gupta kindly provided us with the Xylooligosaccharide HPL standards. Additionally, I extend my profound thanks to Prof. Anjireddy Bhavanam from Dr. B.R. Ambedkar National Institute of Technology, Jalandhar, for generously providing the TGA

analysis of our samples. Further, I would like to extend my heartfelt thanks to all the supporting and technical staff of the Department of Biotechnology who have directly or indirectly helped during my study.

I am indebted to my research colleagues, Mr. Ninian Prem Prasanth Pabbathi and Mr. Aditya Velidandi for their valuable input and constant support throughout this journeyI also want to express my gratitude to Mounica Sarvepalli and Sivasankar M for being good friends and making my time here enjoyable.

I would like to acknowledge the Science and Engineering Research Board, Department of Science and Technology, India for providing us with financial support to carry out the research (Reference No. ECR/2015/000076.).

Finally, I am grateful to my wife and research colleague Ms. Madhavi Latha Chinta for her mental, emotional and intellectual support and critical reviews of my work and manuscripts throughout the journey. Her moral support was very valuable for my research.

I am extremely grateful to my late father Mr. Nagabhushanam Gandham for encouraging me to take up this journey and my mother Ms. Sujatha Gandham for her constant care and love. I would also like to thank my siblings Mr. Dilip Gandham and Ms. Aparanjitha Priyadarshini Gandham for their moral support throughout the period. Lastly, I would like to thank and apologize to all whom I might have missed in this acknowledgement for their support and help.

With sincere appreciation,

(Pradeep Kumar Gandam)
Research scholar
(Roll No 716181)

Abstract

This study investigates the prospect of tailored biorefinery objectives targeting specific anatomical sections of corncobs, an underexplored area in the field. The corncob is dissected into its rigid outer anatomical portion (CO) and its inner soft pith (CP). Initially, the comprehensive biomass composition of both CO and CP was determined through four different methods. CP exhibited a higher carbohydrate content and lower lignin content (83.32% and 13.58%, respectively) compared to CO (79.93% and 17.12%, respectively). The syringyl/guaiacyl (S/G) ratio was higher in CP (1.34) than in CO (1.28). Physical characterization confirmed lower crystallinity and thermal stability in CP compared to CO. Saccharification yield of CP without pretreatment matched that of pure cellulose and xylan controls. Subsequently, sustainable pretreatment methodologies for CO were optimized using central composite design. Results were validated using hybrid-artificial neural network models incorporating metaheuristic optimization of hyperparameters through Teaching-Learning-Based Optimization (TLBO), Particle Swarm Optimization (PSO), and Genetic Algorithm (GA). Three potential pretreatment methodologies—$NaHCO_3$, NaOH, and sequential treatment (NaOH followed by H_2SO_4)—were identified, yielding pretreated CO residues COr1, COr2, and COr3 respectively. A novel strain of *Pichia kudriavzevii* was isolated from ripened Palmyra palm (*Borassus flabellifer*) fruit pulp, exhibiting high tolerance to ethanol, lignocellulose-derived inhibitors, and fermentation of various carbon sources (including xylan) over a pH range of 2.5 to 8.5. Simultaneous saccharification and co-fermentation (SSCF) and separate hydrolysis and fermentation (SHCF) modes were employed to valorise COr1, COr2, and COr3 individually. Achieved ethanol and glycerol concentrations 63%, 5% of their theoretical yield (T.Y) respectively. The techno-economic analysis revealed an overall negative profit margin. However, this disparity is notably narrower for the NaOH pretreatment scenario (USD 18.0). This gap can be readily surmounted, when factoring in the co-product credit from the revenue generated (USD 203.3) through XOS production from CP. The potential of xylooligosaccharides production from CP was demonstrated by saccharifying untreated CP with commercial xylanase, achieving an impressive yield of 77% of its theoretical yield (T.Y.). Among the evaluated scenarios, the SSCF process utilizing COr2 in conjunction with XOS production from CP emerged as the most economically sustainable biorefinery option. Although NaOH pretreatment shows lower exergy performance metrics (process efficiency 0.91, sustainability index 10.90, and environmental

impact 0.09) compared to sequential H_2SO_4 pretreatment, its economic viability and sustainability make it the preferred choice.

Layout of the thesis

Chapter 1: Introduction

Concept of biorefinery, and biomass recalcitrance were introduced, highlighting the importance of corncob as the feedstock, it also underscores the necessity for optimal pretreatment

Chapter 2: Literature Review

A comprehensive literature review of pretreatment and post-processing methodologies reported for corncob biomass were discussed.

Chapter 3: A New Insight into the Composition and Physical Characteristics of Corncob Substantiating Its Potential for Tailored Biorefinery Objectives

The procedure for segregating corncob anatomical portions is discussed, followed by comprehensive characterization using state-of-the-art methodologies.

Chapter 4: Integrated Multi-Objective Optimization of Sodium Bicarbonate Pretreatment for the Outer Anatomical Portion of Corncob Using Central Composite Design, Artificial Neural Networks, and Metaheuristic Algorithms.

The selection and optimization of $NaHCO_3$ pretreatment for CO, using a multi-step strategy that employs both statistical and machine learning approaches synergistically, are discussed.

Chapter 5: Enhancing Saccharification of Sequentially Pretreated Corncob Outer Anatomical Portion Using NaOH and H2SO4: A Study Utilizing RSM-CCD, Validated with ANN

The optimization of two additional pretreatments, such as dilute alkali (NaOH), and a sequential NaOH pretreatment followed by pretreatment with H_2SO_4, is discussed

Chapter 6: Isolation and characterization of lignocellulose derived inhibitor tolerant, high ethanol tolerant, xylose-fermenting ethanologenic yeast strains

The chapter deals with the isolation and characterization of novel yeast strains.

Chapter 7: Co-production of Bioethanol and Glycerol from the Outer Anatomical Portion of Corncob, with Emphasis on Pith: Evaluating Inhibitor Adsorbing Efficiency in Comparison with Established Surfactants

Optimization of simultaneous ethanol and glycerol production is undertaken, while exploring a novel approach involving CP as adsorbent for fermentation inhibitors.

Chapter 8: Chemical-Free Enzymatic Synthesis of Food-Grade Xylooligosaccharides from Corncob Pith for Enhanced Sustainability in Production

The enzymatic production of XOS from untreated raw CP is examined.

Chapter 9: Techno Economic and Exergy analysis of the overall process scenarios

A detailed sustainability analysis of CO and CP biorefinery strategies discussed is conducted.

Chapter 10: Summary and Conclusions

Concluding remarks on the overall outcomes and future prospects of the work are discussed.

Key words

Biorefinery

Corncob

Pretreatment

Response surface methodology

Artificial neural network

Teaching-Learning-Based Optimization

Particle Swarm Optimization

Genetic Algorithm

Xylooligosaccharides

Techno-economic analysis

Chemical exergy analysis

Contents

List of Figures

List of Tables

List of symbols and abbreviations

I002	–	Intensity at about 2θ
$(NH_4)_2SO_4$	–	Ammonium sulfate
[EMIM] OAc	–	1-ethyl-3- methylimidazolium acetate
2FI design	–	Two-level factorial design
AAEMs	–	Alkali and alkaline earth metal species
ABE	–	Acetone, Butanol, Ethanol
AC	–	Avicel
ACB	–	Ballmilled Avicel
Acr	–	Area of all the crystalline peaks ((101), (10$\bar{1}$), (021), (002), (040)) together
ACra1	–	Area of all the crystalline peaks of the sample obtained by peak integration after subtracting the diffraction intensity of the ball-milled AC
ADF	–	Acid detergent fibre
AFEX	–	Ammonia Fibre Explosion
$AlCl_3$	–	Aluminum chloride
ANN	–	Artificial neural network
ARP	–	Ammonia recycle percolation
As	–	Total area of the sample before amorphous subtraction
At	–	Total area of the diffractogram
ATCC	–	American Type Culture Collection
AWB	–	Agricultural waste biomass
BLAST	–	Basic Local Alignment Search Tool
BS 12	–	Dodecyl dimethyl betaine
BTMAC/LA	–	Benzyltrimethylammonium chloride / lactic acid
BX	–	Beachwood Xylan
C.V.%	–	Percentage of Coefficient of variation
$C_2H_2O_4$	–	Oxalic acid
$C_3H_8O_3$	–	Glycerol
$C_4H_4O_4$	–	Maleic acid
$C_4H_6O_4$	–	Succinic acid
$C_4H_6O_5$	–	DL-Malic acid
$C_6H_8O_7$	–	Citric acid

$Ca(OH)_2$	–	Calcium hydroxide
CB	–	Cellobiose
CBP	–	Consolidated bioprocessing
CBU	–	Cellobiase units
CC1	–	Corncob variety 1 (KMH-2589 (Kaveri seed company limited, Secunderabad, India, 500003)
CC2	–	Corncob variety 2 (LTH 22 (Yaaganti Seeds Pvt. Ltd, Hyderabad, India, 500034)
CC3	–	Corncob variety 3 P3533 (Pioneer Hi-Bred Private Ltd, Hyderabad, India, 500081)
CC4	–	Corncob variety 4 BL 900 (Bisco biosciences, Hyderabad, India, 500003)
CCD	–	Central composite design
CCH	–	Corncob hydrolysate
CCr	–	Corncob rrsidue
CH_3COOH	–	Acetic acid
$ChCl_3$	–	Chloroform
CL	–	Cellulose (cotton linters)
CL	–	Cellulose (cotton linters)
Cl_2	–	Chlorine gas
CLB	–	Ballmilled cellulose (cotton linters)
CO	–	Corncob outer
COB	–	Ballmilled CO (corncob outer)
COD	–	Chemical oxygen demand
COr1	–	Corncob outer residue 1 (obtained from $NaHCO_3$ pretreatment)
COr2	–	Corncob outer residue 2 (obtained from NaOH pretreatment)
COr3	–	Corncob outer residue 3 (obtained from H_2SO_4 pretreatment)
CP	–	Corncob pith
CPB	–	Ballmilled CP (corncob pith)
Cra1%	–	Percent crystallinity of the sample calculated by the amorphous subtraction method using cellulose as the amorphous standard
Cra2%	–	Percent crystallinity of the sample calculated by the amorphous subtraction method using the ball-milled sample as the amorphous

		standard
Crd	–	Percent crystallinity calculated by peak deconvolution method
CrI%	–	Percent crystallinity index
$CuCl_2$	–	Copper(II) chloride
DAEM	–	Distributed activation energy model
DESs	–	Deep eutectic solvents
DMA	–	Dimethylacetamide
DMF	–	N, N-Dimethylformamide
DMSO	–	Dimethyl sulfoxide
DNS	–	3,5, di-nitrosalicylic acid
DTG	–	Derivative thermogram
E10	–	10% Ethanol in gasoline
E100	–	100% fuel Ethanol
E27	–	27% Ethanol in gasoline
E30	–	30% Ethanol in gasoline
E85	–	85% ethanol in gasoline
EtOH	–	Ethanol
Exch	–	Chemical exergy
$FeCl_3$	–	Ferric chloride
$FeSO_4$	–	Ferrous sulfate
FPU	–	Filter paper units
FTIR	–	Fourier Transform Infrared Spectroscopy
GA	–	Genetic algorithm
GB100	–	ANN architecture optimized using genetic algorithm and Bayesian regularization with a population size of 100
GB50	–	ANN architecture optimized using genetic algorithm and Bayesian regularization with a population size of 50
Glc	–	Glucose
GlOH	–	Glycerol
H/C	–	Hydrogen to carbon ratio
H/Ceff	–	Hydrogen to carbon ratio
H_2O_2	–	Hydrogen peroxide
H_2O_2	–	Hydrogen peroxide

H_2SO_4	–	Sulphuric acid
H_2SO_4	–	Sulphuric acid
H_3PO_4	–	Phosphoric acid
HBI	–	Hydrogen bond intensity
HCl	–	Hydrochloric acid
HCl	–	Hydrochloric acid
HDPE	–	High-density polyethylene
HF	–	Hydro fluoric acid
HMF	–	Hydroxymethyl Furfural
HNO_3	–	Nitric acid
HPLC	–	High-performance liquid chromatography
HSS	–	High-speed steel
HTP	–	Hydrothermal pretreatment
I_{am}	–	Intensity at the "valley" between the two peaks at about $2\theta = 18°$
IEA	–	International Energy Agency
ISO	–	International organization for standardization
k	–	Dimensionless shape factor (0.89)
K_2HPO_4	–	di-Potassium hydrogen phosphate
K_2SO_4	–	Potassium sulfate
KaOH	–	Potassium hydroxide
KAS	–	Kissinger-Akahira-Sunose
KBr	–	Potassium bromide
$KMnO_4$	–	Potassium permanganate
$KNaC_4H_4O_6.4H_2O$	–	Sodium potassium tartrate
KOH	–	Potassium hydroxide
L	–	Crystallite size in nm
L/S	–	Liquid-to-solid ratio
Lac	–	Lactose
LCA	–	Life cycle analysis/ assessment
LG	–	Lignin
LG	–	Percentage of lignin removed
LHW	–	Liquid hot water
LOI	–	Lateral order index

MAE	–	Mean Absolute Error
MCM-41	–	Mobil Composition of Matter No. 41
$MgCl_2$	–	Magnesium chloride
MIBK -	–	Methyl isobutyl ketone
$MnCl_2$	–	Manganese chloride
MSE	–	Mean squared error
MSP	–	Minimum selling price
Mt	–	Metric tons
n	–	Positive integer.
Na_2CO_3	–	Sodium carbonate
Na_2HPO_4	–	di-Sodium hydrogen phosphate
Na_2SO_3	–	Sodium Sulphite
Na_2SO_4	–	Sodium sulfate
$Na_3C_6H_5O_7$	–	tri-Sodium citrate
NaCl	–	Sodium chloride
NaCl	–	Sodium chloride
$NaClO_2$	–	Sodium hypochlorite
NADH	–	Nicotinamide adenine dinucleotide
NADP	–	Nicotinamide adenine dinucleotide phosphate
$NaHCO_3$	–	Sodium bicarbonate
NaOH	–	Sodium hydroxide
NaOH	–	Sodium hydroxide
NDF	–	Neutral detergent fibre
NH_4OH	–	Ammonia liquor
NIR	–	Near-infrared spectroscopy
NIR-PLS	–	Partial least squares regression model for NIR calibration curve
NMR	–	Nuclear magnetic resonance
NREL	–	National Renewable Energy Laboratory
NREL-LAP	–	National Renewable Energy Laboratory, USA-laboratory analytical procedure
O/C	–	Oxygen to carbon ratio
OFW	–	Ozawa-Flynn-Wall
PB100	–	ANN architecture optimized using particle swarm optimization and

		Bayesian regularization with a population size of 100
PB50	–	ANN architecture optimized using particle swarm optimization and Bayesian regularization with a population size of 50
PCR	–	Polymerase chain reaction
PEG	–	Poly ethylene glycol
PFI	–	Papirindustriens Forskningsinstitutt
PSO	–	Particle swarm optimization
R	–	Gas constant
R2C	–	Coefficient of multiple determinations for calibration
R2P	–	Coefficient of multiple determinations for prediction
R2V	–	Coefficient of multiple determinations for validation
RID	–	Refractive index detector
RMSE	–	Root Mean Squared Error
RPD	–	Residual predictive deviation
RSM	–	Response surface methodology
S/G	–	Syringyl /guaiacyl ratio
SAA	–	Soaking in aqueous ammonia
SEC	–	Standard error of calibration
SEM	–	Scanning Electron Microscopy
SEP	–	Standard error of prediction
SHF	–	Separate hydrolysis and fermentation
Si_{φ}	–	Exergy sustainability index
SLQA	–	Lignosulfonate quaternary ammonium salt
Sn-BTN	–	Tin-loaded Bentonite
Sn-MMT	–	Tin-loaded montmorillonite
SSCF	–	Simultaneous saccharification and co-fermentation
SSF	–	Simultaneous saccharification and fermentation
TB100	–	ANN architecture optimized using teaching learning-based optimization and Bayesian regularization with a population size of 100
TB30	–	ANN architecture optimized using teaching learning-based optimization and Bayesian regularization with a population size of 30
TCI	–	Total crystallinity index
TEA	–	Techno-economic analysis

TGA	–	Thermogravimetric Analysis
THFA	–	Tetrahydrofurfuryl alcohol
TiO_2	–	Titanium dioxide
TLBO	–	Teaching learning-based optimization
TLC	–	Thin layer chromatography
TS	–	Total sugars (reducing) released
TY	–	Theoretical yield
UFLC	–	Ultra performance/fast liquid chromatography
WLN agar	–	Wallenstein Laboratory Nutrient agar
XOS	–	Xylooligosaccharides
XRD	–	X-ray Diffraction
XY	–	Commercial Xylan
Xyl	–	Xylose
YNB	–	Yeast nitrogen base
YPD agar	–	1% yeast extract, 2% peptone, 2% dextrose and 2% agar
YPM8E5	–	10 g/L yeast extract, 20 g/L peptone, 80 g/L maltose, 5% ethanol (v/v), 50 µg/mL kanamycin, 50 µg/mL chloramphenicol
ZnMoO4	–	Zinc molybdate
β	–	Full width at the half maximum (FWHM) of the (002) lattice expressed in radians
θ	–	Peak position in radians (Bragg angle)
λ	–	Wavelength of the incident x-ray (0.1540 nm)
φ	–	Exergy efficiency of the process

Chapter 1
Introduction

1.1 Biorefinery definition

The take, make and dispose approach of rapid industrialization economies of the world has been detrimental to fossil fuels and the ecological sustainability of the globe [1]. To overcome this crisis, the world is moving towards ecologically sustainable, zero-waste economic models, like the circular bio-economy [2]. In a circular bio-economy, biologically-derived inputs or biomass waste can serve as valuable assets for the production of bioenergy and biomaterials in biorefineries. The biorefinery assumes a crucial and innovative role in the circular bio-economy, offering both environmental and economic advantages.

A biorefinery integrates various methods for treating and processing biomass into a unified system, yielding diverse components from a single biomass source, thereby maximizing the economic potential of raw materials and reducing the waste generated. It is a promising solution for converting raw materials into biofuels, amino acids, enzymes, antibiotics, energy etc. In addition to value addition, the biorefinery approach can make the overall process a real green technology. The concept of biorefinery concept is still in its infancy globally. A pivotal challenge is to establish a sustainable model for its effective implementation. Obstacles such as limited raw material availability, challenges in establishing a viable product supply chain, and uncertainties regarding the scalability of the model in, terms of technical efficiency and economic feasibility, are hindering its progression toward commercial-scale development. The National Renewable Energy Laboratory (NREL) in the USA is at the forefront of biorefinery research.

Biorefineries are categorized into generations based on factors such as feedstock, technology, and the range of products obtained. The widely used classification, based on the nature of the feedstock used, categorizes biorefineries into four generations [3]. Food sources such as sugar, starch, vegetable oil, or animal fats are the main raw materials for first-generation biorefineries. Second-generation biorefineries depend on lignocellulosic feedstocks mainly derived from non-edible agricultural waste, forest residues, wood chips, as well as other waste streams generated from the food industry, such as wheat bran, animal fats, and waste cooking oil. Additionally, the usage of certain low-cost and low-maintenance crops grown solely for the purpose of renewable bioenergy production, termed energy crops, is also considered as second-generation feedstocks. These energy crops are often woody (Willow, Poplar) or herbaceous plants (*Miscanthus x giganteus, Pennisetum purpureum*). Algae is the primary source of feedstock for

third-generation biorefineries. Genetically engineered energy crops and algae that sequester high amounts of carbon from the atmosphere to form the bulk of biomass are considered fourth-generation biorefinery feedstocks.

The ambiguous biorefinery classification system was redefined in 2008 by IEA Bioenergy Task 42, which defined the biorefinery as sustainable processing of biomass into a spectrum of marketable products and energy (feed, food, chemicals, materials, fuels, heat and power) [4]. The four main features of this new biorefinery classification system, namely, platforms, products, feedstock, and conversion processes, can accommodate and group a wide variety of biorefining aspects into a streamlined classification system.

A platform can be an intermediate or a final product. The number of platforms involved explains the complexity of a biorefining process. There are two different product groups considered, the energy products (all kinds of biofuels) and material products (chemicals, feed and food), and two different feedstock groups, the energy crops (starch crops, short rotation forestry) and biomass residue (agriculture, forest and industrial biomass waste). Likewise, there are four different conversion processes considered, namely, biochemical conversion, thermochemical conversion, chemical conversion, and mechanical processes.

1.2 Biofuels

Diminishing fossil fuels, increasing petroleum import prices, and changing global politics are forcing nations to look for sustainable alternative measures. The Net Zero Emissions by 2050 Scenario under the United Nations Sustainable Development Goal 7 on Affordable and Clean Energy, aims to rapidly increase the use of bioenergy to replace fossil fuels by 2030 while avoiding negative social and environmental impacts [5], [6]. Since the year 2005, several countries have legislated certain standards to incorporate biofuels for automobile usage. About 98% of the fuel requirement in the road transportation sector has currently been met by fossil fuels and the remaining 2% by biofuels, fuels produced from biomass [7]. Bioethanol is the most extensively produced biofuel in the world. Global biofuel production reached a record 154 billion litres in 2018, of which bioethanol amounts to 110 billion litres, the rest being biodiesel and hydro-treated vegetable oil. Global bioethanol output is anticipated to increase by 20% by 2024, reaching 130 billion litres (Figures 1.1A & 1.1B) [7]. Currently, many countries are blending gasoline with ethanol and aim to increase the gasoline to ethanol ratio in the near future. Increasing demand for biofuels has been the largest driving force for the research and development in biomass valorisation. Up to 10%, anhydrous ethanol blend with petrol (E10) is legalized in many countries, that is used with or without slight engine modifications [8], [7].

Higher ethanol blends of gasoline E85 and E100 can only be used in vehicles with special engine modifications known as flex-fuel vehicles. Brazil is currently using E27 for all transport vehicles, along with E100 in flex-fuel vehicles. The USA sets its renewable energy usage standards every year, currently using ethanol-blended gasoline E30 – E85 in their flex-fuel vehicles. European Union and China are using E10 [8], [7]. Currently, India is importing 85% of its oil requirement. Ethanol-blended petrol E10 is permitted in India, yet the average ethanol blending is just around 5%. However, the inadequate supply of ethanol further restricted this blending to only 50% of the total petrol sold in the country. Indian national policy on biofuels – 2018, aims to achieve a 10% ethanol blend by 2022 and a 20% ethanol blend by 2025. To accomplish this an estimate of 10160 million litres of ethanol requirement is projected by the year 2025 [7]. The current Indian ethanol production capacity is 6840 million litres per year and is mainly produced from molasses and grain-based distilleries. Although molasses and grain supply projections are satisfactory, to achieve the ethanol production goal by 2025 (Figure 1.1C), it is necessary to stress on enhancing the share of lignocellulose-based ethanol [7]. Ethanol produced from non-edible feedstock such as waste from food crops or agricultural waste is categorized as second-generation biofuel. Agricultural waste biomass (AWB) is one such renewable resource that fits these criteria.

However, Biomass recalcitrance is a major obstacle for biorefineries, and various pretreatment approaches have been suggested to overcome it. Despite intensive efforts in emerging lignocellulosic biorefineries, the very first step of the biorefinery, the cost-effective pretreatment to access the recalcitrant lignocellulose components to resolve them into individual components, is still a major obstacle and a key challenge.

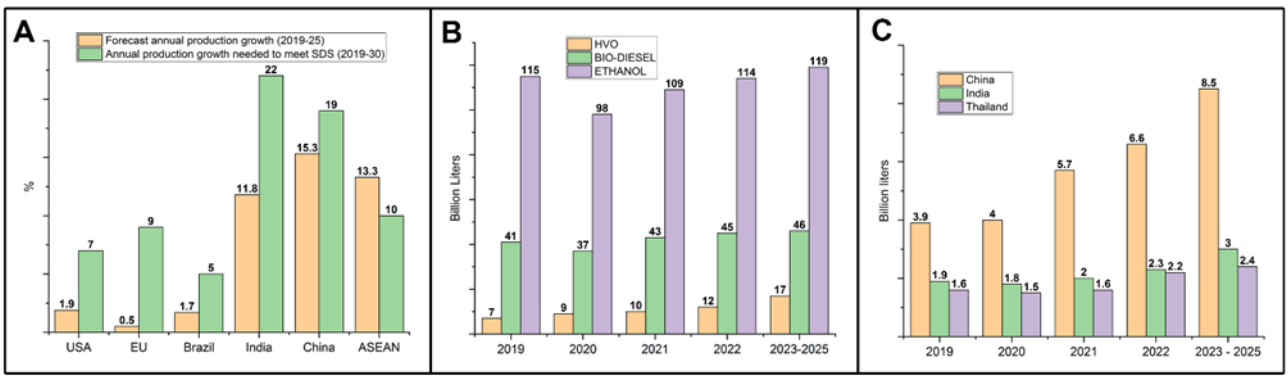

Figure 1.1 Global biofuel production forecasts and scenarios

A. Forecast of annual biofuel production growth vs sustainable development scenario (SDS) requirement; **B**. Global biofuel production in 2019 and forecast to 2025; **C**. Ethanol production

in key Asian markets – forecast 2019 – 2025. Note: ASEAN: The Association of Southeast Asian Nations; HVO: Hydrotreated vegetable oil. The data was collected from [7].

1.3 Corncobs

Corncobs are the AWB derived from maize (*Zea mays*), the most cultivated cereal crop in the world [9], [10] and is proven to be the most promising AWB for biofuel production, owing to its abundance, higher xylan content, lower lignin and lower structural ash content compared to other biomass types (Gandam et al., 2022a).

Global maize production has been predicted to reach 1.17 billion metric tons (Mt) by the end of 2023, with the USA being the top producer with almost 390 million metric tons, followed by China at 277 Mt (U.S. Department of Agriculture, 2023). The huge amounts of corn produced and processed to be used as food, poultry feed and ethanol sources leave a considerable amount of waste that includes 0.3 Mt corncobs per 1.0 Mt maize processed [13]. Large volume with low cost makes corncob a very promising renewable resource. In India, secondary agricultural residues, such as corncobs are mostly disposed of by field dumping, open burning or used as firewood in boilers or furnaces. It was reported that 21% of India's greenhouse gas emissions in the year 2010 resulted from agricultural waste disposal [14]. In addition, economic loss in terms of estimated biogas and energy potential of the disposed agricultural residue is around 1165 million Nm^3 biogas per year [15].

1.4 Biomass recalcitrance and pretreatment

Typically, every biomass is constituted of cellulose, hemicellulose and lignin, along with minor to negligible amounts of extractives (non-structural sugars and waxes), pectin, and structural ash (proteins and metal ions), and the composition of these varies among plant species [16]. Every biorefinery lignocellulose pretreatment approach should start with a compositional analysis of the particular biomass in question to determine the best suitable approach to deconstruct it [17].

The newly formed plant cells usually have a thin, extensible, yet tough primary cell wall surrounding the plasma membrane. The primary cell wall is made of cellulose microfibrils and hemicelluloses. A rigid secondary cell wall is usually deposited inside the primary cell walls of mature cells, with more orderly arranged cellulose microfibrils, hemicellulose and lignin (Figure 1.2). Middle lamella is made of pectin, and it connects the primary cell walls of the adjacent cells [18].

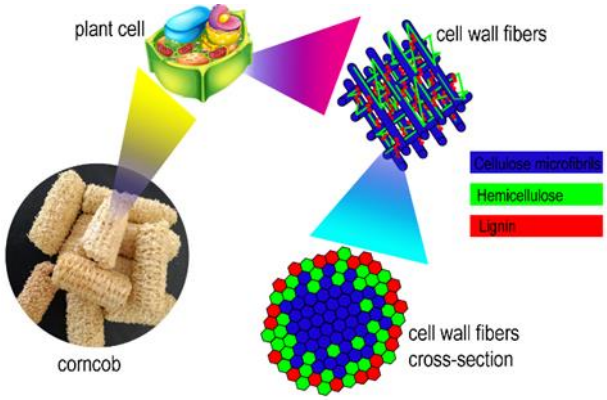

Figure 1.2 Plant cell wall components

Corncob biomass could be valorised to produce different industrially important chemicals including ethanol. Corncobs have a distinctive lignocellulosic composition with a higher xylan content and lower lignin and structural ash content compared to other biomass types [19]. The average reported biomass composition of corncobs derived from NREL analysis methods [20] is, Cellulose 38.9%, hemicellulose 28. 5%, and lignin 20. 5% [21], [22], [23], [24], [25], [26], [27]. A comparative lignocellulose-composition of different second-generation bioethanol feedstocks, such as corncob, corn stover, sugar cane bagasse, wheat straw, and rice straw showed cellulose content up to 36%, 37%, 39%, 36%, 36% respectively, hemicellulose content up to 38%, 30%, 25%, 30%, 27% respectively, and lignin content up to 11%, 20%, 21%, 17%, 9% respectively [28]. High cellulose, xylan contents and lower lignin content make corncob an excellent choice for different biorefinery objectives, especially the ethanol production through biorefinery approach will benefit by channelling the xylan to ethanol production or much more economical co-products like XOS and D-xylitol.

The resistance of biomass to digestibility and hydrolysis is collectively influenced by various structural and compositional properties. These include lignin content and composition, accessible surface area, crystallinity, degree of polymerization of cellulose, and hemicellulose content, all contributing to what is termed as recalcitrance. Pretreatment processes aim to decrease biomass recalcitrance through one or more of these methods, such as lignin and hemicellulose removal, increasing surface area, and reducing cellulose crystallinity, among others [29]. Pretreatment plays a crucial role in the economics, productivity, and lifecycle energy efficiency of the biorefinery, accounting for 18% of the total operating cost of biorefinery [30]. It also affects the upstream and downstream processes, such as the type of biomass used, the content of sugars, lignin, ash, and extractives in the liquid fraction, the neutralization step, the organism used for fermentation, the handling of generated oligomers,

processing of the solid residue, and waste management (Gandam et al., 2022b). Therefore, it is essential to find and optimize a feasible biomass pretreatment for any biorefinery application.

1.5 Research gaps and origin of the current work

We conducted an extensive literature review on corncob-based biorefineries, encompassing both upstream and downstream operations. Our investigation revealed that various methods have been employed for the characterization of biomass. However, none of the studies reported a comprehensive composition analysis of corncob using all available physical and chemical characterization methods.

Furthermore, the corncob pith, which represents an anatomically distinct portion, has never been characterized separately, nor has it been valorized by isolating it from the rest of the corncob biomass. The premise of our current work is rooted in the belief that the corncob pith can be valorized either with mild pretreatment or without any pretreatment, leveraging its unique morphological features to enhance the overall economics of the biorefinery.

Moreover, a comprehensive assessment of various chemical pretreatments on the outer anatomical portion of the corncob, coupled with techno-economic and exergy-based sustainability analyses, has not been previously reported. Based on these findings, in this study, corncob biomass was fractionated into distinct anatomical portions, including the corncob outer (CO) comprising a hard woody ring, chaff, and glume, and a soft inner corncob pith (CP). Both anatomical portions underwent comprehensive characterization using advanced analytical techniques and cutting-edge methodologies such as the National Renewable Energy Laboratory (NREL) Laboratory Analytical Procedures (LAPs), the Van Soest method, Near-Infrared (NIR) Spectroscopy, Thermogravimetric Analysis (TGA), Derivative Thermogravimetry (DTG), Fourier-Transform Infrared Spectroscopy (FTIR), X-ray Diffraction (XRD), and Scanning Electron Microscopy (SEM). This was followed by the optimization of sustainable chemical pretreatment methods for the CO using central composite design, artificial neural networks, and metaheuristic algorithms like Teaching-Learning-Based Optimization (TLBO), Particle Swarm Optimization (PSO), and Genetic Algorithm (GA). Subsequently, valorization strategies for the pretreated CO were developed, including ethanol and glycerol co-fermentation using a novel, xylan-assimilating, inhibitor-tolerant strain of Pichia kudriavzevii, while exploring the innovative approaches such as utilizing CP as adsorbents to enhance fermentation efficiency. Additionally, enzymatic production of xylooligosaccharides from CP without pretreatment was carried out. Furthermore, comprehensive techno-economic and chemical exergy analyses were

conducted to evaluate the sustainability and feasibility of bioprocessing scenarios, providing valuable insights for decision-making.

1.5.1 Objectives of the current work

This study is structured around the following objectives.

1. Comprehensive compositional analysis and characterization of corncob anatomical portions
2. Development of tailored pretreatment approaches for corncob outer anatomical portion
3. Isolation of inhibitors and high ethanol tolerant, xylan utilizing yeast stain for biorefinery applications
4. Optimization of saccharification and fermentation methodologies for pretreated corncob outer anatomical residue.
5. Production of food-grade xylooligosaccharides from corncob pith (inner anatomical portion), without a chemical pretreatment
6. Techno-economic and exergy assessment of sustainability of the optimized process.

Chapter 2
Literature Review

2.1 Types of pretreatments reported for corncob-biomass valorization

Chemical, physicochemical, physical, mechanical, and biological pretreatment approaches were proposed to achieve an economic valorization of corncob lignocellulose. Usually, a single or combination of multiple pretreatment methods was used. There were few reports where whole corncob or corncob-based industrial waste residues were valorized without any pretreatment. The effects of different pretreatment methodologies on lignocellulose are illustrated in Figure 2.3. The ratio of corncob-derived products and objectives reported (Figure 2.4), the frequency of each pretreatment used to valorize corncob biomass (Figure 2.5), and the percentage of different pretreatments used for a particular valorization product/objective is graphically represented (Figures 2.6 & 2.7). Lignocellulose deconstruction efficiency (as percentages of removal or concentration in the hydrolysate [H], and/or as percent recovery or percent concentration left in the CCR [R]). The highest efficiencies reported for each corncob pretreatment type (Table 2.1) and the highest yields or efficiencies of products and objectives reported for corncob valorization (Table 2.2) are tabulated for comparative understanding.

2.1.1 Chemical pretreatments

2.1.1.1 Dilute NaOH pretreatment -efficiency and biorefinery platforms

Chemical treatment of lignocellulose biomass has always been a pretreatment choice for various biorefinery applications. Dilute NaOH pretreatment is the highest reported single chemical pretreatment for the valorization of corncob biomass. NaOH cleaves the α, β-aryl ether linkages that connect hemicellulose to lignin, leading to disruption and detachment of lignin and the uronic acid substitutions of hemicellulose, and the swelling of cellulose as well. Cumulatively increases the porosity of otherwise recalcitrant lignocellulose [32].

Various studies involving a variety of corncob valorization objectives reported dilute NaOH pretreatment. About 85% increase in enzymatic saccharification of CCR was reported from dilute NaOH treatment [33]. The yields of platform sugars obtained were glucose in the range of 32.52 g/L – 59.98 g/L, xylose 10.41 g/L – 33.23 g/L [34], [35], reducing sugars 4.6 g/L – 48 g/L [36], [37], and total sugars 776 g/kg – 932 g/kg [35]. Very few works reported dilute NaOH as a sole pretreatment approach for corncob-based bioethanol production, signifying the importance of combination approaches to achieve better enzymatic saccharification of CCR. Yields of other notable products reported were butanol 9.52 g/L – 12.27 g/L[37], [35], 2,3-

butanediol 0.42 g/g –19.5 g/L[38], [39], acetoin 1.8 g/L [39], lactic acid 122.99 g/L [40], fumaric acid 35.22 g/L [23], and levoglucosan 1.81% – 34.8% [41], [42]. Dilute NaOH pretreatment-derived CCR was used as a carbon source in submerged or solid-state fermentation to produce cellulolytic enzymes. Corresponding yields reported per gram of CCR were: cellulase 11.1 FPU, CMCase 12.96 IU, cellobiase 1.48 IU [43], β-glucosidase 271.76 IU, endoglucanase 163.09 IU, FPase 9.09 IU, β-xylosidase 248.01 IU [44], and xylanase 1334.8 IU [45]. Application of dilute NaOH-treated CCR as an adsorbent to remove water contaminants, where poor dye adsorption (06% /102h) [46] and an excellent nitrate removal capacity (93.3%) were reported [47].

Table 2.1 Highest efficiencies reported for each corncob pretreatment type

Pretreatment	Efficiency of pretreatment	Reference
NaOH	(R) Cellulose 56.51 %	[48]
	(R) Hemicellulose 42.45 %	
	(R) Lignin 1.03 %	
NaOH	(H) Cellulose 13.8%	[47]
	(H) Hemicellulose 44.8 %	
	(H) Lignin 88.2%	
HCOOH→ NH_4OH	(R) Cellulose 82.9%	[49]
	(H) Hemicellulose 83.2%	
H_2SO_4 → NaOH	(R) cellulose 91.1%	[49]
	(H) Hemicellulose 66.8%	
	(H) Lignin 81.0%	
NaOH → H_2O_2	(R) Cellulose 86.18%	[50]
	(R) Hemicellulose 10.68%	
	(R) Lignin 2.21%	
NaOH → Steam explosion	(R) Glucose 83.34%	[51]
	(R) Xylose 6.34%	
	(R) Arabinose 4.27%	
	(R) ASL 2.47%	
	(R) AIL 2.7%	
LHW → NaOH	(R) Cellulose 84.73%	[52]
	(R) Hemicellulose 4.58%	
	(R) Lignin 10.68%	

$Na_2H_3CO_6$	(R) cellulose 91.06%	[53]
	(R) hemicellulose 84.08%	
	(H) lignin 34.09%	
$Ca(OH)_2$	(H) Cellulose 1.3%	[54]
	(H) Hemicellulose 31%	
	(H) Lignin 81.5 %	
$NaClO_2$	(R) Holocellulose 90.3%	[55]
	(R) Lignin 5.4 %	
Na_2SO_3	(R) Cellulose 85.17%	[56]
	(H) Lignin 77.45%	
NH_4OH	(R) Hemicellulose 28.9%	[57]
	(R) Cellulose 83.8%	
	(H) Lignin 84.7%	
KOH	(R) Glucan 82.9%	[58]
	(R) Xylan 2.2%	
	(H) Lignin 89.4%	
Na_2S + NaOH	(R) Cellulose 70.85%	[59]
	(R) Hemicellulose 15.61%	
	(R) Lignin 97.54%	
H_2SO_4	(R) Cellulose 46.1%	[24]
	(R) Hemicellulose 0.0 %	
	(R) Lignin 51%	
	(H) Cellulose 30.5%	
	(H) Hemicellulose 100 %	
	(H) Lignin 9.1%	
H_2SO_4 + Ascorbic acid	(R) Cellulose 54.88%	[60]
	(R) Hemicellulose 11.34%	
	(R) Lignin 19.74%	
H_2SO_4, Steam explosion	(R) Cellulose 58.22%	[61]
	(R) Hemicellulose 1.15%	
	(R) ASL 1.6%	
	(R) AIL 27.07%	
H_2SO_3	(R) Glucan 66.9%	[62]
	(R) Xylan 5.8%	
	(R) Lignin 27.6%	
$C_2H_2O_4$	(R) Lignin 22.4%	[63]

	(R) Glucan 56.1%	
	(R) Xylan 10.8%	
CH_2O_2	(R) XOS yield 38.3%	[64]
	(R) cellulose 36.5%	
	(R) lignin 9.0%	
p-toluenesulfonic acid	(R) Glucan 89.51%	[65]
	(H) Xylan 79.38%	
	(H) Lignin 69.34%	
Solid acid catalyst	(R) Cellulose 64.6%	[66]
	(R) Hemicellulose 7.8%	
	(R) Lignin 21.4%	
Solid acid catalyst	(H) Hemicellulose 100%	[67]
THF+H2O	(R) Cellulose 88.2%	[68]
	(H) Lignin removal 71.9%	
Glycerol	(R) Cellulose 69.1%	[69]
	(R) Hemicellulose 10.3%	
	(R) Lignin 9.2%	
Deep eutectic solvent	(H) Lignin 98.5	[70]
Ionic liquid	(H) Lignin 99%	[71]
H_2O_2 – NaOH	(R) Cellulose 91.8%	[72]
	(R) hemicellulose 89%	
	(R) Lignin 77.5%	
H_2O_2	(H) pentose yield 49.6%	[73]
	(H) Glucan 3.50-4.31%	
$KMnO_4$	(R) cellulose 94.56%	[74]
	(R) hemicellulose 81.47%	
	(H) lignin 46.79%	
Hydrothermal	(R) Cellulose 78.34%	[32]
	(R) Hemicellulose 3.95%	
	(R) Lignin 17.70%	
Steam explosion	(R) Glucan 43.7%	[75]
	(R) Xylan 5.5%	
	(R) Lignin 23.4%	
Torrefaction	(R) Cellulose 47.51%	[76]
	(R) Hemi cellulose 26.71%	
	(R) AIL 18.09%	

Ultra-high pressure	(H) Hemicellulose 0.0%	[77]
	(H) Cellulose 2.2%	
	(H) Lignin 34.2%	
Ultrasonication	(R) Glucose 58.97%	[78]
	(R) Xylose 1.20%	
	(R) Lignin 35.62%	
Ball milling	(R) Glucose 59.04%	[78]
	(R) Xylose 0.82%	
	(R) Lignin 35.70%	
white-rot fungus)	(R) Glucan 33.9%	[79]
	(R) Xylan 38.9%	
	(R) Lignin 16.4%	
	Lignin removal 17.1%	
Laccase	(R) Cellulose 68.12%	[80]
	(R) Hemicellulose 6.04%	
	(R) Lignin 19.14%	

(H) concentration in the hydrolysate (removed); (R) Concentration in the residue

Table 2.2 Highest yields and efficiencies of products and objectives reported for corncob valorization

Product/objective	**Concentration/yield/ efficiency**	**Pretreatment used**	**Reference**
2,3-butanediol	29.18 g/L	$Na_2H_3CO_6$	[53]
ABE	20.5 g/L	Steam explosion	[81]
Acetoin	1.8g/L	NaOH	[39]
propionic acid	71.8 g/L	Industrial CC-molasses	[82]
Levulinic acid	24.5 g/L	Industrial CCR	[83]
Lactic acid yield	39.1 g/L	H_2SO_4	[84]
Acetic acid yield	24.4 g/L	H_2SO_4	[84]
Butyric acid	26.4 g/L	Ionic liquid	[85]
Dye adsorption (MB)	636.94 mg/g.	KOH	[86]
Zn – Adsorption	41%	$KMnO_4$	[87]
Cr(VI) – Adsorption	25.69 mg/g.	o-Phosphoric acid	[88]
Protein – Adsorption	626 mg/L	H_2SO_4	[83]
	212.7 mg/L		

Total metal ion – Adsorption			
Wastewater treatment	COD removal 47.6 mg/g/L Total nitrogen removal 86.6 %	NaOH	[89]
Methane	309.4 L / Kg	Extrusion-NaOH	[90]
Bio-oil	55.15%	Torrefaction	[91]
Hydrogen	713.6 ± 44.1 ml /g	HCl	[92]
Biosurfactant (Surfactin)	3.95 g/L	NaOH	[93]
BTX	51.1%	Torrefaction	[94]
Carbon supercapacitor	specific capacitance 208.5 F g-1 at 1 A g-1	Ultrasonication → centrifugal mill	[95]
Composite	ethanol-processing CCR	Extrusion -twin-screw	[96]
D-Lactate	7.9 g/L	Glycerol	[97]
Carbon source for solid-state/submerged fermentations	Cellulase 11.1 FPU/g, CMCase 12.96 IU/g), Cellobiase 1.48 IU/g	NaOH	[43]
Carbon source for solid state / submerged fermentations	Xylanase activity 3300 U/g	Whole CC	[98]
Ethanol	252 g/kg	H_2SO_4	[99]
FAME yield	86.5%	H_2SO_4	[100]
furfural	89.4%	NaOH→ H_2O_2	[101]
Furfurylamine	0.267 g /g xylan	NaOH → solid acid catalyst	[102]
Furoic acid	9.93 g/L	Solid acid catalyst	[67]
Lactic acid yield	0.77 g/g	NaOH	[40]
Lignin-Sulfonated	1.62 mmol/g	NaOH → HCl	[103]
Lignin purification	purity 99.0%, yield 57.3%	H_2SO_4	[104]
Cellulose acetate	60% acetylation	LHW → NaOH	[52]
Malic acid	38.6 g/L	H_2SO_4	[105]
levoglucosan	37.4%	H_2SO_4	[106]
Pyrolytic yield	Levoglucosan 15.01%	H_2SO_4	[41]

	Total ketones 2.06% Total acids 3.63% Total furans 1.38% Total phenols 2.53%		
Sophorolipids	49.2 g/L	H_2SO_4	[107]
Cellulose conversion	96.83%	H_2SO_4 → NaOH	[108]
Reducing sugar yield	1.37 g/g	laccase	[109]
XOS yield	86.10%	Oxalic acid	[110]
Xylitol	68.4 g/L, 72h	H_2SO_4	[111]
β-farnesene	4.28 g/L, 48 h	H_2SO_4 → NaOH	[108]

2.1.1.2 Dilute NaOH-combination pretreatments

Combining dilute NaOH pretreatment with other types of pretreatment methodologies was shown to be more promising to the overall sugar yield, energy consumption, and reaction times [32]. NaOH treatment combined with dilute sulphuric acid treatment is a widely applied combination pretreatment approach for bioethanol production from corncobs and allows simultaneous saccharification processes with a higher solid loading of CCR. Reported efficiencies of dilute NaOH combination pretreatments were: 81.98% delignification (Na_2SO_3+NaOH) [80], up to 84.7g/L ethanol yield (NaOH+H_2SO_4) [112], up to 96% glucose yield from enzymatic saccharification (NaOH+steam explosion) [51], xylose yield 63.4% (NaOH+Hydrothermal pretreatment (HTP)) [113], cellulose acetate synthesis with 60% acetylation (Liquid hot water (LHW)+NaOH) [114], 67.19% yield of regenerated cellulose (NaOH + BmimCl (1-butyl-3-methylimidazolium chloride)) [32], enhanced nitrate adsorption capacity evident by increased C/N ratio of the effluent water (NaOH+Hydrothermal pretreated CCR) [115], use of CCR as the carbon source for semi-solid fermentation to produce xylanases (NaOH+hydrotehrmal) [113], and production of cellulose fibres with increased crystallinity and thermal stability (NaOH+microwave assisted bleaching) [50].

2.1.1.3 Pretreatment with alkalis other than dilute NaOH

Several alkalis other than NaOH were studied for their efficiency in pretreating lignocellulose biomass. These include $Ca(OH)_2$ (lime) [116], [117], Na_2CO_3 [118], Na_2S, and aqueous ammonia [119]**.**

Aqueous ammonia is the second-largest alkali pretreatment method used for corncobs. Up to 84.7% of lignin removal [57], around 5.5% hemicellulose hydrolysis [120], and a maximum

of 83.8% cellulose recovery were reported [57] using aqueous ammonia. $Ca(OH)_2$ was found to be an efficient delignification agent and a moderate hemicellulose solubilizer at milder temperatures of 30 – 55 ^oC. The same is the case with KOH but at a higher temperature range of 70 – 100 ^oC. Sodium salts like Na_2SO_3, Na_2S, Na_2CO_3 and $Na_2H_3CO_6$ were also employed to pre-treat the corncobs. Among these, the highest delignification ability was shown by Na_2SO_3 individually [56] and Na_2S in combination with 0.5% NaOH [59]. Although hemicellulose solubilization is moderate to low, the cellulose recovery was satisfactory with these alkali-catalyzed pretreatments.

Formic acid pretreatment, followed by aqueous ammonia pretreatment, has proven to be efficient in hemicellulose solubilization (83.2%) and cellulose recovery (82.9%) [112], whereas aqueous ammonia pretreatment followed by hydrogen peroxide pretreatment was efficient for hemicellulose and lignin degradation along with a lower cellulose recovery [40]. A prolonged hydrothermal pretreatment followed by KOH pretreatment of corncob reportedly produced an extremely porous ($1cm^3/g$) lignocellulose suitable for manufacturing supercapacitors [121]. Formic acid pretreatment followed by aqueous ammonia-derived CCR reportedly resulted in cellulose conversion up to 90.8% [112]. KOH pretreatment of corncob reportedly enabled a high solid loading (20%) for enzymatic saccharification, resulting in a glucose yield of 91% [58].

In a comparative study, 15% ammonia pretreatment was proven to achieve a better delignification of corncob than 2% NaOH and 2% H_2SO_4 [122]. At 7.1% sulfite charge, 60% delignification was achieved from corncob industrial residue, and the subsequent enzymatic saccharification of the residue yielded 79.3% reducing sugars and 60 g/L ethanol from the fermentation of the released sugars [123]. An ultrasound (10 W/mL) assisted aqueous ammonia soaking pretreatment with 15% NH_4OH, at a milder temperature (60 ^oC) and shorter duration (<12 min), achieved an 84.7% delignification and 83.8% of cellulose recovery [57]. Sulfide (Na_2SO_3) and sulfite (Na_2S) pretreatment of corncob in the presence of NaOH was proven to be efficient in delignification (97%), where sulfonated lignin becomes more susceptible to delignification with NaOH. Moreover, the subsequent CCR was proven to be a potential carbon source for lactic acid production [59]. Sodium percarbonate pretreatment of corncob showed a 30.09% lignin removal, with cellulose and hemicellulose recoveries of 91.06% and 84.07%, respectively. The surface area of the resulting CCR was also increased, leading to improved 2,3-butanediol production via an SSF (Simultaneous saccharification and fermentation) process [53]. Improved lactic acid productivity (79.47 g/L) was reported in an SSF process using NH_3-

H_2O_2 pretreated CCR as the carbon source compared to control NaOH pretreatment. Moreover, the NH_3-H_2O_2 pretreated CCR does not require any detoxification washing step before its downstream processing, making the overall process environmentally-friendly [40].

2.1.1.4 Dilute H_2SO_4 pretreatment

Dilute sulphuric acid treatment is the second-largest chemical pretreatment approach reported for diverse biorefinery applications from corncobs (Table 2.2), (Figure 2.3), (Figure 2.4). Hemicellulose is more susceptible to mild conditions of acid concentration and heat than cellulose and lignin. This behaviour is exploited in acid pretreatments to solubilize hemicellulose without affecting cellulose. Dilute sulphuric acid is cheaper and corrosion-free than other acids like HCl and easy to handle even for a large-scale operation [124].

The yields of enzymatic saccharification of CCR derived from dilute H_2SO_4 pretreatment were reported as cellulose conversion 52.6% – 89.77%, glucose 75 – 97% of the theoretical yield, xylose 75 – 87.2% of the theoretical yield, total sugars 34 – 84% of the theoretical yield, and reducing sugars 35 g/L – 51.82 g/L

Several biorefinery platforms were reported with dilute H_2SO_4 pretreatment, such as 0.09 ethanol up to 47 g/L [125], 11.64 g/L of ABE (acetone, butanol, ethanol) [126], and up to 9.52 g/L Butanol production [37]. The adsorption properties of dilute sulphuric acid-treated corncob to remove different water contaminants were reported, with the removal of nitrate up to 94.1%, total nitrogen up to 83.6% [47], soluble proteins up to 626 mg/L [127], and total metal ions up to 212.7 mg/L [127]. Adsorption of two different dyes, direct orange-15 and direct blue 6BX with 32.9 mg/g and 22.5 mg/g of the corncob residue, respectively, was also reported [128]. A work reported 39.1 g/L of lactic acid and 24.4 g/L of acetic acid production (Guo et al., 2010), and malic acid production of 38.6 g/L was reported by another [105]. Valorization of hemicellulose in terms of 68.4 g/L xylitol production [111], xylooligosaccharides (XOS) yield 1.82 g/100g of corncob [129], and a few lignin valorizations works, including isolation of lignin (57.3%), and value-added products from isolated lignin were reported [104]. Some of the works reported pyrolytic products from corncob residue; notably, levoglucosan yield of up to 37.4% [106], FAME yield of 86.5% [100], and sophorolipids concentration of up to 49.2 g/L are reported [107].

2.1.1.5 Pretreatment with acids other than dilute H_2SO_4

Both inorganic (H_2SO_4, HNO_3, H_3PO_4, HCl, H_2SO_3) and organic acids (oxalic acid, malic acid, acetic acid) were reported for their application in pretreating lignocellulose biomass feedstocks. The yields and efficiencies of dilute organic acid pretreatment of corncob were reported as HCl (Hydrogen yield up to 713 ml/g CC [92]), acetic acid (92.69% glucan conversion [130], ascorbic acid (27.7% Zn adsorption [87]), formic acid (23 wt% nanocellulose, 8.5 wt% nano lignin yield [64]), gluconic acid (XOS 56.2%, glucose 86.3% [131]), sulfurous acid (ethanol 75% [62]), nitric acid (ABE < 1g/L, 27.42%, Zn adsorption [87]), oxalic acid (ethanol yield up to 20 g/L [132], furfural 81.69% [133]), p-toluenesulfonic acid (ethanol 55 g/L, Lignin sulfonation 2.16 mmol/g [65]).

Ball milling of oxalic acid (15 mM) impregnated corncob, followed by microwave-induced hydrothermal pretreatment, reportedly achieved a xylose sugar yield of 86.10% [110]. A pilot-scale ethanol production study reported 21.1 g/L ethanol from oxalic acid pretreated corncob biomass. This result indicates the scaleup ability of oxalic acid pretreatment [134]. A bio-hydrogen yield of 107.9 ml/g of total volatile solids was reportedly obtained from 10 g/L CCR, generated from 1% HCl pretreatment [135]. Despite showing the highest sugar yield through enzymatic saccharification, H_2SO_4 pretreated CCR showed very poor ABE yield compared to H_3PO_4 treated CCR [126]. Pretreatment of corncob with o-Phosphoric acid, followed by pyrolysis, reportedly produced biochar with Cr(VI) adsorbing efficiency of 93%, satisfying the Langmuir isotherm model. In addition, as a solid fuel, biochar showed a higher heating value of 19.97 MJ/Kg [88]. Gluconic acid pretreatment of corncob resulted in 56.2% XOS and 86.4% saccharification yield [136]. Corncob ball-milled in the presence of oxalic acid, followed by microwave irradiation, resulted in 86.10% xylose and XOS yield. [110]

Pretreatment methods involving both alkali and acid are termed combination pretreatment approaches. Some of the combination pretreatment methods reported are given in Table 2.

Table 2.3 Combination pretreatments reported on corncob for ethanol production

Initial pretreatment → Successive pretreatment	Detoxification	Efficiency Of pretreatment	Bioconversion	Lignocellulose component valorised	Ethanol Yield (Y) Productivity (P) Theoretical yield (TY)	Co-products	Reference
Ammonia steeping 2.9 M NH_4OH (L/S 5), 26°C, 24 h → 0.3 M HCl, 100-108°C, 1 h	CCR: water wash CCH: alkali neutralization → desalting using IRA-94	(H) LG 80-90%	SSF	CL, HC	Y = 45 g/L Y = 86%	None	[137]
2% H_2SO_4 (L/S 10), 121°C, 45 min → 2% NaOH (L/S 6), 80°C	CCR: Water wash CCH: N.A	**NA**	SHF & SSF	CL	strain 45# Y = 3.31 g/100 g 77.7% of TY Angel-EH12 Y = 3.69 g / 100g 86.9 % of TY	None	[138]
1.4% H_2SO_4 (L/S 20), 12 min, 170 °C → NaOH (N.D)	CCR: N.D CCH: N.D	(R) CL 65.7% (R) HC 1.8% (R) LG 3.2%	SSF (batch & fed-batch)	CL	Y = 57.2 g/L	None	[139]
2% H_2SO_4 (L/S 10) 121°C, 45 min →2% NaOH (L/S 6) 80°C, 6h	CCR: water wash CCH: N.D	(R) CL 91.1% (H) HC 66.8% (H) LG 81.0%	SSF (batch & fed-batch)	CL	Y = 69.2 g/l Y = 81.2% Fed bath mode Y = 84.7 g/l Y = 79.6%	None	[112]
Formic acid (L/S 6) 60°C, 6 h →15% NH_4OH (L/S 6) 60°C, 12 h	CCR: water wash CCH: N.D	(H) HC 83.2% (R) CL 82.9%	SSF (batch & fed-batch)	CL	Y = 62.7 g/l Y = 77.3 %	None	[112]
2% HNO_3 (L/S 5), 121°C, 15 min → 1% NaOH (L/S 20), 121°C, 15 min	CCR: water wash CCH: without detoxification	(R) CL78.62% (R) HC3.2% (R) LG 2.0%	SSF	CL, HC, LG	E.Y = 33.14 g/l E 74.49%	Bio gas Lignin extraction	[140]
2% NaOH (L/S N.D),RT,24 hr → 1% H_2SO_4 (L/S N.D), 170 °C, 5 min	CCR: N.D CCH: N.D	(R) CL 92.25%	SHF	CL	Y = 1.8 g/l	None	[141]

1% H_2SO_4 (L/S 10), 120°C, 60 min → 0.075g/g NaOH, 60°C, 120 min	Water wash	(H) XY 88.6% (H) LG 88% (R) GL 94.6%	SSF	CL	Y = 52 g/L 77.2% of TY	N.A	[142]
1.1% H_2SO_4 (L/S 8), 120°C, 3h →2% NaOH (L/S N.D), 65°C, 2h	CCR: Water wash CCH: N.A	(R) CL 66.7% (H) HC 72.6%, (H) LG 62.9%	SHF	CL	Y = 57.8 g/L	None	[143]
1% H_2SO_4 (L/S 10), 120°C, 60 min → NaOH 0.075 g/g dry substrate., 60°C, 2 h	CCR: Water wash CCH: N.A	(R) GL 63.5 % (R) XY 6.7 % (R) LG 17.6%	SSF	CL	Y = 52 g/L 77.2% of TY	None	[144]
pH 5.5, 121 °C, 15 min → *P.chrysosporium* (lignin degrading), 30 °C, 20 days → 10% CCR, Xylanase 800 U/g, 1% Tween-80 pH 5.3, 50°C	CCR: Water wash CCH: over- liming → resin 201X 7 overliming → macroporous resin NKA II overliming → activated charcoal concentration → resin 201X 7 concentration → macroporous resin NKA II concentration → activated charcoal	(H) HC 20.8% (H) CL 18.50% (H) LG 42.7%	Fermentation-CCH SSF (CCR)	CL, HC	Xyl→EtOH Y = 6.65 g/L Y = 0.427 g/g Glc→EtOH Y = 33.3 g/L Y = 0.510 g/g	None	[54]

Note: CC corncob whole, without pretreatment; CCR: pretreatment derived solid Corncob residue; CCH: pretreatment derived corncob hydrolysate; (R) = % recovered or % composition in the solid residue; (H) = % hydrolysed or % concentration in the hydrolysate; L/S = Liquid to solid ratio; N.D = not defined; N.A = Not applicable; Glc: glucose; Xyl: Xylose; Ara: arabinose; Gal: galactose; Man: mannose; GL: glucan; XY: xylan; AR: arabinan; LG: lignin; CL: cellulose; HC: hemicellulose; LC: lignocellulose; TS: total sugars; HSF: hybrid saccharification and fermentation.

2.1.1.6 Solid acid catalyst pretreatment

Solid-acid catalysts are heterogeneous catalysts synthesized by embedding acidic functional groups on the surface of a solid matrix. Various classes of these catalysts include zeolites, mixed metal oxides, single-component metal oxides, heteropoly acids, mounted acids, metal salts, mesoporous materials and cation exchange resins [145].

Magnetic solid acid catalysts are the economically viable option for their ability to be recovered and reused. Sn-BTN (Tin-loaded Bentonite) catalyzed acid pretreatment of corncob-biomass has achieved a 100% hemicellulose removal, further obtaining 53.3% furfural yield upon subsequent downstream conversion.

Although it is not much energy efficient, an interesting combination of ball milling of corncob in the presence of a solid acid catalyst (SO_4^{2-}/SiO_2-Al_2O_3/La^{3+}), followed by ultrasonication, reportedly generated 82.90% of theoretical furfural yield [78].

Solid acid catalyst synthesized by simple sulfonation of microcrystalline cellulose-derived carbon with sulphuric acid reportedly yielded 78.1% xylose from corncobs and 91.6% successive enzymatic saccharification yield in just 48 hrs [146].

Corncob-derived lignin along with other control lignin samples was treated with a solid acid catalyst ($ZnMoO_4$ embedded on mesoporous silicate MCM-41 (Mobil Composition of Matter No. 41), producing the lignin-derived platform chemicals, methyl coumarate and methyl ferulate [147].

In an interesting corncob based biorefinery objective to produce furoic acid from corncob derived furfural, a solid acid tin-bentonite (Sn-BTN) catalyst pretreatment in a biphasic system (5:5 (v/v) Methyl isobutyl ketone (MIBK)-H_2O) reportedly yielded 53.3% furfural and the simultaneous biotransformation with *Brevibacterium lutescens* achieved 100% furoic acid yield within 18 hrs [67].

Bamboo-derived-magnetic-solid-acid catalyst pretreatment of corncobs showed that the catalysts synthesized with less concentrated (0.25%) H_2SO_4 and higher concentrated (2%) KOH pretreatment-derived carbons achieved a higher reducing sugar yield. These results emphasize the importance of hemicellulose removal and delignification without affecting the cellulose content of the biomass to achieve a porous carbon with high acid loading capability and a higher surface area [148].

Alkali (1% NaOH) pretreated corncobs were sequentially treated with an acidified tin-based solid acid catalyst with zirconium oxide support to produce furfural. Simultaneously, the furfural was bio-converted to furfurylamine with a recombinant *Escherichia coli* expressing ω-

transaminase. The results showed that 3g of pretreated corncob yielded 90.3 mM furfural and subsequently 76.3% furfurylamine through bioconversion [102].

An integrated co-catalysis process that included a mineral acid (4% H_2SO_4), an organic acid (3% Acetic acid) and a Lewis acid (5% $FeCl_3.6H_2O$) was proposed [149] to achieve higher furfural yield from corncobs. The results proved the synergetic effect of the three acids to improve furfural yield.

2.1.1.7 Organosolv pretreatment

The use of organic solvents for the pretreatment of lignocellulosic biomass feedstocks, also known as organosolv pretreatment, dates back to the 1970s when organic solvents were used to remove lignin in the pulping process. Various organic solvent types have been reported for biomass valorization, such as low boiling point alcohols (ethanol, methanol), high boiling point alcohols (glycerol, ethylene glycol, THFA (Tetrahydrofurfuryl alcohol)) and organic compounds of other classes (ethers, ketones, phenols, and dimethylsulfoxide) [150].

Glycerol pretreatment for corncob biomass valorization was mostly reported for the production of levoglucosan, and the yields reported (38.0% - 44.5%) were increased hundreds of times than from untreated corncobs [151], [152]. A glucose yield of 83.7% from enzymatic saccharified CCR and a D-lactate yield of 6.1 – 7.9 g/L from the fermentation of spent glycerol were reported [97], [69].

Note that pretreatment with organic acids is usually classified under organosolv pretreatments, but we discussed it under acid pretreatments.

2.1.1.8 Ionic liquids & Deep eutectic solvents (DESs) pretreatment

Ionic liquids are salts of organic cations and organic or inorganic anions, characterized by melting points less than that of water (< 100 ^oC), often below the ambient temperatures, and few with further lower melting points of below 0 ^oC. They exhibit low vapour pressure and high thermal stability. Owing to these physicochemical properties, the processes which use ionic liquids are often termed green technologies [153].

DESs are binary solvents comprising a eutectic mixture of Lewis or Brønsted acids and bases, including a wide variety of anionic and cationic species that act as hydrogen bond donors and hydrogen bond acceptors. Individual melting points of the two components involved are higher than that of their eutectic melting point. Although DESs are being referred to as a new class of ionic liquids due to certain characteristic similarities they share, DESs are technically completely different solvents from ionic liquids.

Sun et al. [154] compared ionic liquids of different [EMIM] OAc (1-ethyl-3-methylimidazolium acetate) combinations, with H_2O, DMF (N, N-Dimethylformamide), DMSO (dimethyl sulfoxide) and DMA (Dimethylacetamide) to study their efficiency to generate platform sugars and lignin from corncob biomass. The highest glucose and xylose yields, 0.41% and 1.81% respectively, were obtained from [EMIM] OAc/ Di.H_2O (3:7) combination, whereas, the highest lignin yield of 9.78% was obtained with [EMIM] OAc/ DMSO (3:7) combination [154]. At the same operating parameters, BTMAC/LA (Benzyltrimethylammonium chloride / lactic acid) deep eutectic combination was proven to be more efficient than BTEAC/LA (Benzyltriethylammonium chloride / lactic acid) for promoting saccharification of the resulting CCR (94% sugar yield) [155]. In another comparative study, different combinations of choline chloride with glycerol, imidazole and urea were studied, and the choline chloride/imidazole (3:7) combination was found to be more efficient in terms of glucan and xylan recovery and acid-soluble lignin removal even at a milder temperature (80 ^oC) [156]. Subsequently, the downstream saccharification of the CCR was also improved. An extensive comparative study, involving different combinations of $ChCl_3$ with several organic acids and alcohols, showed that $ChCl_3$/lactic acid (1:2) combination was most efficient in lignin removal up to 95.5%, and $ChCl_3$/Glycerol (1:2) as the most efficient in promoting downstream saccharification of the CCR with a glucose yield of 96.4% [70]. Another extensive study of ionic liquid pretreatment efficiency, involving both EMIM/AC and BMIM/Cl (1-butyl-3-methylimidazolium chloride), individually and in their combinations, showed that both EMIM-AC/Ethanolamine (60:40) and BMIM-Cl/Ethanolamine (60:40) exhibited the highest lignin removal capacity in the range of 92% - 99%, and promoted subsequent downstream sugar conversion (enzymatic saccharification) in the range of 88.2% - 97%, EMIM-AC/Ethanolamine (60:40) being the best among the two [71]. In an attempt to valorise lignin as well as to improve ionic liquid pretreatment of corncobs, lignin-derived γ-valerolactone was used as a co-solvent along with ionic liquid Mmim/DMP. Further lignin was used in the immobilization of butyric acid-producing strain, *Clostridium tyrobutyricum* [85].

2.1.1.9 Oxidative pretreatment

Oxidizing agents, in general, delignify as well as solubilize hemicellulose. The use of hydrogen peroxide is widely reported for the oxidative pretreatments of corncob, and, to a lesser extent, $NaClO_2$ showed excellent lignin degradation capacity with very minimum effect on

holocellulose. The release of poisonous Cl_2 gas during $NaClO_2$ pretreatment is a major drawback of this process.

$KMnO_4$ is traditionally known for its nontoxic, cost-effective, highly efficient oxidative property that is used in water treatments. An alkaline $KMnO_4$ pretreatment of corncob reportedly resulted in 46.79% delignification, 94.56% and 81.47% cellulose and hemicellulose recoveries, respectively [74] [157].

2.1.1.10 Fenton and metal chlorides pretreatment

Metal chlorides such as $FeCl_3$, $AlCl_3$, $CuCl_2$, $MnCl_2$, $MgCl_2$, NaCl can degrade lignocellulose and sugars, are less corrosive, and recoverable as metal hydroxides. Hence, these are regarded as one of the ideal choices for pretreatment. Metal cations can accept electrons, easily be hydrated in water, and thus, release hydrogen upon hydrolysis. These properties make them act as both Lewis and Brønsted acids [158]. The metal cations were proven to be efficient in solubilizing hemicellulose and lignin. The concentration of the metal chlorides, operating temperature and time are the important factors in determining the efficiency of the pretreatment.

Fenton reaction was adopted from an exclusive, natural biochemical process that a brown-rot fungus (wood rotting, basidiomycete) employs. The brown rot fungus carries a Fe^{2+}, Fe^{3+}, H_2O_2 assisted hydroxyl ($HO^{\cdot}$) and hydroperoxyl ($HOO^{\cdot}$) free radical generation. These free radicals attack the π electron system of recalcitrant plant cell wall lignin and pave the way for a group of lignocellulose-digesting enzymes. This energy-efficient two-step process achieves many glycans and xylan hydrolysis without much lignin degradation [159].

In work reported by several univalents, bivalent and trivalent cation-containing metal chlorides were compared for their pretreatment efficiencies and found that pretreatment with 25 mM $FeCl_3$ at 140 ^oC for 20 min gave the best results, releasing 99% of the xylan, recovering 91% of cellulose, in addition to increasing the downstream saccharification of resulting CCR to nearly 5 fold, compared to that of untreated corncob [160]. In a comparative study of corncob pretreatments, dilute acid-catalyzed steam explosion is found best to hydrolyze the hemicellulose from corncob, whereas ultrasonication-assisted Fenton reaction is found best for lignin removal. The enzymatic hydrolysis of the CCRs derived from each pretreatment approach is 86.8% and 90.34%, respectively [128]. Fenton pretreatment with the synergetic action of Fe, Fe^{2+}, Fe^{3+}, H_2O_2 along with ultrasonication-assisted TiO_2 catalyst, in combination with a prior mild alkali pretreatment, has been proven to be efficient in the delignification of corncob (33.20 g/L) and a subsequent enzymatic XOS production 174.81 mg/g CCR [161].

Organic solvents like DMSO are thought to promote delignification and hemicellulose solubilization, thereby increasing the permeability of lignocellulose materials. This concept was reported in a modified Fenton pretreatment of corncob where DMSO/water was used as a solvent for Fenton reaction with $FeCl_3$ and H_2O_2. When the resulting pretreatment slurry with carbohydrate recovered CCR of up to 94% was enzymatically saccharified without any detoxification, 92% of the theoretical glucose yield was achieved [162]. Ultrasonication-assisted $FeSO_4$ pretreatment of the corncob resulted in CCR with enhanced saccharifying capacity (glucose yield up to 90.3% of theoretical yield) and also improved its dye adsorption capacity [128]

2.1.2 Physicochemical pretreatments

2.1.2.1 Liquid hot water pretreatment

Hydrothermal pretreatment (HTP) or Liquid hot water pretreatment (LHW) causes deoxygenation of the biomass, decreases the production of unwanted acid and ketone by-products, and enhances the hydrophobicity and the grindability of the biomass. Hydrothermal pretreatment is the most applied physicochemical approach with corncobs [163]. A severity factor (log R_0) between 3.64 and 4.25 of HTP can markedly improve hemicellulose solubilization and cellulose saccharification [164]. HTP of corncobs suggests that the S/G (Syringyl /guaiacyl) ratio of the lignin in biomass enhances the hemicellulose solubility and decreases the cellulose digestibility [165].

HTP-mediated AAEMs (alkali and alkaline earth metal species) removal from corncobs and reported pyrolytic yields of hydrothermally-pretreated CCR (HTP-CCR) are satisfactory. Co-pyrolysis of HTP-CCR and High-density polyethylene (HDPE) improved the H/Ceff ratio (optimum ratio 1.2) and thus improved the levoglucosan and furan production [21] [166]. Other notable HTP works on corncobs are HTP (22 g/L XOS, CCR with 65% cellulose and 22% lignin, 100% saccharification yield)[167], HTP in combination with NaOH (regenerated cellulose with better viscoelastic properties) [32], thermostable xylanase in combination with HTP (28.6% XOS from corncob with larger initial size > 100 mm) [168], Sn-MMT (Tin-loaded montmorillonite) catalyzed-microwave assisted-hydrothermal pretreatment in 2-sec-butyl-phenol/NaCl-DMSO system improved xylose and furfural yields up to 86.67 %, 57.80 % respectively [169]. An (SO_4^{2-}/SiO_2-Al_2O_3/La^{3+}) catalyzed HTP process resulted in 7.01 g/L xylan and 21% furfural [170].

2.1.2.2 Steam Explosion

When maintained under highly pressured (0.7 – 4.8 MPa), saturated steam (160 – 260 °C) for a particular time followed by a rapid depressurization, biomass undergoes an explosive decompression. This results in the disruption of carbohydrates and lignin to different extents, ultimately improving the biomass surface area and, thus, the digestibility of the cellulose. Hence, the steam explosion is mostly used in combination with other pretreatment methods. In addition to the decompression effect, hydrolysis of acetate groups of hemicellulose generates acetic acid, which can further contribute to the process's effectiveness through autohydrolysis (acid hydrolysis) effect on biomass [171].

2.1.2.3 Ammonia Fibre Explosion (AFEX) and Aqueous Ammonia Pretreatment

Ammonia fibre explosion is a variant of steam explosion pretreatment, where the process is carried in the presence of liquid ammonia (1:1 or 1:2 S/L ratio), at a temperature range of 60–90 °C, pressure 40 - 50 atm for 10–60 min. In addition to the explosive decompression of biomass, the rapid expansion of ammonia causes swelling and disruption of the biomass, further enhancing the pretreated biomass surface area. Also, ammonia decreases the crystallinity of cellulose. In addition, a small portion of hemicellulose is solubilized, and the lignin structure is disrupted but not degraded. Unlike the steam explosion, the evaporation of the ammonia during AFEX results in only the solid pretreated residue without leaving a liquid slurry. AFEX can be successfully applied to the low lignin-containing biomass feedstocks es than the high lignin biomass feedstocks since the lignin is not removed during the pretreatment [172], [173] Soaking in aqueous ammonia (SAA) is a process in which biomass is soaked in aqueous ammonia at a milder temperature (25–60 °C), for a longer period of 10 – 60 days, in a batch reactor. A selective delignification of the biomass minimizes the sugar loss [174]. Ammonia recycle percolation (ARP) is a process where aqueous ammonia (10 – 15%) is passed through (1- 5 ml/min) a packed bed reactor filled with biomass, at an elevated temperature (150–190 °C), and a residence time up to 120 mins. Later the ammonia is recovered and recycled. To prevent the evaporation of ammonia, the system is slightly pressurized [175]. Some of the hemicellulose is degraded and lost during the process. The low cost, easy recovery and recycling make it feasible to scale up this pretreatment process. Notably, the unrecoverable ammonia present in the pretreatment slurry can be used as a nitrogen source during the downstream fermentation process. [174], In addition, the milder operating conditions produce very few inhibitory

products. Nevertheless, recycling ammonia is an energy-intensive process, and the use of ammonia has serious environmental concerns. [176].

2.1.3 Physical pretreatments of corncobs

2.1.3.1 Torrefaction

Both pyrolysis and torrefaction involve heating raw biomass in an inert, non-oxidizing environment. Nitrogen is commonly used to create such an environment. Pyrolysis is carried at the temperature range of 350 – 650^{o}C, whereas torrefaction is carried at a relatively milder temperature range of 200 – 300^{o}C. The time ranges from a few seconds to hours for both processes. The resulting biomass residue shows decreased H/C and O/C ratios and moisture content and an increased energy density, hydrophobicity, reactivity, and grindability [177].

Both cellulose and hemicellulose decompose at relatively lower pyrolytic temperatures than much resilient lignin. Cellulose decomposition is slower at milder torrefaction conditions and produces fewer volatile products. Hence, torrefaction is a much more suitable biomass pretreatment method than pyrolysis [178].

Torrefaction is always accompanied by downstream fast pyrolysis of CCR and reportedly improves the pyrolytic bio-oil quality. Higher torrefaction temperatures cause crosslinking and charring of biomass, decreasing pyrolytic bio-oil yield [91]. 240^{o}C is the optimum torrefaction temperature for corncob, at which activation energy, H/Ceff ratio, and exponential factor are increased while lowering the oxygen content, mass, and energy content of the corncob. Wet torrefaction reportedly enhanced levoglucosan yield), whereas dry torrefaction caused higher cellulose degradation and charring) [76]. Ozawa-Flynn-Wall (OFW) method is best suitable for activation energy calculation whereas, Kissinger-Akahira-Sunose (KAS) method and distributed activation energy model (DAEM) is suitable for the calculation of pre-exponential factor [179], [94].

2.1.3.2 Ultrasonication

Ultrasound disrupts the lignocellulose biomass in solution through cavitation, shear and the generated free radicals. [180], [181]. Sonication is known to induce hydrolysis; thus, ultrasound-assisted thermochemical pretreatments can be performed at reduced temperature, time and catalyst concentrations. [182], [183], [184]. As discussed earlier, ultrasonication is widely reported as an accessory process along with certain thermochemical pretreatments. Nevertheless, ultrasound alone has also been reported as a corncob pretreatment approach.

2.1.3.3 Ultra-high pressure pretreatment

Ultrahigh pressure pretreatment or high-pressure process is an emerging non-thermal, physical pretreatment process that involves pressure in a range of 100 – 800 MPa. Often, it is also termed as high isostatic pressure and high hydrostatic pressure treatment. [185]. This pretreatment approach has proven successful in the food industry (Knorr et al., 2011). Ultrahigh pressure pretreatment reportedly enhanced the enzymatic saccharification of *Eucalyptus globulus* pulp [186], [187], cotton stalk [188], sugarcane bagasse [189] and corncob (100 MPa for 10 minutes reportedly increased the accessible hemicellulose surface area to promote enzymatic XOS production [77]

The adiabatic expansion was tried as a pretreatment approach before carbonization of the resulting CCR to produce activated carbon to be used as an electrode material for capacitors. The resulting carbon has shown a specific capacitance of 276 F/g at 50 mA/g [190].

Simple heat treatment of corncob at 120 ^{o}C for 40 min reportedly enhanced its organic adsorption capacity of carbon to 11 mg/L and total nitrogen to 0.28 mg/L for 6 days of adsorption [191].

2.1.3.4 Irradiation pretreatment

Several types of ionizing and non-ionizing irradiations have been reported as biomass-pretreatment approaches. They include microwave, ultrasound, gamma rays, and electron beam. Irradiation causes delignification and disruption of cellulose crystallinity, thus causing biomass depolymerization.

Gamma radiation, reportedly, removed the hemicellulose and decreased the crystallinity of cellulose by cleaving β-1,4 glycosidic links and also removed the lignin from biomass, resulting in a biomass residue that is highly susceptible to enzymatic saccharification. [192].

Microwave irradiation has been used as an alternative to conventional heating methods, with the advantage of uniform heat distribution at comparatively low energy input. Studies proved that microwave irradiation could improve the enzymatic saccharification of the pretreated biomass residue. [193]. Often microwave irradiation is reported as a means of heating, aiding the thermochemical pretreatment reactions. Nevertheless, scaling up of microwave technology is not economical [193].

2.1.3.5 Pulsed Electric Field Pretreatment

High-intensity electric fields are known to cause increased permeability and mechanical rupture in cell membranes [178]. This phenomenon is applied in pulsed electric field pretreatment, where short bursts of high intensity (5–20 kV/cm) electric pulses were applied on biomass kept in between two electrodes. The increased porosity of pretreated biomass will then permeate the chemical catalysts to disintegrate it further. Comparatively, the energy requirement is low [178].

2.1.3.6 Plasma pretreatment

It is an unconventional technology reported lately. In this, a feeding gas such as argon, nitrogen, or oxygen is ionized by electricity under the vacuum condition to generate reactive plasma, which effectively removes the lignin and makes the biomass susceptible [194]. It is a highly expensive pretreatment methodology due to the cost of gas used, the specialized equipment required, and the process conditions used [195], [196], [197]. To address this, atmospheric plasma pretreatment was proposed, where the process is carried under atmospheric pressure, with air as the gaseous medium [194]. Although the mechanism is not fully understood, atmospheric plasma pretreatment involves both physical and chemical processes forming a proton-active layer over the biomass surface and the free radical attacks) to disrupt the lignocellulose recalcitrant structure [198], [199], [200], [201], [202].

Atmospheric low-temperature plasma pretreatment of corncob resulted in cleavage of β-O-4 aryl ether linkages of lignin as oxidation of the biomass. The lignin aryl linkages were reduced to 58.7/100Ar after the pretreatment, and overall oxygen content has improved. The thermodynamically favourable reaction pathway involves cleavage of Cβ-O followed by Cβ-Cα covalent bonds [203]

2.1.4 Mechanical pretreatments

Comminution is the first step in valorizing any type of lignocellulose biomass. Even if a particular physical, chemical or biological pretreatment were used, the initial pretreatment step would be the mechanical comminution. Reduction in biomass size increases the total accessible surface area and decreases the degree of polymerization, thus improving the access of enzymes, catalysts, and overall mass and heat transfers. In addition, comminution helps in the densification and storage of biomass. Nevertheless, reducing the size of biomass beyond a critical size will not enhance the post-processing efficiency further [204]. Mechanical

comminution as a solo pretreatment approach is not attractive because it is an energy-demanding process, and it does not remove lignin [205].

2.1.4.1 Milling as a pretreatment

Different types of mills were reported for the comminution of dry lignocellulose biomass (moisture content <15%), namely, knife mill, pin mill, hammer mill, roller mill, cryogenic mill and centrifugal mill. Papirindustriens Forskningsinstitutt (PFI) mills are laboratory-scale refiners, and disc refiners are large-scale industrial equipment. These two are routinely used for pretreatment purposes [206].

Ball milling is the most used mechanical pretreatment for corncobs. The use of balls made of steel, zirconium oxide and glass with varying diameters and rotated at different RPMs was reported. By varying the input corncob to balls ratio between 1:8 and 1:20, the active pyrolytic temperature of the resulting CCR has been altered in the range of 100 – 113.3^{o}C. Ball milling as a solo pretreatment methodology was also proposed to produce platform sugars, XOS, furfural and butanol. Although ball milling of corncobs is mostly performed in dry conditions, an exception was reported where aqueous swelling of the corncobs was done before wet ball milling it. Other types of mills reported for the pretreatment of corncob are RT-34 cutting mill, centrifugal mill, blender, PFI mill, wet disk mill and wet grinding. Mostly, these mills were used to achieve an increased downstream enzymatic production of platform sugars. Furthermore, the results show that these millings achieved the yields of glucose, xylose and arabinose in the range of 36.1% -71.3%, 14.4% - 39.1%, and 10.1% - 18.69%, respectively, with wet disk milling yielding the highest.

Ball milling in combination with other pretreatments has proven to be more successful than ball milling alone for corncob-based biorefinery objectives. Ball milling of organosolv lignin extracted corncob, followed by microwave pretreatment, led to excellent hemicellulose solubilization up to 85.2% and lignin removal, both acid-soluble and insoluble together up to 36.7%. It also improved the further downstream lignin purification with a yield of up to 2063 g/mol and achieved up to 82% of CCR enzymatic saccharification. In another work of corncob lignin valorization, ball milling of dewaxed corncob, followed by organosolv lignin extraction and the downstream plasma treatment of extracted lignin, has improved the aliphatic structure of the lignin with an improvement in overall H, O and N percentages. In a comparative study reported for corncob-based XOS and furfural production, different combinations and single pretreatments were tried: Ball milling alone, Ball milling in the presence of a solid acid catalyst

(SO_4^{2-}/SiO_2-Al_2O_3/La^{3+}), ball milling in combination with successive ultrasonication and ultrasonication alone. The highest furfural production of 64.62 mg/g was achieved by the ball milling-ultrasonication combination, whereas the highest XOS production of 12.05 mg/g was achieved with ball milling alone. Nevertheless, the lignin removal among all these pretreatment variations remained almost constant in the range of 34.84% - 35.70%. Ball milling of corncob in the presence of a solid acid catalyst (SO_4^{2-}/SiO_2-Al_2O_3/La^{3+}), followed by ultrasonication, was proven to be a successful combination pretreatment approach to enhance hydrothermal furfural production, in which a furfural concentration equal to 82.90% of its theoretical yield was obtained at 190°C for 30 minutes [78]. Ball milling, followed by the aqueous swelling of the corncob, reportedly enhanced the enzymatic saccharification of the CCR without the production of inhibitors [37]. Ball milling of corncob has reportedly shown potential biohydrogen production from the derived CCR [207].

Wet disk milling was proven to be successful in promoting ABE fermentation of CCH by *C. acetobutylicum* SE-1 [208]. When wet grinding was compared to other pretreatment methods, like sulfonation and PFI milling, it was proven to be the best in promoting enzymatic saccharification of resulting pretreated corncob residue. After 45 minutes of wet grinding, corncob residue showed 96.7% saccharification [209]. A comparative study involving different physical and chemical pretreatments of corncob proved that milling is the most economical and efficient for improving the dye adsorption capacity of CCR, where 91% of dye adsorption is achieved in 102 hours [46]. Cellular scale fragmentation (50 – 30μm) of the corncob has reportedly enhanced the enzymatic saccharification to 98.3% due to exposure of a higher percentage of polysaccharide chains on biomass surface [210].

2.1.4.2 Extrusion as a pretreatment

Extrusion is one of the simple and cost-effective mechanical methods of pretreatment involving shearing, mixing, and heating. This pretreatment method results in softened surface erosion of biomass by forcing it through a rotating screw and the inner wall of the extruder barrel. Unlike the other mills discussed, extruders can support continuous processing and online monitoring and thus are ideal for large-scale applications [211].

Both single and twin-screw extrusions were proposed for corncob pretreatments. Different industry-derived corncob residues were twin-screw extruded along with HDPE, compatibilizers and coupling agents to form composites of varying physical parameters, among which ethanol-processed corncob residue has produced composites with better physical properties like tensile

and flexural strengths. A specially designed twin-screw extruder was employed to separate xylose from steam-exploded corncob slurry, and the resulting CCR was subjected to enzymatic saccharification. A glucose conversion rate of 90.01% was achieved with 80% xylan removed CCR. A comparative study involving different extrusion modes, such as faster feed rate extrusion, alkali assisted faster feed rate extrusion, and slower feed rate extrusions, with and without subsequent enzymatic saccharification, reported their effect on downstream anaerobic digestibility of their respective CCRs. Methane production in the range of 240.6 - 309.4 L/Kg was achieved, proving alkali assisted faster feed rate extrusion followed by enzymatic saccharification as the best among them. A combination pretreatment of corncob with alkali-assisted extrusion, followed by enzymatic pretreatment, reportedly resulted in methane production that is 22.3% higher than that from untreated corncob. Another combination pretreatment of corncobs, involving steam explosion followed by extrusion with different screw elements in a modified extruder, led to 7% and 80% removal of xylan. Surprisingly, enzymatic saccharification of 7% xylan removed CCR has achieved the highest glucan conversion rate than the latter [212]. A comparative study involving the extrusion of corncob with different types of screw elements demonstrated the influence of the type of screw element used on ultimate enzymatic saccharification of the CCR [213].

2.1.4.3 Biological pretreatment

Broadly, two different approaches were reported for the biological pretreatment of corncobs. The first one is the use of cellulases and xylanases, and the second is lignin-degrading enzymes. The microbes that produce the respective enzymes can also be used to decrease the recalcitrance of the biomass. Various biological methods reported are briefed in Table 2.4

In a corncob-lignin valorization approach, a white-rot fungus (*Theileria Orientalis*-Cui6319) was used to treat the corncobs for 25 days to achieve a 46.5% yield of lignin. In another work of ethanol production, corncob biomass was pretreated with a white-rot fungus (*Irpex. lacteus*) to achieve a 17.1% delignification, and when the resulting CCR was used as a carbon source for the ethanol production in an SSF process, an ethanol yield of 106 mg/g was achieved. A delignification work where corncob biomass was treated with laccase and simultaneously forced through an orifice to create a hydrothermal cavitation effect resulted in 47.4% lignin removal.

Table 2.4 Biological pretreatments of corncob

Biological pretreatment	Efficiency of pretreatment	Detox method	Post-processing	Biorefinery Platforms	Ref
Delignification with *P.chrysosporium*	(H) Hemicellulose 20.8% (H) Cellulose 18.50% (H) Lignin 42.7%	Water wash	SHF CCR + Xylanase+ Tween-80 Xylose + C. shehatae → Ethanol CCH + C. shehatae → ethanol SSF CCR+ Cellulase + *S.cerevisiae* → Ethanol	Xylanase activity (H) Hemicellulose 42.9% Fermentation Xyl→EtOH Ethanol 6.65 g/L Xylan conversion 39.22% Glc→EtOH Ethanol 33.3 g/L Cellulose conversion 71.90%	[54]
Synergetic-Sequential saccharification with thermophilic cellulases, xylanases, and esterase of *C.owensensis*	(H) Xylose 16.8% (H) Arabinose 45.7% (H) Glucose 0%	N.A	ES: commercial cellulase	Glucan conversion rate 37.9% Xylan conversion rate 34.8 %	[75]
ES: Co-hydrolysis *C.owensensis* thermophilic enzymes + commercial cellulase 30mg/g, pH 5.0, 50°C, 72 h	N.A	N.A	N.A	Glucan conversion rate 23.1% Xylan conversion rate 17.4 %	[75]
Synergetic effect of Cellulase and Xylanase	N.A	N.D	Sugar analysis	Glucose 11.5 mg/ml Xylose 2.3 mg/ml	[214]
Delignification with white-rot fungus	(R) Glucan 33.9% (R) Xylan 38.9% (H)Lignin 17.1%	Alkali wash	SSF: Cellulases + Xylanases → *P.tannophilus*	Ethanol 11.5 g/L	[79]
Synergetic-sequential *T.orientalis* (Cui6319-white rot fungus) → *F.pinicola* (Cui12330-Brown rot fungus)	Lignin Yield 62.6%	Lignin Extraction (Dioxane/water) and isolation	Fast pyrolysis of Lignin 600 °C, 60 s, Helium	Toluene 0.6% Phenol 4.3% p-Cresol 6.5% 2-methoxy-4-vinyl phenol 19.2%	[215]

Hydrothermal cavitation-assisted Laccase activity	(H)Lignin 47.4%	N.A	N.A	Cavitation yield 356 X 10^{-5}	[22][54][54][53][52][52](Chen et al., 2010)(Chen et al., 2010)(Chen et al., 2010)(Chen et al., 2010)(Chen et al., 2010)(Chen et al., 2010)[150][29][29][29][150][150][150][150][150]
Combined action of laccase (*Hexagonia hirta* MSF2) + hydrodynamic cavitation	(R) Cellulose 42.25% (R) Hemicellulose 27.38% (R) Lignin 8.14%	N.A	ES	Reducing sugar yield 1.37 g/g	[109]
Note: (H): percent hydrolysis; (R): percent recovery; ES: enzymatic saccharification; N.A: not applicable; Glc: glucose; Xyl: xylose; EtOH: ethanol					

In a combination biological pretreatment, corncob biomass was treated with white-rot fungus (*Theileria orientalis*) for 25 days, followed by treatment with brown rot fungus (*Fomitopsis Pinicola)* for another 7 days, highest delignification ever reported (up to 62.6%) was achieved. A work of corncob delignification [22] reported hydrothermal cavitation assisted laccase activity that depended on orifice plate configuration and fluid pressure. An increase in lignin removal and cellulose recovery was reported by optimizing those parameters.

An efficient synergetic white rot (*T. Orientalis*) and brown rot (*F*. Pinicola) fungal pretreatment of corncob were reported [216]. The physical and structural characterization of the separated lignin revealed a linear structure with decreased phenolic-OH content, decreased p-coumaric acid-glycan ester linkages, absence of methoxyl groups and an increased -COOH content and the S/G ratio. The thermal stability and pyrolytic conversion of lignin were also improved, resulting in a bio-oil with increased alkyl-phenol content.

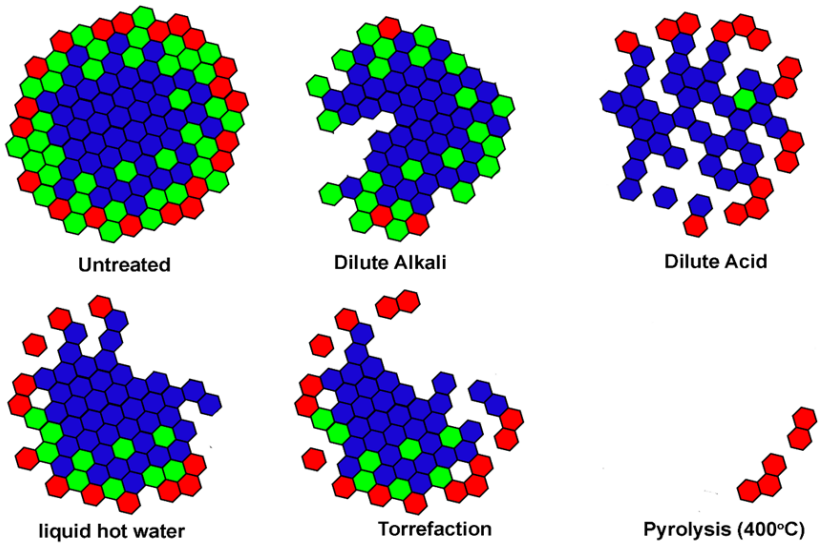

Figure 2.1 Effect of different pretreatments on lignocellulose

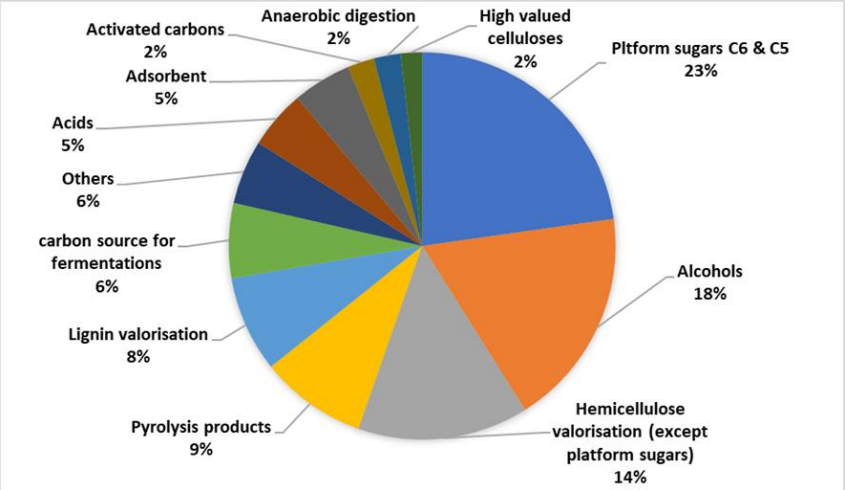

Figure 2.2 Biorefinery platforms products reported from corncob

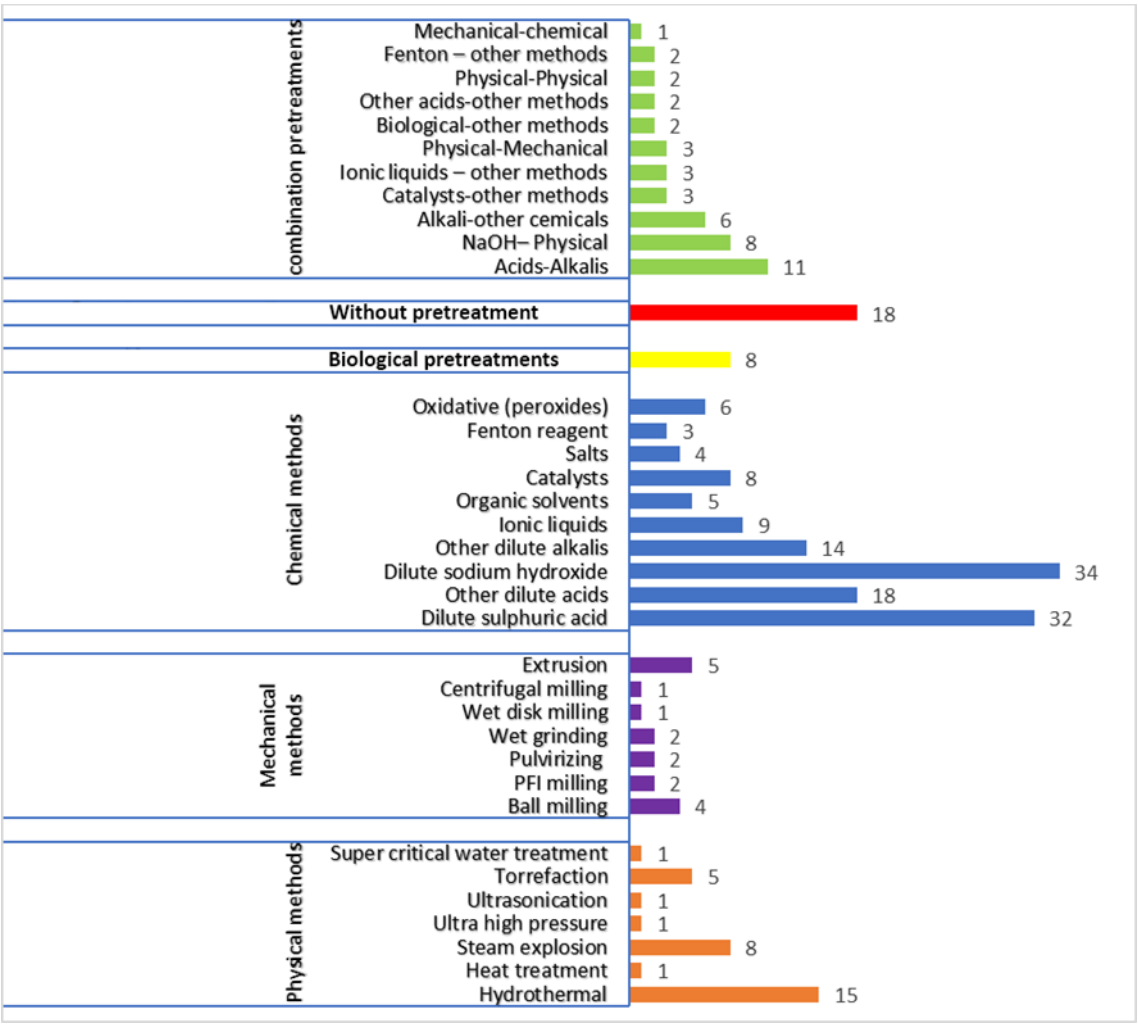

Figure 2.3 Types and frequency of pretreatments reported for corncob biorefinery

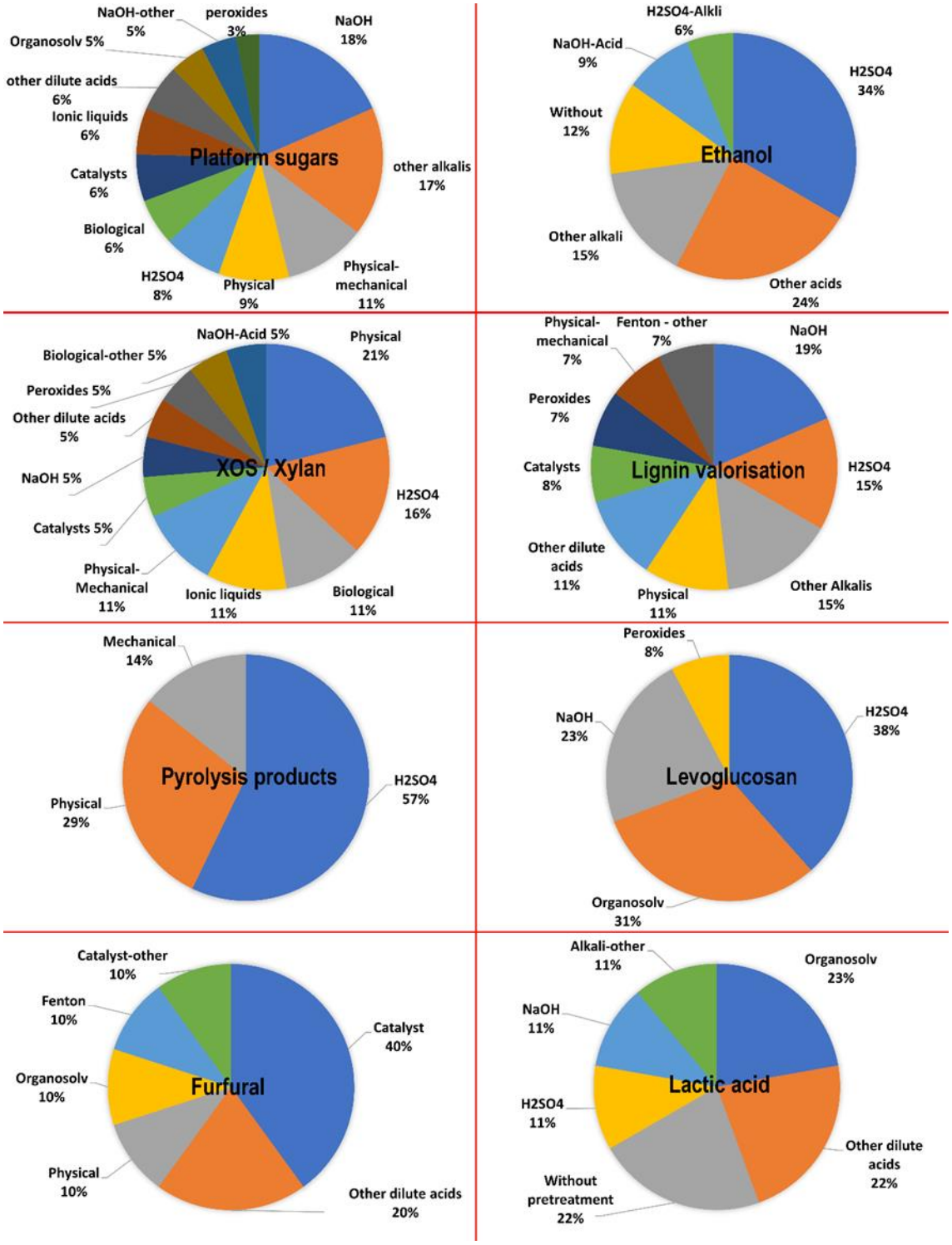

Figure 2.4 Pretreatments used for each corncob derived biorefinery platform

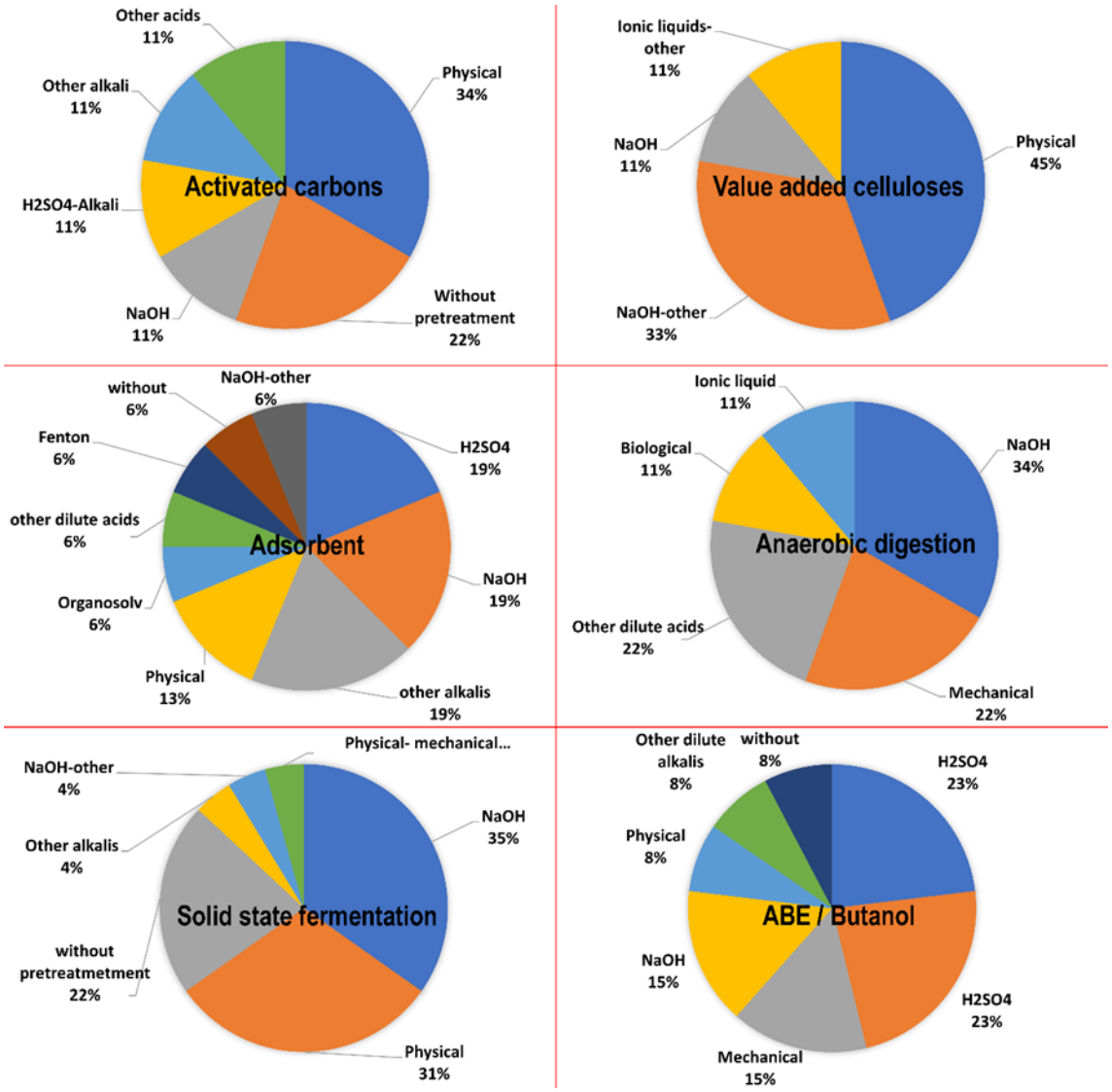

Figure 2.5 Pretreatments used for each corncob derived biorefinery platform

2.2 Detoxification and other strategies to improve saccharification and fermentation yield

Certain compounds formed during pretreatment processes may negatively affect productivity by acting on the saccharifying enzymes and or microorganisms involved. 5-hydroxymethyl furfural from cellulose, sugar, sugar acids, furan aldehydes, carboxylic acids like formic, levulinic and acrylic acids from hemicellulose, phenols like 4-hydroxybenzoic acid, 4-hydroxybenzaldehyde, vanillin, dihydroconiferyl alcohol, coniferyl aldehyde, syringaldehyde, syringic acid etc. from lignin are the common inhibitors formed from pretreatment of lignocellulosic biomass [217]. Accumulation of sugars like cellobiose can inhibit further

saccharification, and ethanol itself may act as an inhibitor in an ethanol production process owing to its antimicrobial properties. Different strategies have been used to counteract these inhibitors. That includes the selection of feedstock that produces fewer inhibitors, and neutralization of inhibitors present in the hydrolysate by various chemical and physical methods such as surfactants, adsorbents, alkalis, reducing agents, enzymes, heat, vaporisation, liquid-liquid and liquid-solid extraction etc. [218]. Certain bio-engineering methods like an adaptation of fermenting strain (adaptive evolution or evolutionary engineering) to the hydrolysate [219]use of recombinant engineered organisms that are high ethanol yielding and inhibitor tolerant (Hasunuma et. al., 2014) were also reported.

2.2.1 Chemical and enzymatic detoxification

Supplementing pretreatment reactions with surfactants was known to enhance the enzymatic saccharification, by emulsifying the hydrophobic lignin derivatives [220], lowering unproductive binding of cellulase with cellulose [221], and bringing certain structural and physiological changes in enzymes and improving the thermal stability of the enzymes [222]. Different surfactants like dodecylbenzene sulfonic acid, polyethylene glycol 4000, and Tween-80, were found to be effective [223]. Tween-80 (15% w/w) supplementation reportedly enhanced the dilute acid pretreatment efficiency of corncob (83.7% hemicellulose removal, 52% delignification), and the enhanced enzymatic saccharification of resulting CCR (maximum glucose and xylose yields 80.54% and 70.66% respectively) at a 41.67% decreased enzyme loading (17.5 PFU/g dry matter). Fermentation of resulting sugars with, *Scheffersomyces stipitis* produced an impressive ethanol yield (0.37 g/g; 1.02 g ethanol/L/h) [223]. An SSF process of industrial CCR supplemented with 0.2 g/L rhamnolipids achieved 61.99% of theoretical ethanol yield with an 82.38% cellulose conversion rate. The hydrophobic interaction between rhamnolipids and lignin derivatives caused by a 12.3% decrease in surface tension of the reaction mixture, improved the productive cellulase binding and decreased the cellulase degradation and effective enzyme dosage [224]. A lignin-based amphoteric surfactant, lignosulfonate quaternary ammonium salt (SLQA), and a betaine-based surfactant, dodecyl dimethyl betaine (BS12), are compared for their relative efficiencies in improving SSF of corncob to produce bioethanol. When supplemented, BS12 has proven to enhance the cellulolytic activity at a concentration as low as 1g/L, however, higher concentrations of BS12 have proven toxic to the yeast cell viability. On the other hand, SLQA also enhanced the cellulolytic activity, without showing the toxic effect on yeast cell growth. These findings paved

a new path to valorize lignin [225]. $CaOH_2$ (lime) is routinely reported for the neutralization of acid-pretreated slurries [226]. A comparative detoxification study of xylan rich corncob acid hydrolysate with lime, zeolites (Clinoptilolite, NaX, ZSM-39) and their combinations, reported that the zeolites decreased the effective concentration of sugars as well as inhibitors by adsorbing them, whereas higher pH caused by lime degraded the sugars. Over-liming alone resulted in higher ethanol fermentability of CCH by both *Pichia stipites* (Ethanol 10.4 g/L/96h; initial reducing sugar 35.9 g/L) *and Candida shehatae* (Ethanol 6.7 g/L/120h; initial reducing sugar 29.1 g/L) [227]. Efficient detoxification of CCH using a non-ionic, styrene divinyl benzene derived polymer (Amberlite-XAD4), achieved >90% removal of 5-HMF, furfural, and vanillin, with a minimum loss (2.5%) of sugars. fermentation of detoxified CCH separately by S. cerevisiae, and P. stipites, showed a 351%, and 473% increase in ethanol production respectively [228]. Use of reverse osmosis to detoxify the oxalic acid pretreated CCH with a laboratory-built membrane filtration device reportedly achieved maximum acetic acid removal (2.6 g/L), complete furfural removal (0.4 g/L), partial 5-HMF removal (0.07 g/L) and relatively unaffected dissolved sugars and total phenolics. Further fermentation of detoxified CCH containing 30.5 g/l of fermentable sugars, 1.2 g/L acetic acid, 0.12 g/L 5-HMF, 2.56 g/L total phenolics, by *Scheffersomyces stipitis*, resulted in a 244% increase in ethanol productivity than the control [134]. The activated charcoal method was found comparatively much more efficient in removing 80%, and 95% of dissolved furans, and phenolics respectively from corncob acid hydrolysate. The other methods used in the study were neutralization, overliming, laccase, and precipitation [229]. Application of laccases in detoxification is evaluated, where delignification and phenol oxidation efficiencies of three different acid laccases [rLacA, (*Trametes hirsute*-AH28-2), rLcc9 (*Coprinopsis cinereaI*), and PIE5 (genetically modified through directed evolution of rLcc9)] were tested on CCH obtained from alkali-pretreated corncob. The comprehensive performances reported are 82%, 63% and 28% respectively. Further, laccase treatment of CCH significantly improved the bioethanol production by *S. cerevisiae* by lowering the adaptation time and improving the cell viability [230].

2.2.2 Evolutionary adaptation & Genetic engineering

S. cerevisiae strain was deadapted against lignin-derived inhibitors (2-furoic acid, guaiacol, p-hydroxybenzoic acid, p-coumaric acid, and ferulic acid) present in industrial CCR hydrolysate. The procedure involved a simple, step-wise gradual addition of CCH over 60 hours of cultivation time. The resulting adapted strain has produced ethanol concentration (62.68 g/L)

and the yield (55.7%), in an SSF process using the CCH as the carbon source [231]. An increase of inhibitor tolerance was reported among different ethanologenic *Saccharomyces cerevisiae* strains, by cultivating the strain initially on molasses alone in aerobic batch mode, followed by adapting the strains on a mixture of molasses and CCH in aerobic fed-batch mode, resulting in high ethanol-yielding strain KE6-12 [62]. Comparison of *Zymomonas mobilis ZM4 and Saccharomyces cerevisiae DQ1* for their relative, lignocellulose derived inhibitor tolerance revealed both the organisms equally tolerant against phenolic aldehydes, but *Zymomonas mobilis ZM4* showed an increased tolerance towards phenolic acids due to its lipopolysaccharide cell wall barrier [232]. Metabolic-engineered acetate-tolerant *Escherichia coli*-MS04 strain reportedly produced 35 g/l of ethanol in 18 h (>80% of the theoretical yield) [233]. Engineering strains for hemicellulolytic activity are quite appropriate to work on xylan rich feedstocks like corncob. Two recombinant *Kluyveromyces marxianus* strains IXPαR and IMPαXPαR were constructed, each with a polycistronic gene IMPX and IMPaX respectively. IMPX codes for extracellular β-mannanase, and β-xylanase, whereas IMPaX codes an extra β-D-xylosidase. The activity of β-mannanase from IMPX is higher than that of IMPaX (21.34 and 15.50 U/mL respectively), whereas the activity of β-xylanase from IMPaX is far higher than that of IMPX (136.17 and 42.07 U/ml). The efficiencies of hemicellulases from both recombinants were tested in fed-batch hybrid saccharification and fermentation process, where hemicellulases from both strains, supplemented with commercial cellulases increased the glucose and xylose concentration, thus improving the ethanol production up to 8.7%. The effect was much more profound in the case of alkali-treated CCR than in acid-treated CCR [234].

2.3 Saccharification of pretreated corncob residue

Hydrolysis of cellulose and hemicellulose fractions of biomass into fermentable monosaccharides is known as saccharification. Often the efficiency of this step is critical for the success of the overall biorefinery [235]. Saccharification is carried out in two major ways, hydrolysis by acids and hydrolysis by enzymes.

2.3.1 Acid saccharification

Dilute mineral acids like H_2SO_4 and HCl are commonly used at a temperature of about 160^oC and pressure of about 10 atm. for hydrolysis of cellulose. However this process is strongly discouraged by the formation of compounds that inhibit fermentation, 5-HMF, and furfural. One has to understand that the acid pretreatment used to solubilize hemicellulose, will be

carried at relatively milder temperatures. The purpose of acid pretreatment is to solubilize the hemicellulose, without causing much damage to the cellulose, whereas the purpose of acid saccharification is to hydrolyse all the sugar content, especially cellulose in the already pretreated biomass residue. [235].

2.3.2 Enzymatic saccharification

Holocellulase is a consortium of endoglucanases (EC 3.2.1.4), exoglucanases or cellobiohydrolases (EC 3.2.1.91), β-glucosidases (EC 3.2.1.21) and lytic polysaccharide monooxygenases (EC 1.14.99.53-56). The presence of β- glucosidase is known to boost the overall cellulase activity, and the ratio between the endoglucanase and β- glucosidase activities, is reportedly an important influencing parameter affecting saccharification efficiency [236], [237]. Hemicellulases include a wide variety of enzymes such as xylanases, endoglucanases, mannanases, β-xylosidase, feruloyl esterases, and arabinofuranosidases [235]. Fungi or bacteria produce these enzymes. Lists of commercial and in-house produced cellulases and hemicellulases, and their sources, reported in corncob based bioethanol production works, are given in Tables 2.5 and 2.6 respectively. In addition to the optimum temperature and pH values, enzyme loading is usually represented as units of enzyme per gram of substrate and solid substrate loading is represented as the percentage of substrate among the overall reaction mixture are the two important factors that need to be optimized for an enzymatic saccharification step. The average total cellulase loadings reported are in the range of 10 – 30 filter paper units (FPU) per gram of the substrate [23], [57], [124], [155], and a wide range of beta-glucosidase, and xylanase loadings were reported 5 – 330 cellobiase units (CBU) and 15 – 3000 units per gram of substrate respectively [79], [238], [239], [113], to a minor extent beta-xylosidase loadings were also reported in corncob valorization works in the range of 1.9 – 18 U/g [208], [79]. Substrate (CCR) loadings were reported in the range of 1 – 20 %. The majority of these enzymatic saccharification reactions were carried for 72 hours with a continuous stirring of the reaction mixture at around 150 rpm [75], [146] Optimization of an enzymatic saccharification reaction always aims to achieve a better saccharification yield with highest possible substrate loading and lowest possible enzyme loading. Different representations were used to report saccharification yields, such as glucan conversion rate 22 – 97.9% [213], [240], xylan conversion rate 17.4 – 90% [75], [233], total sugar conversion up to 97% [71], glucose yield 20 – 97% [241], [242], xylose yield 0.8 – 92% [113], [162], [162], reducing sugar yield 13.8 – 91.5% [214], [55], total sugars 20.9 g/100 g corncob – 932 g/kg corncob [156], [35], and

the works involving xylooligosaccharide (XOS) production usually represents their yields according to the chain length of XOS and or total XOS concentration [23], [243]. These yields do not just depend on the efficiency of the enzyme itself but other crucial factors like the type of pretreatment, detoxification methods employed, additives like surfactants used, and the post processing scenarios involved. [75]. However certain works reported their yields in terms of concentration of sugars per certain volume of reaction mixture, lacking a mass closure on corncob conversion [37], [126]. Cost of the enzymes used is one of the crucial factors that accounts for overall process economics of bioethanol production, any additional measures to save or recycle the enzymes will be rewarded with a positive profit [244].

Table 2.5 Commercial cellulases and xylanases reported for the saccharification of CCR

Commercial name	Manufacturer	Enzyme complex	Optimum conditions	Reference
Accellerase 1000	Genencor/Danisco USA	Exo-1,4-β−glucanase, Endo-1,4-β-glucanase, β-glucosidase, Hemicellulases	pH 4.8, 50^{o}C	[245]
Accellerase 1500	Genencor, USA	Endo-1,4-β-glucanase β-glucosidase	pH 4.8, 60^{o}C	[246]
Accellerase XY	Genencor, USA	Hemicellulase enzyme complex	pH 4.0, 50^{o}C	[247]
Acremonium cellulase	Meiji Seika Co., Japan	Exo-1,4-β−glucanase, Endo-1,4-β-glucanase, β-glucosidase	pH 5.0, 50°C	[208]
Cellic CTec2	Novozymes, Denmark	Exo-1,4-β−glucanase, Endo-1,4-β-glucanase, β-glucosidase, Hemicellulases	pH 5.5, 50^{o}C	[99]
Celluclast 1.5 L	Novozymes, Denmark	Cellobiohydrolases, endo-1,4-β-glucanase	pH 5.0, 50^{o}C	[248]
Cellulase	KDN Biotech Co. Ltd, China	Total cellulase, xylanase, β-glucosidase	pH N.D, 50^{o}C	[249]
Cellulase A1	Shanghai Youtellbio Co., Ltd,	Data unavailable	pH 5.5, 35^{o}C	[250]
Cellulase -T. reesei ATCC 26921	Sigma, USA	Exo-1,4-β−glucanase Endo-1,4-β-glucanase	pH 4.8, 50^{o}C	[251]
Cellulase UTE-1500	Youtell Bio	Exo-1,4-β−glucanase, Endo-1,4-β-glucanase, β-glucosidase, Xylanase	pH 4.0, 50°C	[230]

Cellulase ZC-1700	CTA-TEX Chemical Co. Ltd. in China	Cellulase complex	pH 4.8, 45°C	[125]
Cellulase-C8546	Sigma-Aldrich, USA	Endo-1,4-β-glucanase	pH 5.0, 50°C	[252]
Cellulase-GC220	Genencor	Whole cellulase complex	pH 4.8, 50°C	[112]
Cellulase-Youtell #6	Hunan Youtell Biochemical Co, China	Endo-1,4-β-glucanase, β-glucosidase	pH 4.8, 50°C	[253]
IJT-cellulase	Imperial Jade Bio-Technology Company, China	Data unavailable	pH 5.0, 50°C	[138]
Novozyme-188	Novozymes, Denmark	β-glucosidase	pH 6.0, 50°C	[254]
NS 50010	Novozymes	β-glucosidase	pH 5.0, 50°C	[138]
NS22083	Novozymes, Denmark	Xylanase	pH 4.8, 60°C	[167]
NS22086	Novozymes, Denmark	Exo-1,4-β−glucanase Endo-1,4-β-glucanase	pH 5.5, 38°C	[224]
NS22118	Novozymes, Denmark	β-glucosidase	pH 5.5, 38°C	[255]
Optimase CX40L	Genencor International, Inc	Cellulase	pH 5.0, 50°C	[138]
Optimash™ BG	Genencor®	β-glucosidase, β-xylosidase	pH 5.2, 60 - 70°C	[208]
Palkocel-40	Maps Enzymes Ltd. India	Xylanase, Endoglucanase, β-glucosidase	pH 4.8, 50°C	[33]
Palkofeel-30	Maps Enzymes Ltd. India	Xylanase, Endoglucanase, β-glucosidase	pH 4.8, 50°C	[33]
Xylanase B1	Shanghai Youtellbio Co., Ltd,China	Data unavailable	pH 5.5, 38°C	[250]

Table 2.6 in-house produced cellulases and xylanases reported for the saccharification of CCR

Enzyme	Activity reported	Source organism	Optimum conditions	Reference
Cellulase	0.032 U/ mL	*Actinobacillus sp.* (cattle rumen)	pH 6.0, 40ºC	[122]
Cellulase	N.A	*Metagenome derived (buffalo rumen)*	pH 5.0, 50ºC	[256]
Cellulase	FPU N.D	*P.decumbens JUA10-1*	pH 4.8, N.D	[139]
Cellulase	60 FPU/ml	*T.reesei*	pH 5.0, 48ºC	[143]
Cellulase	146 FPU/g; 12 CBU/g	*T.reesei ZU-02*	pH 4.8, 50ºC	[257]
Cellulase & hemicellulase cocktail	2.0 FPase 6.0 CMCase 20.0 xylanase 2.0 β-glucosidase 2.0 β -xylosidase	*C. thermophile*	N.D	[258]
Cellulase & hemicellulase cocktail	Cellulase total 5.0 FPU/g Endoglucanase 97 CMCU/g Xylanase 4632 U/g β-glucosidase 76 pNPGU/g	*Aspergillus strain (AN-64)*	pH 6.0, 50ºC pH 5.0, 50ºC (β-glucosidase)	[99]
Cellulase & hemicellulase cocktail	Cellulase total 9.0 FPU/g Endoglucanase 193 CMCU/g Xylanase 6840 U/g β-glucosidase 61 pNPGU/g	*M. cinnamomea (CM-10T)*	pH 6.0, 50ºC pH 5.0, 50ºC (β-glucosidase)	[99]
Cellulase & hemicellulase cocktail	Cellobiohydrolase 11 pNPLU/g Cellulase total 14 FPU/g Endoglucanase 199 CMCU/g Xylanase 2162 U/g β-glucosidase 81 pNPGU/g	*S. thermophilium (CM-8T)*	pH 6.0, 50ºC pH 5.0, 50ºC (β-glucosidase & Cello)	[99]

Cellulase & hemicellulase cocktail	Cellulase total 5 FPU/g Endoglucanase 65 CMCU/g Xylanase 110 U/g β-glucosidase 32.5 pNPGU/g	*P.pinophilum*	pH 4.8, 50°C	[33]
Xylanase	3317.71 IU/g	*A. niger SH3*	pH 3.0, 38°C	[44]
Xylanase	0.142 U/mL	*Bacillus sp. PC-01* (Hot spring)	pH 5.0, 50°C	[122]
Xylose isomerase	0.088 U/mL	*Streptomyces griseus* (N.A)	pH 7.0, 70°C	[122]
β-D-Xylosidase (RuXyn)	1 1.25 U/mL	*Kluyveromyces marxianus*-IXPαR	pH 5.5 at 50°C	[234]
β-Gglucosidase	376 CBU/g	*A.niger ZU-07*	pH 4.8, 50°C	[257]
β-Gglucosidase	30 CBU/ml	*Aspergillus.sp*	pH 5.0, 48°C	[143]
β-Glucosidase	1.20 U/mg	*Clavispora NRRL Y-50464*	pH 5.5 at 45°C	[259]
β-Mannanase (M330)	21.34 U/mL	*Kluyveromyces marxianus*-IXPαR	pH 5.5 at 68°C	[234]
β-Xylanase (Xyn-CDBFV)	136.17 U/ml	*Kluyveromyces marxianus*-IMPαXPαR	pH 5.5 at 50°C	[234]
β-Xylosidase	336.49 IU/g	*A. niger SH3*	pH 3.0, 38°C	[44]

Note: U: units; IU: international units; FPU: filter paper units; CBU: cellobiose units; CMCU: carboxy methyl cellulose units; pNPGU: 4-Nitrophenyl β-D-glucopyranoside units; FPase: Total cellulase activity determined by filter paper assay; CMCase: Endoglucanase activity determined by CMC assay; N.A: data not available; N.D: data not defined.

2.4 Fermentation

Several wild type as well as genetically engineered genera of yeasts, fungi, and bacteria were known for ethanol production. Most commonly reported wild type *Saccharomyces cerevisiae* can only ferment hexose sugars to ethanol. Whereas certain genetically modified, as well as wild type microbes were known to ferment both glucose and xylose together improving ethanol yield [260]. The details of different microbes reported for bioethanol production from corncob are given in Table 2.7. Simultaneous saccharification and fermentation (SSF), and separate hydrolysis and fermentation (SHF), are the two classical processes, used to carry out the conversion of pretreated biomass to ethanol.

Table 2.7 microbes reported for ethanol fermentation from corn cob derived carbon sources

organism	Carbon source	Ethanol	Reference
Angel instant dry yeast (commercial)	Glc	E.Y = 75.07 g/L E.Y = 89.38%	[253]
C.glabrata	Glc	E.Y = 31.32 g/L E.T.Y = 89%	[261]
C.tropicalis W103	Glc Xyl	E 25.3 g/l E 82% of TY	[262]
Clavispora NRRL Y-50464	CB	Y = 23 g/L	[259]
E. coli KO11	Glc, Xyl	E.Y = 104.0 g/ l	[263]
E. coli -MS04	Glc, Xyl	E 35 g/l E 80% of TY	[233]
K.marxianus	Glc	E.Y = 33.14 g/l E 74.49%	[140]
K.marxianus 6556	Glc	28% of TY	[251]
P.guilliermondii	Glc	E.Y = 56.3 g/l E.P = 0.47 g/l/h	[264]
P.kudriavzevii	Glc,Xyl	31.89 of TY	[252]
P.stipitis CBS 6054	Glc, Xyl, CB	74% of T.Y	[223]
P.stipitis NCIM 3499	Glc, Xyl	16.08 g/L	[229]
Pichia kudriavzevii	Glc, Xyl	85.95% of TY	[265]
Pichia kudriavzevii N-X	Glc, Xyl	Y = 67.1 g/L	[266]
S. cerevisiae -1400	Glc, Xyl	E.Y = 45 g/L E.Y = 86%	[137]
S. cerevisiae BCRC 21812	Glc	E.Y = 32.3 g/l E.Y = 0.64 g/g	[267]
S. cerevisiae CAT-1-BGAL	Glc, Lac	E.Y = 54.7 % E. P = 1.42 g/L/h	[268]
S. cerevisiae CAT-1-C	Glc, CB	E.Y = 95.1 % E. P = 0.814 g/L/h	[268]
S. cerevisiae- F106-KR	Glc, Xyl	Y = 0.48 g/g	[260]
S. cerevisiae MP 3013	Glc	E.Y = 131.3 g / kg cc	[249]
S. cerevisiae W13	Glc, Xyl	Y= 44.6 g/L	[266]
S. cerevisiae W303-1A	Glc	75.6% of TY	[138]

S. cerevisiae -W303-1A-45	Glc, CB	E 3.31 g/100 g E% 77.7% TY	[138]
S. cerevisiae- XR-K270R	Glc, Xyl	93.9% of TY	[260]
S. cerevisiae-KE6-12	Glc,Xyl	75% of TY	[62]
S. stipitis CBS 6054	Gl, Xyl	58% of TY	[226]
S.cerevisiae BJ1824	Glc	0.142% (v/v)	[122]
S.cerevisiae CICC 31014	Glc	E.Y = 60.8 g/l E.T.Y = 72.2%	[123]
S.cerevisiae DQ1	Glc	E 48.6 g/L	[232]
S.cerevisiae HAU	Glc, Xyl	16.08 g /L 0.43 g/g	[229]
S.cerevisiae NBRC2114	Glc	E.Y = 77%	[269]
S.cerevisiae TC-5	Glc	E.Y = 31.96 g/L E.P = 0.222 g/L/h	[270]
S.passalidarum U1-58	Glc, Xyl	E.Y = 53.24 g/L E.Y = 75.35%	[250]
Saccharomyces cerevisiae-KE6-12	Glc, Xyl	76% of TY	[62]
Saccharomyces cerevisiae-RHD-15	Glc, Xyl	53% of TY	[62]
Spathaspora passalidarum U1-58	Glc, Xyl	75.35% of TY	[271]
Z. mobilis-CP4	Glc, Xyl	E 60.5 g/l E% 81% TY	[272]
Z. mobilis-TISTR405	Glc	35.93 of TY	[141]
Z.mobilis ZM4	Glc	E 54.42 g/L	[232]

Note: Glc: glucose; Xyl: xylose; CB: cellobiose; Lac: lactose

2.4.1 Simultaneous saccharification and fermentation (SSF)

SSF is the widely applied economical approach that involves running both saccharification and fermentation simultaneously by adding hydrolysing enzymes and ethanol fermenting organisms together [123]. The presence of inhibitors, mass transfer effects, optimum temperature and pH are the major factors affecting an SSF process. SSF prevents the accumulation of cellobiose that could otherwise inhibit cellulase activity [123]. An SSF process of oxalic acid pretreatment derived CCR with Acellerase 1000 and *Pichia stipitis*, resulted in an ethanol concentration of 20 g/l in 48 h. It was reported that extracellular β-glucosidase secreted by *Pichia stipitis*, owing to its cellobiose hydrolysing activity accelerated and enhanced ethanol fermentation beyond the

expected theoretical yield [273]. SSF of CCR obtained from dilute sulphuric acid pretreatment at 10% solid loading resulted in 40.3 g/L ethanol concentration accounting for 71.2% of the theoretical yield, while increasing the solid loading to 14% improved the ethanol concentration (50.2 g/L), but decreased the overall theoretical yield (70.4%), owing to poor mass transfer effect and lignin-derived inhibitors [125]. The advantage of fed-batch culture over batch culture to achieve higher ethanol yield has been proposed by many other studies [274]. In a comparative study, acid-alkali pretreatment derived CCR yielded 69.2 g/L ethanol (81.2% of theoretical yield) though batch SSF, and 84.7 g/L ethanol (79% of theoretical yield) through fed-batch mode. 19% dry mass, with 22.8 FPU/g glucan cellulase, 5 g/L *Saccharomyces cerevisiae* was used in both modes [112]. To match the optimum temperatures of both saccharifying enzyme and ethanol fermenting mesophilic *Saccharomyces cerevisiae* (~35^{o}C), a cold-active holocellulase (~38^{o}C) was produced from a psychrotolerant *A.niger* strain. Maximum ethanol concentration of 13.05 g/L accounts for (~48.85% of the theoretical yield) obtained through the SSF process carried at 38^{o}C for 72 hours [44]. Slight variations and improvements for the classical SSF approach were proposed by several authors. A prehydrolysis step was proposed in an SSF process, where a commercial cellulase treatment was carried on CCR for up to 12 hours, before initiating the SSF by adding an inhibitor adapted *Saccharomyces cerevisiae* strain [231].

2.4.2 Simultaneous saccharification and co-fermentation (SSCF)

SSCF involves the fermentation of both glucose and xylose present in CCH and or obtained from saccharification of CCR by a suitable single microbe or a consortium of organisms. An SSCF of whole corncob slurry (CCR+CCH) with a pre-fermentation step fermenting glucose before adding the saccharifying enzymes achieved high xylose consumption (79%) and ethanol yield (>75% of theoretical yield) with high solid loading. The pre-fermentation step counteracted the inhibitory effects of glucose [62].

xylose reductase and xylose dehydrogenase genes of a known xylose-fermenting *Saccharomyces cerevisiae* - F106-KR strain were engineered to alter their cofactor preference from $NADH^{+}$ to $NADP^{+}$, the resulting mutant (XR-K270R) with altered redox potential lost its ability to convert xylose to xylitol. And the mutant used in the corncob based SSCF process achieved an ethanol yield of up to 93.9% of the theoretical yield in 36 h [260].

2.4.3 Separate hydrolysis and fermentation (SHF)

In SHF saccharification and fermentation processes will be conducted separately. A low xylan to lignin ratio (0.3) of dilute acid pretreated CCR was reported as the key to achieving higher ethanol yield (14.35 g/l) through an SHF process employing *Pichia stipitis CBS 6054* [275]. An ethanol yield of 235 L/ton of corncob (82% of TY) by separately fermenting, acid pretreatment derived xylose rich CCH, and glucose-rich hydrolysate derived from enzymatic saccharification of CCR by *Scheffersomyces stipitis CBS 6054* was reported [226]. A two-stage staggered ethanol fermentation was reported, where xylan rich CCH and the glucose-rich CCR hydrolysate were mixed and initially CCR hydrolysate was fermented anaerobically with *Saccharomyces cerevisiae* at 30^{o}C, shaking at 180 rpm for 48 hours, later inactivated by raising the temperature to 50^{o}C for 6 hours, then CCH fermentation was carried by inoculating *Pichia stipites* semi-aerobically at 30^{o}C by shaking at 180 rpm for 48 hours. yielding 4.2% v/v ethanol accounted for 252 g ethanol/g of corncob [99]. An SHF process with CCR 180 g /L, cellulase complex with 20FPU/g: 7 CBU/g at 48^{o}C, for 48 hours released 128 g/L reducing sugars, later fermented it with *Zymomonas mobilis* to achieve an ethanol yield of 57.8 g/L. the study revealed the saccharification efficiency influencing parameters in the order of substrate concentration > FPU: CBA > time[143]. A consortium (1:1:1) of cellulase from *Actinobacillus* species (cattle rumen isolate), xylanase from *Bacillus* species (hot spring isolate) and xylose isomerase from *Streptomyces griseus* was used to saccharify CCR at their respective temperature and pH optimums until no further activity was measured (Cellulase at 40^{o}C, pH 6, followed by Xylanase at 50^{o}C, pH 5, and then by xylose isomerase at 70^{o}C, pH 7) to achieve highest reducing sugar quantity by 4.5 hours [122]. Although SSF is widely reported as more efficient than the SHF process for ethanol production, a few exceptions where the advantage of SHF is reported [261].

2.4.4 Consolidated bioprocessing (CBP)

CBP is to carry the production of glycolytic enzymes, saccharification, and fermentation, all in a single step by a single or consortium of different organisms. Wild strains such as *Saccharomyces cerevisiae*, and *Escherichia coli* are modified via metabolic engineering to be CBP suitable microbes [276], [277]. It requires minimal pretreatment of the biomass, thereby lowering the chances of inhibitor formation. This process reduces the cost of operation and increases the production of ethanol and other objectives from biomass [278]. A recombinant *Saccharomyces cerevisiae* strain with high xylanolytic activity was constructed to display three

different enzymes on its surface (*Abdopus aculeatus* β-glucosidase 1 (plasmid pI23-BGL1-kanMX), *Aspergillus oryzae* β-xylosidase (plasmid pI5-XylA-NatX) and *Trichoderma reesei* endoxylanase II (plasmid pδW-XYN-kanMX). The CBP of hydrothermal pretreatment derived, non-detoxified corncob slurry, with the recombinant yeast, resulted in an ethanol yield of up to 102.8 kg/tonne of corncob, whereas the SSF of the same feedstock supplemented with commercial cellulase and xylanase cocktail and the same yeast strain resulted in only 57.8 kg ethanol/tonne of the corncob. The low performance of the SSF process is thought due to the higher amount of acetic acid produced by acetyl xylan esterase present in the commercial enzyme cocktail [276]. Three genetically modified *Saccharomyces cerevisiae -Y33 strains* were constructed with exoglucanase gene (GeneBank: AY861348), endoglucanase (GeneBank: EU169241) and β- glucosidase genes (GeneBank: AF163097), using a linearized plasmid. A one-step CBP of untreated corncob powder with this consortia showed a 25%
enhanced ethanol and glycerol production (2.02 g/L, and 0.85 g/L respectively in 96 hours) than that of a single organism with all three enzymes [277].

2.5 Valorisation of untreated biomass and Industrial residues without pretreatment

Waste corncob residue, obtained from corncob-based industrial xylitol or furfural production, has proven to be an excellent raw material for further biorefinery applications. An estimate made in 2011 revealed that around half a million tons of industrial CCR are produced yearly in china itself [279]. Since most of the hemicellulose is already solubilized, CCR is rich in cellulose and is readily accessible for cellulases without any further pretreatment or can be valorized with a very mild pretreatment approach.

Table 2.8 Valorization of corncob industrial residue for bioethanol production without a pretreatment

Pretreatment	Efficiency of pretreatment	Detoxification	Bioconversion	Lignocellulose component valorised	Ethanol Yield (Y) Productivity (P) Theoretical yield (TY)	Co-products	Reference
Whole CC-Without pretreatment	N.A	N.A	SSF	CL	Y = 2.02 g/L	Glycerine	[277]
Industrial CCR hydrolysate	N.A	N.A	repeated fed-batch fermentations	CL, HC	Y = 56.3 g/l P = 0.47 g/l/h 3 times repetition Y = 51.2 g/l P = 1.11 g/l/h	None	[264]
Industrial CCR – without pretreatment	N.A	Strain adaptation	SSF	CL	Y = 62.68 g/L Y = 55.7%	None	[231]
Industrial CCR – without pretreatment	N.A	N.A	SSF	CL	Y = 54.42 g/L Y = 48.6 g/L	None	[232]
Industrial CCR – without pretreatment	N.A	N.A	SSF	CL	Y = 75.07 g/L 89.38% of TY	None	[253]

Industrial CCR – without pretreatment	N.A	N.A	SSF	CL	Y = 72.7%	None	[244]
Industrial CCR – without pretreatment	N.A	Without detoxified	SSF	CL	Y = 61.99%	None	[224]
Industrial CCR – without pretreatment	N.A	Without detoxified	SSF	CL	Y = 86.56%	None	[280]
Industrial CCR – without pretreatment	N.A	N.A	SSF	CB	Y = 23 g/l	N.A	[259]
Industrial CCR – without pretreatment	N.A	N.A	SSF (fed-batch)	CL	Y = 31.96 g/L P = 0.222 g/L/h	None	[270]

Note: CC corncob whole, without pretreatment; CCR: pretreatment derived solid Corncob residue; CCH: pretreatment derived corncob hydrolysate; (R) = % recovered or % composition in the solid residue; (H) = % hydrolysed or % concentration in the hydrolysate; L/S = Liquid to solid ratio; N.D = not defined; N.A = Not applicable; Glc: glucose; Xyl: Xylose; Ara: arabinose; Gal: galactose; Man: mannose; GL: glucan; XY: xylan; AR: arabinan; LG: lignin; CL: cellulose; HC: hemicellulose; LC: lignocellulose; TS: total sugars; HSF: hybrid saccharification and fermentation.

Notable examples are L-lactic acid production from CCR enzymatic hydrolysate by *Bacillus coagulans* ZX25 [281], D-lactic acid production by *S. inulinus* YBS1-5 using CCR hydrolysate as a carbon source, and cottonseed as a nitrogen source [282]**,** solid-state fermentation to produce xylanase by *Aspergillus foetidus* using CCR as the carbon source [98], levulinic acid production [83], and butanol [283]. Precipitated lignin-derived phenolics adsorbed on industrial CCR are obstacles to this valorization route [231]. Different surfactants such as tea seed cake were proposed to overcome this by effectively nullifying the inhibitory effects of lignin derivatives, even with unwashed CCR [280]**.** Lignin associated with industrial CCR is purified (acid-soluble lignin 2.94 – 3.23%, acid-insoluble lignin 88.8 – 90.6%) and valorized [284]. Industrial corncob molasses, rich in hemicellulose hydrolysate, is another biorefinery choice that can be utilized without further extensive pretreatment strategies. Propionic acid at a satisfactory concentration (71.8 g/L) was reportedly produced by *P. acidipropionici*, using hemicellulose rich corncob molasses [82] (Table 2.8).

Corncob-derived biochar from hydrothermal processes was further valorized as a soil improver [285]. Powdered, untreated corncob was proposed to be valorized as a carbon source for xylanase (3300 U/g), ethanol (2.02 g/L), and glycerol (0.85 g/L) production and could be used as an adsorbent to remove COD and total nitrogen for water remediation [277], [286].

2.6 Techno-economic and Lifecycle analysis

Techno-economic analysis (TEA) is an assessment tool used to evaluate the technical and economic feasibility of a process or a system. A comprehensive TEA may encompass all the upstream and downstream unit operations of a process concerning their capital and costs of operation, with an essential focus on the production phase, and establishes the profitable minimum selling price (MSP) of the final product. However, TEA does not take the environmental impacts of the technology in the study into consideration [287]. On the other hand, life cycle analysis/ assessment (LCA) is a quantitative approach, currently being used to evaluate the impact of all the processes, chemicals, materials, and infrastructures involved from the production of raw material to the end usage and disposal of the final product (complete life cycle), on natural resources, ecosystem and human health. [288]. The goal, scope, inventory preparation, choice of boundaries, and impact assessment criteria were defined by two leading standards 14040, 14044, set by the international organization for standardization (ISO). [289], [290]. A comprehensive LCA must include all the phases of biomass valorization, along with different sensitivity, uncertainty, and varying scenario analysis. Though TEA and LCA are

performed separately, recent studies suggest the advantages of integrating both TEA and LCA to get a better perspective on the trade-off between environmental and economic aspects of the process. There are very few works, that reported TEA and LCA of corncob-based 2G-bioethanol production. In addition, most of the LCA studies reported were not comprehensive [288]. Two recent comprehensive reviews compiled enormous TEA data reported on 2G-bioethanol productions from different feedstocks, but none of their cited works reported a TEA of corncob-based bioethanol production. Nevertheless, they both reported studies involving corn stover as a feedstock. [291], [292]. The details of TEA and LCA studies on corncob-based ethanol biorefineries were summarized in Tables 2.9 and 2.10 respectively. Pang et al. proposed a corncob-biorefinery strategy, to consecutively produce xylose, ethanol, and a lignin-phenol-adhesive, based on an existing industrial process. The additional valorization step involves the conversion of lignin to adhesive. TEA of the proposed process considering a plant size of 1t ethanol production was economical and further reduction in operating cost can be achieved by increasing the phenol-lignin substitution, using lignin-derived phenol, and by producing XOS from hemicellulose instead of xylose [293]. LCA of the proposed biorefinery revealed 79.6% valorization of the total renewable carbon in the corncob, the water recycling unit incorporated in the process achieved 57.8% reduction in waste water generation, and other environmental impacts calculated were less than that of base cases [293]. TEA of a corncob-based biorefinery producing ethanol (C6 based), xylose (C5 based), Heat, and electricity (Lignin based), is comparatively better than bioethanol production costs reported from corn stover and rice husk. Although hexose-only fermentation resulted in lesser bioethanol production, the process is still economical due to the higher market value of xylose than ethanol and the additional revenue generated by selling excess heat and electricity [294]. The environmental impact analysis of the proposed biorefinery significantly performed better than the base cases [294]. In a comparative TEA study of different feedstocks, the raw material cost of corncob was higher than that of sugar cane bagasse but lower than that of rice husk, and the production was found to be highly sensitive to the raw materials cost (5447 USD ton/h of corncob conversion). In addition, the cost of utilities (water and natural gas consumption) was highest for the corncobs, making the overall processing of corncob to ethanol, slightly higher than that of other biomass types. Nevertheless, the highest xylose content of the corncob resulted in an experimental ethanol yield with a positive profit margin for the corncob based process [295]. Consequently, corncob showed the highest environmental impact, in terms of energy consumption, and COD was the highest environmental impact contributor for all the fed stocks, while 39% of the environmental

impact generated due to the cultivation and processing of feed stocks is depredated upon ethanol production from them [295]. LCA of E10 and E85 blends of gasoline with bioethanol produced through three different corncob biorefinery scenarios (case 1: ethanol, biogas, heat, and power; case 2: ethanol, heat, and power; case 3: ethanol, xylose, heat, and power), indicated that irrespective of the type of biorefinery, all the ethanol-blended fuels performed better than that of pure gasoline [296]. An estimate of around 71.6% of the fermentable carbon in corncobs was converted to ethanol and microbial lipids (CCR and CCH as carbon sources respectively) in a biorefinery, depredating 33% of the initial COD in the acid hydrolysate [249]. A comparative LCA of the impact of 2G ethanol-biorefineries on the local water bodies in China revealed that the grey water foot print accounts for the largest proportion of total life cycle water footprint [297]. lifecycle energy consumption and carbon emissions of 2G ethanol processes from different raw materials were found to be similar, and the small observed differences were mainly attributed to the changes in pretreatments used [298]. Exergy analysis of a corncob biorefinery showed an ethanol yield of up to 179.7 L/t biomass, with a positive net energy ratio (1.6) attributed to the combined heat and power system involved, and the overall process was economical due to the co-product credit of xylose [299]

Table 2.9 TEA of corncob biorefineries

Proposed Biorefinery	Base cases	Process innovations	Costs	Production, revenue and other improvements	Reference
CL → EtOH HC → Xylose LG + Phenol→ Adhesive	CL → EtOH HC → Xylose LG separation	incorporating a water recycling unit		Overall revenue of the proposed biorefinery reached 111 times that of the base case (1414.55 USD / t ethanol) 79.6% of the renewable carbon is valorised 57.8% reduction in waste water generation	[300]
CL → EtOH HC → Xylose LG → CHP	CL → EtOH HC+LG → CHP CL+HC → EtOH LG → CHP		Production cost = 0.5 USD / L ethanol Feedstock cost = 68.9% of the production cost	36.8% reduction in cooling utilities 60.6% reduction in heating utilities Ethanol 194.2 kg/ t dry biomass	[294]
CL+HC → EtOH	Other biomass types	N.A	Total Operational cost Raw materials54.7% Utilities cost 45.3% Total Capital cost Separation equip. 50% Pretreatment equip. 27% Transformation equip. 23% Cost of utilities (water and natural gas consumption) is highest for the corncobs	0.43 kg ethanol/kg CC (highest ethanol production compared to other biomass types) Profit margin 2200 USD/day (4th place)	[295]

Note: CL: cellulose; HC: hemicellulose; LG: lignin; EtOH: ethanol; CHP: combined heat and power;

Table 2.10 LCA and environmental analysis of corncob biorefineries

Goal & Scope	Contribution analysis	Sensitivity analysis	Scenario analysis	Reference
GHGs intensities of a biorefinery, with an existing biorefinery as base case. cradle-to-grave & cradle-to-gate	Total emissions = acid treatment (CCR 61.0%, CCH 39.0%); Post-processing (ethanol 14.7%, lignin-phenol-adhesive 85.3%).	co-products prices steam consumption and electricity use are the most sensitive factors to impact	Impact of alternative sources for steam generation; Coal 111.7 g CO_2 eq./MJ, Natural gas 77.8 g CO_2 eq./MJ, Biomass 37.8 g CO_2 eq./MJ	[300]
Environmental impact of each unit of a biorefinery, with two simulated biorefineries as base cases gate-to-gate	Exergy allocation: Bioethanol 47.9%, Electricity 5.6%, Steam 0%, Xylose 20.9%, Mother liquor 25.6%	Pretreatment, SSF, and WWT, contributed to highest FD & GWP and the proposed biorefinery performed better than the base cases	N.A	[294]
Environmental performance of corncob-derived bioethanol-blended fuels (E10, E85) with pure gasoline as the reference. cradle-to-grave	Exergy allocation: Both E10 & E85 showed decreased impact on FDP, GWP, and HTP. Showed increased impact on ODP, AP and EP GWP, HTPI ODP, EP, AP	An increase in ethanol theoretical yield must be accompanied by increased feed stock utilization and co-product credit, to show a profound lowering effect on FDP and GWP.	N.A	[296]
Life-cycle water footprint (WF) of 2G	WF of corn cob bio-ethanol production 317 m^3/t.	WF was most affected by crop yield,	N.A	[297]

biofuels in different provinces of China. cradle-to-grave	GWF = Cassava stalk > Corncob; BWF = wheat straw > rice straw > corncob; GyWF = wheat straw > corncob	GyWF is most affected by the chemical fertilizers and the natural nitrogen.		
Estimation of lifecycle energy consumption and carbon emissions of corncob ethanol cradle-to-grave	fossil fuel consumption 0.51–0.84 MJ/MJ EtOH CO_2 emissions 39.44–49.97 gCO2eq/MJ EtOH Feedstock processing 5.18 – 6.95 g /MJ EtOH Feed stock conversion 50.57 – 61.6 g /MJ EtOH	glucose and xylose co-fermentation emits about 20% fewer GHGs	Hybrid and plug-in hybrid electric vehicles have 18–20% lower emissions than internal combustion engine vehicles, and flexible-fuel vehicles (E85)	[301]
Exergy analysis of a biorefinery	Exergy efficiency: Overall processes 84.7% WWT 81.6% CHP 58.0% Products 36.6%	N.A	N.A	[299]
Environmental impact of production stage cradle-to-gate	Corncob-based ethanol highest energy consumer showed the highest environmental impact 8 PEI/h.	N.A	N.A	[295]
CHP: combine heat and power; WWT: wastewater treatment; PEI: potential environmental impact; GWF: green water foot print; BWF: blue water foot print; GyWF: grey water foot print; FD: fossil depletion; GWP: global warming potential, HTPI: human toxicity potential by ingestion; ODP: ozone depletion potential, EP: eutrophication potential, AP: acidification potential; CCR: corncob residue; CCH: corncob hydrolysate; N.A not available				

Chapter 3

A New Insight into the Composition and Physical Characteristics of Corncob Substantiating Its Potential for Tailored Biorefinery Objectives

3. 1 Materials and Methods

3.1.1 Sample Selection and Preparation

Four different Zea mays varieties (https://iimr.icar.gov.in/cultivars-2/, accessed on 02/12/2022), KMH-2589 (Kaveri seed company limited, Secunderabad, India, 500003), LTH 22 (Yaaganti Seeds Pvt. Ltd, Hyderabad, India, 500034), P3533 (Pioneer Hi-Bred Private Ltd, Hyderabad, India, 500081), and BL 900 (Bisco biosciences, Hyderabad, India, 500003), which were produced and cultivated around Telangana state, India (18.1124° N, 79.0193° E), were chosen for the study. These were termed CC1, CC2, CC3, and CC4, respectively. Five kilograms of shelled corncobs of each variety were directly collected from the fields, thoroughly washed, and air-dried for several months as per the National Renewable Energy Laboratory, USA-laboratory analytical procedure (NREL-LAP) [302]. The pith was separated from air-dried corncobs by drilling it out using a homogenizer motor attached with a high-speed steel (HSS) drill bit (twist bit) of a 6 mm size. The average weight ratio of the separated outer and inner anatomical portions of the corncob was 49:1, with densities of 403.6 kg/m3 and 128 kg/m3, respectively. These portions were separately milled to obtain a particle size in the range of 0.85–0.18 mm (−20/+80 sieve fraction) [303]. The woody ring of the corncob outer was more resilient to milling, and it required a heavy-duty knife mill to comminute it to the desired size. Two corncob-derived samples (−20/+80 fractions)—the corncob outer (CO), and corncob pith (CP) were considered for further biomass composition analysis (Figure 3.1). The CP is relatively homogenous, whereas the CO is a mix of chaff, glume, and woody ring. Hence, for biomass composition analysis by the NREL and near-infrared (NIR) spectroscopy-based rapid methods, sampling was performed by selecting 50 random 5 g selections from thoroughly mixed individual CO and CP fractions of each corncob variety to achieve a uniform distribution of all anatomical variations among the samples. For physical characterization, single CO and CP samples that were an equal mix of all the corncob varieties used were selected.

Commercial microcrystalline cellulose (Avicel® PH-101, Sigma Aldrich, Burlington, MA, U.S.A, 01805) and cellulose-cotton litres (Sigma Aldrich, Burlington, M.A, U.S.A, 01805) were taken as pure cellulose references. Lignin alkali (Sigma Aldrich, Burlington, M.A, U.S.A, 01805) and xylan from beech wood (Megazyme, Wicklow, Ireland, A98YV29) were used as

pure lignin and xylan references. These were termed AC, CL, LG, and XY, respectively. Unless otherwise mentioned, all of the samples are processed in triplicates through all of the analytical procedures.

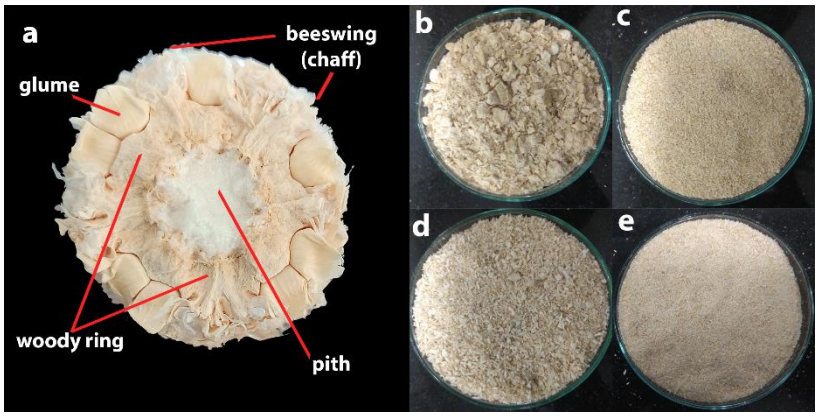

Figure 3.1 Corncob cross-sectional anatomy and the samples prepared. (a) corncob crosssection showing CO and CP regions; (b) CO comminuted to 2–10 mm; (c) CO comminuted to 0.85–0.18 mm (−20/+80 mesh); (d) CP comminuted to 2–5 mm; (e) CP comminuted to 0.85–0.18 mm (−20/+80 mesh).

3.1.2 Scanning Electron Microscopy (SEM) Analysis

Morphological images of the samples were recorded with a scanning electron microscope (VEGA3 TESCAN LMU). Small amounts of dry individual samples (moisture <1%) were fixed on to sample-holding stubs using carbon tape and were subjected to gold and palladium sputtering under a vacuum (Gold Sputter Coater-SPI-MODULE). The SEM instrument was operated in secondary electrons detection mode with a 5–15 kV accelerating voltage and a working distance of around 10 mm. Each sample was scanned at three different levels of magnification, ranging from 600× to 5000× [129].

3.1.3 NREL Method for Biomass Composition Analysis

The biomass composition analysis was carried out as per the NREL-LAPS (https://www.nrel.gov/bioenergy/biomass-compositional-analysis.html, accessed on 02/12/2022). The monosaccharides analysis was carried out using high-performance liquid chromatography (HPLC) (Prominence UFLC, Shimadzu, Kyoto, Japan, 604-8442) equipped with Rezex-RPM-monosaccharide-Lead (II) ion column (Phenomenex, Torrance, C.A, U.S.A, 90501-1430) and a suitable guard column. The HPLC analysis of acetate was performed using a Repromer-H (Dr. Maisch GmbH, Beim Brückle, Germany, 1472119) column along with an

appropriate guard column. We ran 20 μL of the samples through the respective columns maintained at 80°C in isocratic mode using HPLC-grade water as the mobile phase. The retention data were collected using a refractive index detector with a flow cell temperature of 50°C. Analysis of sucrose was carried out using a biochemistry analyzer (YSI-2950-D, Xylem, Washington, D.C U.S.A, 20003) equipped with an immobilized enzyme membrane (YSI-2703). The standards used for all analytical procedures were HPLC-grade chemicals purchased from Sigma Aldrich, Burlington, M.A, U.S.A, 01805.

3.1.4 Van Soest Method for Fiber Analysis

Detergent partitioning of the fibre fraction of the lignocellulose materials followed by gravimetric analysis, which was proposed by Van Soest et al. [304], was used to determine the composition of the CO, CP, AC, and CL. Initially, neutral detergent fibre (NDF) (hemicellulose + cellulose + lignin + ash), acid detergent fibre (ADF) (cellulose + lignin +ash), and acid detergent lignin (ADL) (lignin) were determined among the samples. Further, the respective percentages of cellulose, hemicellulose, and lignin were gravimetrically calculated using Equations 2.1–2.3 [304]. The respective digestions were carried in 250 mL round bottom flasks in a heating mantle. The filtration followed by drying and ashing was carried out in borosilicate filtration crucibles with grade-2 porosity.

$$Hemicellulose = NDF - ADF \quad \text{(equation 2.1)}$$

$$Cellulose = ADF - ADL \quad \text{(equation 2.2)}$$

$$Lignin = ADL \quad \text{(equation 2.3)}$$

3.1.5 NIR Spectroscopy Method for Rapid Biomass Composition Analysis

The NIR spectra of the CO and CP samples were collected in the diffuse reflection mode using a Cary Varian 5000-UV-Visible-NIR spectrophotometer, Agilent, USA. The spectra were acquired by placing around 1 g of the sample in the powder cell at ambient temperature. Each sample was scanned in triplicates in the range of 1000 nm to 2500 nm, with 64 scans per spectrum. The average of the triplicate spectrum was considered for further analysis. Reflectance (R) data was converted to absorbance (A) using the equation A = log (1/R) [305]. A NIR calibration model with partial least squares regression (PLS) was built using the Unscrambler®-X software, version 10.4 (Aspen Technology, Inc, Bedford, M.A, U.S.A, 01730). Preprocessing of the spectral data was carried out using Savitzky-Golay smoothing and multiplicative scatter correction techniques. The PLS calibration models were built based on

the full range of the spectrum, where two-thirds of the sample scans were taken as a reference set and the remaining scans were taken as the test set. Both sets were carefully selected to have equal representation from all four samples. The coefficient of multiple determination for calibration (R^2C), coefficient of multiple determination for validation (R^2V), coefficient of multiple determination for prediction (R^2P), standard error of calibration (SEC), standard error of prediction (SEP), and residual predictive deviation (RPD) are the important indicators used for the NIR-PLS model evaluation [305].

3.1.6 Thermogravimetric Analysis (TGA)

TGA (TGA 4000, Perkin Elmer, Waltham, M.A, U.S.A, 02451) of the samples was separately carried out in isothermal mode under an inert atmosphere (N2 flow around 19.8 mL/min), and oxidative atmosphere (air). The temperature range used was 30 °C–800 °C at a constant heating rate of 200 °C/min. The TGA curve with mass percentage remaining against temperature was plotted using OriginPro2018 software, Ver.b9.5.1.195 (OriginLab Corporation, Northampton, M.A, U.S.A, 01060). The instrument-generated first derivative data was smoothened with the adjacent averaging method at 70-point smoothing, and the mass loss percentage per minute against temperature was plotted. This curve was used as an alternative to the derivative thermogram (DTG); hence, hereafter it is referred to as the DTG curve. The lignocellulosic composition of the samples was calculated using Equation 2.4–2.6. Their relative thermal degradation percentages were obtained from the respective TGA curves, where the inflection points were selected based on the corresponding superimposed DTG curve [306]. Additionally, the DTG curve is normalized and inverted by integrating the sample weight percentage at each time fraction of the derivative data (m_i) to the initial (m_0) and end (m_∞) mass% of the sample using Equation 2.7 [307]. The peak deconvolution was separately performed on normalized DTG curves of both CO and CP by manually selecting the peaks at each devolatilization stage, and a multiple peak fit was performed using the Gaussian function. Peaks were manually marked and iterations were performed until the fit converged and a chi-square tolerance value of 1×10^{-9} was reached. All the converged peaks have shown R^2 and adjusted R^2 values above 0.99. Moisture, hemicellulose, cellulose, and lignin peaks were assumed as pseudo-components [308], and their compositions were calculated based on the respective areas of the peaks using Equation 2.8.

$$\%\ \text{Hemicellulose} = (W - H) \quad \text{(equation 2.4)}$$

$$\%\ \text{Celulose} = (A - C) \quad \text{(equation 2.5)}$$

$$\%\ \text{Lignin} = (C - L) \quad \text{(equation 2.6)}$$

$$X_i = \frac{m_i - m_\infty}{m_0 - m_\infty} \quad \text{(equation 2.7)}$$

$$\%\ \text{PC} = (a/A) \times 100 \quad \text{(equation 2.8)}$$

where: *W* = % mass after dehydration; *H* = % mass measured after hemicellulose removal; *C* = % mass measured after cellulose removed; *L* = % mass measured after lignin removed (% Ash content); *PC* = pseudo-component; *a* = area of a peak; *A* = total area under the curve.

3.1.7 Fourier Transform Infrared Spectroscopy (FTIR) Analysis

FTIR spectra were measured using a BRUKER Alpha II compact FTIR spectrometer. Both the CO and CP samples were milled to pass through an 80-mesh sieve, and the commercial control samples AC, CL, and LG were used in their manufactured form without any additional milling. The samples were prepared as per the standard KBr pelleting method [309]. Spectra were collected in the absorbance mode with 32 scans per spectrum at a resolution of 4 cm^{-1}, within a wavenumber range of 4000–400 cm^{-1} [310]. Each sample was pelleted in triplicates and an average spectrum was considered. Processing, mathematical analysis, and deconvolution of the obtained spectra were performed using OriginPro2018 software. The total crystallinity index (TCI) was calculated as the height ratio of the absorption peaks at 1372 cm^{-1} and 2900 cm^{-1} [311]. The lateral order index (LOI) or empirical crystallinity index was calculated as the area ratio of the peaks at 1430 cm^{-1} and 893 cm^{-1} [312]. Hydrogen bond intensity (HBI) was calculated as the area ratio of the peaks around 3340–3330 cm^{-1} and 1320 cm^{-1} [313]. Additionally, two different S/G ratios 1462 cm^{-1}/1510 cm^{-1} [314] and 1595 cm^{-1}/1509 cm^{-1} [315], lignin to total carbohydrate ratios 1515 cm^{-1}/1374 cm^{-1}, 1515 cm^{-1}/1162 cm^{-1}, and 1515 cm^{-1}/898 cm^{-1}, and hemicellulose to total carbohydrate ratio 1734 cm^{-1}/1374 cm^{-1} [316] were calculated. Unless otherwise mentioned, the areas of the respective peaks were used to calculate all of the above-mentioned ratios.

3.1.8 X-ray Diffraction (XRD) Analysis

XRD data of the samples were recorded with X'Pert Powder XRD (Malvern Panalytical Ltd, Malvern, U.K, WR141XZ). The scans were performed at a step size of 0.0167113 in the 2θ angle range of 6o–80o with 5 s of exposure at each step using Ni-filtered Cu Kα radiation at wavelengths of 1.540598 (Kα1) and 1.544426 (Kα2). The operating generator voltage and tube currents were 45 kV and 30 mA, respectively. Smoothing, baseline subtraction, peak integration, and peak deconvolution of the digitally obtained diffraction data between the 2θ angles from 10o to 40o were performed using OriginPro2018 software. The crystallinity of the samples was calculated by four different methods. The percent crystallinity index (CrI%) was calculated by the peak height method using equation 2.9 [317]. Percent crystallinity (Crd) was calculated by the peak deconvolution method using equation 2.10. This method assumes that the peak broadening is contributed by the amorphous content [318]. The percent crystallinity of the sample (Cra_1) was calculated by the amorphous contribution subtraction method using the ball-milled AC as the amorphous standard for all of the samples using equation 2.11 [319]. This method needs an additional normalization step to bring the diffractogram of the amorphous standard below the sample diffractogram to avoid negative values making the process prone to errors or bias [319]. To overcome this problem, we reported a modified version of the amorphous contribution subtraction method where the percent crystallinity (Cra_2%) was measured using the ball-milled form of the sample itself as an amorphous standard instead of a common standard. The crystallite sizes of the (002) lattice of each sample were calculated using the Scherrer equation (Equation 2.12) [320], and the interplanar distances between the crystal lattices, known as d-spacing, were calculated using Bragg's law (Equation 2.13) [321].

$$CrI\% = \left(\frac{I_{002} - I_{am}}{I_{002}}\right) \times 100 \qquad \text{(equation 2.9)}$$

$$Cr_d\% = \left(\frac{A_{cr}}{A_t}\right) \times 10 \qquad \text{(equation 2.10)}$$

$$Cr_{a1}\% = \left(\frac{A_{Cra1}}{A_s}\right) \times 100 \qquad \text{(equation 2.11)}$$

$$L = k\lambda/\beta \cos\theta \qquad \text{(equation 2.12)}$$

$$d = n\,\lambda/(2\sin\theta) \qquad \text{(equation 2.13)}$$

where I_{002} = Intensity at about 2θ = 22.6° (represents the diffraction from both crystalline and amorphous materials) I_{am} = Intensity at the "valley" between the two peaks at about 2θ = 18° (represents the diffraction contributed by amorphous material), A_{cr} is the area of all the

crystalline peaks ((101), (10$\bar{1}$), (021), (002), (040)) together, and A_t is the total area of the diffractogram. A_{Cra1} is the area of all the crystalline peaks of the sample obtained by peak integration after subtracting the diffraction intensity of the ball-milled AC and A_s is the total area of the sample before amorphous subtraction. L is the crystallite size in nm, k is the dimensionless shape factor (0.89), λ is the wavelength of the incident x-ray (0.1540 nm), β is the full width at the half maximum (FWHM) of the (002) lattice expressed in radians, θ is the peak position in radians (Bragg angle), and n is a positive integer.

3.1.9 Enzymatic Saccharification of Untreated Corncob Samples

Both the CO and CP were separately saccharified with cellulase (*Trichoderma reesei* ATCC 26921, Sigma-C2730, initial activity around 650 filter paper units (FPU)/g), and xylanase (endo-1,4-β-Xylanase M1 from *Trichoderma viride*, Megazyme, E-XYTR1, initial activity around 1650 units (U)/mL), without any pretreatment. The CL and XY were also saccharified as the substrate controls with the respective enzymes. A typical enzymatic reaction process involved a 5 g dry weight of the substrate, taken in 250 mL Erlenmeyer flasks along with 50 mM of sodium citrate buffer, pH 4.8 (cellulase reaction), and pH 4.5 (xylanase reaction). Each enzyme was appropriately diluted in their respective buffers to achieve 20 FPU of cellulase and 30 U of xylanase per 1 g of dry mass of the substrate, achieving a liquid-to-solid ratio of 20 at a total reaction volume of 100 mL. A set of substrate blanks was incubated along with the test flasks by including all the ingredients mentioned above except the respective enzymes. The reactions were carried at 50 °C with shaking at 130 RPM for 50 h. Sample aliquots of 0.05 mL were collected at every 5 h interval. All the aliquots were appropriately diluted with respective buffer solutions to measure the total reducing sugars released using a micro-DNS assay, where the total reaction volume was minimized to 1.5 mL while maintaining the sample-to-reagent ratio mentioned in the original macro-DNS assay, as proposed by T.K. Ghose [322]. The absorbance of substrate blanks was subtracted from that of the corresponding test sample of the same time interval, and the resulting spectral data were plotted against time to visualize the enzymatic saccharification effect on each substrate. Enzyme activity (saccharification) was measured as per the procedure reported by Asmarani et al. [122]. The obtained saccharification yield was expressed as the percent of the total theoretical yield (TY), calculated using the equation of Mandels and Sternberg [323]. Anhydro correction factors of 0.9 and 0.88 were used for the cellulase and xylanase activities, respectively [323], and the total glucan and xylan

concentrations obtained from the NREL analysis were taken as the respective initial substrate concentrations [324].

3.2 Results and Discussion

3.2.1 SEM Analysis

The SEM images revealed the varied morphological features of the samples (Figure 3.2). The CO is compact and tightly packed in contrast to the loosely packed foam-like CP. The pores observed in the CP explain its soft airy features. A huge contrast in physical recalcitrance can be observed between the CO and CP at every magnification (50 μm, 20 μm, and 5 μm). Several previously reported studies described the morphology of whole corncob particles as a sheet-like bulky structure [325], solid-tight structure [139], highly ordered rigid structure [326] and agglomerated unbroken surface [327], and those findings exactly coincide with the morphology of the CO of this study. In addition, these reports also presented an increase in corncob porosity upon pretreatment.

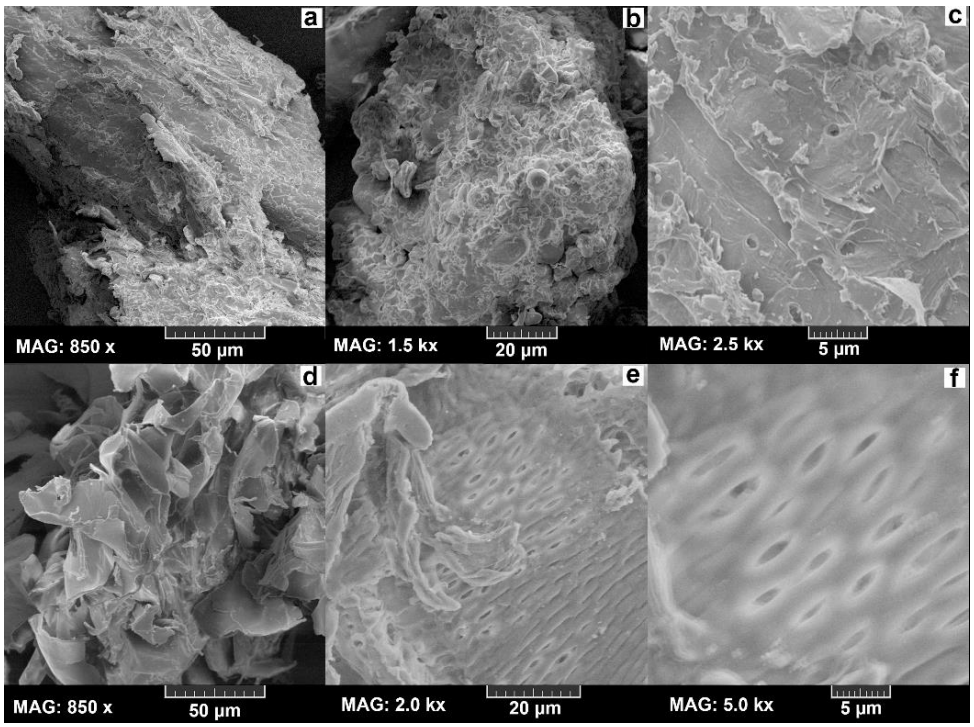

Figure 3.2. SEM images. Note: (**a**–**c**) are the CO and (**d**–**f**) are the CP. All the images were scanned at a constant accelerated voltage (H.V) of 5.0 kV by maintaining a working distance (W.D) ranging between 10.04 and 10.34 mm.

3.2.2 NREL Method for Biomass Composition Analysis

The compositional differences among all four different corncob varieties of the study were tabulated (Table 3.1, 3.1.1). None of the CO and CP samples showed mannose, while a small percentage of mannose was found in both the CL and AC references. Both cellulose and hemicellulose percentages of all the CP samples were slightly greater than that of CO samples due to the comparatively lower total lignin percentage in the CP. Overall hemicellulose percentage among both the CO and CP samples was greater than the cellulose percentage (Table 3.1, 3.1.1). The total water and ethanol extractives and the sucrose concentration in all CP samples were greater than that of the CO samples. The total protein was less in the CP than that of CO (Table 3.1, 3.1.1). Many works reported biomass composition analysis of the whole corncob by the NREL method. However, most of these works reported just the cellulose, hemicellulose, and total lignin concentrations rather than the particulars of individual monosaccharide concentrations, the information about extractives, and the protein content. The lignocellulose composition of CO reported in this work is closer to that of the whole corncob composition reported in the literature [25], which could be due to the higher percentage of CO in the whole corncob. The HPLC chromatograms for structural carbohydrate analysis of CO and CP are given in Figures 3.3 and 3.4

SHIMADZU LabSolutions **Analysis Report**

<Sample Information>

Sample Name	: CO2-structural-25ulin1ml-apr21		
Sample ID	: CO2-structural-25ulin1ml-apr21		
Data Filename	: CO2-structural-25ulin1ml-apr21.lcd		
Method Filename	: Cb-Glc-Xyl-Gal-Ara-Man-RezexPb+2-80C-50C-calibration.lcm		
Batch Filename	:		
Vial #	: 1-1	Sample Type	: Unknown
Injection Volume	: 5 uL	Level	: 1
Date Acquired	: 4/15/2021 9:20:26 PM	Acquired by	: NIT
Date Processed	: 5/27/2021 10:26:04 AM	Processed by	: Pradeep

<Chromatogram>

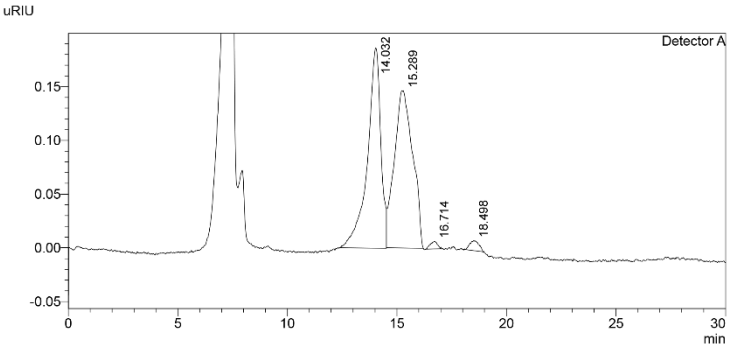

<Peak Table>

Detector A

Peak#	Ret. Time	Area	Height	Conc.	Unit	Mark	Name
1	14.032	7924	187	0.092	mg/ml	M	Glucose
2	15.289	8617	147	0.089	mg/ml	M	Xylose
3	16.714	161	7	0.055	mg/ml	M	Galactose
4	18.498	276	9	0.028	mg/ml	M	Arabinose
Total		16978	349				

Figure 3.3 Chromatogram for Structural carbohydrates of CO

SHIMADZU LabSolutions **Analysis Report**

<Sample Information>

Sample Name	: CP2-structural-25ulin1ml-apr21		
Sample ID	: CP2-structural-25ulin1ml-apr21		
Data Filename	: CP2-structural-25ulin1ml-apr21.lcd		
Method Filename	: Cb-Glc-Xyl-Gal-Ara-Man-RezexPb+2-80C-50C-calibration.lcm		
Batch Filename	:		
Vial #	: 1-1	Sample Type	: Unknown
Injection Volume	: 5 uL	Level	: 1
Date Acquired	: 4/15/2021 10:33:09 PM	Acquired by	: NIT
Date Processed	: 5/27/2021 10:33:41 AM	Processed by	: Pradeep

<Chromatogram>

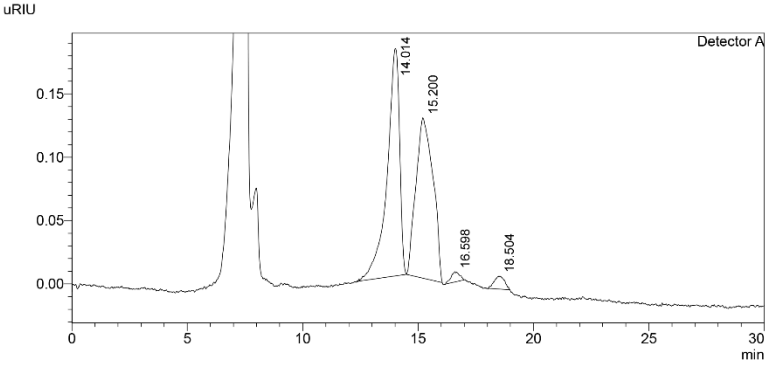

<Peak Table>

Detector A

Peak#	Ret. Time	Area	Height	Conc.	Unit	Mark	Name
1	14.014	6746	180	0.088	mg/ml	M	Glucose
2	15.200	6530	127	0.082	mg/ml	M	Xylose
3	16.598	208	8	0.055	mg/ml	M	Galactose
4	18.504	321	10	0.028	mg/ml	M	Arabinose
Total		13805	325				

Figure 3.4 Chromatogram for Structural carbohydrates of CP

Table 3.1 Biomass composition of samples by the NREL method

Corn Variety/ Reference	Sample	%AIL	%ASL	%Glucan	%Xylan	%Galactan	%Arabinan	%Mannan	%Protein (Structural)	%Water Extractives	%Ethanol Extractives	%Sucrose	%Acetate
CC1	CO	14.52 ± 0.23	1.85 ± 0.13	36.68 ± 0.13	25.42 ± 0.26	10.1 ± 0.04	5.29 ± 0.26	N.D	0.62 ± 0.1	2.26 ± 0.15	1.17 ± 0.22	2.58 ± 0.2	5.24 ± 0.38
	CP	11.11 ± 0.16	1.72 ± 0.12	39.13 ± 0.37	24.39 ± 0.34	11.14 ± 0.05	6.28 ± 0.28	N.D	0.39 ± 0.13	3.49 ± 0.05	1.58 ± 0.04	3.84 ± 0.31	5.21 ± 0.07
CC2	CO	15.44 ± 0.33	2.04 ± 0.31	37.04 ± 0.36	25.77 ± 0.19	11.45 ± 0.24	5.77 ± 0.06	N.D	0.79 ± 0.05	2.46 ± 0.37	1.55 ± 0.15	2.89 ± 0.27	5.84 ± 0.2
	CP	11.18 ± 0.24	2.11 ± 0.35	39.66 ± 0.35	25.39 ± 0.1	11.52 ± 0.39	7.39 ± 0.12	N.D	0.48 ± 0.13	3.59 ± 0.07	1.96 ± 0.25	4 ± 0.29	5.73 ± 0.19
CC3	CO	14.52 ± 0.15	2.51 ± 0.12	37.22 ± 0.26	25.86 ± 0.1	10.63 ± 0.16	6.55 ± 0.12	N.D	0.69 ± 0.37	2.28 ± 0.36	1.77 ± 0.39	2.87 ± 0.08	5.57 ± 0.2
	CP	11.42 ± 0.14	2.49 ± 0.37	40.44 ± 0.06	24.89 ± 0.17	11.26 ± 0.16	7.16 ± 0.05	N.D	0.49 ± 0.32	3.35 ± 0.36	1.68 ± 0.28	4.19 ± 0.1	5.56 ± 0.13
CC4	CO	15.52 ± 0.14	2.1 ± 0.26	37.71 ± 0.21	26.66 ± 0.09	11.65 ± 0.17	5.93 ± 0.03	N.D	0.7 ± 0.14	2.85 ± 0.19	1.64 ± 0.29	2.76 ± 0.16	5.87 ± 0.33
	CP	12.04 ± 0.17	2.25 ± 0.11	39.64 ± 0.18	25.14 ± 0.34	12.15 ± 0.1	7.72 ± 0.33	N.D	0.52 ± 0.07	3.37 ± 0.07	1.9 ± 0.27	4.21 ± 0.25	5.25 ± 0.3
Reference	CL	0.33 ± 0.27	0.35 ± 0.07	66.66 ± 0.24	15.47 ± 0.26	N.D	N.D	10.8 ± 0.2	ND	0.34 ± 0.07	0.25 ± 0.14	ND	ND
	AC	N.D	0.32 ± 0.1	71.88 ± 0.11	15.83 ± 0.13	N.D	N.D	9.77 ± 0.36	ND	0.09 ± 0.34	0.07 ± 0.3	0 ± 0.25	0 ± 0.36
Note: AIL: acid-insoluble lignin; ASL: acid-soluble lignin; N.D: not detected.													

Table 3.1.1 Summation of structural sugar and lignin composition of corncob anatomical portions CO and CP

Constituent	CO (avg. %)	CP (avg. %)	CO (g/Kg CO)	CP (g/Kg CP)	CO g/kg corncob	CP g/kg corncob
Lignin (Total)	17.1 ± 0.6	13.6 ± 0.6	171	136	167.58	2.72
Glucan	37.2 ± 0.4	39.7 ± 0.5	371.625	397.175	364.1925	7.9435
Xylan	25.9 ± 0.5	25 ± 0.4	259.275	249.525	254.0895	4.9905
Galactan	11 ± 0.7	11.5 ± 0.4	109.575	115	107.3835	2.3
Arabinan	5.9 ± 0.5	7.1 ± 0.6	58.85	71.375	57.673	1.4275
Mannan	0	0	0	0	0	0

3.2.3. Van Soest Method for Fiber Analysis

The NDF value of all CP samples was higher than that of CO and was similar to that of the pure cellulose references CL and AC. Although ADF values of CP were slightly higher than CO, they were almost half that of CL and AC. The composition analysis shows that the hemicellulose percentages of both the CO and CP samples were higher than their respective cellulose percentages. In addition, the CP samples showed comparatively higher cellulose and hemicellulose as well as lower lignin percentages compared with CO samples (Table 3.2). These results are consistent with the NREL method results reported in this work. Whole corncob fibre analysis results reported by many previous works [328] were closer to that of the CO in this work.

Table 3.2 Fiber analysis and lignocellulose composition analysis by the Van Soest method.

Corn Variety/ control	Sample	% NDF	% ADF	% ADL	% Hemicellulose	% Cellulose	% Lignin
CC1	CO	87.17 ± 0.3	45.25 ± 0.14	6.75 ± 0.07	41.92 ± 0.07	38.5 ± 0.15	6.75 ± 0.1
	CP	92.76 ± 0.1	49.35 ± 0.16	1.7 ± 0.32	43.41 ± 0.16	47.65 ± 0.32	1.7 ± 0.12
CC2	CO	85.56 ± 0.08	47.88 ± 0.1	9.47 ± 0.31	37.68 ± 0.3	38.41 ± 0.17	9.47 ± 0.15
	CP	95.62 ± 0.25	51.77 ± 0.22	4.12 ± 0.31	43.85 ± 0.13	47.65 ± 0.18	4.12 ± 0.11
CC3	CO	88.02 ± 0.28	46.91 ± 0.3	9.34 ± 0.13	41.11 ± 0.24	37.57 ± 0.28	9.34 ± 0.09
	CP	94.43 ± 0.15	49.64 ± 0.24	2.36 ± 0.32	44.79 ± 0.24	47.28 ± 0.1	2.36 ± 0.11
CC4	CO	86.21 ± 0.09	46.31 ± 0.19	8.3 ± 0.25	39.9 ± 0.27	38.01 ± 0.3	8.3 ± 0.1
	CP	95.1 ± 0.24	50.62 ± 0.21	1.8 ± 0.16	44.48 ± 0.12	48.82 ± 0.17	1.8 ± 0.19
Control	CL	98.1 ± 0.31	95.51 ± 0.13	0	2.59 ± 0.28	95.51 ± 0.21	0
	AC	98.62 ± 0.17	97.31 ± 0.22	0	1.31 ± 0.11	97.31 ± 0.11	0

3.2.4 NIR Method for Rapid Biomass Composition Analysis

The NIR spectra of both the CO and CP were analogous to that of other biomass types reported [329], with all the characteristic peaks of lignocellulose. The results of PLS calibration, validation, and prediction performances of the individual models as per their full spectral pretreatment are presented in Figure 3.5. All the statistical parameters of both calibration and validation sets were similar. Among the models generated with the unprocessed spectra of CO, the glucan model achieved the highest prediction, followed by the models of sucrose and protein. Meanwhile, the highest predictive models of CP were obtained for xylan and protein, followed by sucrose, glucan, and lignin.

R2C/R2P ratios close to one, lower SEC and SEP values, and higher RPD values (>2) indicate a better fit of the models. The performances of all the models were significantly improved by

the spectral pretreatments, decreasing the differences among calibration and validation sets. Savitzky-Golay smoothing of both the CO and CP spectra achieved models with the highest predictive performance.

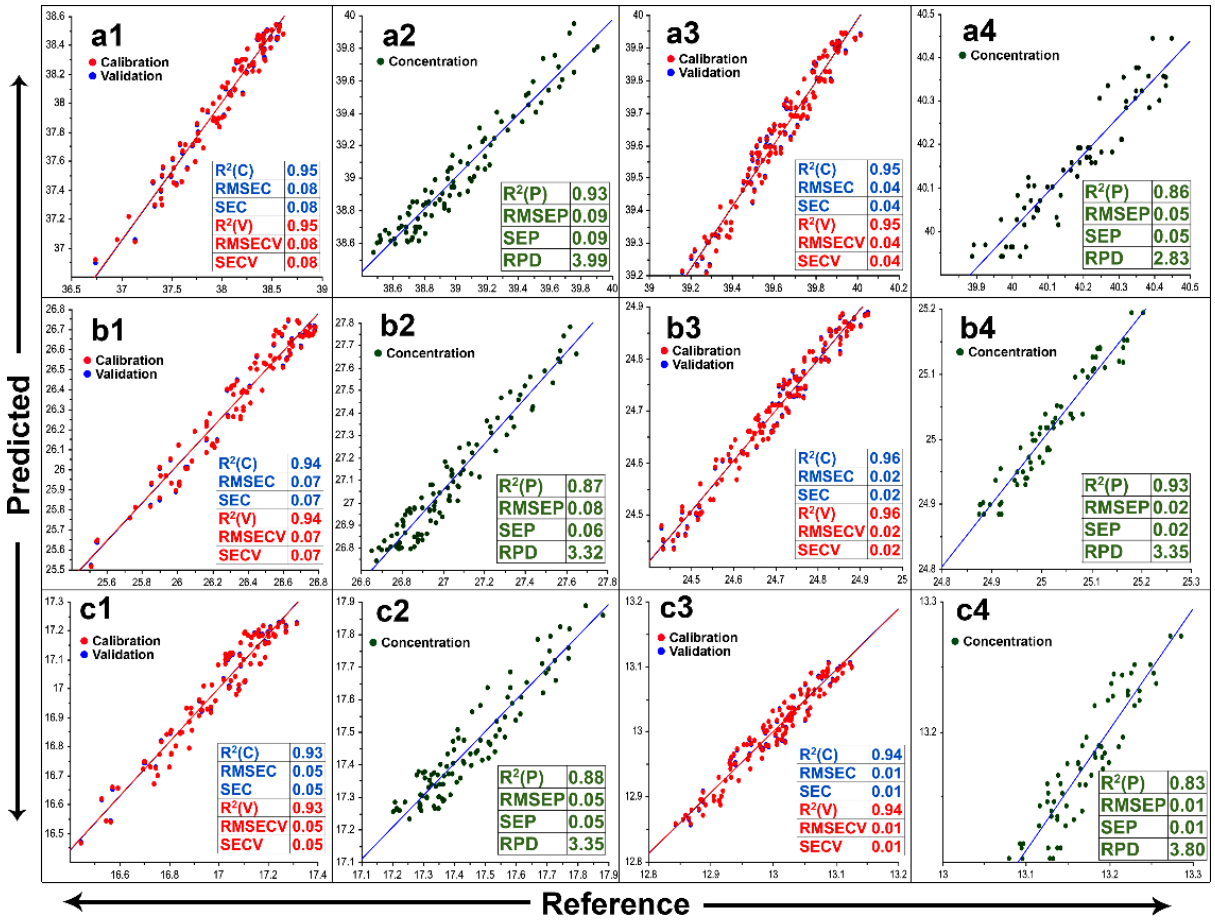

Figure 3.5. NIR-PLS calibration models. Note: (**a1**–**c1**) are calibration and validation models of the glucose, xylose, and lignin of CO, respectively; (**a2**–**c2**) are prediction performances of the models (**a1**–**c1**), respectively; (**a3**–**c3**) are calibration and validation models of the glucose, xylose, and lignin of CP, respectively; (**a4**–**c4**) are prediction performances of the models (**a3**–**c3**), respectively. Savitzky-Golay smoothing was used for the respective NIR spectra of all above models; R2(C): coefficient of multiple determination for the calibration; R2(V): coefficient of multiple determination for the validation; R2(P): coefficient of multiple determination for the prediction; SEC: standard error of the calibration; SEP: standard error of the prediction; RPD: residual predictive deviation.

3.2.5 TGA Analysis

Under an inert environment, devolatilization started at 30 °C and maximum dehydration occurred between 50.5 and 67 °C. The end of the dehydration stage, denoted by the start of the first mass loss plateau, was observed in the range of 90.8–240 °C. An abrupt weight loss due to hemicellulose decomposition was observed at 298 °C for both the CO and CP [308], while the cellulose degradation peaks of the CO, CP, AC, and CL were in the range of 340–352 °C; the complete degradation of the same samples was in the range of 381–400 °C. No additional peaks were observed after 400 °C for all samples except for LG. In contrast, the thermal decomposition curve of all samples under the oxidative environment was comparatively complex, with additional devolatilization peaks observed at 423–472 °C for CO and CP, and around 591–598 °C for AC and CL. Maximum decomposition under the oxidative environment for CO and CP was achieved at 539 °C and 494 °C, respectively. The absence of a hemicellulose degradation peak in both AC and CL indicates their purity. The pyrolytic profile of LG under both inert and oxidative environments was quite complex with multiple decomposition steps, spanning a wide range of temperatures. Evidently, LG needs a temperature beyond 800 °C for complete decomposition. Both CO and CP achieved a higher mass loss under the oxidative environment. On the contrary AC, CL, and LG attained maximum weight loss under the inert environment (Figure 3.6). Despite showing similar degradation temperatures, the extent of pyrolysis among CO and CP is different, with CP showing a higher mass loss percentage at each inflection point. The three-stage thermal degradation profile of whole-native corncob reported by Yao et al. [330] is quite similar to that of the CO in this study, the starting, peak, and final temperatures of the TGA profile, including the maximum weight loss reported, were similar. The same is the case with the TGA of the whole corncob reported by Zheng et al. [41]. The alteration of the TGA profile reported for dilute sulfuric acid-pretreated corncob with that of native corncob showed the exact thermal decomposition temperature range of hemicellulose [41]. The lignocellulose composition of CO and CP calculated by the TGA analysis under both inert and oxidative environments clearly showed lower lignin and residue content along with a higher hemicellulose percentage in CP. The lignocellulose composition calculated as pseudo-components by the peak deconvolution method revealed a similar difference between CO and CP (Table 3.3, Figure 3.7). AC and CL have shown a pure cellulose devolatilization peak without traces of hemicellulose or lignin. These results are consistent with the compositions determined by the other methods reported in this work.

Table 3.3 Mass (%) of the lignocellulose components in thermally degraded samples.

	CO-i	CO-o	CO-dc	CP-i	CP-o	CP-dc	AC-i	AC-o	CL-i	CL-o
HC	24.23	24.97	25.31	29.93	32.83	45.09	0	0	0	0
CE	51.85	45.88	18.03	48.64	49.1	31.2	94.76	86.58	100	87.95
LG	12.15	24.99	16.58	10.09	13.91	13.16	5.24	12.01	0	9.09
A and C	11.35	4	N.A	10.9	4		0	1.37	0	2.9
TC	76.09	70.86	43.34	78.57	81.93	76.29	94.76	86.58	100	87.95
HC/TC	0.32	0.35	0.58	0.38	0.4	0.59	0	0	0	0
LG/TC	0.16	0.35	0.38	0.13	0.17	0.17	0.06	0.14	0	0.1

i: inert environment; o: oxidative environment; dc: peak deconvolution; HC: Hemicellulose; CE: cellulose; LG: lignin; TC: total carbohydrate; A and C: ash and residual carbon at 800 °C.

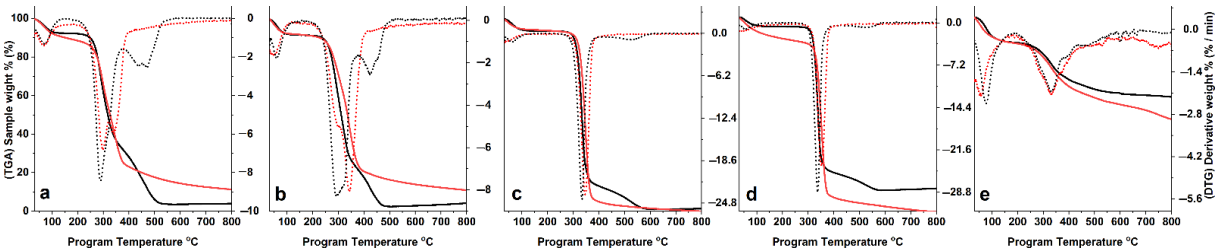

Figure 3.6 TGA profiles of the samples along with their first derivatives.

Note: black solid and dotted lines: the thermogram and its derivative under the oxidative environment, respectively; red solid and dotted lines: the thermogram and its derivative under the inert environment, result; (**a**,**b**,**c**,**d**,**e**): CO, CP, AC, CL, and LG, respectively. The left-Y axis is common for all of the graphs.

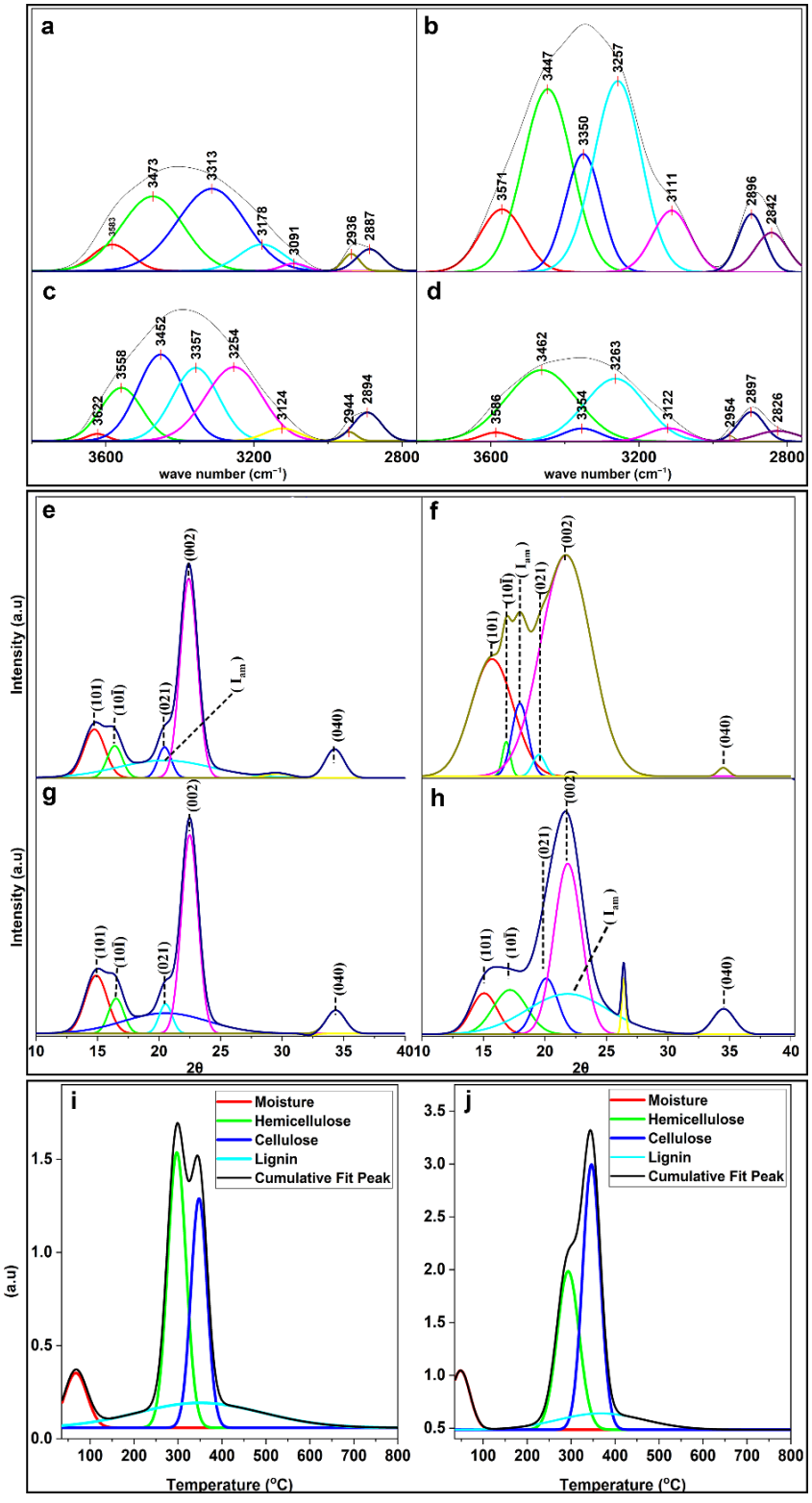

Figure 3.7 Peak deconvolutions of the FTIR, XRD, and DTG curves.

Note: FTIR peak deconvolutions of (**a**) CO, (**b**) AC, (**c**) CP, and (**d**) CL; XRD peak deconvolutions of (**e**) CO, (**f**) AC, (**g**) CP, and (**h**) CL; DTG peak deconvolutions of (**i**) CO and (**j**) CP.

3.2.6 FTIR Analysis

The characteristic FTIR peaks of lignocellulose observed among all of the samples were tabulated (Table 3.4). The unprocessed spectra of all samples showed the characteristic –OH stretch in the range of 3700–3000 cm^{-1}, specifically at 3350 cm^{-1} for both AC and CL and in the higher wavenumber region in the case of CO, CP, and LG. The –OH stretching peak of CP was much sharper and showed higher absorption than that of CO (Figure 3.7). Deconvolution of the broad stretching region between 3800 and 2800 cm^{-1} showed around five different peaks for each sample (Figure 3.7). The relative peak intensities of the characteristic intramolecular hydrogen bonds (3586–3559 cm^{-1}, 3475–3448 cm^{-1}, and 3358–3351 cm^{-1}) were in the order of AC > CP > CO > CL, AC > CL > CO > CP, and AC > CP > CL, respectively. Furthermore, the intensities of intermolecular hydrogen bond peaks (3179–3112 cm^{-1}) were in the order of AC > CO > CL > CP. CP clearly showed an increased carbohydrate percentage compared with CO in both crystalline (1428 cm^{-1}, 1162 cm^{-1}) and amorphous regions (1335 cm^{-1}, 897 cm^{-1}, 668 cm^{-1}, 527 cm^{-1}, 993 cm^{-1}). In addition, CP showed an increased hemicellulose percentage (1734 cm^{-1}, 1248 cm^{-1}), and total carbohydrate percentage (1205 cm^{-1}, 1111 cm^{-1}) than the CO. The abundance of guaiacyl-type lignin was detected in CO (862 cm^{-1}, 1516 cm^{-1}) with an overall increase in lignin content (1459 cm^{-1}), while CP showed more syringyl lignin and less total lignin compared with CO.

Table 3.4 FTIR peaks obtained and their assignments.

Wave Number Range (cm^{-1})	Samples and Their Obtained Peaks (cm^{-1})					Generic Functional Group Assignment, Reference	Lignocellulose Specific Assignment
	CO	CP	AC	CL	LG		
3650–3600						Non-bonded free –OH stretching. [331]	
3400–3200						Bonded –OH stretching. [331]	
	3584	3559	3571	3586		Intramolecular hydrogen bond O(2)H–O(6). [332]	Cellulose
	3475	3453	3448	3465		Intramolecular hydrogen bond O(2)H–O(6). [332]	Cellulose
					3430	–OH (bonded) stretching. [333]	Lignin *
		3358	3351	3355		Intramolecular hydrogen bond O(3)H–O(5), [332]	Cellulose
	3179	3124	3112	3123		Intermolecular hydrogen bond O(6)H–O(3), [332]	Cellulose
3000–2850						C–H stretching: Alkanes/O–H stretching carboxylic acid/Aldehyde. [334]	
2970–2860						CH–stretching region (saturated aliphatic group frequencies). [335]	
					2937	C–H stretch methyl and methylene groups (2942 HW lignin, 2938 SW lignin). [336]	SW.Lignin
	2886	2898	2904	2902		Symmetric C–H stretching. [333]	Cellulose *
					2842	C–H stretch O–CH3 group. [336]	Lignin
1780–1640						C=O stretching: Ester/Aldehyde/Ketone/Carboxylic acid; C=C stretching: Alkene [334]	
	1731	1733				Ketone/Aldehyde C=O stretching (unconjugated) [337]	Hemicellulose *
					1711	Non–conjugated carbonyl [338]	Lignin
	1643	1635	1639	1641	1643	Intramolecular hydrogen bond/absorbed water/Aromatic ketones stretching [333]	
1600–1475						C=C stretching–skeletal vibration of phenolic compounds such as lignin, –CH2 bend. [334]	
	1606	1604				Aromatic skeleton vibration [336]	Lignin * (S > G; G-con. > G-eth.)
					1598	The aromatic ring (C=C), C=O stretching vibrations [315].	Lignin * (S > G; G-con. > G-eth.)
	1516	1516			1510	Aromatic ring (C=C) stretching [315].	Lignin * (G > S)
	1456	1462		1458	1464	Asymmetric bending of CH3 in methoxy groups//CH2 bending vibration [337]	Lignin * (S > G), Cellulose, Hemicellulose
	1425	1427	1429	1431		Scissoring motion of –CH2 [311]	Cellulose-I * Crystallinity peak
						O–CH3 C–H deformation symmetric [336]	Lignin
	1372	1374	1372	1372	1376	Symmetric and asymmetric C–H deformation [334]	Cellulose, Hemicellulose, Lignin
	1335		1337	1337		C–H, –OH in-plane bending/weak C–O stretching [339]	Cellulose amorphous

					1327	Stretching of C–O in syringyl ring [340]	Lignin-S *
		1318	1316	1314		–CH2 wagging [341]	Cellulose I crystalline
1300–1000						C=O/C–O–C/C–O–H; Alcohols, ethers, esters, carboxylic acids, anhydrides [342]	
			1281	1281		C–H bending [340]	Cellulose crystalline *
					1269	Aromatic ring vibration [334]	Lignin-G
	1248	1251				C–O–C and C–O Stretching [343]	Hemicellulose *
					1220	C=O stretching of guaiacyl ring [344]	Lignin G
	1205	1203	1201	1203		O–H in-plane bending [338]	Carbohydrates *
	1158	1162	1164	1166		C–O–C stretching, Asymmetric stretching of C–O, C–C, O–H stretching of C–OH group [343]	Crystalline cellulose, β-glycosidic bond
					1137	C–H (aromatic) in-plane deformation, secondary alcohols, C–O stretch [310],	Lignin G
	1111	1113	1113	1115		Asymmetric stretching of C–O–C; Cellulose characteristic peak [333]	Cellulose *
					1082	C–O deformation, secondary alcohol, an aliphatic ether [336]	Lignin
	993	993	987	986		C–O and C–C, C–H bending or CH2 (amorphous band) stretching [345]	Cellulose
1000–650						Out-of-plane bend Alkenes/Aromatics, aromatic C–H stretching [334]	
	899	899	897	895		C–O–C stretching at β-1,4 glycosidic link [333]	Amorphous band *
	862				858	C–H out of the plane in positions 2, 5, and 6 of G-ring [346]	Lignin-G
				814	817	The vibration of mannan. CH out-of-plane bending in phenyl rings [347]	Glucomannan, Lignin G
			714	714		Alcohol, OH out-of-plane bend. [348]	Cellulose Iβ *
	668	668	668	668		–OH out-of-plane-bending [349]	Cellulose amorphous
	607	617	619	617	617	Alkyne C–H bend, Alcohol, OH out-of-plane bend [344]	Carbohydrates/Lignin
	524	527	520	518	520	C–O–C bending, C–C–C ring deform [350]	Cellulose, β-glycosidic bond

SW: softwood; HW: hardwood; * characteristic peaks; G: guaiacyl; S: syringyl; G-con: condensed guaiacyl ring; G-eth: etherified guaiacyl ring.

In addition, the adsorbed water content was less in the case of equally dried CP compared with CO. These findings showed an overall increase in the carbohydrate to lignin ratio, hemicellulose to total carbohydrate ratio, and hemicellulose to lignin ratios in CP compared with that of CO (Table 3.5). The absence of lignin and hemicellulose peaks in the spectrum of AV and CL indicates their purity. The FTIR spectrum previously reported for the whole corncob was quite similar to that of both the CO and CP of this study [75]. The lignin to carbohydrate ratios previously reported were the same as that of CO, and these values were shown to get closer to that of CP when the corncob was pretreated with dilute acids and alkalis, proving the lignocellulosic construct of CP reported in this work [82]. The HBI value previously reported for the whole corncob is quite similar to that of the CO of this study and is reportedly decreased upon pretreatment [48]. The TCI, LOI, and CrI% values of a xylose-extracted corncob residue reported by Chi et al. [103] were slightly more than that of the CO in this work, indicating the decreased crystallinity of the biomass due to the presence of relatively amorphous constituents such as hemicellulose and lignin. On the other hand, the TCI and LOI values of the pure cellulose reference AC reported in the literature [104] are consistent with this work. All of the FTIR peaks of a whole corncob as reported by Zheng et al. [105] were also observed in the case of the CO. The S/G ratios of CO reported in this work are consistent with that of the whole corncob reported by HPLC [106] and NMR methods [107].

Table 3.5 Lignocellulose composition ratios measured by FTIR data.

Ratio	Wave Number Range (cm^{-1})	CO	CP	LG
S/G	1462/1510–1508	1.34	1.38	0.52
S/G	1595/1510–1508	1.28	1.34	2.54
LG/TC	1510–1508/1374	1.03	0.71	8.75
LG/TC	1510–1508/1162	0.45	0.34	N.A1
LG/TC	1510–1508/898	2.89	1.93	N.A1
XY/TC	1734/1374	1.16	1.88	N.A2
XY/TC	1734/1162	0.50	0.90	N.A2
LG/XY	1510–1508/1734	0.88	0.37	N.A1

S/G: syringyl/syringyl + guaiacyl ratio; LG/TC: lignin/total carbohydrate ratio; XY/TC: xylan/total carbohydrate ratio; LG/XY: lignin/xylan ratio; N.A1: lignin-related peaks are present but carbohydrate peaks are absent; N.A2: carbohydrate-related peaks are absent.

3.2.7 XRD Analysis

Diffractograms of the CO, CP, AC, and CL showed the lignocellulose characteristics of crystal lattice peaks with different intensities [351], such as (101) in the 2θ angle range of 14–15°, (10Ī) in the 16.5–17° range, (021) around 20.8°, (002) around 22.6°, and (040) around 34.3°. An amorphous characteristic plateau spanning between the peaks (10Ī) and (002) with its centre around 18o was also observed (Figure 3.8). The results of crystallinity measurements by all four of the methods used were consistent (Table 3.6). The measured crystallinity of the samples was in the order of AC > CL > CO > CP. The results of Cra1% and Cra2% were similar for all samples. The method followed for the analysis of Cra2% was found to be advantageous to that of Cra1%, as the former can achieve the result without an additional step of normalization that could otherwise misinterpret the data (Figure 3.9), (Table 3.6). The d-spacing of all samples was comparable (Table 3.6), whereas the crystallite sizes of the 002 lattice (L) of CO were the highest, and those of CP was the smallest. All results of AC and CL were similar. The observed differences between CO and CP strongly reflect the differences in their lignocellulosic construct (Table 3.6). The crystallinity (CrI%) and crystallite size (L) values reported for AC are consistent with the reported values in the literature [352]. Moreover, the difference between the values of CrI% and Crd% is consistent with the values reported in the literature for different types of cellulosic compounds [353]. The CrI values of the whole corncob previously reported were in the range of 35.19–39.2%; these values are almost half of that shown by CO in this work, proving the effect of separating amorphous CP from the whole corncob. Additionally, these works reported the increase in the CrI of the corncob residue after removing its amorphous content (xylose or lignin) by the pretreatments employed [129]. Both the XRD (CrI%, Crd%, Cra1%, Cra2%) and FTIR (TCI, LOI, HBI) methods used for crystallinity measurement showed a lower crystallinity of CP compared with that of CO, AC, and CL, explaining the amorphous nature of CP due to its higher hemicellulose and syringyl lignin (Table 3.5). However, the CO showed slightly higher crystallinity than AC and CL in the FTIR measurement and a lower crystallinity in the XRD measurement. This observed difference in crystallinity among two different methods can be explained by two reasons: crystallinity measurement by FTIR methods is not absolute but is relative, and the readings are greatly influenced by the amorphous content (hemicellulose and lignin) of the sample [354]; the XRD readings are dependent on crystallite size rather than particle size, thus the AC and CL having pure cellulose crystallite provided much sharper peaks than CO. The patterns of the FTIR, XRD, and TGA curves were consistent with that of the whole corncob reported [50].

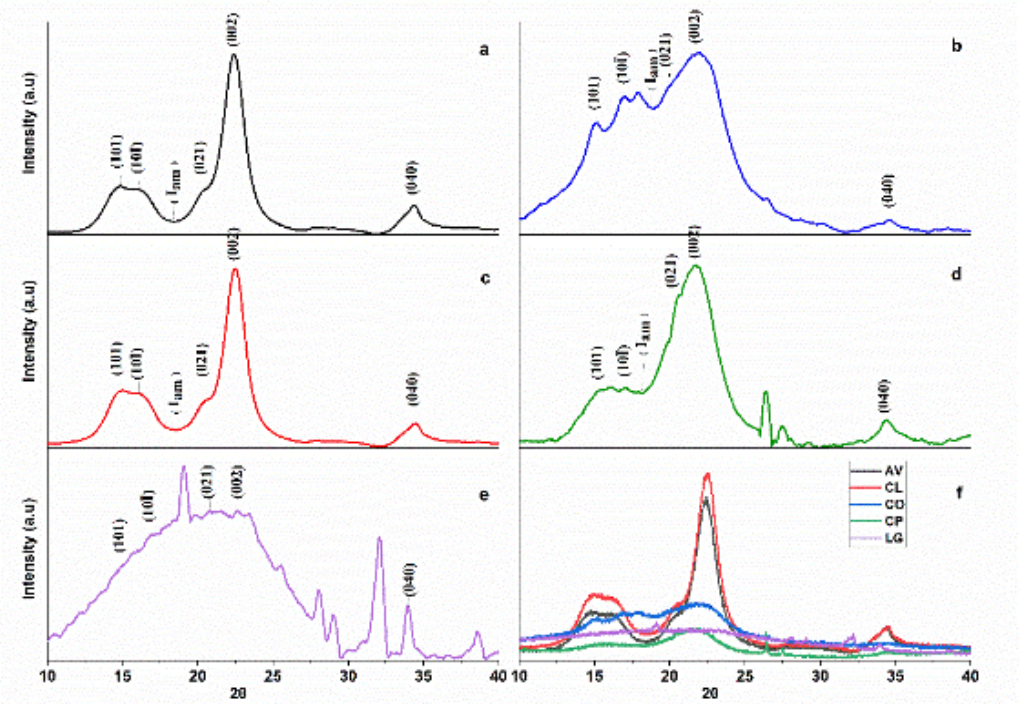

Figure 3.8 XRD profiles of the samples
Note: a) AC; b) CO; c) CL; d) CP; e) LG; f) all

Table 3.6 Crystallinity measurements of samples by both the XRD and FTIR-based indices.

	XRD Analysis						FTIR Analysis		
Sample	**CrI%**	**Crd%**	**Cra1%**	**Cra2%**	**L**	**d**	**TCI**	**LOI**	**HBI**
CO	70.0	93.0	26.48	25.20	5.75	0.34	2.82	2.35	2.46
CP	31.0	73.0	20.06	23.84	2.94	0.41	1.47	0.87	2.03
AC	93.0	78.0	48.04	48.04	4.67	0.40	1.72	1.29	2.15
CL	91.0	77.0	44.28	36.01	4.73	0.39	1.8	0.96	1.89

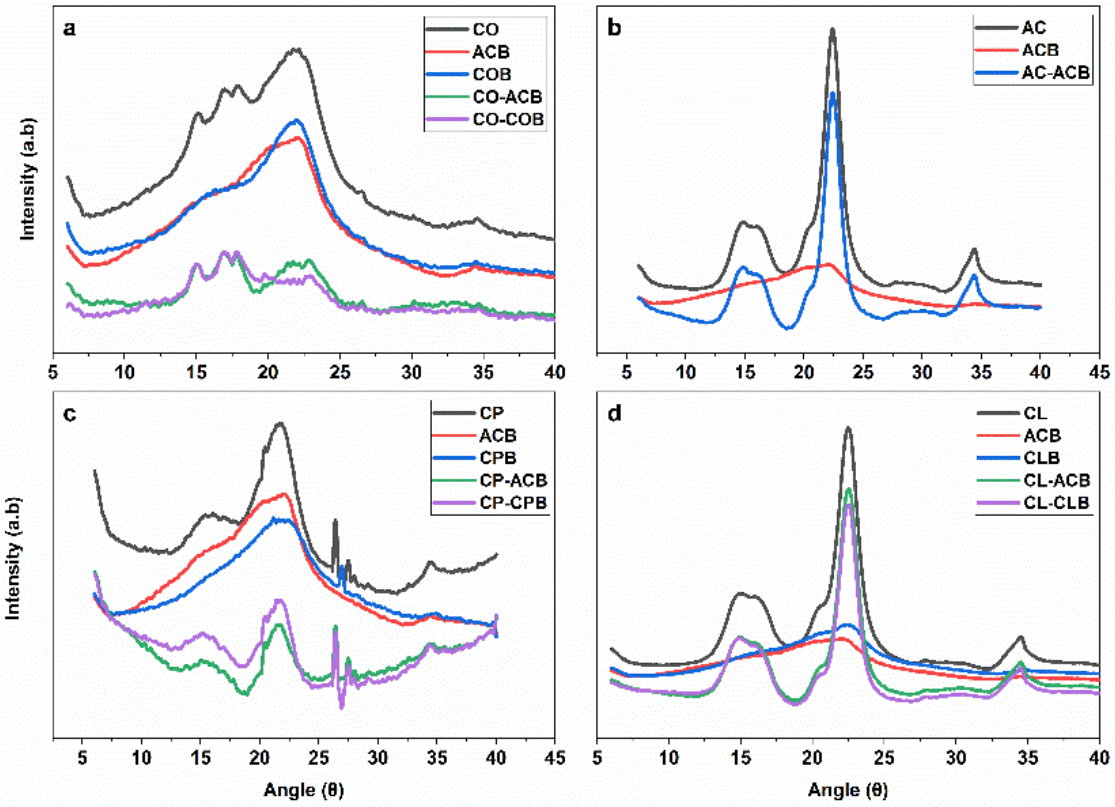

Figure 3.9 Amorphous contribution subtraction of XRD diffraction.

Note: ACB, CLB, COB, and CPB are the diffraction patterns of the ball-milled AC, CL, CO, and CP, respectively; the negative sign indicates the diffraction of the sample after subtracting the diffraction of amorphous standards from it. For example, CO–ACB: diffraction of CO after subtracting amorphous contribution using diffraction of ACB; (**a**), (**b**), (**c**), (**d**): Decrease in diffraction of around 18° and sharpening of the crystalline lattice by around 22° indicate the amorphous subtraction; (**a**) and (**c**): Diffraction patterns of CO and CP are significantly different, suggesting their varied crystallinities. Both COB- and CPB-subtracted samples showed slightly sharper patterns than that of ACB-subtracted samples; (**d**) CLB achieved a better amorphous subtraction than ACB.

3.2.8 Enzymatic Saccharification of Untreated Corncob Samples

A saccharification yield of 50–60% of the theoretical yield (TY) of CL and XY was obtained during the first 5 h of the incubation, which later gradually increased to 72.8% and 90.13%, respectively, after 40 h and 30 h. The saccharification of CP gradually increased and achieved a maximum yield close to that of controls, which was 70.57% of its TY at 50 h with cellulase and 88.70% of its TY at 50 h with xylanase. CO showed comparatively poor enzymatic saccharification susceptibility, showing no significant improvement from a minute

saccharification yield of 15–18% of its TY obtained at the 10 h interval with both enzymes (Figure 3.10).

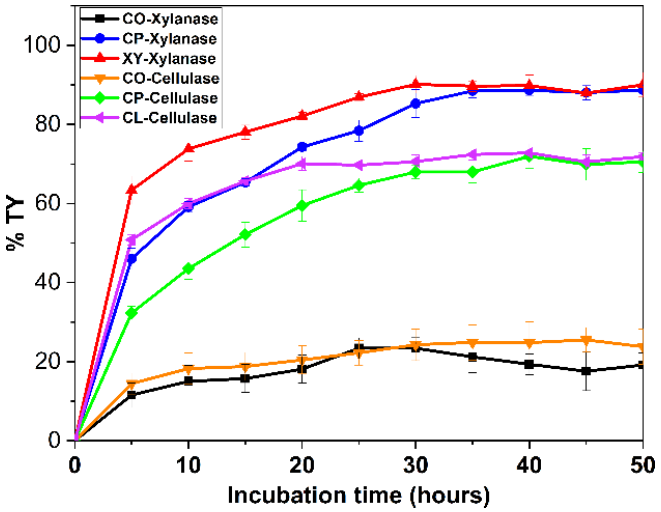

Figure 3.10 Enzymatic saccharification of the samples.

Note: CO/CP/XY-xylanase: samples of CO, CP, or XY treated with xylanase; CO/CP/CL-cellulase: samples of CO, CP, or CL treated with cellulase; %TY: percentage of the theoretical yield (saccharification) achieved.

The maximum TY of CO with xylanase was around 26% of the reference XY, whereas CP achieved 98.4% of it. The maximum TY of CO with cellulase was around 35% of reference CL, whereas CP achieved 98.8% of it. These results are perfectly correlated with the chemical and physical characterization of the respective corncob anatomical portions. As per the NREL method of composition analysis, CP on average showed a 20.7% lower lignin percentage along with a higher percentage of cellulose, hemicellulose, and extractives (6.8%, 1.9%, and 21.4%, respectively). A similar difference was observed from other composition analysis methods reported in this work. In addition, the S/G and XY/TC ratios of CP were 3.8%, which was 67.4% higher; the LG/TC and LG/XY ratios of CP were 31.8% and 57.9% lower than that of CO, respectively. The crystallinity values of the CP measured by both the XRD (CrI%, Crd%, Cra1%, and Cra2%) and FTIR (TCI, LOI, and HBI) methods were 55.7%, 21.5%, 24.2%, 5.3%, 47.8%, 62.9%, and 17.4% lower than that of CO, respectively. A huge contrast observed in enzymatic saccharification susceptibility of untreated CO and CP can be essentially attributed to their chemical compositional differences, especially to their lignin-to-carbohydrate ratios and to their differences in crystallinity. Although CP has a slightly higher syringyl percentage than CO, the S/G ratio appears to be a comparatively minor deciding factor for their saccharification susceptibilities.

The saccharification profile of CO in this study is similar to that of the whole corncob without pretreatment as previously reported by many other researchers as a control in their respective studies [355]. Whole corncob ground to a similar mesh as that of the CO in this study reportedly achieved a similar saccharification yield by the first 10 h interval and was unchanged thereafter using cellulase of the same make as that used in this study [70] and when using cellulase procured from a different manufacturer [356]. Similar yields and patterns were reported even when the cellulase activity was complimented with β-glucosidase [55]. On the other hand, many works reported enzymatic production of xylooligosaccharides from pretreated whole corncob, either by in-house-produced xylanases [161] or with commercial xylanases [357]; however, none of these studies showed the effect of xylanases on an untreated corncob. Nevertheless, we found a report where the whole corncob without any chemical pretreatment was used as a control for in-house-produced *T.viride*-derived xylanase; the enzyme activity profile reported for the untreated whole corncob was similar to that of the CO in this study, but the peak activity was achieved at 48 h of incubation [358]. However, we did not find any work reporting the saccharification of individual anatomical portions of corncob to date.

Chapter 4

Integrated Multi-Objective Optimization of Sodium Bicarbonate Pretreatment for the Outer Anatomical Portion of Corncob Using Central Composite Design, Artificial Neural Networks, and Metaheuristic Algorithms.

4.1 Materials and methods

4.1.1 Sample Selection and Preparation

Shelled corncobs (Zea mays) were collected from a corn processing unit located at Hanamkonda, Telangana, India. After being thoroughly cleaned and sun-dried for two weeks, the corncob was separated into pith (CP) and outer portion (CO) (Gandam et al., 2022b). The CO portion was selected as the biomass for this study, while cotton linters (CL) (Sigma Aldrich,101802987) served as a pure cellulose reference. Analytical-grade chemicals (FINAR Chemicals, India) were used, and samples were processed in triplicate for all analytical procedures.

4.1.2 Fixed factor screening of various chemical pretreatments

A total of 28 different chemicals, including acids, alkalis, and salts, were screened (Table 4.1), for their ability to remove lignin and sugars from CO. Each chemical was assigned a number from 1 to 28 and an alphabet 'a,' 'b,' 'c,' or 'd' to indicate the four different concentrations used: 0.1%, 1.0%, 5%, and 10%, respectively (Table 4.1). Each set of pretreatment was carried out with 500 mg of the CO taken in 50 ml screw-cap culture tubes (Borosil, India) individually at three different temperatures: 50°C, 100 °C, and 125 °C, using a vertical, temperature-controlled autoclave sterilizer (Model SLEDD-7411-5576, Equitron medica Pvt. ltd, India). The liquid-to-solid ratio (L/S) and reaction time (minutes) were kept constant at 10:1 and 60 minutes, respectively. The liquid fraction obtained after pretreatment was analyzed for the released lignin using the NREL method for acid-soluble lignin [359], and for reducing sugars using the DNS method [322]. The percentage of lignin removed (LG), and the amount of reducing sugars released (TS) per gram of CO were calculated based on the total lignin and reducing sugar content of CO reported earlier (Gandam et al., 2022b). The corncob residue with the highest lignin removal was selected from each screened chemical pretreatment and subjected to neutralization with water washing using a vacuum filtration setup with Grade-2 filtration crucibles, and the amount of water consumed (in millilitres) was measured. Later, the neutralized residue was subjected to enzymatic saccharification using commercial cellulase from Trichoderma reesei (C2730, Merck, India) at a concentration of 15 FPU/g, with a 15%

solid loading, and a pH of 4.8 maintained using a 0.05M sodium citrate buffer. The reaction was carried out for 70 hours in plugged Erlenmeyer flasks, maintained at 50°C and 130 RPM in an orbital shaker. The total reducing sugars released were measured against a cellobiose standard, and the obtained saccharification yield was expressed as a percentage of the total theoretical yield (TY) of the CO reported earlier. (Gandam et al., 2022b).

Table 4.1 Chemicals screened for their pretreatment efficiency on CO

Serial Code	Chemical Name	Molecular formula
1	Sodium hydroxide	NaOH
2	Potassium hydroxide	KaOH
3	Calcium hydroxide	$Ca(OH)_2$
4	Ammonia liquor	NH_4OH
5	Sodium Sulfite	Na_2SO_3
6	Sodium carbonate	Na_2CO_3
	Sodium bicarbonate	$NaHCO_3$
8	Ammonium sulfate	$(NH_4)_2SO_4$
9	di-Potassium hydrogen phosphate	K_2HPO_4
10	di-Sodium hydrogen phosphate	Na_2HPO_4
11	Potassium sodium tartrate	$KNaC_4H_4O_6.4H_2O$
12	Sodium sulfate	Na_2SO_4
13	Potassium sulfate	K_2SO_4
14	tri-Sodium citrate	$Na_3C_6H_5O_7$
15	Sodium chloride	NaCl
16	Hydrochloric acid	HCl
17	Sulphuric acid	H_2SO_4
18	Nitric acid	HNO_3
19	Phosphoric acid	H_3PO_4
20	Hydro fluoric acid	HF
21	Acetic acid	CH_3COOH
22	Oxalic acid	$C_2H_2O_4$
23	Citric acid	$C_6H_8O_7$
24	Succinic acid	$C_4H_6O_4$
25	DL-Malic acid	$C_4H_6O_5$
26	Maleic acid	$C_4H_4O_4$
27	Glycerol	$C_3H_8O_3$
28	Hydrogen peroxide	H_2O_2

4.1.3 Regular two-level factorial design

Four different alkalis (NaOH, KOH, Na_2CO_3, and $NaHCO_3$) were chosen for this study based on their observed pretreatment performances during the initial fixed factor screening. A 2FI design with resolution IV and 8 runs was constructed using Design-Expert software (version

11.1.2.0; Stat-Ease, U.S.A.). The 2FI design was used to determine the most important factors affecting the pretreatment efficiency of each alkali chosen. The factors tested were alkali concentration (A) 0.5% to 2%, temperature (B) 50°C to 120°C, time (C) 30 to 90 minutes, and liquid-to-solid ratio (D) 7 to 10 ml. The significance of these factors was measured at two levels (-1 and +1), with three dependent variables: lignin removal (R1), sugar loss (R2), and solid recovery (R3), measured following the procedures in section 1.2. To reduce bias, the study was randomized without blocks, and no centre points were included in the design to assess measurement precision. The experimental data was used to create linear regression models that predict the responses, and ANOVA was used to determine significant model terms that maximize R1 and minimize R2 while keeping R3 in the desired range. Additionally, CO-residues from the harshest pretreatment conditions used in each model (run 8) were washed with distilled water as described in section 1.2.

4.1.4 Central composite design

Based on the findings from the 2FI model discussed in section 1.3, $NaHCO_3$ was chosen for further optimization through CCD. The factors were reduced to three, and varied at two levels (-1 and +1): alkali concentration (A) 0.5% – 1.5%, temperature (B) 60 °C – 100 °C, and time (C) 30 – 90 minutes, while maintaining a constant L/S ratio of 10:1. The responses assessed were lignin removal (Y1), total reducing sugar loss (Y2), and enzymatic saccharification yield (Y3). The CCD was randomized, with 20 runs, without blocks. The LG and TS analysis was carried out as outlined in section 1.2. The enzymatic saccharification of pretreated biomass was conducted as described in Section 2.1. An aliquot of 65 µL was collected at five-hour intervals to measure the total reducing sugars released. Samples of untreated CO and commercial cellulose were used as controls. The second-order polynomial equation (equation 4.1) of the quadratic model was used to fit the response surfaces for each of the three response variables Y1, Y2, and Y3, in relation to the linear and quadratic terms for each independent variable, and their interaction terms.

$$Y = b0 + b1A + b2B + b3C + b11A^2 + b22B^2 + b33C^2 + b12AB + b13AC + b23BC$$

(equation 4.1)

where Y is the response variable, coefficient b0 represents the value of Y when all independent variables are zero. The b1, b2, and b3 coefficients represent the linear effects of A, B, and C, respectively. The b11, b22, and b33 coefficients represent the quadratic effects of A, B, and C, respectively. The b12, b13, and b23 coefficients represent the interaction effects between A and B, A and C, and B and C, respectively.

The quality of the models was evaluated by the analysis of variance (ANOVA) and determination coefficient (R^2) values.

Three different criteria were chosen to optimize the CCD results for each pretreatment, each with a different set of objectives and constraints. The ultimate goal of all three optimization criteria is to enhance the ES%. The detailed factor and response objectives and constraints chosen for each criterion are provided in Table 4.2

Table 4.2 CCD-numerical optimization criteria used

Criteria	1	2	3
Alkali or Acid percentage	in range	minimize	minimize
Temperature	in range	minimize	minimize
Time	in range	in range	in range
TL%	in range	in range	maximize
TS mg/g	in range	in range	in range
ES%	maximize	maximize	maximize

4.1.5 ANN-Hyper parameter optimization

The CCD-generated pretreatment model was validated using ANN. The optimization of three hyperparameters, hidden layer number (x1), hidden layer size (x2), and learning rate (x3), for generating the best-fitting ANN model was done using three metaheuristic algorithms (TLBO, PSO, and GA). The software used for this purpose was MATLAB R2020a (MathWorks, Inc, U.S.A). The response data obtained from CCD was standardized using z-score normalization (equation 4.2), while the factors data set was not normalized since it had lower diversity compared to the response data set.

$z = (x - \mu)/\sigma$ (Equation 4.2)

Where, z: is the standardized value or z-score, x: is the original data point; μ: is the mean of the data set, and σ: is the standard deviation of the data set.

4.1.5.1 Designing TLBO, PSO, and GA Algorithms

Three algorithms were created to generate a vector-x of size [1,3] as input arguments for the cost function, using decision variables x1, x2, and x3. The lower and upper bounds of the decision variables were set at [1,3,0.01] and [5,20,0.9] respectively. The maximum number of iterations was set at 100 with a termination tolerance of $1e^{-6}$. The algorithms were run at three

different population sizes: 30, 50, and 100. The algorithms generated new solutions by learning from the best solution, the mean solution, and two randomly selected solutions from the population. The worst solution in the population was then replaced with the new solution if it had better fitness. The algorithms stopped when the maximum number of iterations was reached. The convergence of the algorithms was monitored by recording the best cost value achieved at each iteration. The Matlab codes used are given as Tables AI.1 to AI.4 in Appendix-I.

4.1.5.2 Generating a Cost Function to train ANN with selected hyperparameters

A cost function was designed to take the metaheuristic generated vector-x (section 1.5.1) as the input argument, to train the ANN with CCD-derived factors and responses as input (x) and target (t) data respectively. x and t were preprocessed and randomly divided into three sets for training (60%), validation (20%), and testing (20%). Three different training algorithms, namely Levenberg-Marquardt backpropagation (trainlm), Bayesian Regularization backpropagation (trainbr), and scaled conjugate gradient backpropagation (trainscg) were employed individually, to train the ANN. The cost function evaluates the performance of the trained model using the mean squared error (MSE) and obtains the predicted values at the lowest MSE. The coefficient of determination (R^2), is measured manually to compare the fitness of each hybrid-ANN model. The hybrid-ANN models are named based on a specific convention. The first letter represents the type of metaheuristic algorithm used, while the second letter represents the type of ANN training algorithm employed. Additionally, the numeric value in the name corresponds to the population size utilized. For instance, if the TLBO optimization technique is applied to an ANN with a population size of 100 using the trainbr algorithm, the resulting model would be named TB100. The Matlab codes used are available in our Github repository. The Matlab codes used are given as Tables AI.1 to AI.4 in Appendix-I.

4.1.6 Operating cost of chemical requirement

The operating cost of the chemical requirement for the pretreatment in terms of $NaHCO_3$ usage is calculated. This calculation considers the optimal amount of $NaHCO_3$ determined at a liquid-to-solid ratio of 10, and the current market price of 99.99% pure food-grade $NaHCO_3$ in the local wholesale market of India, which is 0.43 USD per kilogram. However, readers should not confuse this with the total operating cost of the pretreatment.

4.2 Results and discussion

4.2.1 Fixed factor screening of various chemical pretreatments

Lignin removal is one of the measurable factors considered to assess the reduction of biomass recalcitrance. A high cellulose content, along with greater lignin removal, reportedly enhances the enzymatic saccharification of the pretreated biomass residue. Alkalis demonstrated better lignin removal efficiency than acids and salts at all concentration levels and temperatures, with 10% NaOH and 10% KOH achieving the highest efficiency (98%) at 125°C. KOH outperformed NaOH at lower temperatures. 10% NH_4OH, 5% Na_2CO_3, 10% H_2SO_4, and 10% succinic acid achieved the second-highest lignin removal efficiency (93.9%). At 125°C, the lignin removal efficiency (86.7%) of some acids (10% HCl, 5% citric acid, 5% succinic acid, 10% DL-Malic acid, and 10% Maleic acid) was comparable to that of NaOH and KOH at lower concentrations and temperatures. The alkalis showed varying lignin removal efficiencies in the order of KOH > NaOH > Na_2CO_3 > NH_4OH > $Ca(OH)_2$ > $NaHCO_3$. Similarly, the acids exhibited different lignin removal efficiencies in this order of H_2SO_4 > succinic acid > HCl > citric acid > DL-Malic acid > Maleic acid. Pretreatment with 0.1% KOH and $NaHCO_3$ at 50°C resulted in the least sugar loss (1.7 and 1.9 mg/g of CO, respectively), followed by 0.1% NaOH at the same temperature (2.2 mg/g of CO). $NaHCO_3$ caused less sugar loss even at higher concentrations and temperatures, indicating its effectiveness. For instance, 5% $NaHCO_3$ at 100°C resulted in a sugar loss of 2.9%. However, higher concentrations of KOH caused increased sugar loss even at lower temperatures. Pretreatment with 5% KOH at 50°C resulted in a sugar loss of 3%. Among the evaluated salt pretreatments (Na_2HPO_4, K_2HPO_4, tri-sodium citrate, and Na_2SO_4), sugar loss was reasonably lower in the range of 3.1–3.8 mg/g. Maleic acid caused the least sugar loss among the evaluated acids, followed by other organic acids. 0.1% maleic acid at 100°C resulted in a sugar loss of 3.5 mg/g of CO. In contrast, pretreatment with 10% HCl at 125°C resulted in the highest sugar loss of 61.7 mg/g, with H_2SO_4 causing a slightly lower sugar loss of 60.9 mg/g, This could be because H_2SO_4 causes dehydration of released sugars into furfural and 5-hydroxyl methyl furfural. The order of alkalis affecting the highest sugar loss is Na_2CO_3 > tri-sodium citrate > KH2PO4 > Na_2HPO_4 > KOH > $NaHCO_3$. On the other hand, a significant challenge lies in the amount of water required to neutralize the pretreated residue. All the alkalis and acids that showed a better reduction of recalcitrance, supporting higher enzymatic saccharification, also consumed a significant amount of water for neutralizing their respective pretreated residues. In comparison, the $NaHCO_3$ pretreated residue consumed a smaller amount of water. Four alkalis (NaOH, KOH, Na_2CO_3, and $NaHCO_3$) were selected for further

optimization based on their lignin removal efficiency, with the least possible sugar loss, thereby promoting a higher enzymatic saccharification yield. The lower retail price of these alkalis was also a factor for their consideration. Figures 4.1 and 4.2 illustrate the graphical representation of the results of fixed factor screening, and the corresponding tabulated values can be found in Tables 4.3 and 4.4. Figure 4.1 depicts the lignin removal efficiencies of the pretreatments and their effects on sugar loss, while Figure 4.2 illustrates the overall impact of each pretreatment, including their water consumption and enzymatic saccharification yields.

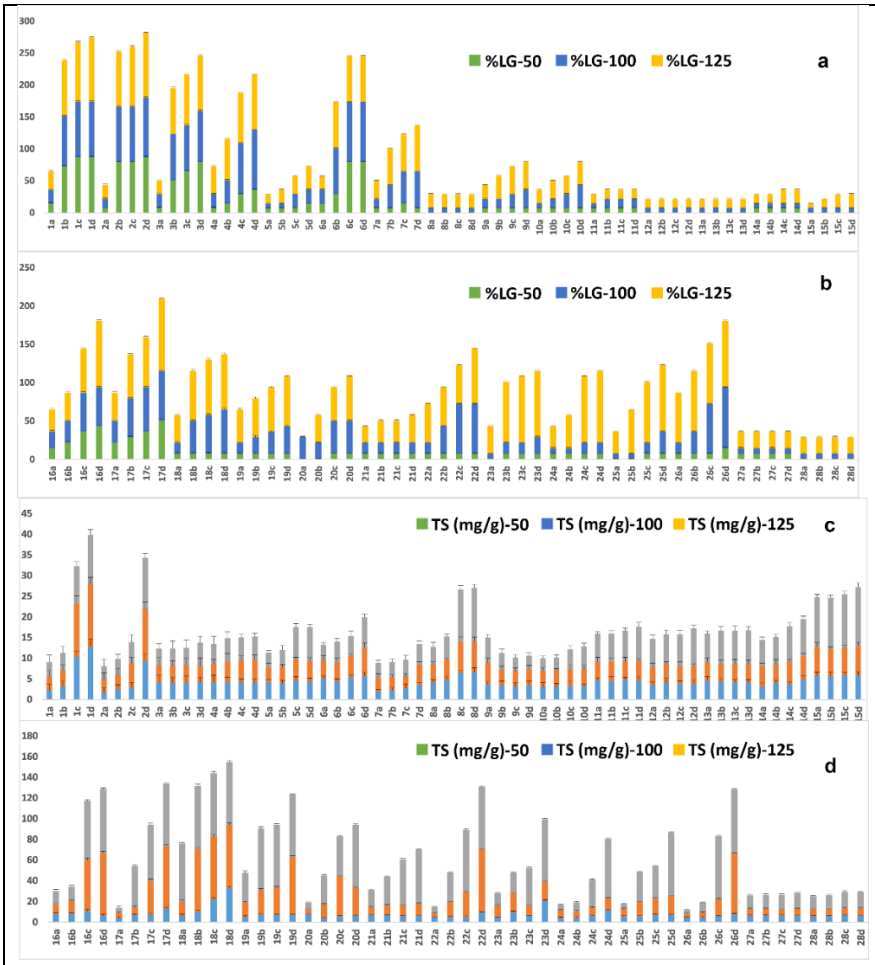

Figure 4.1 Lignin removal efficiency and the sugar loss effect of the screened pretreatments.
a) lignin removal efficiencies of alkalis and salts; b) lignin removal efficiencies of the acids; c) sugar loss with alkalis and salt pretreatments; d) sugar loss with acid pretreatments; % LG-50/100/125 = lignin removal % at the corresponding temperatures; TS (mg/g)-50/100/125 = total reducing sugar loss at the corresponding temperatures.

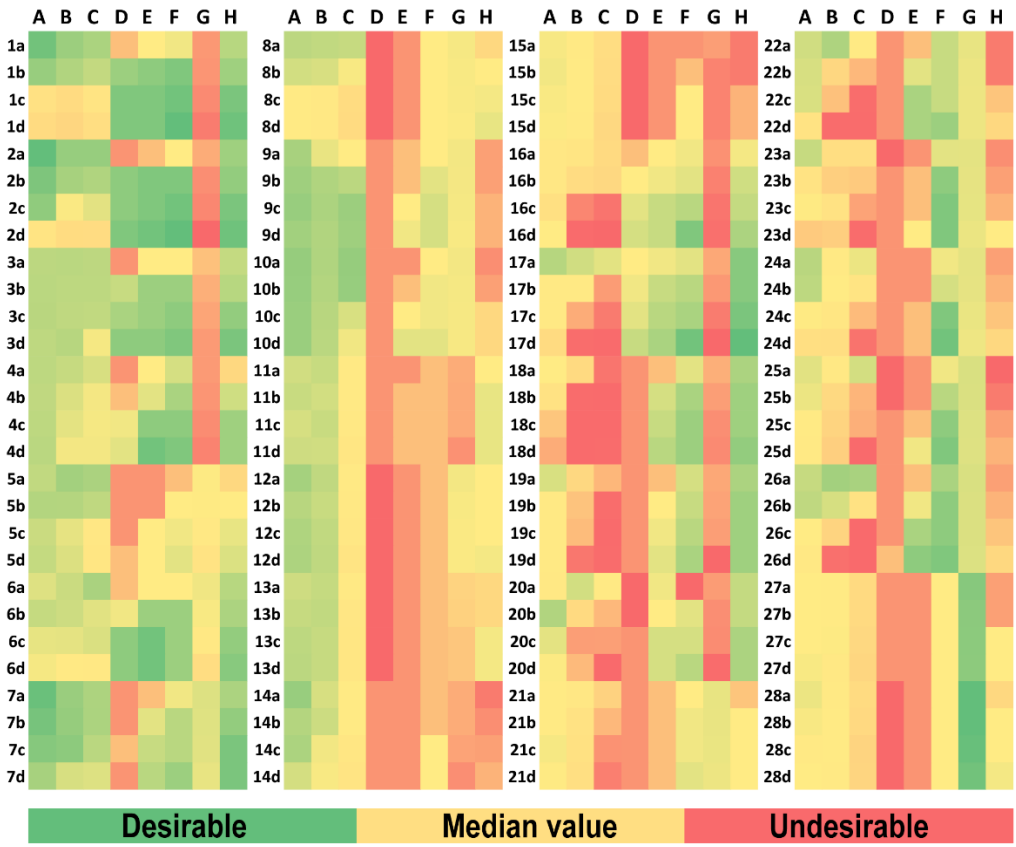

Figure 4.2 Heat map illustrating the impact of each chemical on reducing the recalcitrance of the CO

Note: Each number in the range of 1 – 28 represents a chemical screened for its efficiency in pretreating corncob outer (CO). The variables a, b, c, and d represent four different concentrations of each chemical used. The variable ABC represents the amount of reducing sugar loss (mg/ml) at three different pretreatment temperatures: 50 °C, 100 °C, and 125 °C. The variables D, E, and F represent the amount of lignin removal achieved at the three different temperatures mentioned earlier. The variable G represents the amount of water required (ml/g) to neutralize the pretreated CO residue. Lastly, the variable H represents the enzymatic saccharification percentage. A three-color scale is used, where green represents the desired outcome, red denotes the undesired outcome, and yellow represents the percentile mid-value of the dataset. In this scale, the lowest sugar loss, highest lignin removal, lowest water usage, and highest saccharification rate are considered as the desirable factors.

Table 4.3 Fixed factor screening of chemicals for their lignin removal efficiency

Pretreatment	% LG-50	% LG-100	% LG-125
1a	14.45 ± 1.5	21.67 ± 1.7	28.89 ± 1.7
1b	72.23 ± 1.4	79.45 ± 1.4	86.67 ± 1.6
1c	86.67 ± 1.4	86.67 ± 1.8	93.9 ± 1.2
1d	86.67 ± 1.9	86.67 ± 1.6	101.12 ± 1.3
2a	7.22 ± 1.2	14.45 ± 1.5	21.67 ± 1.7
2b	79.45 ± 1.1	86.67 ± 1.6	86.67 ± 1.2
2c	79.45 ± 1.2	86.67 ± 1.5	93.9 ± 1.9
2d	86.67 ± 1.7	93.9 ± 1.7	101.12 ± 1.1
3a	7.22 ± 1.7	21.67 ± 2	21.67 ± 1.2
3b	50.56 ± 1.2	72.23 ± 1.1	72.23 ± 1.9
3c	65.01 ± 1.6	72.23 ± 1.9	79.45 ± 2
3d	79.45 ± 1.3	79.45 ± 1.9	86.67 ± 1.5
4a	7.22 ± 1.7	21.67 ± 1.1	43.34 ± 1.9
4b	14.45 ± 1.1	36.11 ± 2	65.01 ± 1.6
4c	28.89 ± 0.8	79.45 ± 1.2	79.45 ± 0.8
4d	36.11 ± 0.9	93.9 ± 1.1	86.67 ± 0.8
5a	7.22 ± 0.5	7.22 ± 1.1	14.45 ± 0.5
5b	7.22 ± 0.8	7.22 ± 0.7	21.67 ± 1.1
5c	7.22 ± 1	21.67 ± 0.5	28.89 ± 0.9
5d	14.45 ± 0.9	21.67 ± 0.9	36.11 ± 0.7
6a	14.45 ± 0.8	21.67 ± 1	21.67 ± 0.6
6b	28.89 ± 0.7	72.23 ± 1.1	72.23 ± 0.8
6c	79.45 ± 0.6	93.9 ± 0.6	72.23 ± 1.2
6d	79.45 ± 0.9	93.9 ± 1.1	72.23 ± 0.8
7a	7.22 ± 0.5	14.45 ± 1.1	28.89 ± 0.6
7b	7.22 ± 0.7	36.11 ± 0.6	57.78 ± 0.7
7c	14.45 ± 1.1	50.56 ± 0.8	57.78 ± 1.1
7d	7.22 ± 0.6	57.78 ± 0.8	72.23 ± 0.9
8a	0	7.22 ± 0.7	21.67 ± 1.1
8b	0	7.22 ± 0.6	21.67 ± 0.6
8c	0	7.22 ± 1.1	21.67 ± 0.9
8d	0	7.22 ± 1.1	21.67 ± 0.8
9a	7.22 ± 0.8	14.45 ± 1.1	21.67 ± 0.8
9b	7.22 ± 1.1	14.45 ± 1	36.11 ± 1
9c	7.22 ± 0.9	21.67 ± 0.8	43.34 ± 0.7
9d	7.22 ± 1.1	28.89 ± 1	43.34 ± 0.7
10a	7.22 ± 1	7.22 ± 0.9	21.67 ± 0.5
10b	7.22 ± 0.8	14.45 ± 0.5	28.89 ± 0.6
10c	7.22 ± 1.2	21.67 ± 1.1	28.89 ± 0.9
10d	7.22 ± 0.6	36.11 ± 1.1	36.11 ± 0.9
11a	7.22 ± 0.6	7.22 ± 1.1	14.45 ± 0.5
11b	7.22 ± 1.1	14.45 ± 1	14.45 ± 0.7
11c	7.22 ± 0.5	14.45 ± 1	14.45 ± 0.6
11d	7.22 ± 1.1	14.45 ± 0.5	14.45 ± 1.1
12a	0	7.22 ± 1	14.45 ± 1
12b	0	7.22 ± 0.7	14.45 ± 1.1
12c	0	7.22 ± 1.1	14.45 ± 1
12d	0	7.22 ± 0.6	14.45 ± 0.9
13a	0	7.22 ± 1.1	14.45 ± 0.7
13b	0	7.22 ± 0.9	14.45 ± 1
13c	0	7.22 ± 1.1	14.45 ± 1.2
13d	0	7.22 ± 1.1	14.45 ± 0.9

14a	7.22 ± 1	7.22 ± 0.7	14.45 ± 0.7
14b	7.22 ± 0.8	7.22 ± 1.2	14.45 ± 0.6
14c	7.22 ± 0.5	7.22 ± 0.5	21.67 ± 1
14d	7.22 ± 0.9	7.22 ± 0.7	21.67 ± 0.7
15a	0	7.22 ± 1.1	7.22 ± 0.7
15b	0	7.22 ± 0.6	14.45 ± 0.6
15c	0	7.22 ± 0.6	21.67 ± 0.8
15d	0	7.22 ± 0.8	21.67 ± 1
16a	14.45 ± 0.7	21.67 ± 0.5	28.89 ± 0.7
16b	21.67 ± 1.2	28.89 ± 1.2	36.11 ± 1
16c	36.11 ± 0.7	50.56 ± 0.8	57.78 ± 1.1
16d	43.34 ± 1	50.56 ± 0.7	86.67 ± 1.1
17a	21.67 ± 1.2	28.89 ± 0.8	36.11 ± 1.1
17b	28.89 ± 0.7	50.56 ± 0.9	57.78 ± 0.6
17c	36.11 ± 0.5	57.78 ± 0.8	65.01 ± 1
17d	50.56 ± 0.7	65.01 ± 1	93.9 ± 1.2
18a	7.22 ± 0.8	14.45 ± 1.2	36.11 ± 1.1
18b	7.22 ± 1.1	43.34 ± 0.8	65.01 ± 0.7
18c	7.22 ± 0.7	50.56 ± 0.7	72.23 ± 1.1
18d	7.22 ± 0.8	57.78 ± 0.5	72.23 ± 0.9
19a	7.22 ± 0.7	14.45 ± 0.6	43.34 ± 0.9
19b	7.22 ± 0.7	21.67 ± 0.8	50.56 ± 1.2
19c	7.22 ± 0.7	28.89 ± 1.1	57.78 ± 1.1
19d	7.22 ± 0.9	36.11 ± 1	65.01 ± 0.7
20a	0	28.89 ± 1.2	0 ± 0.8
20b	0	21.67 ± 1	36.11 ± 0.8
20c	7.22 ± 0.9	43.34 ± 1.1	43.34 ± 0.5
20d	7.22 ± 1	43.34 ± 0.6	57.78 ± 1.2
21a	7.22 ± 0.6	14.45 ± 0.9	21.67 ± 0.8
21b	7.22 ± 0.9	14.45 ± 0.6	28.89 ± 0.7
21c	7.22 ± 1.2	14.45 ± 1	28.89 ± 1.1
21d	7.22 ± 1.1	14.45 ± 0.6	36.11 ± 0.5
22a	7.22 ± 1.1	14.45 ± 0.8	50.56 ± 0.9
22b	7.22 ± 0.7	36.11 ± 0.7	50.56 ± 0.8
22c	7.22 ± 1.1	65.01 ± 0.6	50.56 ± 1
22d	7.22 ± 1	65.01 ± 0.5	72.23 ± 0.7
23a	0	7.22 ± 1	36.11 ± 0.8
23b	7.22 ± 0.8	14.45 ± 1	79.45 ± 1
23c	7.22 ± 0.7	14.45 ± 0.8	86.67 ± 0.7
23d	7.22 ± 0.7	21.67 ± 0.7	86.67 ± 0.7
24a	7.22 ± 1	7.22 ± 0.8	28.89 ± 0.8
24b	7.22 ± 0.6	7.22 ± 1.1	43.34 ± 0.9
24c	7.22 ± 0.7	14.45 ± 0.9	86.67 ± 1
24d	7.22 ± 1	14.45 ± 1.2	93.9 ± 1.2
25a	0	7.22 ± 0.9	28.89 ± 1.2
25b	0	7.22 ± 0.9	57.78 ± 1
25c	7.22 ± 1.2	14.45 ± 0.8	79.45 ± 0.5
25d	7.22 ± 0.8	28.89 ± 0.9	86.67 ± 1.2
26a	7.22 ± 0.6	14.45 ± 0.7	65.01 ± 0.7
26b	7.22 ± 0.9	28.89 ± 1.2	79.45 ± 0.8
26c	7.22 ± 0.5	65.01 ± 0.9	79.45 ± 1.1
26d	14.45 ± 1.1	79.45 ± 0.6	86.67 ± 0.9
27a	7.22 ± 1.1	7.22 ± 0.6	21.67 ± 0.8
27b	7.22 ± 0.9	7.22 ± 0.9	21.67 ± 0.6

27c	7.22 ± 1	7.22 ± 1	21.67 ± 0.9
27d	7.22 ± 0.7	7.22 ± 1.2	21.67 ± 0.6
28a	0	7.22 ± 1	21.67 ± 0.9
28b	0	7.22 ± 0.8	21.67 ± 1
28c	0	7.22 ± 0.5	21.67 ± 0.7
28d	0	7.22 ± 0.8	21.67 ± 0.8

Note: % LG 50, % LG 100, and % LG 125 indicate the percentage of lignin removed at the respective temperatures; under pretreatment column, the number represents a chemical (information is given in Table 4. 1), and the letters a,b,c,d represents the four different concentrations of each chemical used

Table 4.4 Fixed factor screening of chemicals for their sugar degrading effect

Pretreatment	TS (mg/g)-50	TS (mg/g)-100	TS (mg/g)-125
1a	2.2 ± 1.5	3.3 ± 1.7	3.7 ± 1.7
1b	3.2 ± 1.4	3.8 ± 1.4	4.3 ± 1.6
1c	10.4 ± 1.4	12.8 ± 1.8	9.1 ± 1.2
1d	12.8 ± 1.9	15.2 ± 1.6	11.8 ± 1.3
2a	1.7 ± 1.2	3.2 ± 1.5	3.1 ± 1.7
2b	2.5 ± 1.1	3.6 ± 1.6	3.8 ± 1.2
2c	3 ± 1.2	5.8 ± 1.5	5.2 ± 1.9
2d	9.3 ± 1.7	12.6 ± 1.7	12.3 ± 1.1
3a	4.1 ± 1.7	4.1 ± 2	4.1 ± 1.2
3b	4.1 ± 1.2	4.2 ± 1.1	4.2 ± 1.9
3c	4 ± 1.6	4.2 ± 1.9	4.3 ± 2
3d	4.2 ± 1.3	4 ± 1.9	5.7 ± 1.5
4a	4.2 ± 1.7	4.4 ± 1.1	4.9 ± 1.9
4b	4.2 ± 1.1	5 ± 2	5.6 ± 1.6
4c	4.2 ± 0.8	5.2 ± 1.2	5.7 ± 0.8
4d	4.1 ± 0.9	5.6 ± 1.1	5.6 ± 0.8
5a	4.3 ± 0.5	3.5 ± 1.1	3.7 ± 0.5
5b	3.9 ± 0.8	3.9 ± 0.7	4.2 ± 1.1
5c	4.5 ± 1	5.2 ± 0.5	7.8 ± 0.9
5d	4.4 ± 0.9	5 ± 0.9	8.2 ± 0.7
6a	5 ± 0.8	4.5 ± 1	3.6 ± 0.6
6b	4.4 ± 0.7	4.6 ± 1.1	5.1 ± 0.8
6c	5.3 ± 0.6	5.2 ± 0.6	4.9 ± 1.2
6d	5.7 ± 0.9	7 ± 1.1	7.3 ± 0.8
7a	1.9 ± 0.5	3.2 ± 1.1	3.7 ± 0.6
7b	2.3 ± 0.7	3.1 ± 0.6	3.7 ± 0.7
7c	2.7 ± 1.1	2.9 ± 0.8	4.1 ± 1.1
7d	3.6 ± 0.6	4.8 ± 0.8	5 ± 0.9
8a	4.1 ± 0.7	4.3 ± 0.7	4.4 ± 1.1
8b	4.7 ± 0.9	4.9 ± 0.6	5.7 ± 0.6
8c	6.5 ± 0.6	7.5 ± 1.1	12.6 ± 0.9
8d	6.6 ± 1.2	7.5 ± 1.1	13 ± 0.8
9a	3.6 ± 0.8	5.3 ± 1.1	6.1 ± 0.8

9b	3.3 ± 1.1	3.8 ± 1	4.1 ± 1
9c	3.2 ± 0.9	3.7 ± 0.8	3.3 ± 0.7
9d	3.4 ± 1.1	3.8 ± 1	3.4 ± 0.7
10a	3.1 ± 1	3.8 ± 0.9	3.1 ± 0.5
10b	3.1 ± 0.8	3.9 ± 0.5	3.1 ± 0.6
10c	3.2 ± 1.2	4 ± 1.1	4.9 ± 0.9
10d	3.2 ± 0.6	4.1 ± 1.1	5.5 ± 0.9
11a	4.7 ± 0.6	4.4 ± 1.1	6.8 ± 0.5
11b	4.4 ± 1.1	4.7 ± 1	6.8 ± 0.7
11c	4.8 ± 0.5	4.4 ± 1	7.4 ± 0.6
11d	4.6 ± 1.1	4.7 ± 0.5	8.3 ± 1.1
12a	3.5 ± 0.8	4.2 ± 1	6.9 ± 1
12b	4 ± 1.1	4.5 ± 0.7	7.3 ± 1.1
12c	3.8 ± 0.7	4.3 ± 1.1	7.8 ± 1
12d	3.7 ± 1	4.2 ± 0.6	9.3 ± 0.9
13a	4.6 ± 0.9	4.4 ± 1.1	7 ± 0.7
13b	4.4 ± 0.7	4.3 ± 0.9	8 ± 1
13c	4.2 ± 0.6	4.4 ± 1.1	8.2 ± 1.2
13d	4.1 ± 0.7	4.4 ± 1.1	8.3 ± 0.9
14a	3.2 ± 1	4.9 ± 0.7	6.4 ± 0.7
14b	3.9 ± 0.8	4.6 ± 1.2	6.7 ± 0.6
14c	3.7 ± 0.5	5.6 ± 0.5	8.5 ± 1
14d	4.8 ± 0.9	5.7 ± 0.7	9 ± 0.7
15a	5.7 ± 0.9	7 ± 1.1	12 ± 0.7
15b	5.6 ± 1	6.6 ± 0.6	12.5 ± 0.6
15c	5.8 ± 0.9	6.7 ± 0.6	13 ± 0.8
15d	5.8 ± 0.9	7.1 ± 0.8	14.2 ± 1
16a	7.8 ± 0.7	8.8 ± 0.5	13.3 ± 0.7
16b	7.9 ± 1.2	12.3 ± 1.2	14.1 ± 1
16c	10.7 ± 0.7	49.5 ± 0.8	57.1 ± 1.1
16d	6 ± 1	60.8 ± 0.7	61.7 ± 1.1
17a	4 ± 1.2	4.7 ± 0.8	5.2 ± 1.1
17b	6.8 ± 0.7	7.2 ± 0.9	40.2 ± 0.6
17c	7.1 ± 0.5	33 ± 0.8	54.1 ± 1
17d	12.8 ± 0.7	60.3 ± 1	60.9 ± 1.2
18a	6 ± 0.8	13.3 ± 1.2	56.6 ± 1.1
18b	10 ± 1.1	60.6 ± 0.8	61 ± 0.7
18c	21.9 ± 0.7	61 ± 0.7	61.1 ± 1.1
18d	33 ± 0.8	60.9 ± 0.5	60.7 ± 0.9
19a	4.9 ± 0.7	14.3 ± 0.6	28.4 ± 0.9
19b	7.2 ± 0.7	23.3 ± 0.8	60.2 ± 1.2
19c	7 ± 0.7	26.5 ± 1.1	60.9 ± 1.1
19d	7 ± 0.9	55.9 ± 1	60.5 ± 0.7
20a	7.6 ± 1	4.7 ± 1.2	7 ± 0.8
20b	3.8 ± 0.9	13.3 ± 1	28 ± 0.8
20c	5.2 ± 0.9	39.3 ± 1.1	38.6 ± 0.5

20d	5.8 ± 1	26.9 ± 0.6	61.4 ± 1.2
21a	6.7 ± 0.6	7.6 ± 0.9	17 ± 0.8
21b	6.4 ± 0.9	9.8 ± 0.6	28.1 ± 0.7
21c	5.7 ± 1.2	10.5 ± 1	44.4 ± 1.1
21d	5.9 ± 1.1	11.4 ± 0.6	52.6 ± 0.5
22a	4.7 ± 1.1	3.8 ± 0.8	6.4 ± 0.9
22b	4.8 ± 0.7	14.8 ± 0.7	28.2 ± 0.8
22c	4.9 ± 1.1	24.2 ± 0.6	60.2 ± 1
22d	9.4 ± 1	60.7 ± 0.5	60.6 ± 0.7
23a	4.4 ± 0.5	11.9 ± 1	11.7 ± 0.8
23b	9.8 ± 0.8	18.1 ± 1	20.1 ± 1
23c	5.9 ± 0.7	9.8 ± 0.8	36.8 ± 0.7
23d	20.2 ± 0.7	18.6 ± 0.7	60.6 ± 0.7
24a	4 ± 1	7 ± 0.8	5.4 ± 0.8
24b	4.2 ± 0.6	6 ± 1.1	9 ± 0.9
24c	5.9 ± 0.7	8.5 ± 0.9	26.6 ± 1
24d	11.3 ± 1	11.5 ± 1.2	57.7 ± 1.2
25a	5.1 ± 0.6	7.4 ± 0.9	4.7 ± 1.2
25b	5.4 ± 1.1	14 ± 0.9	29.3 ± 1
25c	6.6 ± 1.2	15.8 ± 0.8	31.7 ± 0.5
25d	7 ± 0.8	18.1 ± 0.9	61.2 ± 1.2
26a	4.4 ± 0.6	3.5 ± 0.7	3.6 ± 0.7
26b	4.2 ± 0.9	4.8 ± 1.2	9.8 ± 0.8
26c	5.9 ± 0.5	16.1 ± 0.9	61.4 ± 1.1
26d	7.5 ± 1.1	59 ± 0.6	61.5 ± 0.9
27a	6.1 ± 1.1	6.6 ± 0.6	13.2 ± 0.8
27b	6.1 ± 0.9	6.7 ± 0.9	13.5 ± 0.6
27c	6.2 ± 1	5.9 ± 1	14.3 ± 0.9
27d	5.7 ± 0.7	7.4 ± 1.2	15.1 ± 0.6
28a	5.4 ± 0.9	6.8 ± 1	13 ± 0.9
28b	5.7 ± 1.2	6.5 ± 0.8	13.8 ± 1
28c	6.8 ± 1.1	6.7 ± 0.5	15.8 ± 0.7
28d	6.1 ± 1	7 ± 0.8	15.7 ± 0.8

Note: TS represents the total reducing sugar

4.2.2 Regular two-level factorial design

The ANOVA analysis showed that alkali concentration, temperature, and time had significant effects on the responses with the respective P-values < 0.05 and higher f-values, while the L/S ratio had a negligible effect. The R^2 values for all responses were between 0.96 and 0.99, and the predicted R^2 values were in good agreement with the Adjusted R^2 values (difference < 0.2). All the models achieved adequate signal-to-noise ratios (adequate precision >4) (Tables 4.5, and 4.6). The linear regression model equations for all the responses of each pretreatment are shown as coded equations 4.3 to 4.14. NaOH and KOH had higher lignin removal efficiencies

(>98%) than Na_2CO_3 and $NaHCO_3$, with Na_2CO_3 achieving only 70.48% lignin removal at 84°C. However, Na_2CO_3 had higher sugar loss (4.20 mg/g) than NaOH and KOH. $NaHCO_3$ achieved 54.74% lignin removal with the least amount of sugar loss (3.53 mg/g) at 92.05 °C, it exhibited the least amount of sugar loss even at such higher temperature. The amount of water needed to neutralize CO-residue was the least for $NaHCO_3$ (250-280 ml/g) and the highest for NaOH and KOH (350-380 ml/g), and the same for the Na_2CO_3 pretreatment is in the range of 290-310 ml/g. Optimized solutions for each design are shown in Figure 4.3

$$LG - NaOH = 125.619 + 60.045 \times A + 8.525 \times B + 7.26 \times C \quad \text{(equation 4.3)}$$

$$TS - NaOH = 4.4725 + 2.6325 \times A + 0.67875 \times B + 0.23625 \times C \quad \text{(equation 4.4)}$$

$$SR - NaOH = 72.8 + -13.05 \times A + -1.885 \times B + -1.57 \times C \quad \text{(equation 4.5)}$$

$$LG - KOH = 133.124 + 70.2375 \times A + 9.22375 \times B + 7.49375 \times C \quad \text{(equation 4.6)}$$

$$TS - KOH = 5.8475 + 3.6225 \times A + 0.64875 \times B + 0.28875 \times C \quad \text{(equation 4.7)}$$

$$SR - KOH = 71.0683 + -15.315 \times A + -2.03 \times B + -1.625 \times C \quad \text{(equation 4.8)}$$

$$LG - Na_2CO_3 = 128.449 + 76.065 \times A + 10.595 \times B + 7.43 \times C \quad \text{(equation 4.9)}$$

$$SR - Na_2CO_3 = 6.89917 + 3.57 \times A + 0.5275 \times B + 0.38 \times C \quad \text{(equation 4.10)}$$

$$SR - Na_2CO_3 = 71.9558 + -16.5525 \times A + -2.30875 \times B + -1.61875 \times C \quad \text{(equation 4.11)}$$

$$LG - NaHCO_3 = 119.347 + 77.3475 \times A + 12.3087 \times B + 6.52875 \times C \quad \text{(equation 4.12)}$$

$$TS - NaHCO_3 = 6.4575 + 3.51 \times A + 0.475 \times B + 0.325 \times C \quad \text{(equation 4.13)}$$

$$SR - NaHCO_3 = 73.9358 + -16.8225 \times A + -2.66875 \times B + -1.42375 \times C \quad \text{(equation 4.14)}$$

Where, the initial numeric value represents the intercept term, and the multiplied numerics are the coefficients of the respective factors. The intercept term represents the expected response when all the factors are at their baseline (or zero) levels, and the coefficients indicate the change in the response due to a one-unit change in the corresponding factor while holding all the other factors constant.

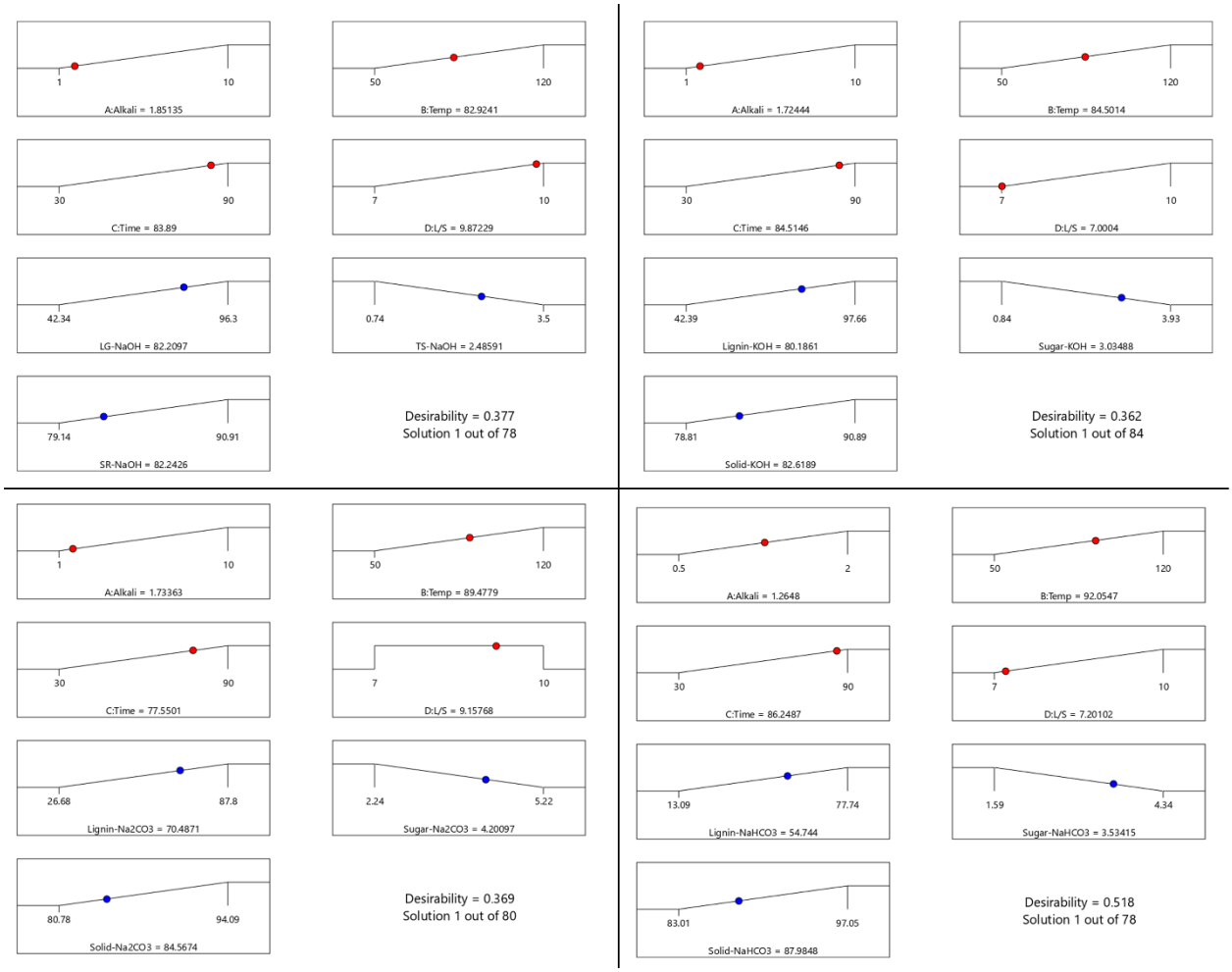

Figure 3.3 Numerical representation of the optimization results of Regular two-level factorial designs

Note: The two numerals given on each ramp are the lower and upper limits of the factors and responses; the red dot represents the optimized value of the factors, and the blue dot represents the corresponding optimized response.

Table 4.5 ANOVA for Regular two-level factorial design

	Sum of Squares	**df**	**Mean Square**	**F-value**	**p-value**	
Model	1804.27	3	601.42	63.32	0.0008	**LG-NaOH**
A-Alkali	801.20	1	801.20	84.35	0.0008	
B-Temp	581.40	1	581.40	61.21	0.0014	
C-Time	421.66	1	421.66	44.39	0.0026	
Residual	37.99	4	9.50			
Cor Total	1842.26	7				
Model	5.67	3	1.89	47.91	0.0014	**TS-NaOH**
A-Alkali	1.54	1	1.54	39.02	0.0033	
B-Temp	3.69	1	3.69	93.40	0.0006	
C-Time	0.4465	1	0.4465	11.31	0.0282	
Residual	0.1579	4	0.0395			

Cor Total	5.83	7				
Model	85.99	3	28.66	63.52	0.0008	**SR-NaOH**
A-Alkali	37.85	1	37.85	83.87	0.0008	
B-Temp	28.43	1	28.43	62.99	0.0014	
C-Time	19.72	1	19.72	43.70	0.0027	
Residual	1.81	4	0.4513			
Cor Total	87.79	7				
Model	2226.16	3	742.05	89.27	0.0004	**LG-KOH**
A-Alkali	1096.29	1	1096.29	131.89	0.0003	
B-Temp	680.62	1	680.62	81.88	0.0008	
C-Time	449.25	1	449.25	54.05	0.0018	
Residual	33.25	4	8.31			
Cor Total	2259.41	7				
Model	6.95	3	2.32	34.96	0.0025	**TS-KOH**
A-Alkali	2.92	1	2.92	44.01	0.0027	
B-Temp	3.37	1	3.37	50.81	0.0020	
C-Time	0.6670	1	0.6670	10.07	0.0338	
Residual	0.2650	4	0.0663			
Cor Total	7.22	7				
Model	106.21	3	35.40	94.58	0.0004	**SR-KOH**
A-Alkali	52.12	1	52.12	139.24	0.0003	
B-Temp	32.97	1	32.97	88.07	0.0007	
C-Time	21.13	1	21.13	56.43	0.0017	
Residual	1.50	4	0.3743			
Cor Total	107.71	7				
Model	2625.42	3	875.14	513.09	< 0.0001	**LG-** Na_2CO_3
A-Alkali	1285.75	1	1285.75	753.82	< 0.0001	
B-Temp	898.03	1	898.03	526.51	< 0.0001	
C-Time	441.64	1	441.64	258.93	< 0.0001	
Residual	6.82	4	1.71			
Cor Total	2632.25	7				
Model	6.21	3	2.07	54.90	0.0010	**TS-** Na_2CO_3
A-Alkali	2.83	1	2.83	75.07	0.0010	
B-Temp	2.23	1	2.23	59.01	0.0015	
C-Time	1.16	1	1.16	30.62	0.0052	
Residual	0.1509	4	0.0377			
Cor Total	6.36	7				
Model	124.49	3	41.50	501.10	< 0.0001	**SR-**Na_2CO_3
A-Alkali	60.89	1	60.89	735.22	< 0.0001	
B-Temp	42.64	1	42.64	514.93	< 0.0001	
C-Time	20.96	1	20.96	253.14	< 0.0001	
Residual	0.3312	4	0.0828			
Cor Total	124.82	7				
Model	2882.51	3	960.84	398.60	< 0.0001	**LG-**$NaHCO_3$
A-Alkali	1329.47	1	1329.47	551.53	< 0.0001	
B-Temp	1212.04	1	1212.04	502.81	< 0.0001	
C-Time	341.00	1	341.00	141.46	0.0003	
Residual	9.64	4	2.41			
Cor Total	2892.16	7				
Model	5.39	3	1.80	67.42	0.0007	**TS-**$NaHCO_3$
A-Alkali	2.74	1	2.74	102.78	0.0005	
B-Temp	1.80	1	1.80	67.76	0.0012	
C-Time	0.8450	1	0.8450	31.72	0.0049	

Residual	0.1065	4	0.0266			
Cor Total	5.49	7				
Model	136.08	3	45.36	406.87	< 0.0001	**SR-**$NaHCO_3$
A-Alkali	62.89	1	62.89	564.08	< 0.0001	
B-Temp	56.98	1	56.98	511.07	< 0.0001	
C-Time	16.22	1	16.22	145.46	0.0003	
Residual	0.4460	4	0.1115			
Cor Total	136.53	7				

Note: the sum of squares is Type III partial; LG = percent of lignin removal; TS = total reducing sugars lost; SR = solid recovery percent; cor total = corrected total; df = degree of freedom.

Table 4.6 Regular two-level factorial design fitness statistics of each model

Std. Dev.	3.08	**R^2**	0.9794	**LG-NaOH**
Mean	68.91	**Adjusted R^2**	0.9639	
C.V. %	4.47	**Predicted R^2**	0.9175	
		Adeq Precision	23.6713	
Std. Dev.	0.1987	**R^2**	0.9729	**TS-NaOH**
Mean	1.99	**Adjusted R^2**	0.9526	
C.V. %	10.00	**Predicted R^2**	0.8917	
		Adeq Precision	19.2749	
Std. Dev.	0.6718	**R^2**	0.9794	**SR-NaOH**
Mean	85.13	**Adjusted R^2**	0.9640	
C.V. %	0.7891	**Predicted R^2**	0.9178	
		Adeq Precision	23.7053	
Std. Dev.	2.88	**R^2**	0.9853	**LG-KOH**
Mean	66.79	**Adjusted R^2**	0.9742	
C.V. %	4.32	**Predicted R^2**	0.9411	
		Adeq Precision	27.8849	
Std. Dev.	0.2574	**R^2**	0.9633	**TS-KOH**
Mean	2.43	**Adjusted R^2**	0.9357	
C.V. %	10.61	**Predicted R^2**	0.8531	
		Adeq Precision	16.9350	
Std. Dev.	0.6118	**R^2**	0.9861	**SR-KOH**
Mean	85.53	**Adjusted R^2**	0.9757	
C.V. %	0.7153	**Predicted R^2**	0.9444	
		Adeq Precision	28.6971	
Std. Dev.	1.31	**R^2**	0.9974	**LG-** Na_2CO_3
Mean	56.61	**Adjusted R^2**	0.9955	
C.V. %	2.31	**Predicted R^2**	0.9896	
		Adeq Precision	66.4929	
Std. Dev.	0.1942	**R^2**	0.9763	**TS-** Na_2CO_3
Mean	3.53	**Adjusted R^2**	0.9585	
C.V. %	5.51	**Predicted R^2**	0.9052	
		Adeq Precision	21.8799	
Std. Dev.	0.2878	**R^2**	0.9973	**SR-**Na_2CO_3
Mean	87.59	**Adjusted R^2**	0.9954	
C.V. %	0.3285	**Predicted R^2**	0.9894	
		Adeq Precision	65.7173	
Std. Dev.	1.55	**R^2**	0.9967	**LG-**$NaHCO_3$
Mean	46.30	**Adjusted R^2**	0.9942	
C.V. %	3.35	**Predicted R^2**	0.9867	

		Adeq Precision	57.8018	
Std. Dev.	0.1632	**R^2**	0.9806	**TS-**$NaHCO_3$
Mean	3.14	**Adjusted R^2**	0.9661	
C.V. %	5.19	**Predicted R^2**	0.9224	
		Adeq Precision	24.0020	
Std. Dev.	0.3339	**R^2**	0.9967	**SR-**$NaHCO_3$
Mean	89.82	**Adjusted R^2**	0.9943	
C.V. %	0.3717	**Predicted R^2**	0.9869	
		Adeq Precision	58.4178	

4.2.3 Central composite design

The ANOVA analysis reveals that A, B, C, AB, AC, BC, A^2, B^2, and C^2 are significant factors for lignin removal, while A, B, AB, AC, BC, B^2, and C^2 are significant for sugar loss. Additionally, A, B, C, AC, BC, and B^2 are significant factors for enzymatic saccharification, as supported by the corresponding P-values that are less than 0.05 and the higher f-values obtained. The Predicted R^2 values were reasonably close to the Adjusted R^2 values, with a difference of less than 0.2. Additionally, all the models had adequate signal-to-noise ratios, with an adequate precision > 4 (Tables 4.7, 4.8, 4.9). The equations labelled 4.15, 4.16, and 4.17 correspond to the coded quadratic model for the three responses Y1, Y2, and Y3, respectively.

$$Y1 = 21.3877 + 5.94214 * A + 21.8429 * B + 2.70257 * C + 4.92919 * AB + 1.97381 * AC + 3.27941 * BC + -1.1237 * A^2 + 11.1678 * B^2 + 1.91545 * C^2 \quad \text{-- (equation 4.15)}$$

$$Y2 = 5.18103 + -0.460346 * A + 0.757998 * B + -0.005096 * C + -0.62821 * AB + -0.264525 * AC + -0.203998 * BC + -0.0609164 * A^2 + -0.423576 * B^2 + -0.215346 * C^2 \quad \text{--(equation 4.16)}$$

$$Y3 = 78.2868 + 3.1488 * A + 9.52109 * B + 2.1499 * C + -0.254723 * AB + -1.03661 * AC + -0.827779 * BC + -0.621959 * A^2 + -4.67555 * B^2 + -0.421339 * C^2 \quad \text{-- (equation 4.17)}$$

The interaction plots between model responses and the factors indicated that alkali concentration alone had a minimal but linear improvement on the responses TL%, TS, and ES, in comparison to temperature. The effect of temperature on these responses was very pronounced; both TL% and ES% exhibited exponential increases as the temperature rose, even up to 120 °C. In contrast, TS experienced a steep decline as the temperature increased from 90 °C. While it was anticipated that temperature would have a negative impact on free sugars, the degree of this sharp decline in sugar concentration came as a surprise (Figure 4.4).

Table 4.7 CCD design layout

Std order	Run order	Factor 1 A:Alkali %	Factor 2 B:Temperature Degrees Celsius	Factor 3 C:Time minutes	Response 1 Y1 %	Response 2 Y2 mg/g of CO	Response 3 Y3 %
1	13	0.5	60	30	12.68	3.05138	54.8686
2	18	1.5	60	30	11.1629	4.00047	64.9749
3	10	0.5	100	30	40.4423	6.39028	76.7402
4	17	1.5	100	30	57.892	4.6473	84.0394
5	20	0.5	60	90	8.16009	4.02037	64.3652
6	2	1.5	60	90	13.7883	3.73213	68.5368
7	11	0.5	100	90	48.2901	6.36405	81.1375
8	8	1.5	100	90	74.385	3.7422	86.0784
9	12	0.5	80	60	14.37	5.52053	75.081
10	19	1.5	80	60	26.1357	4.62105	80.051
11	15	1	60	60	10.939	4.08788	63.5319
12	14	1	100	60	54.1498	5.32838	83.4929
13	5	1	80	30	21.0023	4.8265	76.7645
14	16	1	80	90	25.5817	5.00622	78.7687
15	7	1	80	60	21.1878	5.37488	78.1539
16	6	1	80	60	21.784	5.0766	78.3088
17	9	1	80	60	21.5962	5.0628	77.1149
18	4	1	80	60	21.385	5.2062	78.5999
19	1	1	80	60	21.2911	5.36198	79.6265
20	3	1	80	60	21.1268	5.20102	78.3118

Table 4.8 ANOVA for CCD of *$NaHCO_3$* pretreatment optimization

Source	Sum of Squares	df	Mean Square	F-value	p-value	
Model (Y1)	6197.23	9	688.58	5856.00	< 0.0001	significant
A-Alkali	353.09	1	353.09	3002.84	< 0.0001	
B-Temperature	4771.12	1	4771.12	40575.71	< 0.0001	
C-Time	73.04	1	73.04	621.15	< 0.0001	
AB	194.38	1	194.38	1653.05	< 0.0001	
AC	31.17	1	31.17	265.06	< 0.0001	
BC	86.04	1	86.04	731.69	< 0.0001	
A^2	3.47	1	3.47	29.53	0.0003	
B^2	342.98	1	342.98	2916.87	< 0.0001	
C^2	10.09	1	10.09	85.81	< 0.0001	
Residual	1.18	10	0.1176			
Lack of Fit	0.8583	5	0.1717	2.70	0.1496	not significant
Pure Error	0.3176	5	0.0635			
Cor Total	6198.40	19				
Model (Y2)	13.84	9	1.54	77.54	< 0.0001	significant
A-Alkali	2.12	1	2.12	106.83	< 0.0001	
B-Temperature	5.75	1	5.75	289.64	< 0.0001	
C-Time	0.0003	1	0.0003	0.0131	0.9112	
AB	3.16	1	3.16	159.15	< 0.0001	
AC	0.5598	1	0.5598	28.22	0.0003	
BC	0.3329	1	0.3329	16.78	0.0022	
A^2	0.0102	1	0.0102	0.5144	0.4896	
B^2	0.4934	1	0.4934	24.87	0.0005	
C^2	0.1275	1	0.1275	6.43	0.0296	
Residual	0.1984	10	0.0198			
Lack of Fit	0.1086	5	0.0217	1.21	0.4196	not significant
Pure Error	0.0897	5	0.0179			
Cor Total	14.04	19				
Model (Y3)	1209.45	9	134.38	136.15	< 0.0001	significant
A-Alkali	99.15	1	99.15	100.45	< 0.0001	
B-Temperature	906.51	1	906.51	918.45	< 0.0001	
C-Time	46.22	1	46.22	46.83	< 0.0001	
AB	0.5191	1	0.5191	0.5259	0.4850	
AC	8.60	1	8.60	8.71	0.0145	
BC	5.48	1	5.48	5.55	0.0402	
A^2	1.06	1	1.06	1.08	0.3236	
B^2	60.12	1	60.12	60.91	< 0.0001	
C^2	0.4882	1	0.4882	0.4946	0.4979	
Residual	9.87	10	0.9870			
Lack of Fit	6.61	5	1.32	2.03	0.2280	not significant
Pure Error	3.26	5	0.6518			
Cor Total	1219.32	19				

Note: the sum of squares is Type III partial; model (Y1)/(Y2)/(Y3) = ANOVA for the fit model of the respective responses; cor total = corrected total; df = degree of freedom.

Table 4.9 Fit statistics of CCD for *$NaHCO_3$* pretreatment optimization

Std. Dev.	0.3429	**R^2**	0.9998	**Y1**
Mean	27.37	**Adjusted R^2**	0.9996	
C.V. %	1.25	**Predicted R^2**	0.9982	
		Adeq Precision	272.5117	
Std. Dev.	0.1408	**R^2**	0.9859	**Y2**
Mean	4.83	**Adjusted R^2**	0.9732	
C.V. %	2.92	**Predicted R^2**	0.9196	
		Adeq Precision	33.0475	
Std. Dev.	0.9935	**R^2**	0.9919	**Y3**
Mean	75.43	**Adjusted R^2**	0.9846	
C.V. %	1.32	**Predicted R^2**	0.9343	
		Adeq Precision	42.1917	

Note Y1 = percent of lignin removal; Y2= total reducing sugars lost; Y3 = enzymatic saccharification yield; Std. Dev. = standard deviation; C.V. % = coefficient of variation; R^2= coefficient of determination

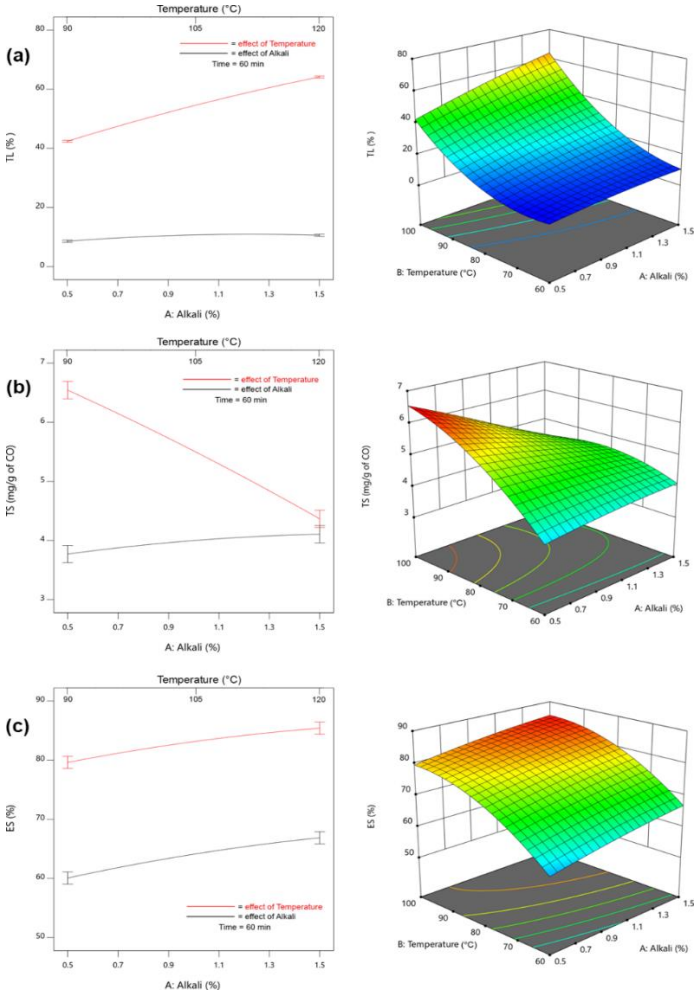

Figure 4.4 Effect of $NaHCO_3$ concentration and temperature on responses

4.2.4 Differential CCD optimization of $NaHCO_3$ pretreatment

The optimum values of factors and their corresponding responses resulting from CCD numerical optimization using three different criteria can be found in Table 4.10, and Figure 4.5. Among the three criteria, Criterion 1 yielded the highest enzymatic saccharification percentage (ES%) for $NaHCO_3$ pretreatment, albeit with a higher total sugar loss (TS mg/g). Criterion 3 secured the second-best ES% with a comparatively lower sugar loss. Criterion 2 demonstrated a notable balance, offering a considerably high ES% with the lowest TS mg/g in comparison. However, the selection of the optimal pretreatment configuration for the proposed bio-refinery depends on whether to valorize the pretreatment slurry for its sugar content. Nonetheless, all criteria consistently demonstrated a clear unidirectional relationship between factors (alkali concentration, temperature) and all the responses under investigation.

Table 4.10 Differential CCD optimization results of $NaHCO_3$ pretreatment

$NaHCO_3$ Pretreatment	Alkali%	Temperature	Time	TL%	TS mg/g	ES%	Desirability
Criteria 1	1.44	100	37.85	58.36	4.73	84.63	0.954
Criteria 2	0.5	76.3	41.61	12.22	5.04	70.34	0.716
Criteria 3	0.53	90.15	89.99	30.83	6.06	80.8	0.542

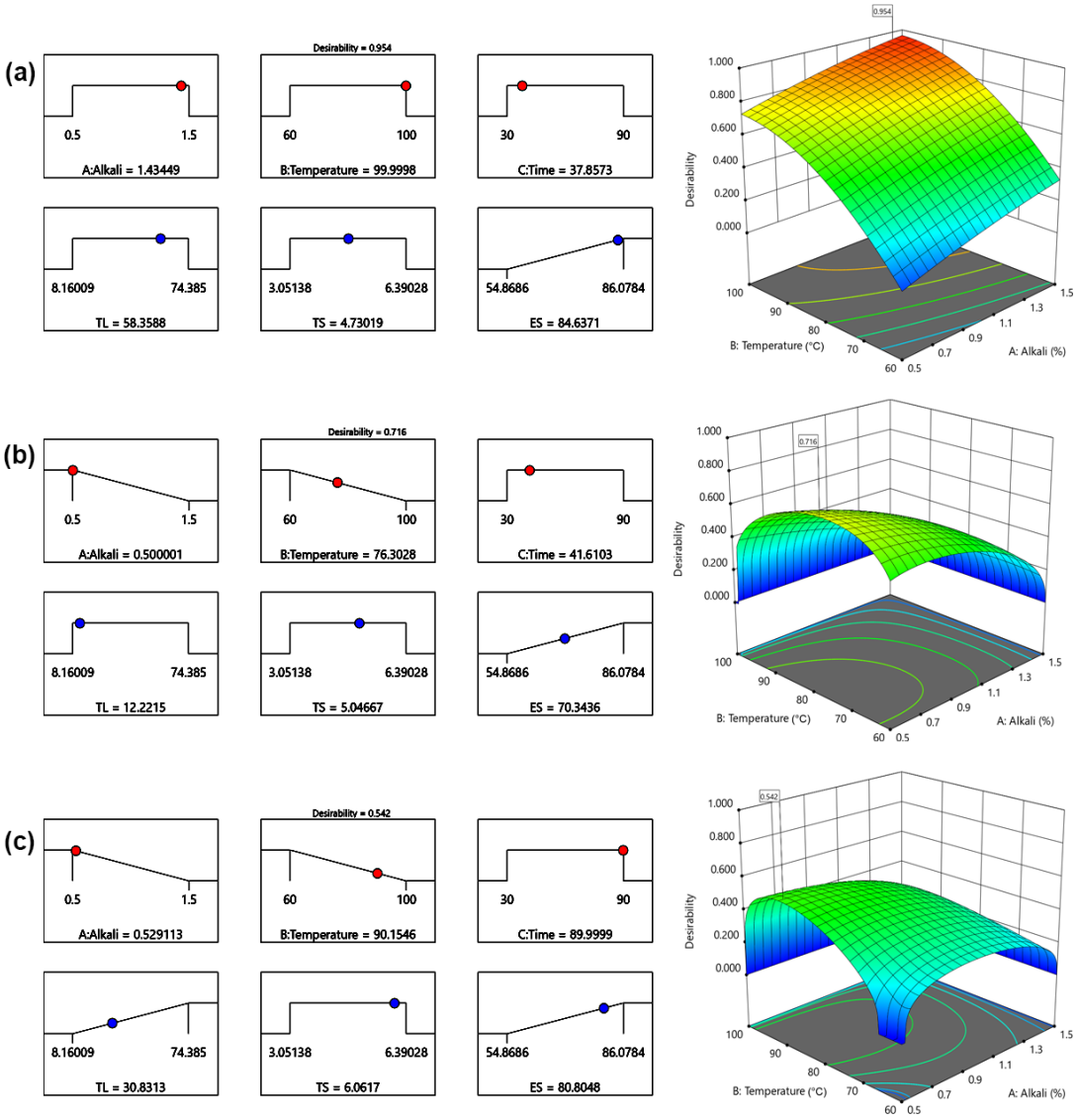

Figure 4.5 Differential CCD optimization results of $NaHCO_3$ pretreatment

Additionally, Figure 4.6 shows the enzymatic saccharification yields of CO derived from each run of the CCD. Maximum saccharification was observed around 65 hours of incubation, with the highest saccharification achieved with CL (86.47%), followed by the CO residue from run 8 of the CCD (86.08%). The control CO showed the least saccharification. These findings are consistent with the results of an earlier work (Gandam et al., 2022b).

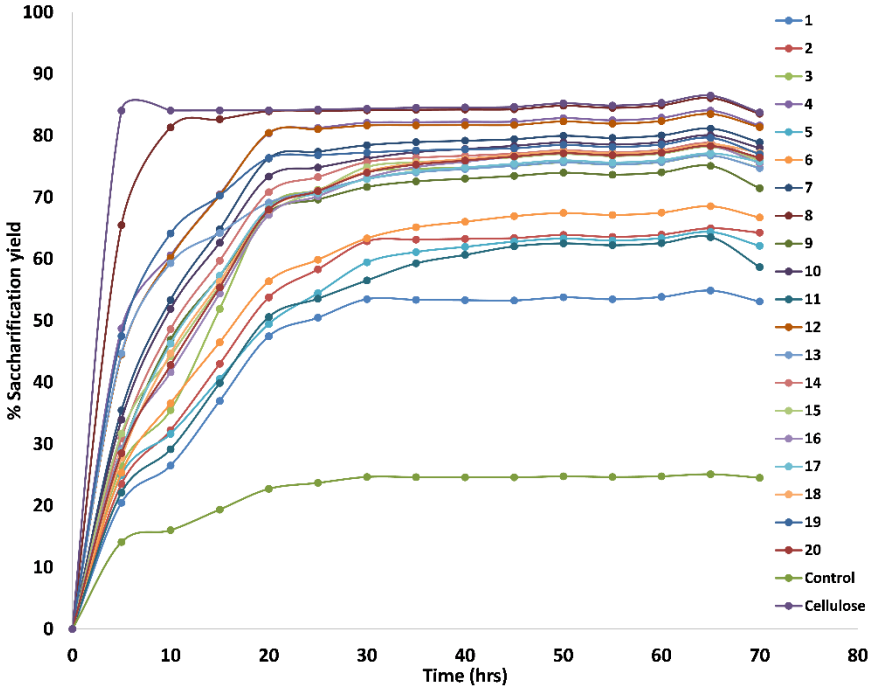

Figure 4.6 Enzymatic saccharification yield %, of the CO derived from each run of CCD.

Note: legends 1 – 20 are the CO derived from each run of the CCD. Pretreated CO residue obtained from each run of the CCD was washed to neutralize it; control = CO without pretreatment; cellulose = commercial cellulose taken as the positive control.

4.2.4 Hybrid-ANN models

The best fitness values for the metaheuristic optimized-ANN models were TB100, TB30, PB50, PB100, GB50, and GB100, in that order. GB50 and GB100 achieved the same cost value but with different x1, x2, and x3 results (Table 4.11). The TLBO and PSO optimizations were terminated at the maximum number of generations, while GA was terminated when the algorithm converged to a solution with an average change in fitness value smaller than the tolerance value. Figure 4.7 shows the convergence, performance, error histogram, and regression plots of the best cost achieved by each optimization run. The predicted values of the best of each hybrid-ANN model, along with the CCD experimental and predicted values, are shown in Table 4.12. "trainbr" was identified as the optimal ANN training algorithm for the data set. TB100 achieved the best fitness and predicted responses at iteration 64. PSO-optimized ANN (PB50) and GA-optimized ANN (GB100) achieved their best cost values at iterations 37 and 59, respectively. TB100 demonstrated the best training performance with a training set MSE of < 0.001 and a test set MSE of < 0.1, resulting in an overall training performance of 0.0010147. PB50 and GB100 also performed well, although slightly lower than TB100 but still

acceptable. A low and uniform error has been observed among all the hybrid-ANN models. TB100 had superior fitness compared to that of all other hybrid-ANN models, including CCD predictions. This was demonstrated by lower RMSE (Root Mean Squared Error), and MAE (Mean Absolute Error) values and higher R^2 values for all response predictions.

PB50 outperformed CCD for response Y3, and GB100 outperformed CCD for response Y2. However, the Y1 and Y2 predictions of PB50 and GB100 are slightly lower but closer to those of CCD. The performance of the selected hybrid-ANN models was evaluated using R^2 as the regression metric for training, testing, and total datasets (Figure 4.8). R^2 values for training data were above 0.99, indicating excellent fit. R^2 values for test data were slightly lower, but still above 0.99 for TB100 and GB100, and just below 0.99 for PB50, indicating good generalization ability. TLBO and GA generally outperformed PSO with higher R^2 values for all metrics. However, the performance differences between the three algorithms were relatively small.

4.2.5. Operating cost of chemical requirement

The optimal amount of $NaHCO_3$ required for pretreatment is determined to be 91 grams per kilogram of CO. Consequently, the estimated cost for treating each kilogram of CO is 0.039 USD.

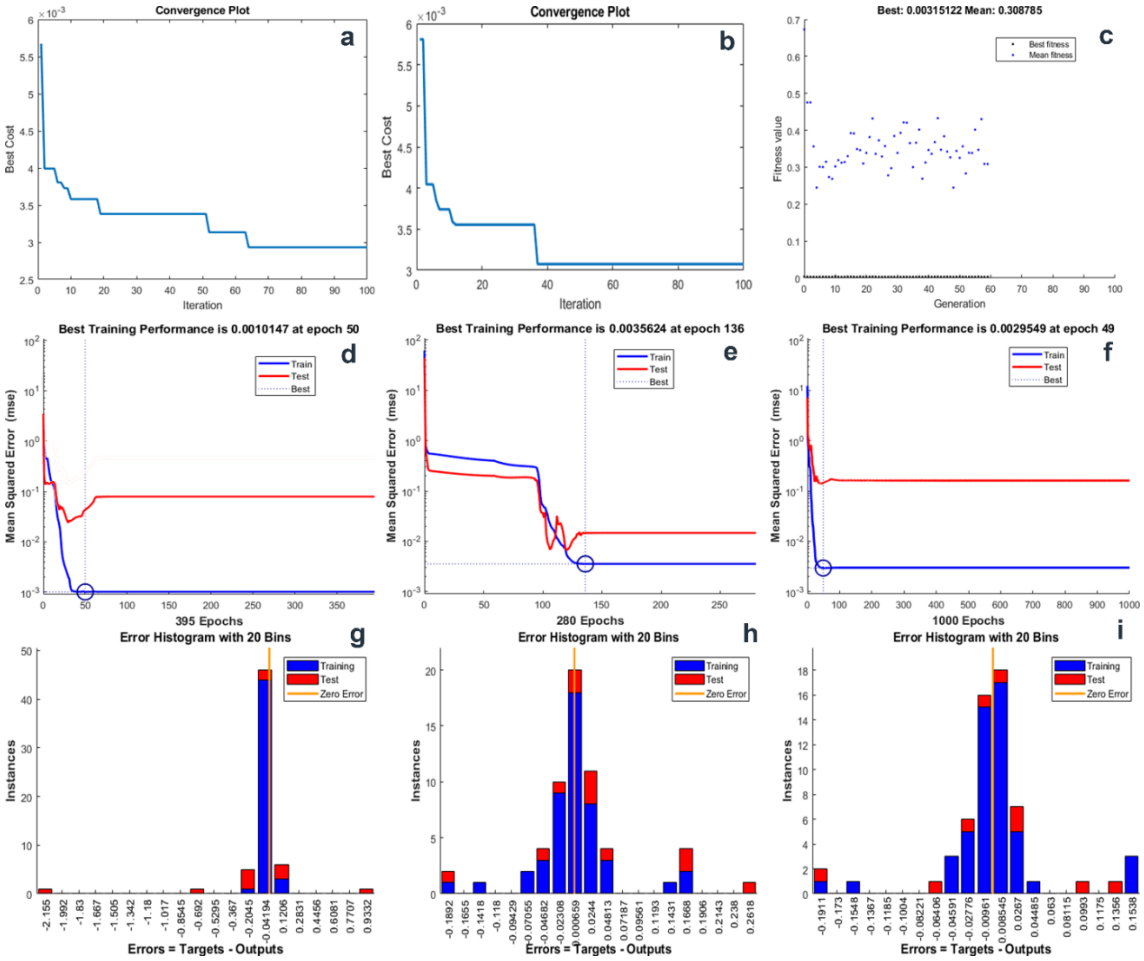

Figure 4.7 Convergence and fitness of the ANN hyperparameter optimizations

Note: a), b), c) = convergence plots for TB100, PB50, and GB100 respectively; d), e), f) = performance plots for TB100, PB50, and GB100 respectively; g), h), i) = error histogram plots for TB100, PB50, and GB100 respectively

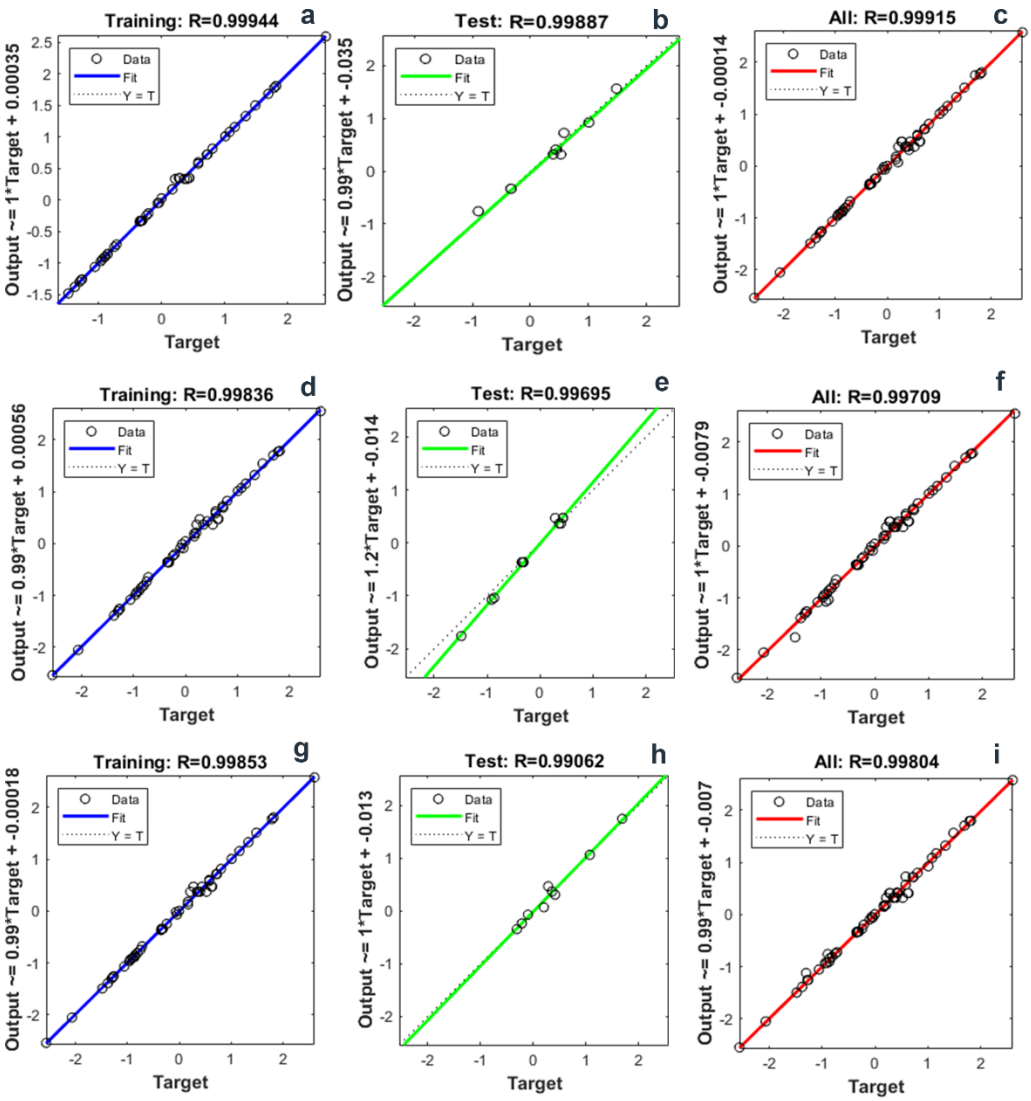

Figure 4.8 Regression plots for ANN-hyperparameter optimizations

Note: a), b), and c) = TB100 regression analysis of training data set, test data set, and entire data set respectively; d), e), and f) = PB50 regression analysis of training data set, test data set, and entire data set respectively; g), h), and i) = GB100 regression analysis of training data set, test data set, and entire data set respectively

Table 4.11 Result of metaheuristic optimization of ANN hyperparameters

optimization	Best cost	Best x1	Best x2	Best x3	convergence
TL30	0.013164	1	3	0.67336	49
TL50	0.007047	1	3	0.32025	82
TL100	0.022869	1	3	0.61312	48
TB30	0.003033	1	43	0.057136	61
TB50	0.0035	1	18	0.60777	11
TB100	0.002933	1	20	0.51572	64
TS30	0.024632	1	4	0.67416	56
TS50	0.021886	1	4	0.01	21
TS100	0.027988	1	3	0.50456	22
PL30	0.021034	1	3	0.9	18
PL50	0.01796	1	5	0.9	4
PL100	0.024566	5	3	0.9	63
PB30	0.004579	1	9	0.001	13
PB50	0.003076	1	50	0.9	37
PB100	0.003143	1	50	0.9	77
PS30	0.03068	1	3	0.01	27
PS50	0.014198	5	50	0.9	22
PS100	0.029028,	1	3	0.01	58
GL30	0.0273	1	3	0.8741	96
GL50	0.0157	1	4	0.5528	84
GL100	0.0147	1	4	0.8567	100
GB30	0.0035	1	15	0.5697	55
GB50	0.0034	2	14	0.6975	53
GB100	0.0032	1	10	0.1518	59
GS30	0.0178	3	11	0.8929	100
GS50	0.0528	1	4	0.022	100
GS100	0.0298	1	4	0.7214	100

Note: the letter T, P, and G represents TLBO, PSO, and GA optimizations respectively; and the letters L, B, and S represents the type of ANN-training algorithm used, trainlm, trainbr, and trainscg respectively; 30, 50, and 100 are the total number of iterations (generations) used for optimization; Best cost = best cost value obtained; Best x1 = number of hidden layers at best cost; Best x2 = hidden layer size at best cost; convergence = iteration at which the best cost is found.

Table 4.12 Comparison of model fitness-CCD and hyperparameter-optimized ANN

	CCD	CCD	CCD	CCD	CCD	CCD	TLBO	TLBO	TLBO	PSO	PSO	PSO	GA	GA	GA
std.	**Y1**	**Y2**	**Y3**	**Y1.p**	**Y2. p**	**Y3. p**	**Y1.p**	**Y2. p**	**Y3. p**	**Y1.p**	**Y2. p**	**Y3. p**	**Y1.p**	**Y2. p**	**Y3. p**
1	12.68	3.05	54.87	12.71	3.09	55.63	13.04	3.07	54.99	12.77	3.07	55.48	12.72	3.07	55.16
2	11.16	4	64.97	11.04	3.96	64.51	11.12	4	64.99	14.31	3.83	63.47	12.73	3.81	65.42
3	40.44	6.39	76.74	40.19	6.27	76.84	40.31	6.38	76.91	40.35	6.37	77.01	40.33	6.38	76.99
4	57.89	4.65	84.04	58.99	4.62	84.7	58.11	4.63	84.06	58.17	4.65	84.05	56.58	4.69	84.55
5	8.16	4.02	64.37	8.06	4.02	63.66	7.94	4.03	64.25	8.15	4.03	64.74	8.44	4.03	64.48
6	13.79	3.73	68.54	13.88	3.83	68.39	13.91	3.74	68.6	13.98	3.74	68.89	13.83	3.74	68.78
7	48.29	6.36	81.14	48.25	6.38	81.55	48.33	6.35	81.23	51.14	5.82	81.98	48.16	6.35	81.29
8	74.38	3.74	86.08	73.88	3.68	85.27	74.02	3.75	86.17	73.97	3.76	85.8	73.7	3.75	86.17
9	14.37	5.52	75.08	15.08	5.58	74.52	14.32	5.53	74.95	15.07	5.53	74.66	19.5	5.35	72.85
10	26.14	4.62	80.05	27.01	4.66	80.81	26.21	4.62	80.14	26.87	4.62	80.08	26.75	4.61	80.31
11	10.94	4.09	63.53	10.85	4	64.09	10.71	4.07	63.43	10.34	4.07	63.32	10.45	4.07	63.8
12	54.15	5.33	83.49	54.63	5.52	83.13	54.4	5.35	83.57	57.35	5.23	82.95	54.73	5.35	83.89
13	21	4.83	76.76	20.72	4.97	75.72	20.6	4.83	76.53	20.57	4.85	76.41	20.59	4.88	74.67
14	25.58	5.01	78.77	26.09	4.96	80.02	26.01	4.89	77.95	25.37	5	78.81	25.99	5	79.27
15	21.19	5.37	78.15	21.16	5.18	78.29	21.39	5.23	78.46	21.45	5.21	78.48	21.3	5.21	78.49
16	21.78	5.08	78.31	21.16	5.18	78.29	21.39	5.23	78.46	21.45	5.21	78.48	21.3	5.21	78.49
17	21.6	5.06	77.11	21.16	5.18	78.29	21.39	5.23	78.46	21.45	5.21	78.48	21.3	5.21	78.49
18	21.38	5.21	78.6	21.16	5.18	78.29	21.39	5.23	78.46	21.45	5.21	78.48	21.3	5.21	78.49
19	21.29	5.36	79.63	21.16	5.18	78.29	21.39	5.23	78.46	21.45	5.21	78.48	21.3	5.21	78.49
20	21.13	5.2	78.31	21.16	5.18	78.29	21.39	5.23	78.46	21.45	5.21	78.48	21.3	5.21	78.49
RMSE				0.4494	0.0995	0.7024	0.2420	0.0727	0.4580	1.2354	0.145	0.6227	1.27913	0.08905	0.83658
MAE				0.332	0.081	0.58	0.2045	0.045	0.2705	0.7115	0.0775	0.4565	0.647	0.059	0.5585
R^2				0.9993	0.9858	0.9919	0.9998	0.9924	0.9965	0.9950	0.9700	0.9936	0.99472	0.98870	0.98852

Note: std. = CCD standard run order; CCD Y1, CCD Y2, CCD Y3 = experimentally obtained responses; CCD Y1p, CCD Y2.p, CCD Y3.p = CCD predicted responses; (TLBO/PSO/GA) Y1.p, Y2.p, Y3.p = predicted responses from hyperparameter optimized ANN with TLBO, PSO, and GA respectively.

Chapter 5

Enhancing Saccharification of Sequentially Pretreated Corncob Outer Anatomical Portion Using NaOH and H_2SO_4: A Study Utilizing RSM-CCD, Validated with ANN

5.1 Material and methods

5.1.1 RSM-CCD Optimization of Sequential pretreatments

Based on the findings from the fixed factor screening (section 4.2.1) and 2FI model (section 4.2.2), NaOH and H_2SO_4 were selected for sequential pretreatment of the CO. These sequential pretreatments were individually conducted and optimized using CCD. The optimization process began with the refinement of NaOH pretreatment parameters through CCD. Subsequently, the CO residue obtained from the optimal NaOH treatment underwent sequential pretreatment with CCD-optimized H_2SO_4. The outcomes of both CCD optimizations were then validated using ANN.

Three factors varied at two levels (-1 and +1) were selected for NaOH pretreatment: alkali concentration (A) ranging from 0.5% to 1.5%, temperature (B) varying between 90 °C and 120 °C, and time (C) spanning 30 to 90 minutes, all while maintaining a constant L/S ratio of 10:1. The responses assessed were % total lignin removal (TL%), total reducing sugar loss in milligrams per gram of CO (TS), and percent enzymatic saccharification yield at 60 hours of saccharification (ES%). Similar design was chosen for the subsequent H_2SO_4 pretreatment where the factors are (A) Acid concentration ranging from 0.1% to 1%, temperature (B) varying between 90 °C and 120 °C, and time (C) spanning 30 to 90 minutes, all while maintaining a constant L/S ratio of 10:1. TS and ES% are the two responses assessed for the sequential H_2SO_4 pretreatment. The CCDs were randomized, with 20 runs without blocks, to systematically examine the parameter space. The TL and TS analysis was carried out as outlined in section 1.2. The enzymatic saccharification of pretreated biomass was conducted as described in Section 2.1. An aliquot of 130 µL was collected at 60 hours of saccharification to measure the total reducing sugars released. Samples of untreated CO and commercial cellulose were used as controls.

Quadratic models were employed to fit response surfaces for the assessed responses, incorporating linear and quadratic terms for each independent variable, along with their interaction terms. The quality of the models was assessed through analysis of variance (ANOVA) and determination coefficient (R^2) values. The three different criteria described in Table 4.2 were used to optimize the CCD results of sequential pretreatments.

5.1.2 Validation of Sequential Pretreatment CCD Model Using ANN

The CCD-generated pretreatment models were validated using hyper parameter optimized ANN architecture (Section 4.1.5.2). With a set of hyperparameters- hidden layer number, hidden layer size, and learning rate set at 2, 20, 0.51 respectively (section 3.2.4), using MATLAB R2020a (MathWorks, Inc, U.S.A).

The response data obtained from CCD was standardized using z-score normalization (Equation 4.2), while the factors data set was not normalized since it had lower diversity compared to the response data set. The datasets were randomly divided into training, validation, and test sets for training the neural network using trainbr. Iterations continued until both the training and test values achieved R^2 values above 0.9, accompanied by corresponding MSE values less than zero. The termination tolerance of 1×10^{-6} was set and reached. A comparative statistical analysis to assess the fitness of the ANN models was conducted by evaluating the proximity of ANN-predicted values to the CCD experimental values, in comparison with CCD-predicted values. The performance metrics used were RMSE, MAE, and R^2 values.

5.2 Results and discussion

5.2.1 Central composite design

The complete design of the models for these sequential pretreatments, along with the experimentally obtained responses are available in Tables 5.1 and 5.2. The ANOVA analysis with Type III – Partial Sum of squares of NaOH pretreatment, revealed that A, B, AB, A^2 are significant factors for lignin removal (TL), A, B, C, AB, A^2, C^2 are significant for sugar loss (TS), and, A, B, C, A^2 are significant factors for enzymatic saccharification (Table 5.3). For the sequential H_2SO_4 pretreatment, the significant model terms for the response TS are A, B, C, AB, AC, A^2, C^2, and for the response ES are A, B, C, A^2 (Table 5.4).

The significance of these factors is determined by their corresponding P-values less than 0.05 and the higher f-values obtained. The Predicted R^2 values were reasonably close to the Adjusted R^2 values, with a difference of less than 0.2. Additionally, all the models had adequate signal-to-noise ratios, with an adequate precision > 4, indicating that the models can be used to navigate the design space (Tables 5.5, and 5.6). Final Equations in Terms of Coded Factors obtained for each response model are given (Equations 5.1 to 5.5)

Table 5.1 CCD design for NaOH pretreatment

	Factor 1	Factor 2	Factor 3	Response 1	Response 2	Response 3
Std	**A:Alkali%**	**B:Temperature (°C)**	**C:Time (min)**	**TL %**	**TS (mg/g)**	**ES %**
1	0.5	90	30	18.0	4.09146	29.3746
2	1.5	90	30	53.6	4.7598	71.4837
3	0.5	120	30	21.9	4.97857	41.4909
4	1.5	120	30	82.6	6.34325	92.1964
5	0.5	90	90	23.2	4.39295	34.6691
6	1.5	90	90	61.5	5.27205	87.5418
7	0.5	120	90	19.3	4.94789	50.16
8	1.5	120	90	84.4	7.15166	94.8728
9	0.5	105	60	23.5	4.13415	40.0946
10	1.5	105	60	77.1	5.33475	93.0982
11	1	90	60	63.6	4.38894	76.0073
12	1	120	60	63.8	5.94039	88.0509
13	1	105	30	66.3	5.34942	80.9237
14	1	105	90	63.2	5.76163	79.5855
15	1	105	60	67.5	5.48016	84.3855
16	1	105	60	67.7	5.3761	83.2655
17	1	105	60	67.1	5.28006	82.2909
18	1	105	60	76.7	5.29473	86.16
19	1	105	60	72.1	5.62156	89.1855
20	1	105	60	65.5	5.58821	81.7237

Table 5.2 CCD design for Sequential H_2SO_4 pretreatment

	Factor 1	Factor 2	Factor 3	Response 1	Response 2
Std	**A:Acid %**	**B:Temperature (°C)**	**C:Time (min)**	**TS mg/g CO**	**ES%**
1	0.1	90	30	114.561	30.8433
2	1	90	30	133.274	75.0578
3	0.1	120	30	139.4	43.5655
4	1	120	30	177.611	96.8062
5	0.1	90	90	123.002	36.4026
6	1	90	90	147.617	91.9189
7	0.1	120	90	140.11	48.668
8	1	120	90	200.246	99.6164
9	0.1	105	60	115.756	42.0993
10	1	105	60	152.18	97.7531
11	0.55	90	60	132.2	79.8077
12	0.55	120	60	166.331	92.4535
13	0.55	105	30	149.784	84.9698
14	0.55	105	90	161.326	83.5648
15	0.55	105	60	153.444	88.6048
16	0.55	105	60	150.531	87.4288
17	0.55	105	60	147.842	86.4055
18	0.55	105	60	148.252	90.468
19	0.55	105	60	149.804	93.6448
20	0.55	105	60	149.97	85.8098

Table 5.3 ANOVA for Quadratic models of NaOH pretreatment responses

Source	Sum of Squares	df	Mean Square	F-value	p-value	
Model (TL)	9313.86	9	1034.87	54.61	< 0.0001	significant
A-Alkali	6411.07	1	6411.07	338.30	< 0.0001	
B-Temperature	270.87	1	270.87	14.29	0.0036	
C-Time	8.39	1	8.39	0.4428	0.5208	
AB	334.72	1	334.72	17.66	0.0018	
AC	6.20	1	6.20	0.3271	0.5800	
BC	24.00	1	24.00	1.27	0.2867	
A^2	801.54	1	801.54	42.30	< 0.0001	
B^2	36.73	1	36.73	1.94	0.1940	
C^2	18.87	1	18.87	0.9958	0.3419	
Residual	189.51	10	18.95			
Lack of Fit	101.29	5	20.26	1.15	0.4416	not significant
Pure Error	88.22	5	17.64			
Cor Total	9503.37	19				
Model (TS)	9.95	9	1.11	27.92	< 0.0001	significant
A-Alkali	3.99	1	3.99	100.73	< 0.0001	
B-Temperature	4.17	1	4.17	105.24	< 0.0001	
C-Time	0.4015	1	0.4015	10.14	0.0098	
AB	0.5106	1	0.5106	12.89	0.0049	
AC	0.1378	1	0.1378	3.48	0.0918	
BC	0.0002	1	0.0002	0.0041	0.9502	
A^2	0.5891	1	0.5891	14.87	0.0032	
B^2	0.0029	1	0.0029	0.0739	0.7913	
C^2	0.3529	1	0.3529	8.91	0.0137	
Residual	0.3961	10	0.0396			
Lack of Fit	0.2888	5	0.0578	2.69	0.1506	not significant
Pure Error	0.1073	5	0.0215			
Cor Total	10.35	19				
Model	8479.73	9	942.19	74.34	< 0.0001	significant
A-Alkali	5924.53	1	5924.53	467.44	< 0.0001	
B-Temperature	458.26	1	458.26	36.16	0.0001	
C-Time	98.34	1	98.34	7.76	0.0193	
AB	0.0238	1	0.0238	0.0019	0.9663	
AC	2.85	1	2.85	0.2245	0.6458	
BC	12.52	1	12.52	0.9877	0.3437	
A^2	782.65	1	782.65	61.75	< 0.0001	
B^2	5.68	1	5.68	0.4483	0.5183	
C^2	28.37	1	28.37	2.24	0.1655	
Residual	126.74	10	12.67			
Lack of Fit	87.91	5	17.58	2.26	0.1954	not significant
Pure Error	38.83	5	7.77			
Cor Total	8606.47	19				

Table 5.4 ANOVA for Quadratic models of H_2SO_4 pretreatment responses

Source	Sum of Squares	df	Mean Square	F-value	p-value	
Model (TS)	7485.86	9	831.76	102.15	< 0.0001	significant
A-Acid	3171.94	1	3171.94	389.54	< 0.0001	
B-Temperature	2994.40	1	2994.40	367.73	< 0.0001	
C-Time	332.60	1	332.60	40.85	< 0.0001	
AB	378.39	1	378.39	46.47	< 0.0001	
AC	96.79	1	96.79	11.89	0.0063	
BC	0.0393	1	0.0393	0.0048	0.9460	
A^2	468.10	1	468.10	57.49	< 0.0001	
B^2	13.93	1	13.93	1.71	0.2202	
C^2	200.56	1	200.56	24.63	0.0006	
Residual	81.43	10	8.14			
Lack of Fit	61.53	5	12.31	3.09	0.1204	not significant
Pure Error	19.89	5	3.98			
Cor Total	7567.29	19				
Model (ES)	9588.40	9	1065.38	96.81	< 0.0001	significant
A-Acid	6737.86	1	6737.86	612.28	< 0.0001	
B-Temperature	449.96	1	449.96	40.89	< 0.0001	
C-Time	83.68	1	83.68	7.60	0.0202	
AB	2.48	1	2.48	0.2258	0.6449	
AC	10.15	1	10.15	0.9220	0.3596	
BC	26.31	1	26.31	2.39	0.1531	
A^2	880.68	1	880.68	80.03	< 0.0001	
B^2	7.86	1	7.86	0.7146	0.4177	
C^2	34.74	1	34.74	3.16	0.1060	
Residual	110.04	10	11.00			
Lack of Fit	67.23	5	13.45	1.57	0.3163	not significant
Pure Error	42.82	5	8.56			
Cor Total	9698.45	19				

Table 5.5 Quadratic model Fit Statistics for NaOH pretreatment

Std. Dev.	4.35	R^2	0.9801
Mean	56.93	Adjusted R^2	0.9621
C.V. %	7.65	Predicted R^2	0.9101
		Adeq Precision	21.2256
Std. Dev.	0.1990	R^2	0.9617
Mean	5.27	Adjusted R^2	0.9273
C.V. %	3.77	Predicted R^2	0.7630
		Adeq Precision	20.9998
Std. Dev.	3.56	R^2	0.9853
Mean	73.33	Adjusted R^2	0.9720
C.V. %	4.86	Predicted R^2	0.8527
		Adeq Precision	27.2076

Table 5.6 Quadratic model Fit Statistics for H_2SO_4 pretreatment

Std. Dev.	2.85	R^2	0.9892
Mean	147.66	Adjusted R^2	0.9796
C.V. %	1.93	Predicted R^2	0.8810
		Adeq Precision	40.5213
Std. Dev.	3.32	R^2	0.9887
Mean	76.79	Adjusted R^2	0.9784
C.V. %	4.32	Predicted R^2	0.9043
		Adeq Precision	30.3179

$TL = 68.60 + 25.32A + 5.20B + 0.9161C + 6.47AB + 0.8803AC - 1.73BC - 17.07A^2 - 3.65B^2 - 2.62C^2$ (equation 5.1)

$TS = 5.34 + 0.6316A + 0.6457B + 0.2004C + 0.2526AB + 0.1312AC - 0.0045BC - 0.4628A^2 - 0.0326B^2 + 0.3582C^2$ (equation 5.2)

$ES = 84.09 + 2\ 4.34A + 6.77B + 3.14C + 0.0545AB + 0.5964AC - 1.25BC - 16.87A^2 - 1.44B^2 - 3.21C^2$ (equation 5.3)

$TS = 148.79 + 17.81A + 17.30B + 5.77C + 6.88AB + 3.48AC + 0.0701BC - 13.05A^2 + 2.25B^2 + 8.54C^2$ (equation 5.4)

$ES = 88.36 + 25.96A + 6.71B + 2.89C + 0.5573AB + 1.13AC - 1.81BC - 17.90A^2 - 1.69B^2 - 3.55C^2$ (equation 5.5)

The interaction plots between model responses and the factors show that up to 1.3% alkali concentration linearly improved TL%, TS, and ES. Thereafter, a further increase in alkali concentration decreased these responses, indicating the detrimental effect of higher alkali concentration on monolignols and free sugars. The temperature exhibited a similar pattern, with peak response values observed around 100–110 °C, followed by a subsequent decrease (Figures 5.1, 5.2). Subsequent H_2SO_4 pretreatment also followed the same pattern of effects on both TS and ES% responses, where an acid concentration up to 0.7% and temperature up to 110 °C linearly improved the responses. Thereafter, a further increase in these factors showed a negative effect on the responses.

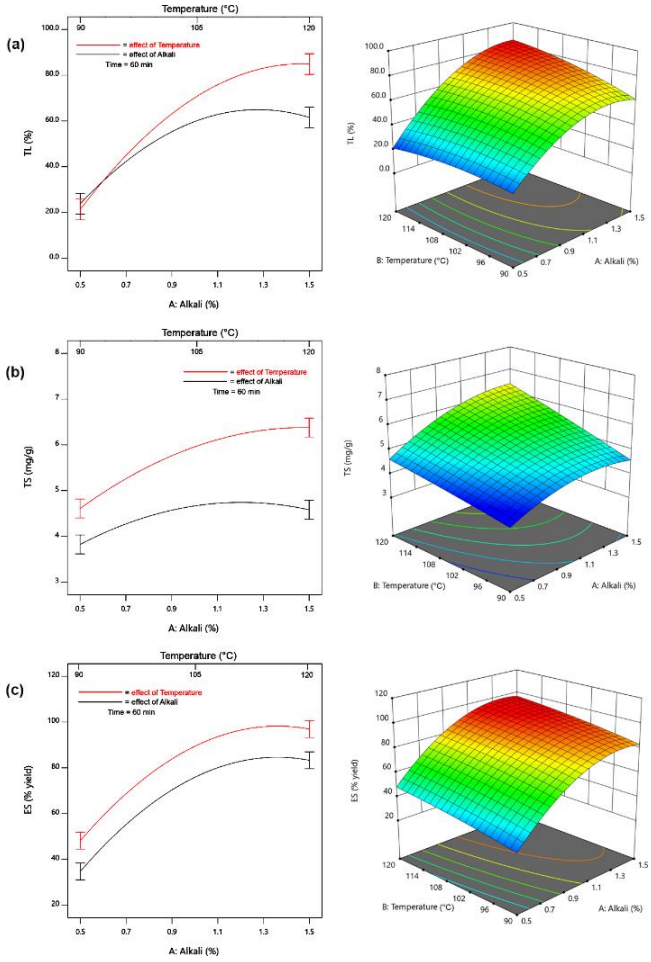

Figure 5.1 Effect of NaOH concentration and temperature on CCD responses

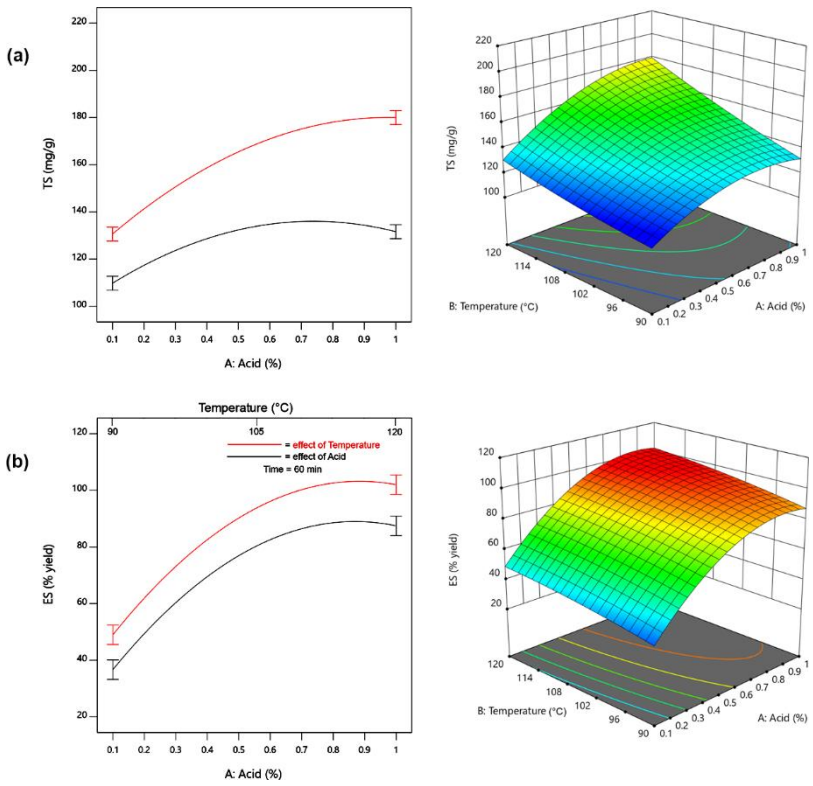

Figure 5.2 Effect of H_2SO_4 concentration and temperature on CCD responses

Differential optimization outcomes as listed in Table 5.7, and Figure 5.3, 5.4 revealed that Criterion 1 yielded the highest enzymatic saccharification percentage (ES%) for both NaOH and sequential H_2SO_4 pretreatments, albeit with a higher total sugar loss (TS mg/g). Notably, a significant sugar loss occurred during sequential H_2SO_4 pretreatment, which is a crucial consideration for achieving an economically viable bio-refinery design. Criterion 3 secured the second-best ES% with a comparatively lower sugar loss. Criterion 2 demonstrated a notable balance, offering a considerably high ES% with the lowest TS mg/g in comparison. However, the selection of the optimal pretreatment configuration for the proposed bio-refinery depends on whether to valorize the pretreatment slurry for its sugar content. Nevertheless, all criteria consistently exhibited a clear unidirectional relationship of catalyst concentration, temperature, and total lignin removal percentage (TL%) on ES%, where an increase in these parameters consistently increased ES%.

Table 5.7 Differential CCD optimization results of sequential NaOH and H_2SO_4 pretreatments

NaOH pretreatment	Alkali %	Temperature	Time	TL%	TS mg/g	ES%	Desirability
Criteria 1	1.44	110.59	76.12	81	6.13	95.54	1
Criteria 2	0.87	90	83.1	54.2	4.88	70.06	0.73
Criteria 3	1	90	89.33	59.9	5.2	77.18	0.692
H_2SO_4 pretreatment	**Acid%**	**Temp**	**Time**	**TL%**	**TS mg/g**	**ES%**	**Desirability**
Criteria 1	0.85	108.97	82.06	N.A	171.47	99.9	1
Criteria 2	0.44	90	78.9	N.A	136.79	74.14	0.73
Criteria 3	0.54	92.02	90	N.A	149.49	81.76	0.615

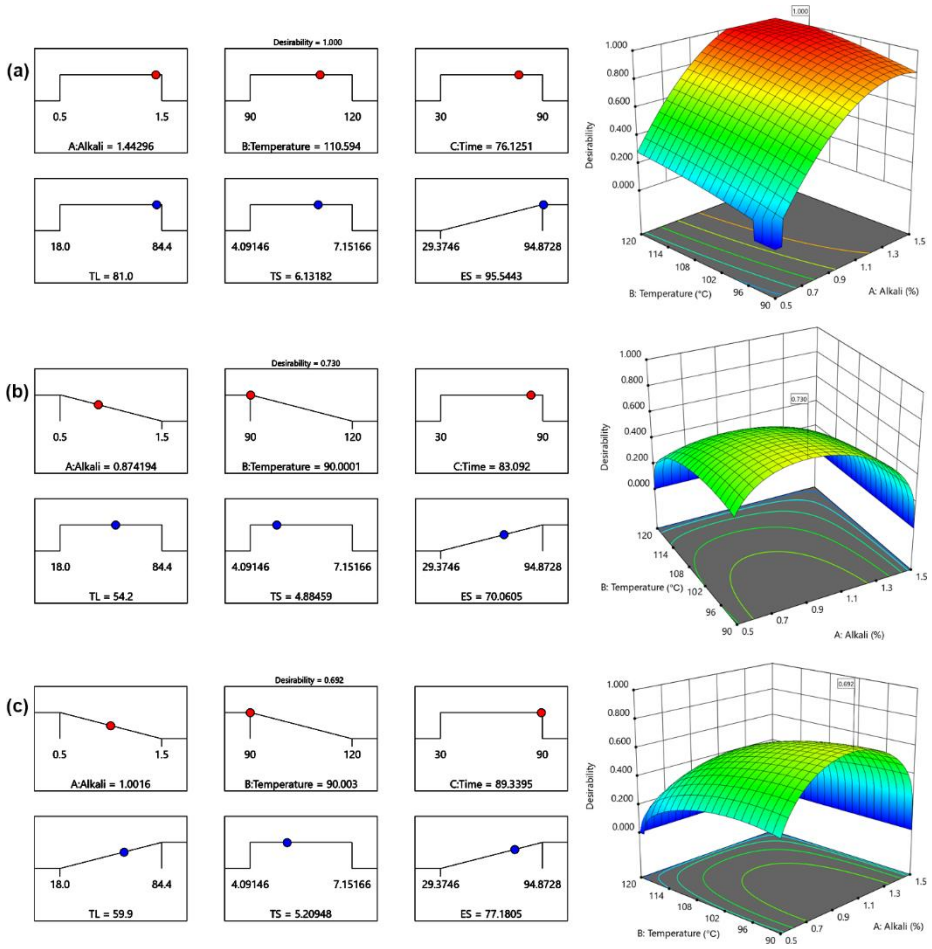

Figure 5.3 NaOH pretreatment CCD optimization criteria

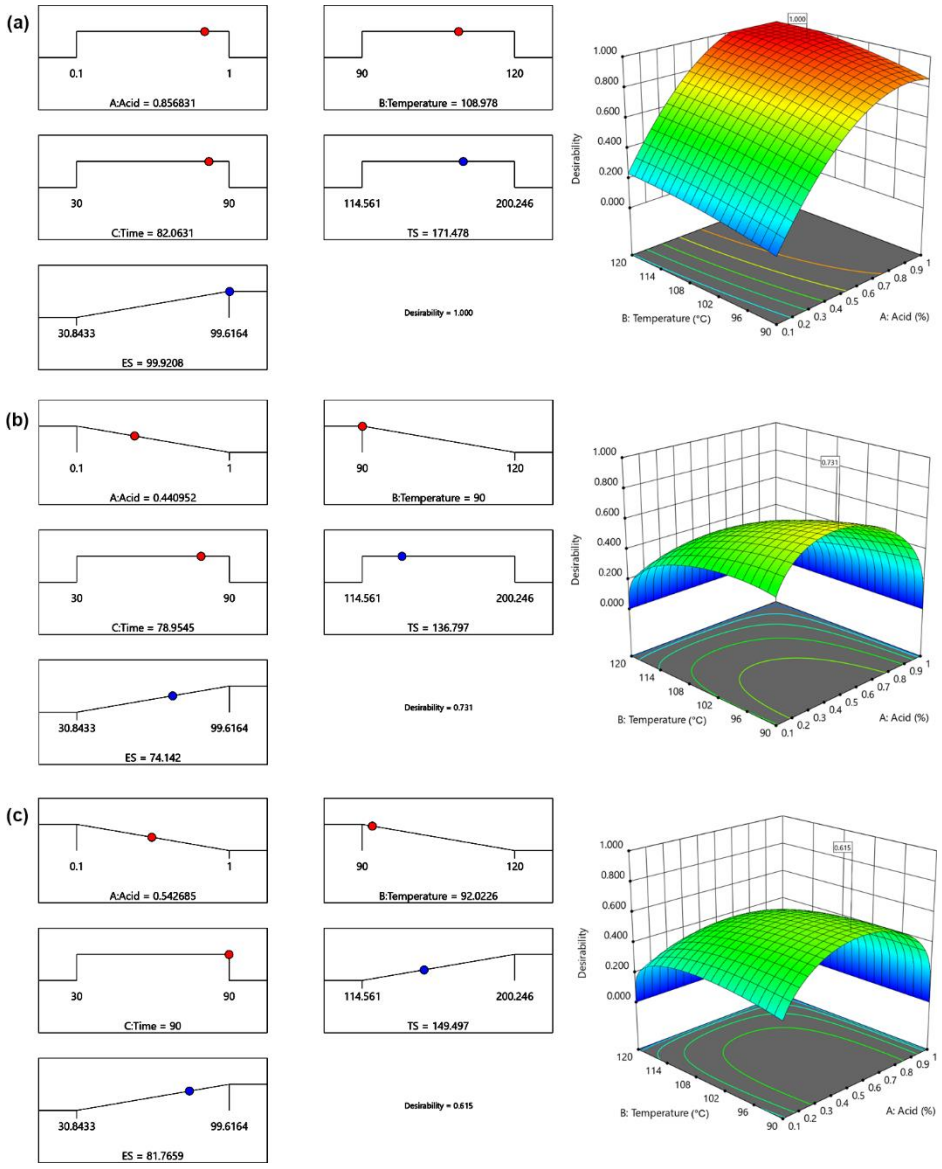

Figure 5.4 H_2SO_4 pretreatment CCD optimization Criteria

5.2.2 Validation of Sequential Pretreatment CCD Model Using ANN

Figures 5.5 and 5.6 depict the performance, error histogram, and regression plots of the best fitting ANN models selected for each stage of the sequential pretreatment. The selection of optimal models was based on R^2 metrics during training, testing, and across the total datasets, as depicted in the figures. R^2 values for both training and test datasets were above 0.98, indicating an excellent fit and good generalization ability of the model. The sequential H_2SO_4 pretreatment model showed slightly improved performance metrics than the preceding alkali pretreatment, indicating a more linear relationship between factors and responses in the former.

The predicted values of both ANN models, along with their corresponding CCD experimental and predicted values, are presented in Tables 5.8 and 5.9 respectively. ANN models have demonstrated superior fitness compared to CCD predictions; the ANN-predicted values are closer to the experimentally obtained values, indicating the efficiency of ANN in understanding the unexpected non-linearity that may arise during pretreatment and considering it. The superior fitness of ANN models was also statistically demonstrated by their lower RMSE (Root Mean Squared Error) and MAE (Mean Absolute Error) values and higher R^2 values for all response predictions.

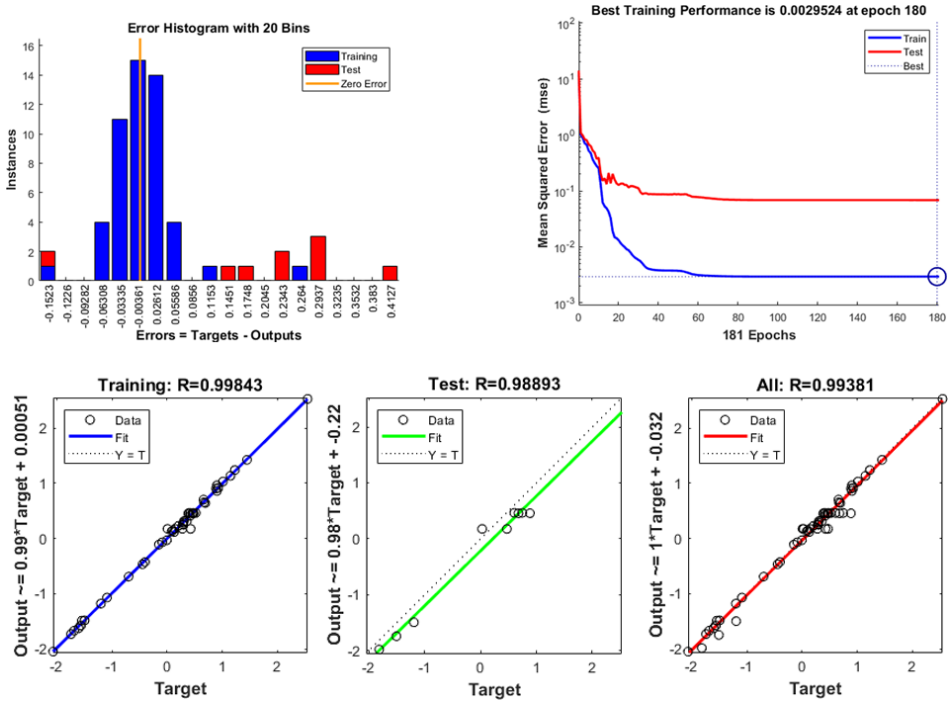

Figure 4.5 Performance plots of ANN model for NaOH pretreatment

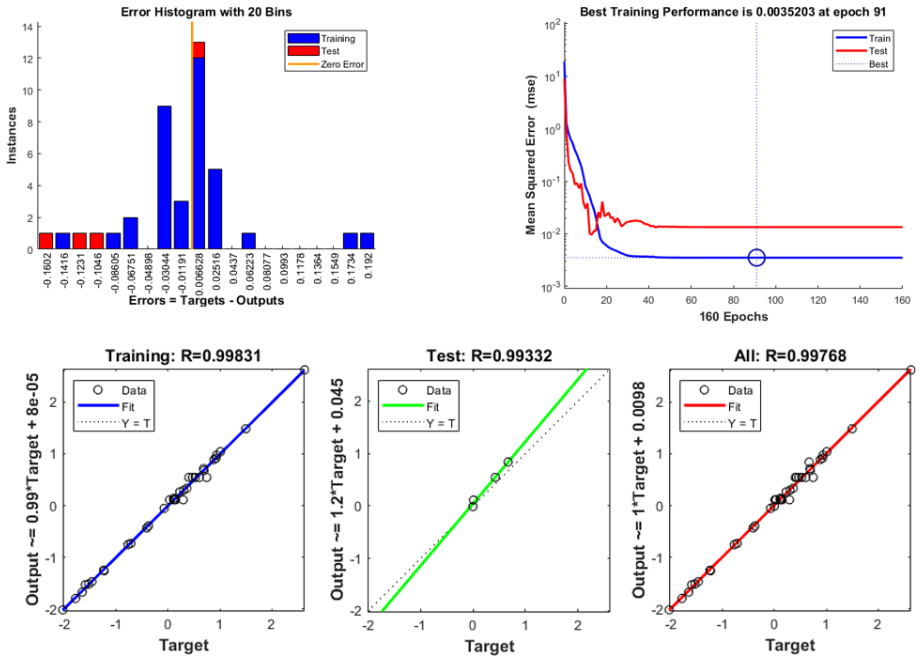

Figure 5.6 Performance plots of ANN model for H_2SO_4 pretreatment

Table 5.8 Comparison of model fitness of NaOH pretreatment-CCD and ANN predictions

	Experimental results			CCD predictions			ANN predictions		
std.	**TL%**	**TS mg/g**	**ES%**	**TL%**	**TS mg/g**	**ES%**	**TL%**	**TS mg/g**	**ES%**
1	18.00	4.09	29.37	19.43	4.11	27.72	18.21	4.08	29.73
2	53.60	4.76	71.48	55.37	4.60	75.10	54.48	4.77	71.92
3	21.90	4.98	41.49	20.37	4.90	43.65	21.71	4.96	41.76
4	82.60	6.34	92.20	82.18	6.41	91.25	82.33	6.33	92.58
5	23.20	4.39	34.67	22.97	4.25	35.30	17.86	4.17	31.10
6	61.50	5.27	87.54	62.43	5.28	85.07	62.06	5.25	87.29
7	19.30	4.95	50.16	16.97	5.03	46.23	19.60	4.93	50.56
8	84.40	7.15	94.87	82.31	7.06	96.21	84.67	7.14	95.30
9	23.50	4.13	40.09	26.21	4.25	42.88	23.73	4.18	39.79
10	77.10	5.33	93.10	76.85	5.51	91.56	76.20	5.37	92.82
11	63.60	4.39	76.01	59.74	4.66	75.88	62.46	4.40	75.82
12	63.80	5.94	88.05	70.15	5.96	89.42	64.02	5.98	87.00
13	66.30	5.35	80.92	65.06	5.50	77.74	66.16	5.38	79.98
14	63.20	5.76	79.59	66.90	5.90	84.01	62.65	5.79	79.46
15	67.50	5.48	84.39	68.60	5.34	84.09	67.13	5.40	83.18
16	67.70	5.38	83.27	68.60	5.34	84.09	67.13	5.40	83.18
17	67.10	5.28	82.29	68.60	5.34	84.09	67.13	5.40	83.18
18	76.70	5.29	86.16	68.60	5.34	84.09	67.13	5.40	83.18
19	72.10	5.62	89.19	68.60	5.34	84.09	67.13	5.40	83.18
20	65.50	5.59	81.72	68.60	5.34	84.09	67.13	5.40	83.18
			RMSE	3.066	0.141	2.517	2.754	0.093	1.807
			MAE	2.352	0.117	2.131	1.416	0.064	1.081
			R^2	0.980	0.961	0.985	0.984	0.983	0.992

Table 5.9 Comparison of model fitness of H_2SO_4 (sequential) pretreatment-CCD and ANN predictions

	Experimental results		CCD predictions		ANN predictions	
std.	**TS mg/g**	**ES%**	**TS mg/g**	**ES%**	**TS mg/g**	**ES%**
1	114.56	30.84	116.08	29.54	114.30	31.31
2	133.27	75.06	130.99	78.08	133.06	75.59
3	139.40	43.57	136.79	45.46	139.05	43.63
4	177.61	96.81	179.21	96.24	177.28	96.85
5	123.00	36.40	120.52	36.70	122.52	36.29
6	147.62	91.92	149.34	89.75	147.42	95.75
7	140.11	48.67	141.51	45.37	139.84	48.60
8	200.25	99.62	197.84	100.65	199.95	100.33
9	115.76	42.10	117.93	44.51	117.15	42.58
10	152.18	97.75	153.55	96.43	152.96	97.49
11	132.20	79.81	133.74	79.97	132.64	79.51
12	166.33	92.45	168.35	93.38	167.12	92.19
13	149.78	84.97	151.56	81.92	150.50	84.39
14	161.33	83.56	163.10	87.70	161.90	83.55
15	153.44	88.60	148.79	88.36	149.90	89.10
16	150.53	87.43	148.79	88.36	149.90	89.10
17	147.84	86.41	148.79	88.36	149.90	89.10
18	148.25	90.47	148.79	88.36	149.90	89.10
19	149.80	93.64	148.79	88.36	149.90	89.10
20	149.97	85.81	148.79	88.36	149.90	89.10
		RMSE	2.018	2.345	1.116	1.734
		MAE	1.838	1.933	0.758	1.090
		R2	0.989	0.989	0.997	0.994

Table 5.10 Summary of the CO pretreatment optimization

Pretreatment option	**Total sugar loss (g/Kg CO)**	**water usage for neutralization (l/kg CO)**	**ES %**	**Total fermentable sugar yield (g/Kg CO)**
$NaHCO_3$_criteria 1	4.73	265.75 ± 7.1	84.63	338.52
$NaHCO_3$_criteria 2	5.04		70.34	281.36
$NaHCO_3$_criteria 3	6.06		80.8	323.2
NaOH_Criteria 1	6.13	364.75 ± 3.5	95.54	382.16
NaOH_Criteria 2	4.88		70.06	280.24
NaOH_Criteria 3	5.2		77.18	308.72
H_2SO_4_Criteria 1	171.47	366.25 ± 2.1	99.9	399.6
H_2SO_4_Criteria 2	136.79		74.14	296.56
H_2SO_4_Criteria 3	149.49		81.76	327.04

Chapter 6

Isolation and characterization of lignocellulose derived inhibitor tolerant, high ethanol tolerant, xylose-fermenting ethanologenic yeast strains

6.1 Materials and methods

6.1.1 Isolation of the yeast

Four samples from sources such as decaying saw dust, corncobs, and pulp of the ripened Palmyra palm (*Borassus flabellifer*) fruit, were collated aseptically into commercially available sterile polypropylene sample containers of 50 ml volume (TARSONS, India. cat# 510030), and stored at 4°C until further processing. 1 gram of each sample was aseptically added to 20 mL of YPM8E5 enrichment medium (1% yeast extract, 2% peptone, 8% maltose, 5% ethanol (v/v), 50 µg/mL kanamycin, 50 µg/mL chloramphenicol, ampicillin 5 mg/ml taken in individual Erlenmeyer flasks of volume 100 ml, and incubated 30°C, for 72 hours in an orbital shaker incubator set at 150 rpm [360]. 30 µL of enrichment culture of each sample was plated on Wallenstein Laboratory Nutrient agar (WLN) (Himedia, M115), and incubated at 30°C, for 72 hours in a static incubator (Thermo). The colonies were screened for yeast morphology by performing simple staining with methylene blue and observed under a compound microscope, later the colonies were also visualized using a phase contrast microscope at 1000x magnification. Colonies with yeast morphology were plated on YPD agar medium (1% yeast extract, 2% peptone, 2% dextrose, and 2% agar). Pure isolates of the selected strains were mixed with 40% glycerol and stored at -80°C.

6.1.2 Screening for Ethanol producing yeasts

Durham tube fermentation test [361] was used to screen the yeast isolates for their ability to ferment the glucose. All cultures were grown in YPD broth for 60 hours. Subsequently, the culture broth was filtered through 0.2 µ syringe-driven filters, and the filtrate was appropriately diluted. The diluted solution was then passed through a Repromer H 300 x 8 mm (Dr. Maisch, Germany) HPLC column, connected to a UFLC system. The injection volume was 20 µL, and HPLC-grade water served as the mobile phase in isocratic mode. The column temperature was maintained at 60 °C, and a refractive index detector (RID 10A) with its cell temperature held at 60 °C was used for elution detection. To identify the ethanol peak, a pure ethanol standard with a concentration of 2

g/L was employed. The strains that can produce ethanol were selected for further biochemical characterization.

6.1.3 Media preparations for biochemical characterization

All the stock media solutions for biochemical characterization were prepared in 2x concentrations. The working 1X compositions of these media are as follows.

6.1.3.1 Carbon source assimilation and fermentation test

2% solutions of selected carbon sources (Galactose, Mannose, D-xylose, D-ribose, L-arabinose, Maltose, Lactose, Sucrose, Cellobiose, Salicin, starch, CMC (carboxymethyl cellulose), Cellulose, Avicel, Xylan, Methanol, Ethanol, Glycerol, Xylitol, DL-lactate, Succinic acid, and Citrate) were prepared by dissolving the respective carbon sources in 2 ml of yeast nitrogen base (YNB, Himedia), as outlined by C. Kurtzman et al. [362].

6.1.3.2 Nitrogen source assimilation test

The required weight of selected nitrogen sources (Ammonium sulphate, Ammonium citrate, Potassium nitrate, Sodium nitrite, Creatinine, Urea, D-proline, L-lysine) was calculated using equation 5.1, and separately dissolved in 2ml Yeast carbon base (Himedia), prepared according to the method described by [362]

$$x = \frac{0.108 \times FW^2}{100 \times NW}$$ (Equation 5.1)

Where x is the grams of nitrogen source containing 0.108 grams of nitrogen, FW is the formula weight of the nitrogen source, and NW is the per-molecule weight of the nitrogen in the source.

6.1.3.3 Inhibitor tolerance test

The selected inhibitors (4-Hydroxy Benzoic acid, Cinnamic acid, Gallic acid, Syringaldehyde, Tannic acid, Vanillin, Furfural, HMF, Acetic acid, Formic acid, Levulinic acid), were appropriately dissolved in sterile distilled water, to achieve six different concentrations each 0.01 g/l, 0.05 g/l, and 0.1 g/l (lower concentration range), and 1 g/l, 4 g/l, 7 g/l higher concentration range, these concentration ranges were selected based on the inhibitor studies available in the literature.

6.1.3.4 Osmotolerance tests

5% to 50% solutions of equal mixtures of glucose and fructose, as well as glucose and xylose, were prepared along with 1% yeast extract and 2% peptone.

6.1.3.5 pH tolerance tests

YPD media with different pH values ranging from 2.5 to 9.5 were prepared.

6.1.3.5 Yeast inoculum for biochemical characterization:

Inoculum for biochemical tests was prepared by starving the yeast cultures that were previously grown on YPD agar plates, by inoculating them into yeast nitrogen base medium with only 0.1% glucose, these cultures were incubated for 24 hours before they were used as inoculum. Later the turbidity of all the cultures was equally adjusted using 0.5 McFarland standard as the reference [363], where a sterile YNB solution without added carbon source was used to dilute the cultures if necessary.

6.1.3.6 Microplate assay for biochemical characterizations

130 µl of appropriate biochemical test media (2x concentration) was pipetted into 96 well plates, and 130 µl of yeast inoculum was added. The plates were incubated at 30 °C while shaking at 60 rpm in a microplate reader (Varioskan LUX, Thermo), the absorbance values were obtained at 595 nm at a kinetic interval of 15 minutes for 20 hours.

6.1.4 Genetic characterization and phylogenetic analysis of the selected yeasts

The genomic DNA of yeast cultures was extracted using the HiPurA Fungal DNA purification spin column kit (MB543-250PR, HiMedia, India) and subsequently analyzed by electrophoresis on a 1% agarose gel. Following this, the fungal-specific D1/D2 Domain of the 26S rRNA gene (680bp) was amplified via PCR, following the method described by HESHAM et al., 2017. The PCR reaction, constituting a total volume of 25 µL, included 12.5 µL of EmeraldAmp GT PCR Master Mix, 2x (Takara Bio USA), 1 µL of DNA template (50–100 ng), 1.25 µL (10 µM) of each primer (NL-1 and NL-4), and 9 µL of free-nuclease water. Amplification involved 36 cycles with specific temperature settings using the Applied Biosystems Veriti Thermal Cycler. The resulting PCR

products were visualized on a 1% agarose gel using GelRed Nucleic Acid Gel Stain and a UV transilluminator (ProteinSimple Red Imager SA-1000).

Subsequently, the PCR products underwent purification using the Exonuclease I and Shrimp Alkaline Phosphatase Purification Kit (New England Biolabs, Inc). Sequencing of the purified PCR products was carried out using the BigDye Terminator v.3.1 Cycle Sequencing Kit (Applied Biosystems, USA) and an Applied Biosystems 310 automatic sequencer. The sequencing conditions involved denaturation at 96°C for 1 min, followed by 28 cycles of 96°C for 1 min, 50°C for 05 s, and 60°C for 4 min. The cycle-sequenced amplicons were further purified using the sodium acetate ethanol method (Thermo Fisher Scientific) and analyzed on a 3500xL Genetic Analyzer (Applied Biosystems, USA). The generated sequencing files (.ab1) were edited using CHROMASLITE (version 1.5) and subsequently analyzed through the Basic Local Alignment Search Tool (BLAST - NCBI). Pairwise alignment was then employed to calculate sequence similarity values between the query sequence and those identified in the initial search, with each isolate reported based on the first five to ten hits in the database.

For accurate species prediction and understanding of evolutionary relationships, multiple sequence alignment and phylogenetic analysis were conducted. The evolutionary history was inferred using the Neighbor-Joining method, resulting in an optimal tree with a sum of branch length equal to 0.32425891. Bootstrap testing (1000 replicates) indicated the percentage of replicate trees where associated taxa clustered together, displayed above the branches. The tree was drawn to scale, with branch lengths in the same units as the evolutionary distances calculated using the Kimura 2-parameter method. The analysis involved 12 nucleotide sequences, excluding positions with gaps and missing data, resulting in a final dataset of 530 positions. The entire evolutionary analysis was executed using MEGA6.

6.2 Results and discussion

6.2.1 Screening of ethanol producing strain

All isolated strains, Y1 to Y6, exhibit yeast-like morphology, as evidenced by phase-contrast microscopy (Figure 6.1). Except for Y3 and Y7, all other yeast strains are fermentative. This has been confirmed through the Durham test and HPLC analysis (Figure 6.2).

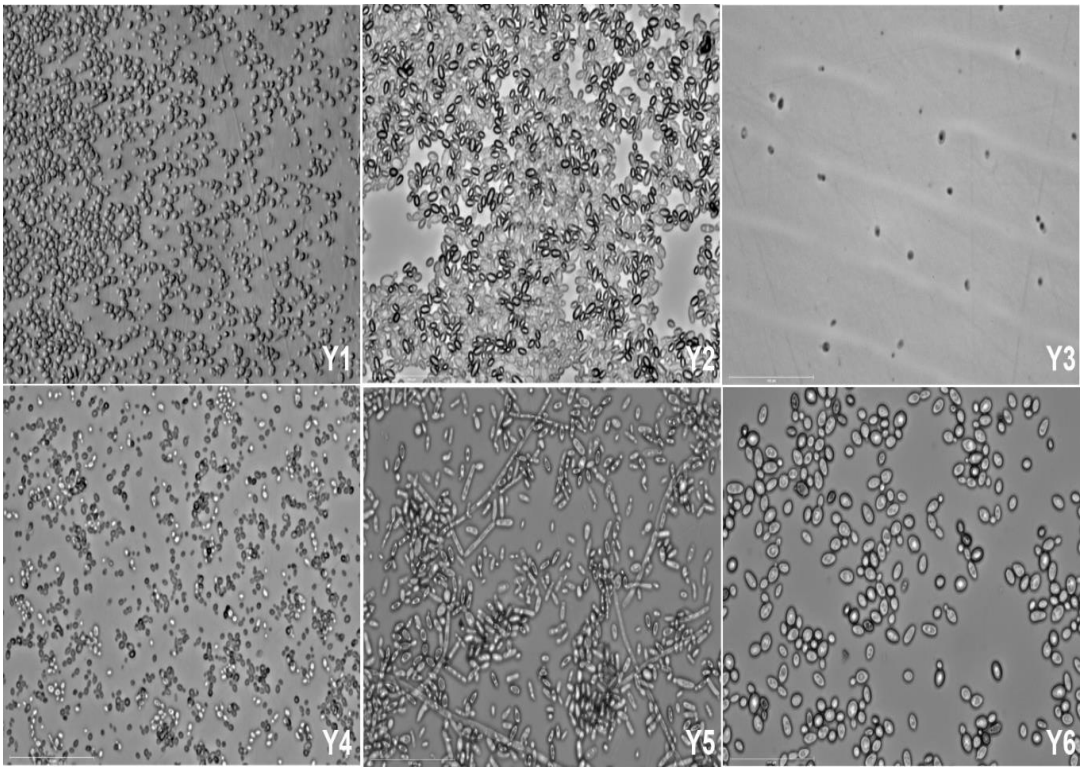

Figure 6.1 Morphology of the isolated cultures

Phase contrast microscopic images of isolated yeasts

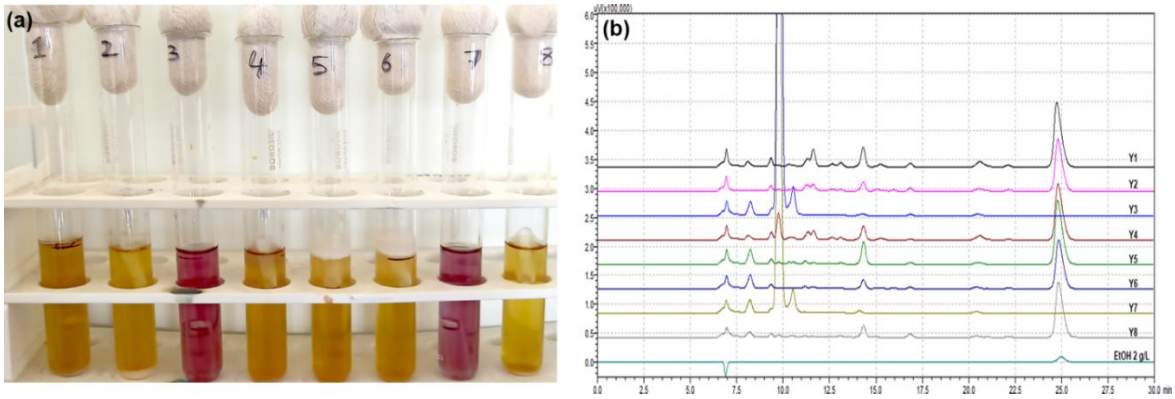

Figure 6.2: Ethanol fermentation test

a) Durham tube test: Except for Y3 and Y7, all other strains exhibit fermentation, as evidenced by the visible color change of the indicator. This is further confirmed by the presence of an ethanol peak around retention time 24 minutes in the HPLC analysis (b), observed in all strains except Y3 and Y7

6.2.2 Inhibitor tolerance

Yeasts Y2 and Y5 have demonstrated enhanced resistance to most of the inhibitors studied. Y2 and Y5 exhibit excellent resistance against all concentration ranges of lignin-derived inhibitors (4-Hydroxy Benzoic acid, Cinnamic acid, Gallic acid, Syringaldehyde, Vanillin), while Y1, Y4, and Y6 display moderate resistance. Y2 shows moderate resistance to tannic acid at lower concentrations and weak resistance at higher concentrations, whereas all other yeasts are inhibited. Against sugar-derived inhibitors such as Levulinic acid, Furfural, and 5-Hydroxy Methyl Furfural, both Y2 and Y5 exhibit significant resistance. Y5 demonstrates better resistance against furfural than Y2, and Y2 exhibits better resistance against HMF than Y5. All yeast strains are completely inhibited by acetic acid and formic acid at all concentration ranges, whereas Y2 and Y5 show weak tolerance against formic acid at a concentration of 0.01 g/L. (Figure 6.3)

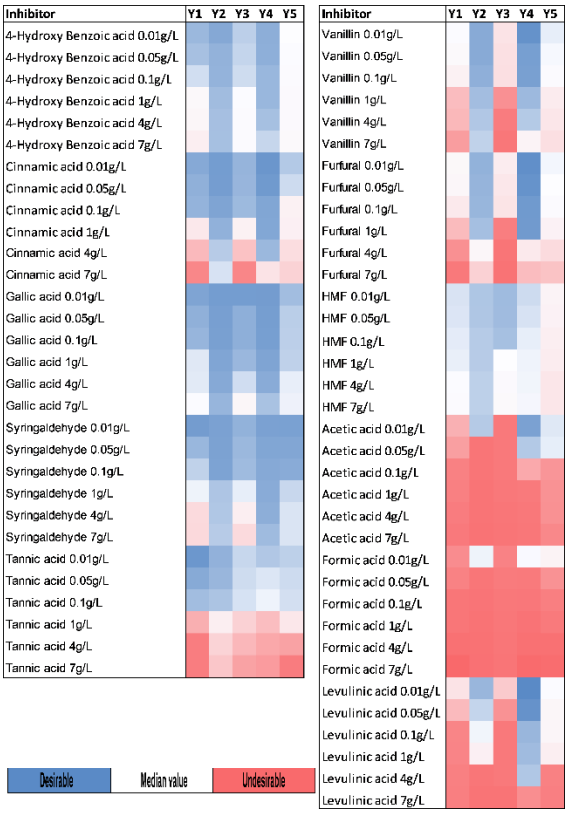

Figure 6.3 Heat map for inhibitor tolerance of selected yeasts
Y1, Y2, Y4, Y5, Y6 represent the yeast isolates that were studied, the colour blue represents the desirable trait, and the colour red represents the undesirable trait, and the colour white represents the median value of the two extremes.

6.2.3 Carbon source assimilation

All yeast strains exhibited assimilation of both galactose and D-Xylose. Y1 and Y4 demonstrated the best assimilation of galactose among the strains, while Y6 and Y5 exhibited the best assimilation of D-Xylose. Y5 showed superior assimilation of mannose compared to the other strains. Y1 and Y4 assimilated cellobiose better than the rest of the strains. Y1, Y2, and Y4 displayed weak assimilation of cellulose and Avicel, while Y5 performed comparatively better than the others. Y5 exhibited good assimilation of Xylan. Both Y2 and Y5 displayed the best assimilation of Dl-lactate, Succinate, and citrate, while others showed moderate assimilation of these carbon sources. Additionally, Y2 and Y5 exhibited moderate but better assimilation of Methanol and ethanol compared to the other strains. All the strains showed equally moderate assimilation of glycerol and xylitol.

6.2.4 Osmotolerance

Both Y2 and Y5 have shown excellent tolerance at all concentrations of glucose and fructose combination. They also exhibited excellent tolerance at all concentrations of glucose and xylose, but a moderate tolerance at 50% of the glucose and xylose combination. The remaining strains demonstrated moderate to good tolerance at lower concentrations of both sugar combinations but were inhibited at higher concentrations. (Figure 6.4)

6.2.5 pH tolerance

Y1 is active around pH 4.5 to 5.5, with moderate to zero growth observed when the pH is moved to either extreme. Y2 showed growth across the entire pH range tested, with the highest growth in the range of pH 4.5 to 8.5. Y4 is active around pH 4.5 to 7.5. Y5 exhibited excellent growth from pH 2.5 to 8.5, and the growth rate of Y5 in this entire pH range surpasses that of all other strains at their respective optimum ranges. Y6 is active in the range of 4.5 to 6.5.

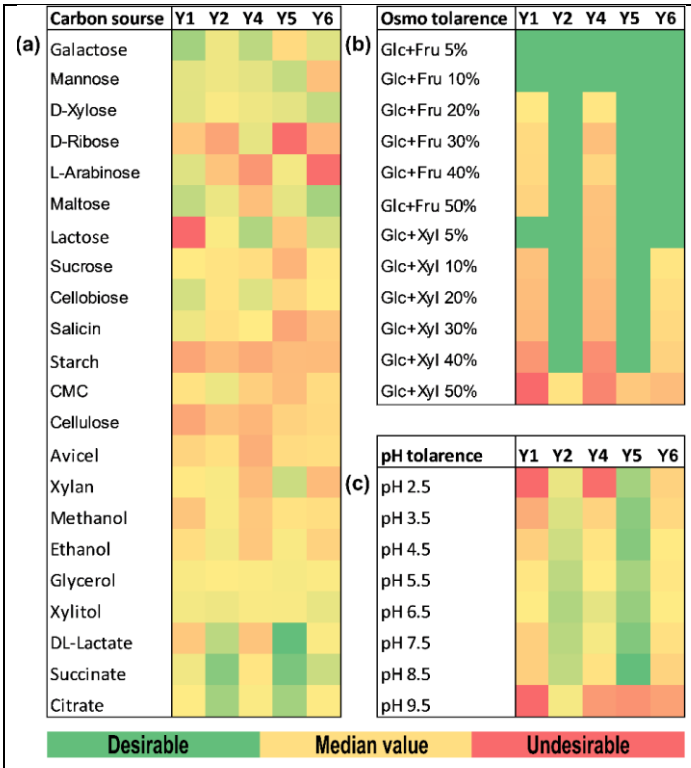

Figure 6.4 Heat map for carbon source assimilation, pH and Osmotolerance

Y1, Y2, Y4, Y5, Y6 represent the yeast isolates that were studied, the colour green represents the desirable trait, and the colour red represents the undesirable trait, and the colour yellow represents the median value of the two extremes.

6.2.6 Genetic characterization and phylogenetic analysis of the selected yeasts

The partial sequencing of the large subunit ribosomal RNA gene revealed that isolates Y2 and Y5 belong to *Candida tropicalis* and *Pichia kudriavzevii*, respectively. These genome sequences have been uploaded to GenBank-NCBI with accession numbers PP527166 and PP527167, respectively.

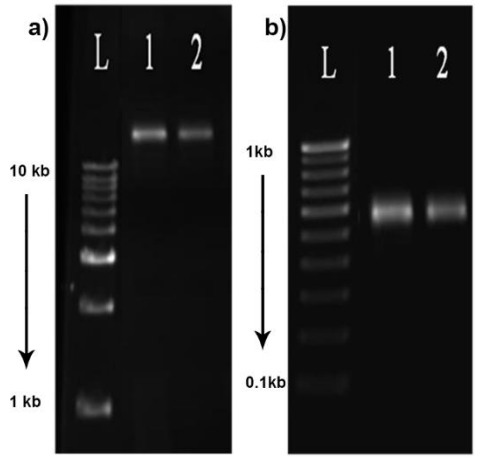

Figure 6.5 Agarose gel runs of the a) genomic DNA isolates and b) PCR products. L1 = DNA ladder, 1 = Yeast Y2, and 2 = yeast Y5

Table 6.1 Raw Genomic sequences of D1/D2 Domain of the 26S rRNA gene of Y2

```
>NL4RC_NL1_Seq159_Y2_NC111223A
CATATCAATAAGCGGAGGAAAAGAAACCAACAGGGATTGCCTTAGTAGC
GGCGAGTGAAGCGGCAAAAGCTCAAATTTGAAATCTGGCTCTTTCAGAG
TCCGAGTTGTAATTTGAAGAAGGTATCTTTGGGTCTGGCTCTTGTCTATGT
TTCTTGGAACAGAACGTCACAGAGGGTGAGAATCCCGTGCGATGAGATG
ATCCAGGCCTATGTAAAGTTCCTTCGAAGAGTCGAGTTGTTTGGGAATGC
AGCTCTAAGTGGGTGGTAAATTCCATCTAAAGCTAAATATTGGCGAGAG
ACCGATAGCGAACAAGTACAGTGATGGAAAGATGAAAAGAACTTTGAA
AAGAGAGTGAAAAAGTACGTGAAATTGTTGAAAGGGAAGGGCTTGAGA
TCAGACTTGGTATTTTGTATGTTACTTCTTCGGGGGTGGCCTCTACAGTTT
ATCGGGCCAGCATCAGTTTGGGCGGTAGGAGAATTGCGTTGGAATGTGG
CACGGCTTCGGTTGTGTGTTATAGCCTTCGTCGATACTGCCAGCCTAGAC
TGAGGACTGCGGTTTATACCTAGGATGTTGGCATAATGATCTTAAGTCGC
CCGTCTTGAAACACGGACCA

>NL1_Seq156_Y2_NC111223A
TTTGAAGAAGGTATCTTTGGGTCTGGCTCTTGTCTATGTTTCTTGGAACAGAAC
GTCACAGAGGGTGAGAATCCCGTGCGATGAGATGATCCAGGCCTATGTAAAGT
TCCTTCGAAGAGTCGAGTTGTTTGGGAATGCAGCTCTAAGTGGGTGGTAAATTC
CATCTAAAGCTAAATATTGGCGAGAGACCGATAGCGAACAAGTACAGTGATGG
AAAGATGAAAAGAACTTTGAAAAGAGAGTGAAAAAGTACGTGAAATTGTTGA
AAGGGAAGGGCTTGAGATCAGACTTGGTATTTTGTATGTTACTTCTTCGGGGGT
GGCCTCTACAGTTTATCGGGCCAGCATCAGTTTGGGCGGTAGGAGAATTGCGTT
GGAATGTGGCACGGCTTCGGTTGTGTGTTATAGCCTTCGTCGATACTGCCAGCC
TAGACTGAGGACTGCGGTTTATACCTAGGATGTTGGCATAATGATCTTAAGTCG
CCCGTCTTGAAACACGGACCA

>NL4_Seq156_Y2_NC111223A
```

GAAGCCGTGCCACATTCCAACGCAATTCTCCTACCGCCCAAACTGATGCTGGCC
CGATAAACTGTAGAGGCCACCCCCGAAGAAGTAACATACAAAATACCAAGTCT
GATCTCAAGCCCTTCCCTTTCAACAATTTCACGTACTTTTTCACTCTCTTTTCAA
AGTTCTTTTCATCTTTCCATCACTGTACTTGTTCGCTATCGGTCTCTCGCCAATA
TTTAGCTTTAGATGGAATTTACCACCCACTTAGAGCTGCATTCCCAAACAACTC
GACTCTTCGAAGGAACTTTACATAGGCCTGGATCATCTCATCGCACGGGATTCT
CACCCTCTGTGACGTTCTGTTCCAAGAAACATAGACAAGAGCCAGACCCAAAG
ATACCTTCTTCAAATTACAACTCGGACTCTGAAAGAGCCAGATTTCAAATTTGA
GCTTTTGCCGCTTCACTCGCCGCTACTAAGGCAATCCCTGTTGGTTTCTTTTCCT
CCGCTTATTGATATG

>NL4_Seq156_Y2_NC111223A_RC(Reverse Complement)
CATATCAATAAGCGGAGGAAAAGAAACCAACAGGGATTGCCTTAGTAGCGGC
GAGTGAAGCGGCAAAAGCTCAAATTTGAAATCTGGCTCTTTCAGAGTCCGAGT
TGTAATTTGAAGAAGGTATCTTTGGGTCTGGCTCTTGTCTATGTTTCTTGGAAC
AGAACGTCACAGAGGGTGAGAATCCCGTGCGATGAGATGATCCAGGCCTATGT
AAAGTTCCTTCGAAGAGTCGAGTTGTTTGGGAATGCAGCTCTAAGTGGGTGGT
AAATTCCATCTAAAGCTAAATATTGGCGAGAGACCGATAGCGAACAAGTACAG
TGATGGAAAGATGAAAAGAACTTTGAAAAGAGAGTGAAAAAGTACGTGAAAT
TGTTGAAAGGGAAGGGCTTGAGATCAGACTTGGTATTTTGTATGTTACTTCTTC
GGGGGTGGCCTCTACAGTTTATCGGGCCAGCATCAGTTTGGGCGGTAGGAGAA
TTGCGTTGGAATGTGGCACGGCTTC

Table 6.2 nBLAST results for the Yeast Y2

S.No	Description	Scientific Name	Max Score	Total Score	Query Cover	E value	Per. Ident	Acc. Len	Accession
1	*Candida tropicalis* ATCC 750 28S rRNA, partial sequence; from TYPE material	*Candida tropicalis*	1099	1099	97%	0	100.00%	865	NG_054834.1
2	*Candida tropicalis* strain ATCC 750 28S large subunit ribosomal RNA gene, partial sequence	*Candida tropicalis*	1094	1094	96%	0	100.00%	592	KU729147.1
3	*Candida sojae* strain CBS 7871 small subunit ribosomal RNA gene, partial sequence; internal transcribed spacer 1, 5.8S ribosomal RNA gene, and internal transcribed spacer 2, complete sequence; and large subunit ribosomal RNA gene, partial sequence	*Candida sojae*	1079	1079	100%	0	98.38%	2656	MK394120.1
4	*Candida neerlandica* strain CBS 434 small subunit ribosomal RNA gene, partial sequence; internal transcribed spacer 1, 5.8S ribosomal RNA gene, and internal transcribed spacer 2, complete sequence; and large subunit ribosomal RNA gene, partial sequence	*Candida neerlandica*	1055	1055	100%	0	97.72%	2658	MK394121.1
5	*Candida neerlandica* culture CBS:434 large subunit ribosomal RNA gene, partial sequence	*Candida neerlandica*	1055	1055	100%	0	97.72%	912	KY106596.1

Table 6.3 Raw Genomic sequences of D1/D2 Domain of the 26S rRNA gene of Y5

>NL4RC_NL1_Seq159_Y5_NC121223
TGCATATCAATAAGCGGAGGAAAAGAAACCAACAGGGATTGCCTCAGTAGCG
GCGAGTGAAGCGGCAAGAGCTCAGATTTGAAATCGTGCTTTGCGGCACGAGTT
GTAGATTGCAGGTTGGAGTCTGTGTGGAAGGCGGTGTCCAAGTCCCTTGGAAC
AGGGCGCCCAGGAGGGTGAGAGCCCCGTGGGATGCCGGCGGAAGCAGTGAGG
CCCTTCTGACGAGTCGAGTTGTTTGGGAATGCAGCTCCAAGCGGGTGGTAAATT
CCATCTAAGGCTAAATACTGGCGAGAGACCGATAGCGAACAAGTACTGTGAAG
GAAAGATGAAAAGCACTTTGAAAAGAGAGTGAAACAGCACGTGAAATTGTTG
AAAGGGAAGGGTATTGCGCCCGACATGGGGATTGCGCACCGCTGCCTCTCGTG
GGCGGCGCTCTGGGCTTTCCCTGGGCCAGCATCGGTTCTTGCTGCAGGAGAAG
GGGTTCTGGAACGTGGCTCTTCGGAGTGTTATAGCCAGGGCCAGATGCTGCGT
GCGGGGACCGAGGACTGCGGCCGTGTAGGTCACGGATGCTGGCAGAACGGCG
CAACACCGCCCGTCTTGAAACACGGACCAA
>NL1_Seq156_Y5_NC111223A
ACTTCCCTTGGAACAGGGCGCCCAGGAGGGTGAGAGCCCCGTGGGATGCCGGC
GGAAGCAGTGAGGCCCTTCTGACTAGTCGAGTTGTTTGGGAATGCAGCTCCAA
GCGGGTGGTAAATTCCATCTAAGGCTAAATACTGGCGAGAGACCGATAGCGAA
CAAGTACTGTGAAGGAAAGATGAAAAGCACTTTGAAAAGAGAGTGAAACAGC
ACGTGAAATTGTTGAAAGGGAAGGGTATTGCGCCCGACATGGGGATTGCGCAC
CGCTGCCTCTCGTGGGCGGCGCTCTGGGCTTTCCCTGGGCCAGCATCGGTTCTT
GCTGCAGGAGAAGGGGTTCTGGAACGTGGCTCTTCGGAGTGTTATAGCCAGGG
CCAGATGCTGCGTGCGGGGACCGAGGACTGCGGCCGTGTAGGTCACGGATGCT
GGCAGAACGGCGCAACACCGCCCGTCTTGAAACACGGACCAA
>NL4_Seq156_Y5_NC121223
AACCGATGCTGGCCCAGGGAAAGCCCAGAGCGCCGCCCACGAGAGGCAGCGG
TGCGCAATCCCCATGTCGGGCGCAATACCCTTCCCTTTCAACAATTTCACGTGC
TGTTTCACTCTCTTTTCAAAGTGCTTTTCATCTTTCCTTCACAGTACTTGTTCGCT
ATCGGTCTCTCGCCAGTATTTAGCCTTAGATGGAATTTACCACCCGCTTGGAGC
TGCATTCCCAAACAACTCGACTCGTCAGAAGGGCCTCACTGCTTCCGCCGGCAT
CCCACGGGGCTCTCACCCTCCTGGGCGCCCTGTTCCAAGGGACTTGGACACCGC
CTTCCACACAGACTCCAACCTGCAATCTACAACTCGTGCCGCAAAGCACGATTT
CAAATCTGAGCTCTTGCCGCTTCACTCGCCGCTACTGAGGCAATCCCTGTTGGT
TTCTTTTCCTCCGCTTATTGATATGCA
>NL4_Seq156_Y5_NC121223_RC(Reverse Complement)
TGCATATCAATAAGCGGAGGAAAAGAAACCAACAGGGATTGCCTCAGTAGCG
GCGAGTGAAGCGGCAAGAGCTCAGATTTGAAATCGTGCTTTGCGGCACGAGTT
GTAGATTGCAGGTTGGAGTCTGTGTGGAAGGCGGTGTCCAAGTCCCTTGGAAC
AGGGCGCCCAGGAGGGTGAGAGCCCCGTGGGATGCCGGCGGAAGCAGTGAGG
CCCTTCTGACGAGTCGAGTTGTTTGGGAATGCAGCTCCAAGCGGGTGGTAAATT
CCATCTAAGGCTAAATACTGGCGAGAGACCGATAGCGAACAAGTACTGTGAAG
GAAAGATGAAAAGCACTTTGAAAAGAGAGTGAAACAGCACGTGAAATTGTTG
AAAGGGAAGGGTATTGCGCCCGACATGGGGATTGCGCACCGCTGCCTCTCGTG
GGCGGCGCTCTGGGCTTTCC

Table 6.4 nBLAST results for the Yeast Y5

S.No	Description	Scientific Name	Max Score	Total Score	Query Cover	E value	Per. Ident	Acc. Len	Accession
1	*Pichia kudriavzevii* strain CBS 5147 18S small subunit ribosomal RNA gene, partial sequence; internal transcribed spacer 1, 5.8S ribosomal RNA gene, and internal transcribed spacer 2, complete sequence; and 26S large subunit ribosomal RNA gene, partial sequence	*Pichia kudriavzevii*	1120	1120	99%	0	99.84%	2746	MH545928.1
2	*Pichia kudriavzevii* strain CBS 5147 small subunit ribosomal RNA gene, partial sequence; internal transcribed spacer 1, 5.8S ribosomal RNA gene, and internal transcribed spacer 2, complete sequence; and large subunit ribosomal RNA gene, partial sequence	*Pichia kudriavzevii*	1120	1120	99%	0	99.84%	2607	MK394162.1
3	*Pichia kudriavzevii* strain CBS5147 chromosome 1, complete sequence	*Pichia kudriavzevii*	1120	1120	99%	0	99.84%	2861343	CP028531.1
4	*Pichia kudriavzevii* strain CBS5147 chromosome 2, complete sequence	*Pichia kudriavzevii*	1114	1114	99%	0	99.67%	2715831	CP028532.1
5	*Pichia kudriavzevii* culture CBS:5147 large subunit ribosomal RNA gene, partial sequence	*Pichia kudriavzevii*	1094	1094	99%	0	99.18%	805	KY108833.1

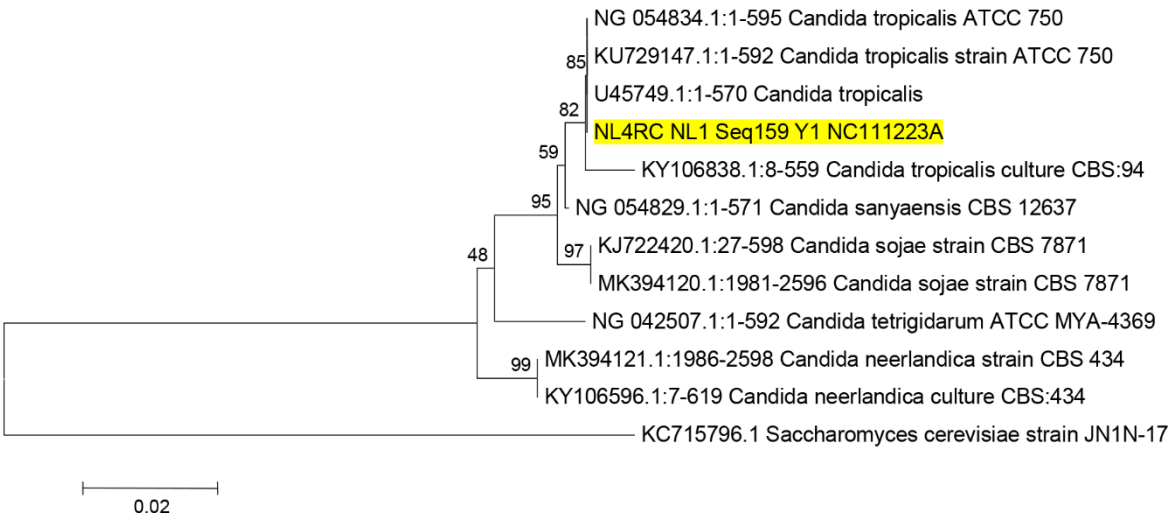

Figure 6.6 Phylogenetic analysis of yeast Y2

The assessment of evolutionary relationships among taxa utilized the Neighbor-Joining method [9]. The resulting optimal tree, with a sum of branch length equal to 0.21509139, is presented. The bootstrap test (1000 replicates) revealed the percentage of replicate trees wherein the associated

taxa clustered together, displayed above the branches [10]. The tree was meticulously drawn to scale, with branch lengths expressed in the same units as those employed in determining the evolutionary distances for phylogenetic inference. The evolutionary distances were computed using the Kimura 2-parameter method [11], measured in the units of the number of base substitutions per site. This analysis involved 12 nucleotide sequences, and positions with gaps or missing data were systematically eliminated. The final dataset comprised a total of 536 positions. All evolutionary analyses were executed using MEGA6 [12].

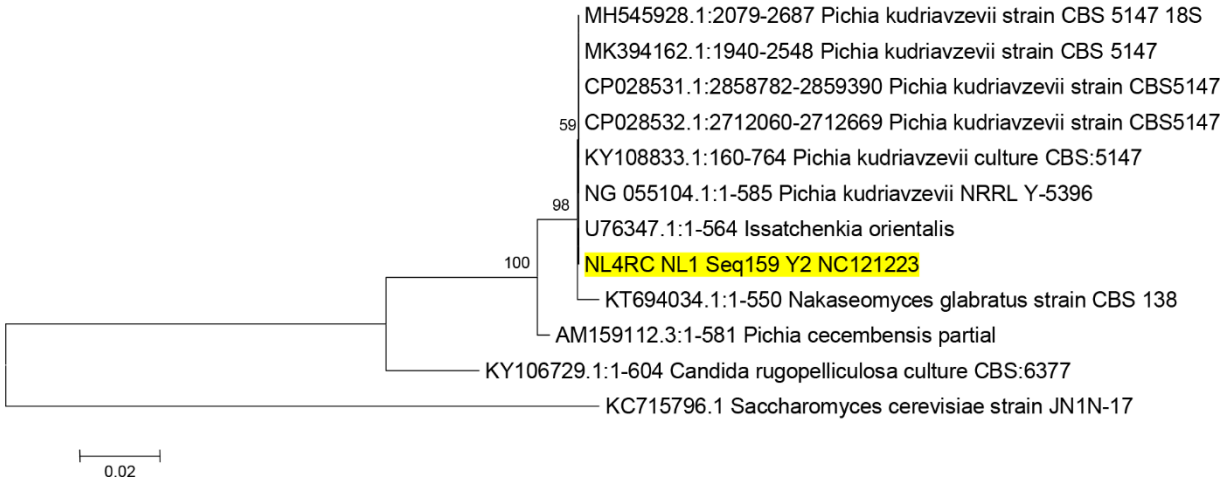

Figure 6.7 Phylogenetic analysis of yeast Y5

The investigation into the evolutionary relationships among taxa employed the Neighbor-Joining method [9]. The resultant optimal tree, depicting a sum of branch lengths equal to 0.32425891, is presented. Above the branches, the percentage of replicate trees wherein the associated taxa clustered together in the bootstrap test (1000 replicates) is indicated [10]. The tree was accurately drawn to scale, portraying branch lengths in units consistent with those used to infer the phylogenetic tree's evolutionary distances. These distances were computed using the Kimura 2-parameter method [11], expressed in units denoting the number of base substitutions per site. The analysis comprised 12 nucleotide sequences, with systematic removal of positions containing gaps and missing data. The final dataset encompassed a total of 530 positions, and all evolutionary analyses were conducted using MEGA6 [12]

Chapter 7

Co-production of Bioethanol and Glycerol from the Outer Anatomical Portion of Corncob, with Emphasis on Pith: Evaluating Inhibitor Adsorbing Efficiency in Comparison with Established Surfactants.

7.1 Materials and methods

7.1.1 Biomass and other materials

Corncob outer residues derived from three different pretreatments, namely $NaHCO_3$, NaOH, and sequential (NaOH followed by H_2SO_4) are termed as COr1, COr2, and COr3 respectively, are the biomass used in this study. The effect of Corncob pith (CP) to enhance enzymatic saccharification and fermentation as an adsorbant, was compared with certain Surfactants (Amberlite IRA-400 chloride form, Amberlite IRA-96 free base, Polyethylene glycol 6000, Silica gel 100-200 Mesh, Tween 20, and Tween 80) that are known for their ability to improve saccharification and fermentation processes by reducing the effective localized concentration of lignin derived inhibitors by adsorption or flocculation. The commercial enzyme cocktail containing 10 FPU cellulase (sigma Aldrich), 5U β- glucosidase (Himedia), and 10 U Xylanase (Merck) per gram of biomass, and 0.02% (w/v) sodium azide was prepared in 0.05 M sodium citrate buffer, pH 4.8.

7.1.2 Microorganisms used for the fermentation

The yeast Y5 (*Pichia kudriavzevii*) was selected based on its ethanol and lactic acid production capacity. The glycerol stock culture was revived and maintained on YPD broth. The actively growing culture was inoculated into a larger volume YPD broth (500 ml × 4) and cultured for 48 hours, at 30°C, and 150 rpm in an orbital shaker. The culture was then centrifuged in sterile tubes, and the pellets were collected. The pellets were washed, dissolved in the sterile distilled water, and diluted to 0.5 McFarland standard equivalent turbidity [363].

7.1.3 Effect of surfactants and adsorbents on enzymatic saccharification

0.2 grams of COR1, COr2, and COr3 were saccharified individually using the enzyme cocktail, with a final liquid-to-solid ratio of 25. The reaction mixture was added with individual surfactants or adsorbents that were weighed (solids) or diluted (liquids) to achieve three different final concentrations 0.1%, 0.5%, and 1%. The enzymatic saccharification was carried in culture tubes, for 60 hours, at 30 °C, and 150 rpm in an orbital shaker. 50 µl of the sample was collected at three

different time intervals, 10 hrs, 30 hrs, and 60 hrs. Control saccharification was also conducted without including the surfactants or adsorbents. The aliquots were analysed for the total reducing sugars released by the DNS method. Appropriate enzyme and adsorbent controls were used to subtract their absorption. The final concentration of glucose and xylose released was estimated using the HPLC method as described in Chapter 1. The best-performing adsorbent was selected further to saccharify a larger quantity of the corncob residues. At the end of saccharification, the reaction mixture was filtered through the grade 1 Buckner funnel, and the filtrate was analysed for its glucose and xylose concentrations. The filtrate was maintained at 4 °C until the fermentation.

7.1.4 Co-production of bioethanol and Glycerol in Separate hydrolysis and co-fermentation mode (SHCF)

The sugar solution obtained from the saccharification of the CO residues was diluted appropriately to include the exact concentration of glucose and xylose obtained from the enzymatic saccharification of the respective CO residue. 5 g/L yeast extract, 10 g/L Peptone, 2 g/L KH_2PO_4 and 1 g/L $MgSO_4$. $7H_2O$, 0.05 g/L chloramphenicol, were dissolved in the sugar solution, and adjusted the pH to 4.8 to make the fermentation medium, the medium was sterilized by autoclaving. To the 10 ml culture medium taken in 50 ml culture tubes, 0.05 ml of the Y2 inoculum was added, and the tubes were capped aseptically. 0.05 ml aliquots of fermenting broth were collected aseptically at 15hr, 30hr, and 60hr intervals. The aliquots were stored at 4°C until they were analysed for glucose, xylose, glycerol and ethanol using HPLC (Prominence UFLC, Shimadzu, Kyoto, Japan, 604-8442) equipped Repromer-H (Dr Maisch GmbH, Beim Brückle, Germany, 1472119) column and an appropriate guard column maintained at 60°C. 20 µL of the samples were injected and run in isocratic mode using HPLC-grade water as the mobile phase. The peak retention data were collected using a refractive index detector (RID-10A) with a flow cell temperature of 60°C. HPLC grade glucose, xylose, glycerol and ethanol were used as standards to make calibration curves and the resultant peak data was integrated using Labsolutions lite (Shimadzu, Japan) software. The sugar yields and saccharification were calculated using equation 7.1, and the ethanol and glycerol yields were calculated based on equations 7.2 and 6.3 respectively.

7.1.5 Simultaneous saccharification and co-production

0.2 grams of COR1, COr2, and COr3 were taken in a culture media to achieve a final liquid-to-solid ratio of 25. The media consisted of all the constituents that were mentioned in sections 6.1.3 and 6.1.4 for saccharification and fermentation respectively. The final pH was adjusted to 4.8 and the fermentation was carried for 60 hrs. The aliquot collection and their analysis were also done as mentioned in those sections. The respective concentrations and yields were calculated using equations 6.1 to 6.3.

$$\boldsymbol{Saccharification\ yield}\ (\boldsymbol{wt.}\%) = \left\{\frac{[\boldsymbol{sugar}]_{\boldsymbol{COr}}}{[\boldsymbol{sugar\ total}]_{\boldsymbol{NREL}}}\right\} \times \mathbf{100} \qquad \text{equation 7.1}$$

$$\boldsymbol{Ethanol\ yield}\ (\boldsymbol{wt.}\%) = \left\{\frac{[\boldsymbol{EtOH}]_{\boldsymbol{COr}}}{[\boldsymbol{EtOH}]_{\boldsymbol{T.Y}}}\right\} \times \mathbf{100} \qquad \text{equation 7.2}$$

$$\boldsymbol{Glycerol\ yield}\ (\boldsymbol{wt.}\%) = \left\{\frac{[\boldsymbol{GlOH}]_{\boldsymbol{COr}}}{[\boldsymbol{GlOH}]_{\boldsymbol{T.Y}}}\right\} \times \mathbf{100} \qquad \text{equation 7.3}$$

Where, $[sugar]_{COr}$ represents the amount of sugar (glucose or xylose) released from the respective CO residue upon enzymatic saccharification; $[sugar]_{NREL}$ is the total sugar concentration (glucose or xylose) of the COr estimated by the NREL method. $[EtOH]_{COr}$ and $[GlOH]_{COr}$ are the ethanol and glycerol concentrations respectively obtained from the fermentation of sugars released from the respective CO-residues. $[EtOH]_{T.Y}$, $[GlOH]_{T.Y}$ are the theoretical ethanol and glycerol concentrations respectively obtained from the total glucose and xylose concentrations of the respective CO-residues (the theoretical considerations from the yeast metabolic stoichiometric reactions are 1 gr of Glucose or xylose produces 0.511 grams of ethanol or 0.022 grams of glycerol.)

7.2 Results and discussion

7.2.1 The SHCF process

Figure 7.1 illustrates the comparative efficiencies of different surfactants and adsorbents used in the study for their effect on the enzymatic saccharification of the respective CO-residues. Where the CP has promoted the highest productivity, next to it are Tween 20, Tween 80, and PEG respectively.

The results of SHCF can be seen in Tables 7.1, 7.2, and 7.3, for COr1, COr2, and COr3 respectively. The maximum GlOH and EtOH obtained from 1 gram of COr1 are 0.017 g, and 0.119 g respectively, with respective theoretical yields of 5.7% and 39.2 %. For COr2 the maximum obtained GlOH and EtOH are 0.02 g, and 0.13 g respectively, with respective theoretical yields of 5.7% and 39.2 %. For COr3 the obtained GlOH and EtOH are 0.016 g, and 0.11 g respectively, with respective theoretical yields of 5.71% and 39.18 %. CP added media has shown the highest glycerol yield whereas Tween 80 added media showed the highest ethanol production. Figure 7.2 illustrates the analysis of the fermentation yields of the CO residue hydrolysates.

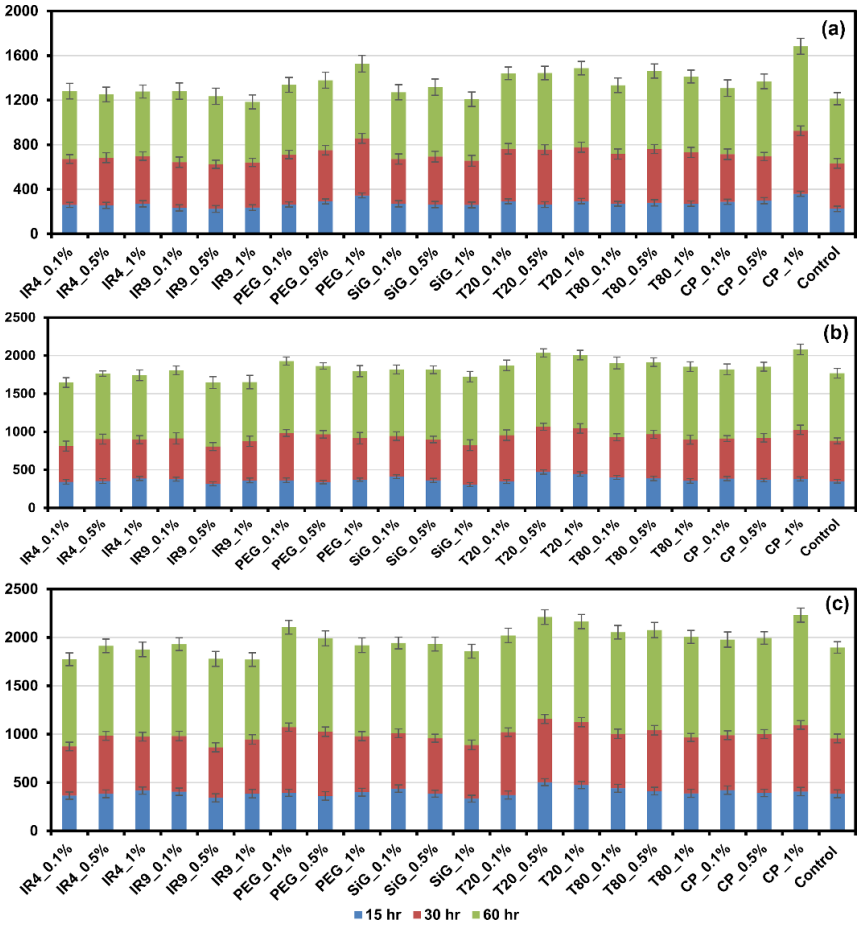

Figure 7.1 Effect of surfactants and adsorbents on enzymatic saccharification

a) b) c) Enzymatic saccharification yields of COr1, COr2, COr3 respectively. The blue, red and green bars represent the concentration of the total sugar (glucose and xylose) released at the time intervals 15 hrs, 30 hrs, and 60 hrs respectively.

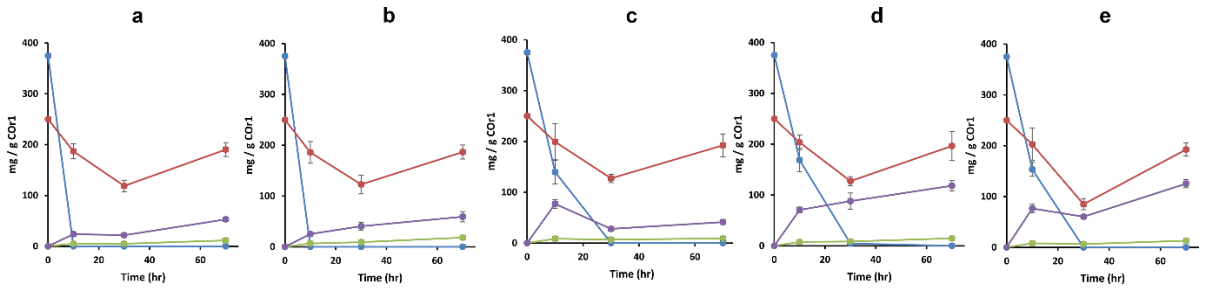

Figure 7.2 Effect of surfactants and adsorbents on the fermentation of sugars obtained from COr1 saccharification.

These are the results of the fermentation of the sugars obtained from the COr1 saccharification, the results of COr2 and COr3 obtained sugars are also almost the same as this. (a) to (e) represents the type of surfactant/adsorbent used in the respective experiments, a) control, b) CP, c) PEG, d) Tween 20, and e) Tween 80.

Table 7.1 SHCF results for COr1

Time (hr)	Adsorbent /control	GlOH g/g COr1	EtOH g/g CO1	GlOH %T.Y_COr1	EtOH %T.Y_CO1
10	PEG	0.008 ± 0.0002	0.073 ± 0.002	2.70	24.10
10	T20	0.007 ± 0.0002	0.067 ± 0.002	2.40	22.10
10	T80	0.008 ± 0.0002	0.073 ± 0.002	2.50	23.90
10	CP	0.006 ± 0.0002	0.024 ± 0.001	2.10	7.90
10	Ctrl	0.005 ± 0.0001	0.023 ± 0.001	1.60	7.50
30	PEG	0.006 ± 0.0001	0.027 ± 0.001	2.10	8.80
30	T20	0.008 ± 0.0002	0.084 ± 0.002	2.70	27.50
30	T80	0.006 ± 0.0002	0.057 ± 0.002	2.00	18.90
30	CP	0.009 ± 0.0003	0.039 ± 0.001	2.90	12.70
30	Ctrl	0.005 ± 0.0001	0.021 ± 0	1.60	6.80
60	PEG	0.009 ± 0.0002	0.039 ± 0.001	2.90	12.90
60	T20	0.014 ± 0.0004	0.113 ± 0.003	4.60	37.00
60	T80	0.012 ± 0.0004	0.119 ± 0.003	4.10	39.20
60	CP	0.017 ± 0.0004	0.056 ± 0.001	5.70	18.50
60	Ctrl	0.011 ± 0.0002	0.05 ± 0.001	3.60	16.60

Time = sample aliquot collection time; PEG = polyethylene glycol; T20 = tween 20; T80 = tween 80; GlOH = glycerol; EtOH = Ethanol; %T.Y = % of the theoretical yield

Table 7.2 SHCF results for COr2

Time (hr)	Adsorbent /control	GlOH g/g COr2	EtOH g/g COr2	GlOH %T.Y_COr2	EtOH %T.Y_CO2
10	PEG	0.009 ± 0.0002	0.08 ± 0.002	2.70	24.10
10	T20	0.008 ± 0.0002	0.08 ± 0.002	2.40	22.20
10	T80	0.009 ± 0.0002	0.08 ± 0.002	2.50	24.00
10	CP	0.007 ± 0.0002	0.03 ± 0.001	2.10	7.90
10	Ctrl	0.006 ± 0.0001	0.03 ± 0.001	1.60	7.50
30	PEG	0.007 ± 0.0002	0.03 ± 0.001	2.10	8.80
30	T20	0.009 ± 0.0003	0.09 ± 0.003	2.70	27.60
30	T80	0.007 ± 0.0002	0.06 ± 0.001	2.00	18.90
30	CP	0.01 ± 0.0003	0.04 ± 0.001	2.90	12.70
30	Ctrl	0.005 ± 0.0001	0.02 ± 0.001	1.60	6.80
60	PEG	0.01 ± 0.0002	0.04 ± 0.001	2.90	12.90
60	T20	0.016 ± 0.0004	0.13 ± 0.003	4.60	37.00
60	T80	0.014 ± 0.0004	0.13 ± 0.003	4.10	39.20
60	CP	0.02 ± 0.0005	0.06 ± 0.002	5.70	18.60
60	Ctrl	0.012 ± 0.0003	0.06 ± 0.002	3.60	16.60

Time = sample aliquot collection time; PEG = polyethylene glycol; T20 = tween 20; T80 = tween 80; GlOH = glycerol; EtOH = Ethanol; %T.Y = % of the theoretical yield

Table 7.3 SHCF results for COr3

Time (hr)	Adsorbent /control	GlOH g/g COr3	EtOH g/g COr3	GlOH %T.Y_COr3	EtOH %T.Y_CO3
10	PEG	0.007 ± 0.0002	0.07 ± 0.002	2.66	24.09
10	T20	0.007 ± 0.0001	0.06 ± 0.001	2.42	22.13
10	T80	0.007 ± 0.0002	0.07 ± 0.001	2.50	23.93
10	CP	0.006 ± 0.0001	0.02 ± 0.001	2.11	7.90
10	Ctrl	0.004 ± 0.0001	0.02 ± 0.001	1.64	7.51
30	PEG	0.006 ± 0.0002	0.02 ± 0.001	2.11	8.76
30	T20	0.007 ± 0.0002	0.08 ± 0.002	2.66	27.53
30	T80	0.006 ± 0.0002	0.05 ± 0.001	2.03	18.85
30	CP	0.008 ± 0.0002	0.03 ± 0.001	2.89	12.67
30	Ctrl	0.004 ± 0.0001	0.02 ± 0	1.56	6.80
60	PEG	0.008 ± 0.0002	0.04 ± 0.001	2.89	12.90
60	T20	0.013 ± 0.0003	0.1 ± 0.003	4.61	36.99
60	T80	0.011 ± 0.0002	0.11 ± 0.003	4.07	39.18
60	CP	0.016 ± 0.0004	0.05 ± 0.001	5.71	18.54
60	Ctrl	0.01 ± 0.0003	0.05 ± 0.001	3.60	16.58

Time = sample aliquot collection time; PEG = polyethylene glycol; T20 = tween 20; T80 = tween 80; GlOH = glycerol; EtOH = Ethanol; %T.Y = % of the theoretical yield

7.2.2 The SSCF process

With COr1 the SSCF process yielded glycerol 0.01 g, and Ethanol 0.09 g with the respective theoretical yields of 2.02 and 24.78. For glycerol, all the surfactants and adsorbents used except the CP yielded the highest, and the highest ethanol yield was obtained from tween 80. For COr2 the yields of glycerol and ethanol are 0.04 g, and 0.23 g / g of Cor2 respectively, with the respective theoretical yields of 5.71% and 63.09%. For COr3 the highest glycerol and ethanol yields are 0.02 and 0.1 g / g COr3 respectively, and these values account for 3.87%, and 35.88% of the theoretical yields respectively.

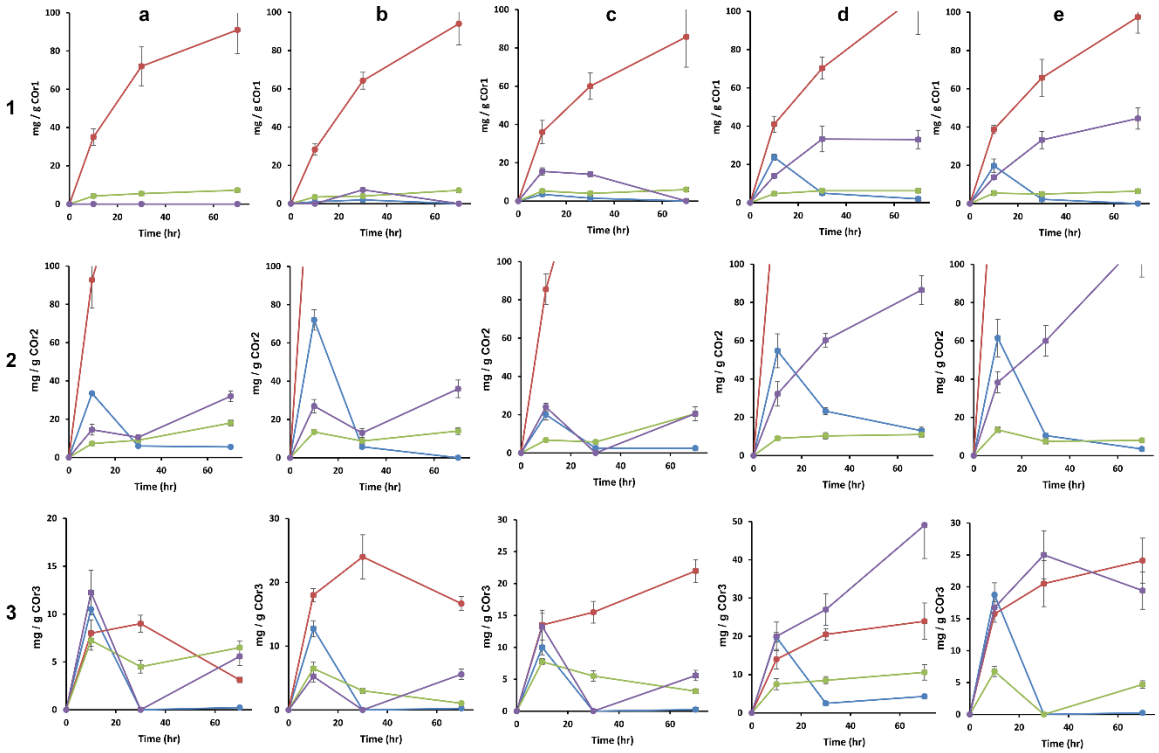

Figure 7.3 Effect of surfactants and adsorbents on the SSCF process

Rows 1, 2, and 3 represent the SSCF results of COr1, COr2, and COr3 respectively. Where columns a, b, c, d, and e represent the type of surfactant or adsorbent used in the media. a) control, b) CP, c) PEG, d) Tween 20, and e) Tween 80.

Table 7.4 SSCF results for COr1

Time (hr)	Adsorbent/control	GlOH g/g CO	EtOH g/g CO	GlOH %TY	EtOH %TY
10	PEG	0.011	0.03	1.46	8.63
10	T20	0.010	0.03	1.32	7.79
10	T80	0.011	0.03	1.53	7.66
10	CP	0.007	0.00	0.97	0.00
10	Ctrl	0.009	0.00	1.18	0.00
30	PEG	0.008	0.03	1.11	7.79
30	T20	0.013	0.07	1.74	18.51
30	T80	0.010	0.07	1.39	18.51
30	CP	0.008	0.01	1.11	4.04
30	Ctrl	0.011	0.00	1.53	0.00
60	PEG	0.012	0.00	1.67	0.00
60	T20	0.013	0.07	1.74	18.37
60	T80	0.013	0.09	1.81	24.78
60	CP	0.014	0.00	1.95	0.00
60	Ctrl	0.015	0.00	2.02	0.00

Table 7.5 SSCF results for COr2

Time (hr)	Adsorbent/control	GlOH g/g CO	EtOH g/g CO	GlOH %TY	EtOH %TY
10	PEG	0.01	0.05	1.88	13.40
10	T20	0.02	0.06	2.51	18.01
10	T80	0.03	0.08	3.76	21.36
10	CP	0.03	0.05	3.76	15.07
10	Ctrl	0.01	0.03	2.02	8.10
30	PEG	0.01	0.00	1.60	0.00
30	T20	0.02	0.12	2.85	33.64
30	T80	0.02	0.12	2.09	33.50
30	CP	0.02	0.03	2.44	7.26
30	Ctrl	0.02	0.02	2.51	5.86
60	PEG	0.04	0.04	5.71	11.45
60	T20	0.02	0.17	3.06	48.30
60	T80	0.02	0.23	2.23	63.09
60	CP	0.03	0.07	3.90	20.10
60	Ctrl	0.04	0.06	5.01	17.87

Table 7.6 SSCF results for COr3

Time (hr)	Adsorbent/control	GlOH g/g CO	EtOH g/g CO	GlOH %TY	EtOH %TY
10	PEG	0.02	0.03	2.83	9.69
10	T20	0.02	0.04	2.74	14.63
10	T80	0.01	0.03	2.47	12.25
10	CP	0.01	0.01	2.38	3.84
10	Ctrl	0.01	0.02	2.65	8.96
30	PEG	0.01	0.00	2.01	0.00
30	T20	0.02	0.05	3.11	19.75
30	T80	0.00	0.05	0.00	18.29
30	CP	0.01	0.00	1.10	0.00
30	Ctrl	0.01	0.00	1.65	0.00
60	PEG	0.01	0.01	1.14	4.09
60	T20	0.02	0.10	3.87	35.88
60	T80	0.01	0.04	1.72	14.20
60	CP	0.00	0.01	0.38	4.09
60	Ctrl	0.01	0.01	2.38	4.09

Chapter 8

Chemical-Free Enzymatic Synthesis of Food-Grade Xylooligosaccharides from Corncob Pith for Enhanced Sustainability in Production

8.1 Materials and methods

The -20/+80 fractions of both corncob pith (CP), and corncob outer (CO) were prepared as described in section 2.1, beechwood xylan (BX) (RM10398-Himedia, India) is taken as a positive control, and cellulose (CL) (Sigma Aldrich, M.A, U.S.A) is taken as a negative control. 0.2 gr of each sample is mixed with 10U/ml Xylanase (1003454250-Merck, USA) solution prepared in 0.05 M sodium citrate buffer of pH 6.0. The liquid-to-solid ratio of 10 was maintained. The saccharification was carried out for 60 hrs at 30°C in an orbital shaker at 130 RPM. The samples were analysed by DNS method, and thin layer chromatography (TLC) for qualitative findings. And with HPLC for quantitative analysis.

8.1.1 TLC method

TLC silica gel -60 plates (Merck) were loaded using the micro capillary technique. The mix of the xylooligosaccharides containing x1 to x6 with 2 mg/ml concentration each in lane 1 labelled as XOS, and the xylanase hydrolysate of CP in lane 2 (CP), xylanase hydrolysate of CO in lane 3 (CO), xylanase hydrolysate of commercial beach wood xylan as a positive control in lane 3 (BX), commercial cellulose (CL) in lane 4, and commercial glucose and cellobiose labelled (GOS) in lane 5 as negative control were ascended using butanol, acetic acid, and water mixture (2:1:1 v/v/v) as mobile phase, and dried, developed with spraying solution containing 2 g diphenylamine and 1 ml aniline, 10 ml phosphoric acid and the rest of the volume made up to 100 with methanol. Followed by spraying plates were heated at 120 °C for 5 minutes.

8.1.2 HPLC analysis

Ion chromatographer (Dionex ICS-5000), a High-Performance Anion Exchange Chromatography system (HPAEC), equipped with a Carbopac PA100 (ID 250 × 4 mm, 8.5 μm particle size) column, was used to run the samples. A gradient elution was carried with 0.1 M NaOH as eluent A, and 0.5 M sodium acetate containing 0.1 M NaOH as eluent B. the gradience used was 0–2 min, 3% B; 2–12 min, 3–24% B; 12–17 min, 100% B; 17–23 min, 3% B, with a flow-rate of1.0 mL/min, and a

column temperature 30 °C. The injection volume of the sample was 20 µL. The samples were detected using Pulsed Amperometric Detector (PAD) All the samples were prepared in 0.2 micron filtered HPLC water. The calibration standard used is a mixture xylooligosaccharides (Xylose, Xylobiose, Xylotriose, Xylotetraose, Xylopentaose, and Xylohexaose) with a concentration range of 0. 04 to 0.33 g/L. the calibration standards used were commercially purchased from Megazyme.

8.2 Results and discussion

Figures 8.1 and 8.2 depict the qualitative and quantitative analysis of the XOS production from CP. The maximum XOS produced from the CP is 20.33 g/ kg CP, while the XOS produced from the pure xylan are 66.86 g/kg. The XOS yield of the CP is 30.40% that of the pure xylan. While the saccharification of untreated-CO yielded about 3.54% that of pure xylan.

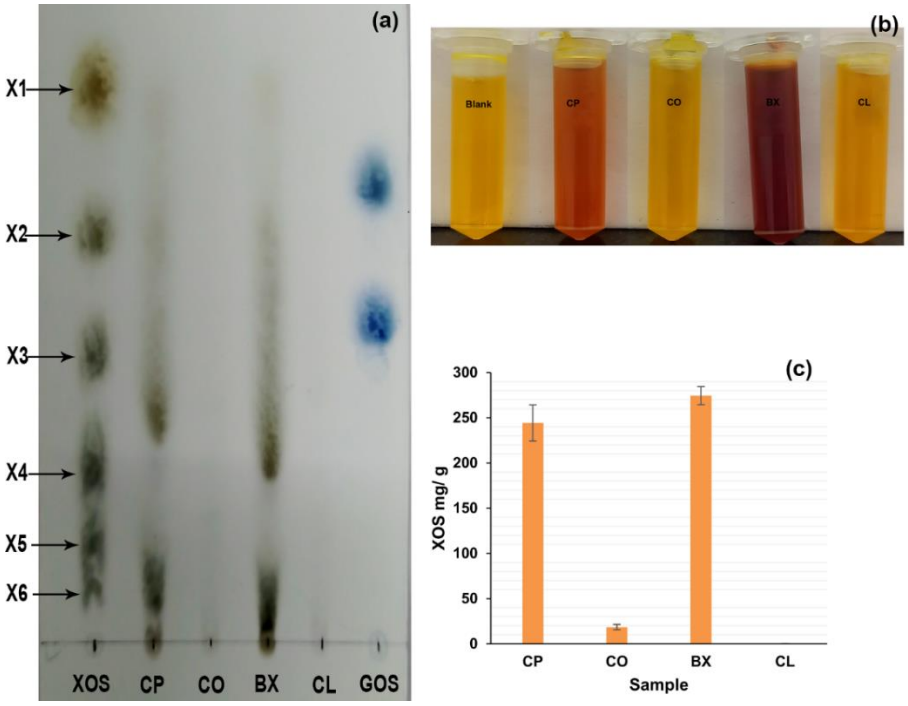

Figure 8.1 Qualitative analysis of XOS production

a) Is the TLC analysis. The colour of XOS in lanes XOS, CP and BX are similar (gryish green), while the colour of glucose and cellobiose is blue (this is the typical colour reaction of the spray reagent used). b) DNS analysis of the samples blank, CP, CO, BX, and CL respectively. C) graphical representation of XOS production from each sample used (DNS total sugar analysis)

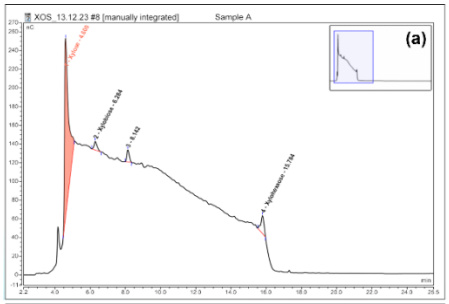

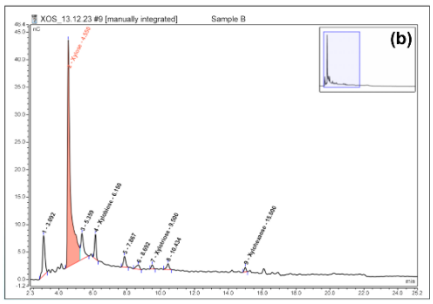

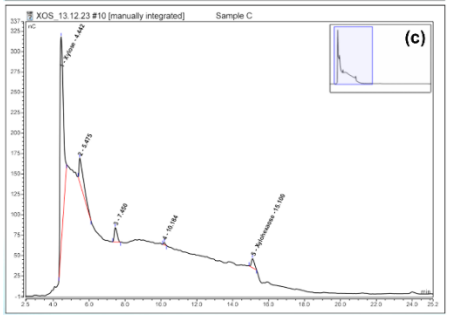

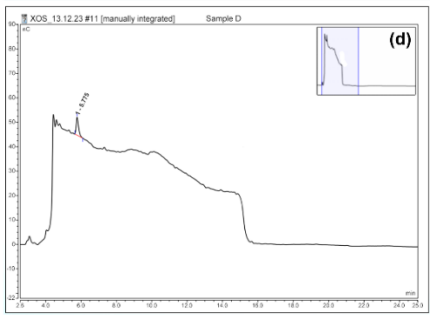

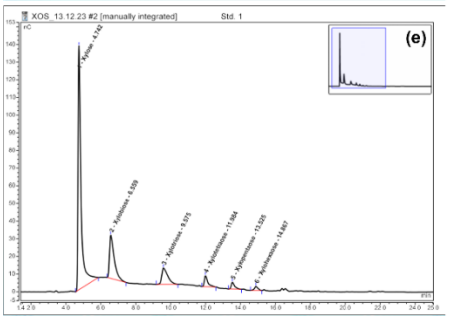

Samples	Retention time	Peak area	Compound	Concentration (g/L)
CP	4.6	46.505	Xylose	0.49
	6.284	1.7574	Xylobiose	0.02
	15.784	4.0196	Xylohexaose	3.54

Samples	Retention time	Peak area	Compound	Concentration (g/L)
CO	4.55	8.8935	Xylose	0.09
	6.15	0.5165	Xylobiose	0.01
	9.5	0.0954	Xylotriose	0.01
	15	0.0984	Xylohexaose	0.00

Samples	Retention time	Peak area	Compound	Concentration (g/L)
BX	4.442	52.1755	Xylose	0.58
	15.1	2.1728	Xylohexaose	1.85

Samples	Retention time	Peak area	Compound	Concentration (g/L)
Standards	4.742		Xylose	
	6.559		Xylobiose	
	9.575		Xylotriose	
	11.984		Xylotetraose	
	13.525		Xylopentaose	
	14.867		Xylohexaose	

Figure 8.2 Quantitative (HPLC) analysis of XOS production

a) sample CP, b) sample CO, c) sample BX, d) sample Cl, d) XOS standards (X1 to X6)

Table 8.1 Concentration of XOS in mg / g of the biomass

Samples	Xylose	Xylobiose	Xylotriose	Xylotetraose	Xylopentaose	Xylohexaose	Total
CP	3.48	0.47	N.D	N.D	N.D	16.37	20.33
CO	1.02	0.30	0.12	N.D	N.D	0.93	2.37
BX	16.24	N.D	N.D	N.D	N.D	50.62	66.86
CL	N.D	N.D	N.D	N.D	N.D	N.D	N.D

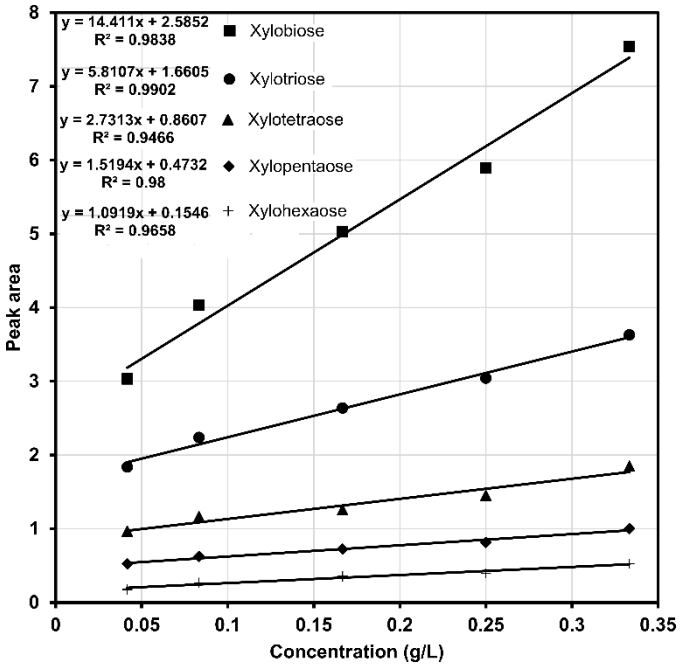

Figure 8.3 HPLC Calibration curve for X2 to X6

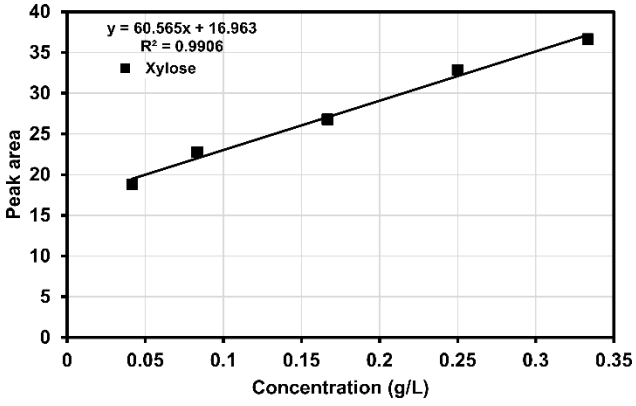

Figure 8.4 HPLC Calibration curve for xylose

Chapter 9

Techno Economic and Exergy analysis of the overall process scenarios

9.1 materials and methods

9.1.1 Techno economic analysis

SuperPro Designer v.13 (Intelligen) trail version was used to simulate the overall process scenarios dived in to pretreatment, SHCF and SSF modes. All the input and output components of each process were registered under pure components under the tasks, the concentration ratios of each stream were registered for 1 kg of the CO residue, calculated based on the experimental values. A batch reactor of maximum 40000 L was selected with the maximum allowable vessel volume set to 65% for all the processes. The operation data for the pretreatment include the charging of catalyst and CO residue in separate streams, and the react at experimentally obtained optimum pretreatment conditions, followed by transfer out the pretreated slurry. Then the slurry is transferred in to a plate and frame filter where the stream is filtered to separate liquid and solid cake. The cake is washed with additional stream of water charged in to the filter and final product is collected, the amount of water used for cake washing was selected based on the laboratory findings. Default values related to the each unit operation were considered. Similar design was employed for saccharification followed by fermentation where two serially connected reactors were taken. And the fermentation was simulated in a batch fermenter, with standard operation settings. After achieving the appropriate material stoichiometric balance, materials cost were input as per the catalogue prices of the commercial analytical grade chemicals used in the laboratory procedures described in the previous chapters, and the cost of utilities such as high-pressure steam, heating, cooling, and electricity requirements were set by the simulation software and the default values were taken. The total operating cost is the summation of material cost and the cost of utilities. Then the economic analysis was performed and the reports were generated. The operating cost in terms of material cost was compared with that of the revenue generated from the output streams manually. This work ignores the other operating costs like labour cost.

9.1.2 Exergy analysis

Exergy analysis is based on second law of Thermodynamics. Chemical exergy represents the maximum work achievable when transitioning a substance from the reference-environment state to the dead state through a process involving heat transfer and substance exchange exclusively with the reference environment. Alternatively, chemical exergy can be perceived as the exergy of a substance at the reference-environment state.

Furthermore, chemical exergy is equivalent to the minimum work required to generate a substance at the reference-environment state from its constituents in the reference environment. It consists of two primary components: reactive exergy, arising from chemical reactions necessary for producing species not stable in the reference environment, and concentration exergy, resulting from the disparity between the chemical concentration of a species in a system and its concentration in the reference environment.

The chemical exergy values in kJ/mol (EX_{ch} or simply denoted as EX in this work), for different streams of the processes involved was calculated using the equation 8.1. A stream contain all the constituents that were input into a process or obtained from the process, based on their respective origins. The solid residue and the liquid filtrate obtained from each pretreatment were calculated as separate individual streams, and when EX_{ch} of the total pretreatment output stream is required, both the values were summated.

The exergetic efficiency (∅) of a process is a measure of how well a system converts available energy into useful work. It is calculated from the ratio of exergy of outputs to exergy of inputs equation 8.2. Usually ∅ is <1. The process exergy sustainability index (SI) is calculated using the equation 8.3. a higher SI value indicates the sustainability of the process. And the environmental impact (EI) is taken as the reciprocal of the SI equation 8.4. Higher the EI value, greater is the impact on the environment.

$$\boldsymbol{Ex_{ch}} = \boldsymbol{n}\left(\sum_i \boldsymbol{x_i}\, \boldsymbol{e_i} + \boldsymbol{RT}\sum_i \boldsymbol{x_i}\, \boldsymbol{ln}(\boldsymbol{x_i})\right) \qquad \text{equation 9.1}$$

$$\emptyset = \frac{\boldsymbol{Exergy\ of\ products}}{\boldsymbol{Exergy\ of\ reactants}} \qquad \text{equation 9.2}$$

$$\text{SI} = \frac{\mathbf{1}}{\mathbf{1}-\emptyset} \qquad \text{equation 9.3}$$

$$EI = \frac{SI}{1} \qquad \text{equation 9.4}$$

Where, **n** is the mole number of the component, x_i is mole fraction of each component of the stream, $\mathbf{e_i}$ is the standard chemical exergy of $\mathbf{i_{th}}$ component, **R** is gas constant, **T** is the process temperature in kelvins.

9.2 Results and discussion

9.2.1 Techno economic analysis

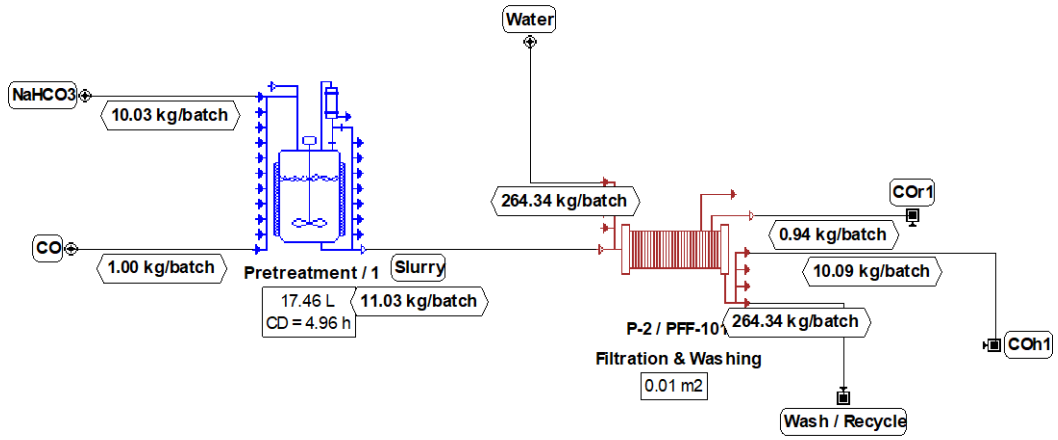

Figure 9.1 Flow diagram for pretreatment process

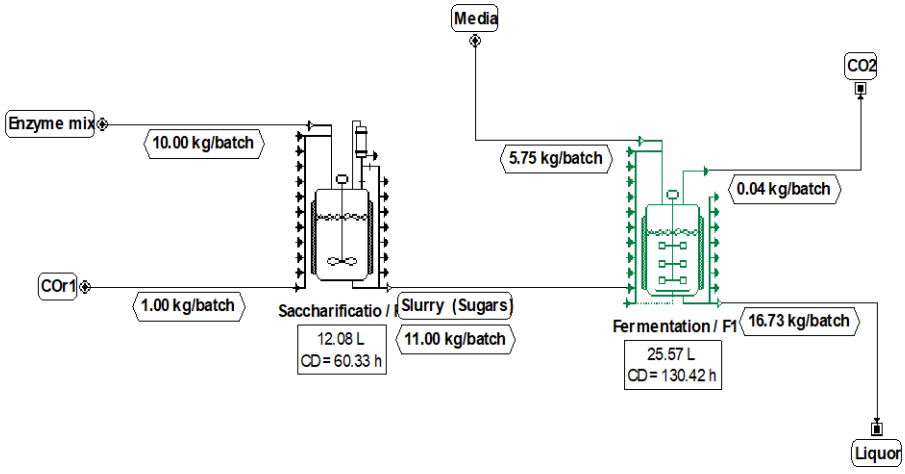

Figure 9.2 Flow diagram for SHCF process

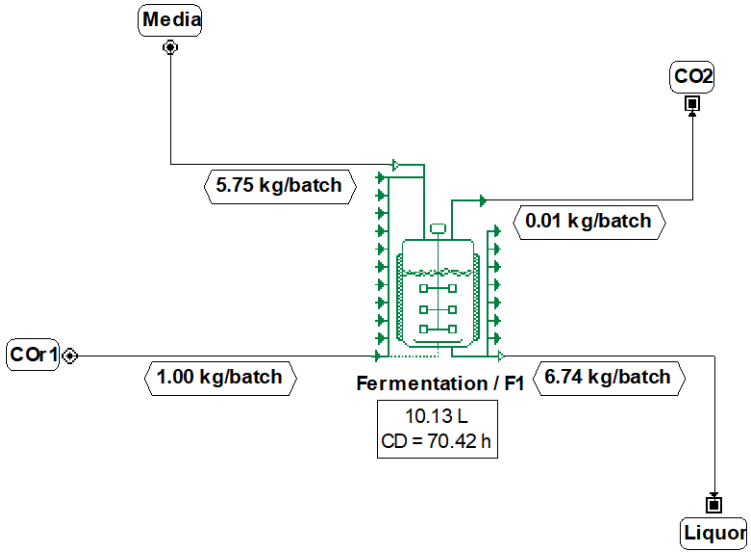

Figure 9.3 Flow diagram for SSCF process

Table 9.1 Total material cost for the processes

					Pretreatment type		
		$NaHCO_3$	**NaOH**	H_2SO_4	$NaHCO_3$	**NaOH**	H_2SO_4
Materials	**Unit Price USD/ kg**	**Requirement/Batch (kg CO)**			**Price USD / Batch (kg CO)**		
Corncob	0.6	1.00	1.00	1.00	0.60	0.60	0.60
Electricity (kWh)	0.42	0.67	0.67	0.67	0.28	0.28	0.28
0.07	0.67	0.67	0.67	0.05	0.05	0.05	0.00
NaOH	4.50	N.A	1.44	0.00	0.00	6.47	0.00
H_2SO_4	3.41	N.A	N.A	0.09	0.00	0.00	0.29
Citric acid anhydrate	13.87	0.09	0.09	0.09	1.22	1.22	1.22
Trisodium citrate, dihydrate	11.45	0.04	0.04	0.04	0.44	0.44	0.44
Cellulase 50 ml (1.5 ml/batch)	3452.00	0.002	0.002	0.002	5.18	5.18	5.18
β-Glucosidase 5 gr	39180.00	0.001	0.001	0.001	39.18	39.18	39.18
Xylanase 10 gr	17449.00	0.001	0.001	0.001	17.45	17.45	17.45
MgSo4	4.40	0.02	0.02	0.02	0.07	0.07	0.07
KH2PO4	12.18	0.03	0.03	0.03	0.38	0.38	0.38
Yeast extract	38.52	0.16	0.16	0.16	6.06	6.06	6.06
Peptone	31.08	0.31	0.31	0.31	9.78	9.78	9.78
Chloramphenicol	2496.00	0.00	0.00	0.00	1.96	1.96	1.96
Yeast	2.30	0.00	0.00	0.00	0.00	0.00	0.00
				Total	**89.162**	**89.082**	**82.899**

Table 9.2 Revenue generated details

Revenue	Unit Price USD / Kg	Production (kg)			Revenue		
Glucose (ES yield of COr)	8.44	0.24	0.27	0.28	2.00	2.26	2.36
Xylose (ES yield of COr)	89.04	0.10	0.11	0.12	9.04	10.21	10.67
Lignin	613.51	0.10	0.14	0.00	61.32	85.10	0.00
Glycerol_SHCF	12.22	0.01	0.01	0.01	0.12	0.14	0.14
Ethanol _SHCF	12.00	0.07	0.08	0.08	0.81	0.92	0.96
Glycerol_SSCF	12.22	0.01	0.04	0.02	0.18	0.50	0.26
Ethanol _SSCF	12.00	0.09	0.23	0.10	1.07	2.71	1.18

Table 9.3 total revenue summation and the total operating cost comparison

	Total obtained revenue		
Process	$NaHCO_3$	**NaOH**	H_2SO_4
Pretreatment	72.36	97.57	13.03
SHCF	0.93	1.06	1.10
SSF	2.06	4.13	2.40
Total from SHCF	73.29	98.62	14.14
Total from SSCF	74.42	101.70	15.43
Total operating cost / batch	**107.012**	**119.742**	**113.809**

Table 9.4 revenue generated from XOS production

XOS (>90% purity) market price USD	XOS revenue / kg CP
10000	203.3

9.2.2 Chemical exergy analysis

For sequential H_2SO_4 pretreatment the input streams of both NaOH (initial pretreatment) and H_2SO_4 (subsequent pretreatment) were considered together, likewise their output streams too. Table 9.5 presents the exergy values calculated for all possible individual streams derived from different pretreatment and post processing scenarios considered. Table 9.6 presents values of ∅, SI and EI calculated based on the exergy values presented in Table 9.5. Note that all the decimal values were rounded to their nearest integers.

Table 9.5 Chemical exergies (Ex_{ch}) of pretreatment and post processing streams

Streams considered	Code	Ex_{ch1} (kJ/mol)	Ex_{ch2} (kJ/mol)	Ex_{ch3} (kJ/mol)
P_input	$\mathbf{EX_{Pi}}$	11314	11515	22834
P_ (solid residue)_ output	$\mathbf{EX_{COr}}$	10582	10468	18933
P_ (liquid filtrate)_ output	$\mathbf{EX_{COh}}$	726	828	3457
ES_input	$\mathbf{EX_{ES\_i}}$	11915	11898	9811
ES_output	$\mathbf{EX_{ES\_o}}$	10293	11406	9772
F_input	$\mathbf{EX_{F\_i}}$	19526	20638	19006
F_output	$\mathbf{EX_{F\_o}}$	1455	1456	1455
(ES + F)_input	$\mathbf{EX_{\_(ES+F)\_i}}$	31442	32536	28817
(ES + F)_output	$\mathbf{EX_{\_(ES+F)\_o}}$	11748	12861	11227
(P+ES+F)_input	$\mathbf{EX_{SHCF\_i}}$	42755	44051	51651
(P+ES+F)_output	$\mathbf{EX_{SHCF\_o}}$	22330	23329	33617
SSCF (ES+F)_input	$\mathbf{EX_{SSCF\_(E+F)i}}$	12174	12156	10071
SSCF (ES+F)_output	$\mathbf{EX_{SSCF\_(E+F)\_o}}$	2503	2508	2503
(P+SSCF)_input	$\mathbf{EX_{SSCF\_i}}$	23488	11529	22845
(P+SSCF)_output	$\mathbf{EX_{SSCF\_o}}$	13086	10471	22393

P = Pretreatment; ES=enzymatic saccharification; F= fermentation; EX_{ch1}, EX_{ch2}, EX_{ch3} = chemical exergies of the processes originated from $NaHCO_3$, NaOH and sequential H_2SO_4 Pretreated residues respectively.

Table 9.6 Chemical exergy (Ex_{ch}) scenario analysis

	Ø_1	Ø_2	Ø_3	SI_1	SI_2	SI_3	EI_1	EI_2	EI_3
COr_{out}/COr_{in}	0.94	0.91	0.75	15.46	11.00	3.97	0.06	0.09	0.25
COh_{out}/COh_{in}	0.06	0.07	0.23	1.07	1.08	1.30	0.94	0.93	0.77
$CO(r+h)_{out}/CO(r+h)_{in}$	1.00	0.98	0.98	1885	52.58	50.31	0.00	0.02	0.02
ES_{out}/ES_{in}	0.86	0.96	1.00	7.35	24.18	251	0.14	0.04	0.00
F_{out}/F_{in}	0.07	0.07	0.08	1.08	1.08	1.08	0.93	0.93	0.92
$SHCF_{out}/SHCF_{in}$	0.37	0.40	0.39	1.60	1.65	1.64	0.63	0.60	0.61
$(P+SHCF)_{out}/(P+SHCF)_{in}$	0.52	0.53	0.49	2.09	2.13	1.96	0.48	0.47	0.51
$SSCF_{out}/SSCF_{in}$	0.21	0.21	0.25	1.26	1.26	1.33	0.79	0.79	0.75
$(P+SSCF)_{out}/(P+SSCF)_{in}$	0.56	0.55	0.51	2.26	2.21	2.05	0.44	0.45	0.49

1, 2, 3 = are the respective pretreatments 1) $NaHCO_3$, 2) NaOH, 3) sequential H_2SO_4; P= pretreatment; COr = solid residue obtained from the pretreatment, COh = pretreatment derived liquid filtrate; ES = enzymatic saccharification, F = fermentation; SHCF=separate hydrolysis and co-fermentation; SSCF = simultaneous saccharification and co-fermentation; Ø = process exergetic efficiency; SI = process exergetic sustainability index; EI = process exergetic environmental impact.

When the pretreatments alone were considered as an isolated process, $NaHCO_3$ was far superior in terms of its process exergy efficiency (Ø) value, with a misleading huge sustainability index (SI) and a zero environmental impact (EI), this is due to comparatively lower optimum pretreatment temperature of the process. However when we look at the individual exergetic efficiencies of enzymatic saccharification and fermentation of the sugars derived from the enzymatic saccharification of the pretreated solid residues (COr), $NaHCO_3$ pretreatment showed a lower efficiency than that of the other two pretreatment methodologies in terms of Ø, SI, and EI values. Same is the case for the respective SHCF and SSCF processes. Hence when considering exergy based sustainability analysis it is always beneficial to look at the overall process than the individual sub-processes. SSCF process scenario based on sequential $NaHCO_3$ pretreatment has showed the better Ø (0.56), SI (2.26), and EI (0.44) values than the other pretreatment methods studied.

Chapter 10

Summary and Conclusions

10.1 Summary and conclusions

The comprehensive characterization of the corncob anatomical portions revealed the striking morphological, structural, and chemical differences among the outer (CO) and pith (CP) sections of each corn variety studied; at the same time, there are no significant differences among the same anatomical portion in different corn varieties. Most of the characteristics of the CO were similar to that of whole corncob characteristics vividly reported in the literature, whereas CP showed unique characteristics, such as lower lignin, protein, and ash contents with an improved xylan and cellulose content. NIR-PLS calibration models along with Savitzky-Golay smoothing of the spectra are proven to be the fittest for the rapid composition analysis of all the biomass components. Both the FTIR and XRD analyses showed that CO is more crystalline than CP. The thermal stability of CP was found to be lower than that of CO. All of these compositional and physical differences led to enhanced enzymatic saccharification of CP by both cellulase and xylanases, which was equal to that of the pure cellulose (AC), and xylan (XY) references. Thus, we propose a tailored enzymatic production of xylooligosaccharides from CPs without pretreatment along with a separate valorisation of CO to achieve an economical biorefinery output from the corncob feedstock. However, the techno-economic evaluation of the proposed process must be carried out to assess the viability of the process given the newly included step of biomass anatomical segregation.

The order of efficiency for alkalis in delignification is as follows: KOH > NaOH > Na_2CO_3 > NH_4OH > $Ca(OH)_2$ > $NaHCO_3$. On the other hand, their impact on sugar loss follows this sequence: Na_2CO_3 > KOH > NaOH > $NaHCO_3$. The $NaHCO_3$ pretreatment, conducted at a $NaHCO_3$ concentration of 1.44%, temperature of 100 °C, and duration of 37.85 min, exhibited favourable results with a significant removal of lignin (58.36%) and a commendable enzymatic saccharification yield (84.63%). However, it was noted that this process incurred a moderate sugar loss of 4.73 mg/g. The NaOH pretreatment, conducted with NaOH at 1.44%, a temperature of 110.59 °C, and a duration of 76.12 min, demonstrated superior performance, achieving a high lignin removal percentage (81%) and an impressive enzymatic saccharification yield (95.54%). However, a slightly higher sugar loss of 6.13 mg/g was observed compared to $NaHCO_3$

pretreatment. The sequential H_2SO_4 pretreatment, conducted with a sequential H_2SO_4 concentration of 0.85%, a temperature of 108.97 °C, and a duration of 82.06 min, revealed remarkable outcomes, achieving an exceptionally high enzymatic saccharification yield (99.9%). However, it came at a substantial cost of sugar loss, reaching 171.47 mg/g.

In addition to its effectiveness as a chemical catalyst for CO pretreatment, $NaHCO_3$ is environmentally friendly because it requires minimal water for neutralizing the treated CO residue. Furthermore, it is cost-effective, with an approximate cost of 0.039 USD per 1 Kg of CO pretreatment. The optimal artificial neural network (ANN) architecture comprises a single hidden layer with 20 neurons and a learning rate of 0.51572. Regarding the hybrid model's performance, it ranks as follows: TLBO-ANN > GA-ANN > PSO-ANN, with "trainbr" being the most suitable training algorithm for these datasets.

Yeast Y5 exhibits exceptional biotechnological potential, particularly in inhibitor tolerance, assimilation capacities, osmotolerance, and pH adaptability. In terms of inhibitor tolerance, Y5 showcases enhanced resistance to various inhibitors, displaying excellent resilience against lignin-derived inhibitors such as 4-Hydroxy Benzoic acid, Cinnamic acid, Gallic acid, Syringaldehyde, and Vanillin. It also demonstrates significant resistance to sugar-derived inhibitors like Levulinic acid, Furfural, and 5-Hydroxy Methyl Furfural, with a unique weak tolerance against formic acid at 0.01 g/L. Y5's assimilation capabilities encompass both galactose and D-Xylose, along with mannose, while also exhibiting moderate to weak assimilation of cellulose and Avicel. Remarkably, it excels in Xylan assimilation and shows superior assimilation of Dl-lactate, Succinate, and citrate. The yeast displays moderate assimilation of Methanol and ethanol, along with glycerol and xylitol. Osmotolerance studies reveal Y5's excellent resilience to combinations of glucose + fructose and glucose + xylose at concentrations from 5% to 40%, maintaining moderate tolerance even at 50%. Furthermore, Y5 showcases a wide pH adaptability, thriving in environments ranging from pH 2.5 to 8.5. Overall, yeast Y5 emerges as a robust and versatile candidate, demonstrating promising attributes for various bioprocessing applications, thereby the yeast Y5 contributing to the advancement of sustainable and efficient bioproduction systems. Further exploration and optimization of Y5's capabilities hold great potential for expanding its industrial applications. The BLAST and phylogenetic analysis of the sequenced D1/D2 domain of the 26S rRNA gene of Y5 revealed that it is a novel strain of *Pichia kudriavzevii*.

The investigation of impact of Corncob Pith (CP) as an adsorbent in comparison to various surfactants (Amberlite IRA-400 chloride form, Amberlite IRA-96 free base, Polyethylene glycol 6000, Silica gel 100-200 Mesh, Tween 20, and Tween 80) known for their ability to enhance saccharification and fermentation processes by mitigating the effective localized concentration of lignin-derived inhibitors through adsorption or flocculation. CP demonstrated notable effectiveness, with the highest productivity observed, closely followed by Tween 20, Tween 80, and Polyethylene glycol 6000 (PEG), respectively. In the Separate Hydrolysis and Co-Fermentation (SHCF) process, 1 gram of COr1 resulted in maximum Glycerol (GlOH) and Ethanol (EtOH) yields of 0.017 g and 0.119 g, respectively, with theoretical yields of 5.7% and 39.2%, respectively. Similarly, COr2 yielded 0.02 g GlOH and 0.13 g EtOH with theoretical yields of 5.7% and 39.2%, and COr3 yielded 0.016 g GlOH and 0.11 g EtOH with theoretical yields of 5.71% and 39.18%, respectively. The media supplemented with CP exhibited the highest glycerol yield, while Tween 80-added media showed the highest ethanol production. In the Simultaneous Saccharification and Co-Fermentation (SSCF) process for COr1, glycerol and ethanol yields were 0.01 g and 0.09 g, respectively, with theoretical yields of 2.02% and 24.78%. For COr2, glycerol and ethanol yields were 0.04 g and 0.23 g per gram of COr2, respectively, corresponding to theoretical yields of 5.71% and 63.09%. COr3 showed glycerol and ethanol yields of 0.02 g and 0.1 g per gram of COr3, accounting for 3.87% and 35.88% of the theoretical yields, respectively (Figure 10.1).

The maximum xylooligosaccharides (XOS) produced from the corncob pith (CP) is 20.33 g/kg CP, whereas the XOS produced from pure xylan amounts to 66.86 g/kg. The XOS yield of CP is 30.40% of that obtained from pure xylan. Additionally, the saccharification of untreated corncob (CO) yielded approximately 3.54% of the XOS produced from pure xylan. Most of the XOS generated in both cases are xylohexaose and xyloses, suggesting that the commercial xylanase utilized was a combination of endo-xylanases (EC 3.2.1.8) and β-xylosidases (EC 3.2.1.37). The process may be further enhanced by incorporating an exo-xylanase (EC 3.2.1.37) into the saccharification mix.

The total revenue generated from the NaOH pretreatment-derived SSCF process is the highest (USD 101.70), so as its total operating cost (USD 119.742), while the exergetic efficiency of the SSCF process through NaOH pretreatment-derived stream showed process efficiency (0.91), Exergy based sustainability index (10.90), and exergy based environmental impact (0.09). These

values are between the two extremes of that of NaHCO3 and sequential H2SO4 pretreatment-derived streams. In summation of techno-economic and exergy-based sustainability analysis, one can select NaOH pretreatment as the best-suited process for the selected biorefinery. However, the revenue generated from the conversion process does not match the total input cost. This can be overcome by the huge co-product credit that can be generated from the XOS production from the CP without any pretreatment which is calculated to be USD 203. 3 per Kg of CP.

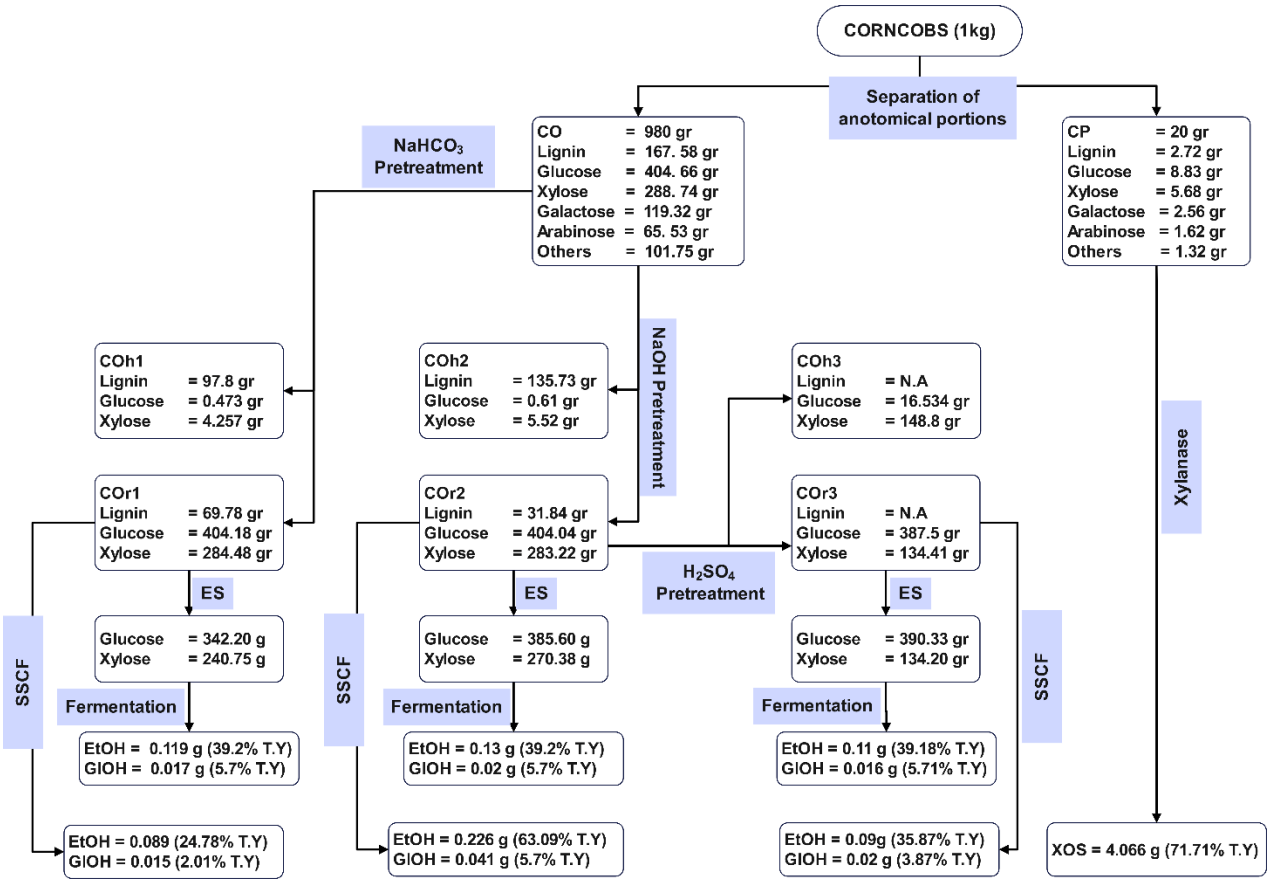

Figure 10.1 Overall process scenario summary

Shaded text are the processes, all the input and output concentrations were calculated for 1 kg of pristine corncob biomass.

10.2 Future prospective of this work

The material cost has the major stake in the overall process, certain high-value inputs like enzymes, and media components increase the overall operating cost. Hence an in-house production of enzymes and the search for alternative nitrogen and other nutrients for fermentation must be

selected from cost-effective raw materials, should be considered. In addition there is a scope for *Pichia kudriavzevii* (Y5) strain improvement, the strain can be metabolically engineered to enhance its productivity towards either one of the products or both, as per the requirement. The XOS production also must be improved by considering in-house produced xylanase cocktails consisting of all endo-xylanase, exo-xylanase, and β-xylosidase. Additionally, other facile, low-cost strategies to enhance XOS production from CO must be explored, in conjunction with the development of purification techniques for XOS. If not for XOS, redirecting the xylan content of the biomass to generate other value-added platforms derived from xylan, such as xylose, xylitol, and furfural, rather than fermenting it into ethanol and glycerol, can further improve overall economics.

Appendix – I

Table AI. 1 Matlab code for optimizing ANN-hyperparameters with TLBO

```
clc; % clear the command window
clear all; % clear the workspace and RAM

% Initialize TLBO parameters
num_vars = 3; % Number of decision variables
var_size = [1 num_vars]; % Size of decision variable vector
lb = [1 3 0.01]; % Lower bound of decision variables
ub = [5 20 0.9]; % Upper bound of decision variables
max_iter = 100; % Maximum number of iterations
n_pop = 50; % Population size

% Initialize TLBO population
pop = repmat(lb, n_pop, 1) + rand(n_pop, num_vars) .* repmat(ub - lb, n_pop, 1);

% Initialize TLBO population
pop = repmat(lb, n_pop, 1) + rand(n_pop, num_vars) .* repmat(ub - lb, n_pop, 1);pop(:, 1:2) =
round(pop(:, 1:2)); % Round first two decision variables

% Initialize variables to store best solution and cost
best_sol = [];
best_cost = inf;
best_iter = 0;

% Initialize variables to store convergence data
convergence_data = zeros(max_iter, 1);
% Main TLBO loop
for i = 1:max_iter
    % Evaluate population
    cost = zeros(n_pop, 1);
    for j = 1:n_pop
        % Call your cost function here with the current decision variable values
        X = pop(j,:);
        cost(j) = ann_cost(X);
    end

    % Find best solution in the population
    [local_best_cost, best_idx] = min(cost);
    local_best_sol = pop(best_idx,:);

    % Update global best solution
    if local_best_cost < best_cost
        best_cost = local_best_cost;
        best_sol = local_best_sol;
        best_iter = i;
    end
```

```
    % Calculate mean solution (centroid)
    mean_sol = mean(pop);

    % Generate new solutions
    for j = 1:n_pop
        % Choose a random solution from the population
        rand_idx1 = randi([1 n_pop]);
        rand_idx2 = randi([1 n_pop]);

        % Generate a new solution by learning
        diff = pop(rand_idx1,:) - pop(rand_idx2,:);
        new_sol = pop(j,:) + rand(1,num_vars) .* diff + rand(1,num_vars) .*
 (best_sol - mean_sol);

        % Apply boundary constraints
        new_sol = max(new_sol, lb);
        new_sol = min(new_sol, ub);

        % Evaluate new solution
        new_cost = ann_cost(new_sol);

        % Replace worst solution in population with new solution
        [worst_cost, worst_idx] = max(cost);
        if new_cost < cost(worst_idx)
            pop(worst_idx,:) = new_sol;
            cost(worst_idx) = new_cost;
        end
    end

    % Store convergence data
    convergence_data(i) = best_cost;
    disp(['Iteration ' num2str(i) ': Best Cost = ' num2str(best_cost) ', Best X1 = '
num2str(round(best_sol(1))) ', Best X2 = ' num2str(round(best_sol(2))) ', Best X3 = '
num2str(best_sol(3))]);
end

% Display best solution found
disp(['Best solution found: x1 = ' num2str(round(best_sol(1))) ', x2 = ' num2str(round(best_sol(2)))
', x3 = ' num2str(best_sol(3))]);
disp(['Best cost = ' num2str(best_cost) ' at iteration ' num2str(best_iter)]);

% Plot convergence data
figure;
plot(1:max_iter, convergence_data, 'LineWidth', 2);
xlabel('Iteration');
ylabel('Best Cost');
title('Convergence Plot');
```

Table AI.2 Matlab code for optimizing ANN-hyperparameters with PSO

```
clc; % clear the command window
clear all; % clear the workspace and RAM

num_particles = 50;     % number of particles
num_iterations = 100;    % maximum number of iterations
inertia_weight = 1.4;   % inertia weight
cognitive_factor = 1.8; % cognitive factor
social_factor = 1.8;    % social factor

% Set decision variable bounds
lb = [1, 3, 0.001]; % lower bounds
ub = [5, 50, 0.9];  % upper bounds

% Initialize particle positions and velocities
particles = zeros(num_particles, 3);
velocities = zeros(num_particles, 3);
for i=1:num_particles
   % Generate random integers for X1 and X2 within bounds
   particles(i,1) = round(rand*(ub(1)-lb(1)) + lb(1));
   particles(i,2) = round(rand*(ub(2)-lb(2)) + lb(2));
   % Generate random value for X3 within bounds
   particles(i,3) = lb(3) + (ub(3)-lb(3)).*rand(1);
   % Set initial velocities
   velocities(i,:) = -1 + 2.*rand(1,3);
end

% Initialize global best
global_best_cost = inf;
global_best_particle = zeros(1,3);

% Store iteration results in matrix
iter_results = zeros(num_iterations, 4);

% Begin PSO
for iter=1:num_iterations
   % Evaluate particle costs
   costs = zeros(1,num_particles);
   for j=1:num_particles
      costs(j) = ann_cost(particles(j,:));
   end

   % Update global best
   [min_cost, min_index] = min(costs);
   if min_cost < global_best_cost
      global_best_cost = min_cost;
      global_best_particle = particles(min_index,:);
      best_iter = iter;
   end
```

```
    % Update particle velocities and positions
    for j=1:num_particles
        % Update velocity
        velocities(j,:) = inertia_weight*velocities(j,:) + ...
            cognitive_factor*rand(1,3).*(particles(j,:) - particles(j,:)) + ...
            social_factor*rand(1,3).*(global_best_particle - particles(j,:));

        % Update position
        particles(j,:) = particles(j,:) + velocities(j,:);

        % Enforce bounds and integer constraints
        particles(j,1) = max(particles(j,1), lb(1));
        particles(j,1) = min(particles(j,1), ub(1));
        particles(j,2) = max(particles(j,2), lb(2));
        particles(j,2) = min(particles(j,2), ub(2));
        particles(j,1:2) = round(particles(j,1:2));
        particles(j,3) = max(particles(j,3), lb(3));
        particles(j,3) = min(particles(j,3), ub(3));
    end

    % Store iteration results in matrix
    iter_results(iter,:) = [global_best_particle, global_best_cost];

    % Display iteration info with best values of X1, X2, and X3
    disp(['Iteration ' num2str(iter) ': Best cost = ' num2str(global_best_cost) ', Best X1 = '
num2str(round(global_best_particle(1))) ', Best X2 = ' num2str(round(global_best_particle(2))) ',
Best X3 = ' num2str(global_best_particle(3))]);

end

% Find final best result among all iterations
[min_cost, min_idx] = min(iter_results(:,end));
final_best_particle = iter_results(min_idx,1:end-1);

% Display final best result separately
disp(['Final best cost = ' num2str(min_cost) ', Best X1 = ' num2str(round(final_best_particle(1))) ',
Best X2 = ' num2str(round(final_best_particle(2))) ', Best X3 = ' num2str(final_best_particle(3)) ',at
iteration =' num2str(best_iter)]);

% Generate convergence plot
figure(1)
plot(iter_results(:,4))
title('Convergence Plot')
xlabel('Iteration')
ylabel('Best Cost')
```

Table AI.3 Matlab code for optimizing ANN-hyperparameters with GA

```
function [best_cost, best_x1, best_x2, best_x3, history] = GA_Final()

% Define optimization problem
nvars = 3;
lb = [1, 3, 0.01];
ub = [2, 10, 0.9];

% Define options for GA
options = optimoptions('ga');
options.Display = 'off';
options.PlotFcn = {@gaplotbestf,};
options.MaxGenerations = 10; % Set the maximum number of generations
options.PopulationSize = 10; % Set the population size

% Initialize history array for storing optimization results
history = struct('Generation', {}, 'Best', {}, 'BestX', {});

% Define cost function
cost_fun = @ann_cost;

% Run GA optimization
[best_x, best_cost, exitflag, output, population, score] = ...
    ga(cost_fun, nvars, [], [], [], [], lb, ub, [], [], options);

% Store best values for each variable
best_x1 = round(best_x(1));
best_x2 = round(best_x(2));
best_x3 = best_x(3);

% Display optimization results
disp('Final solution:');
disp(['Best cost: ', num2str(best_cost)]);
disp(['Best x1: ', num2str(best_x1)]);
disp(['Best x2: ', num2str(best_x2)]);
disp(['Best x3: ', num2str(best_x3)]);

% Store optimization history
history = output;
% Plot convergence
% Store optimization history
history = output;
end


% Define custom output function
    function stop = ga_output(options, state, flag)
        % Extract current generation and best individual
```

```
        gen = state.Generation;
        best_f = state.Best(end);
        best_x = state.Best(1:nvars);
        % Round best_x1 and best_x2 to integers
        best_x(1:2) = round(best_x(1:2));
        % Display current best values
        disp(['Generation: ', num2str(gen)]);
        disp(['Best cost: ', num2str(best_f)]);
        disp(['Best x1: ', num2str(best_x(1))]);
        disp(['Best x2: ', num2str(best_x(2))]);
        disp(['Best x3: ', num2str(best_x(3))]);
        % Update history
        history(gen).Best = best_f;
        history(gen).BestX = best_x;
        % Continue optimization
        stop = false;
        % Plot convergence
    end
```

Table AI.4 Cost function that takes input arguments from metaheuristic algorithms to optimize ANN-hyperparameters

```
function [cost] = ann_cost(x)
% ANN Cost Function for TLBO_PSO_GA Optimizations
% x = [Number of Hidden Layers, hiddenLayerSize, Learning Rate]

% Load input data (factors)
factors = csvread('independent_variables_file_name_.csv');
% Load target data (responses)
responses = csvread('dependent_variables_file_name.csv');

% Set decision variables
hiddenLayers = round(x(1));       % Number of Hidden Layers
hiddenLayerSize = ceil(x(2));     % hiddenLayerSize
learningRate = x(3);        % Learning Rate

% Call the ga_int function to force integer values for X1 and X2
x(:,1:2) = ga_int(x(:,1:2));

% Construct the ANN model
x = factors';
t = responses';
trainFcn = 'trainlm';  % Levenberg-Marquardt backpropagation.
net = fitnet(hiddenLayerSize*ones(1,hiddenLayers),trainFcn);
 % Specify hidden layer structure
net.trainParam.lr = learningRate; % Set learning rate
net.input.processFcns = {'removeconstantrows','mapminmax'};
net.output.processFcns = {'removeconstantrows','mapminmax'};
net.divideFcn = 'dividerand';
net.divideMode = 'sample';
net.divideParam.trainRatio = 70/100;
net.divideParam.valRatio = 15/100;
net.divideParam.testRatio = 15/100;
net.performFcn = 'mse';
net.plotFcns = {'plotperform','plottrainstate','ploterrhist','plotregression', 'plotfit'};

% Train the ANN model
[net,tr] = train(net,x,t);

% Evaluate the ANN model's performance using MSE
y = net(x);
e = gsubtract(t,y);
performance = perform(net,t,y);
cost = performance;
assignin('base', 'predicted_values', y);
end
```

References

[1] M. Toor *et al.*, "An overview on bioethanol production from lignocellulosic feedstocks," *Chemosphere*, vol. 242, p. 125080, 2020, doi: https://doi.org/10.1016/j.chemosphere.2019.125080.

[2] S. S. Kumar, V. Kumar, R. Kumar, S. K. Malyan, and A. Pugazhendhi, "Microbial fuel cells as a sustainable platform technology for bioenergy, biosensing, environmental monitoring, and other low power device applications," *Fuel*, vol. 255, p. 115682, 2019, doi: https://doi.org/10.1016/j.fuel.2019.115682.

[3] P. Cavelius, S. Engelhart-Straub, N. Mehlmer, J. Lercher, D. Awad, and T. Brück, "The potential of biofuels from first to fourth generation," *PLoS Biol.*, vol. 21, no. 3, pp. 1–20, 2023, doi: 10.1371/JOURNAL.PBIO.3002063.

[4] E. de Jong, H. Langewld, and R. van Ree, "IEA Bioenergy Task 42 on Biorefinery," 2009, [Online]. Available: http://www.iea-bioenergy.task42-biorefineries.com/upload_mm/8/5/4/2e500e0f-d19a-4f7f-9360-4e9d5e580b75_Brochure Totaal_definitief_HR%5B1%5D.pdf

[5] International Energy Agency, "Net Zero by 2050: A Roadmap for the Global Energy Sector," *Int. Energy Agency*, p. 224, 2021, [Online]. Available: https://www.iea.org/reports/net-zero-by-2050

[6] International Energy Agency, "International Energy Agency (IEA) World Energy Outlook 2022," *Https://Www.Iea.Org/Reports/World-Energy-Outlook-2022/Executive-Summary*, p. 524, 2022, [Online]. Available: https://www.iea.org/reports/world-energy-outlook-2022

[7] IEA, "Renewables 2019 – Analysis and forecast to 2024," *Int. Energy Agency*, p. 204, 2019, [Online]. Available: https://www.iea.org/reports/renewables-2019

[8] NITI-Aayog, *ETHANOL BLENDING IN INDIA 2020-25*. Ministry of petrolium and natural gases, India, 2020. [Online]. Available: https://niti.gov.in/sites/default/files/2021-06/EthanolBlendingInIndia_compressed.pdf

[9] United States Department of Agriculture, "World agricultural production," *United States Dep. Agric.*, no. 7, pp. 59–65, 2019, doi: 10.32317/2221-1055.201907059.

[10] Government of India, "Third Advance Estimates of Production of Food grains for 2019-20," *Minist. Agric. Farmers Welfare, Dep. Agric. Coop. Farmers Welfare, India.*, vol. 5, no. 1, pp. 43–54, 2020.

[11] P. K. Gandam *et al.*, "Second-generation bioethanol production from corncob – A comprehensive review on pretreatment and bioconversion strategies, including techno-economic and lifecycle perspective," *Ind. Crops Prod.*, vol. 186, no. December 2021, p. 115245, 2022, doi: 10.1016/j.indcrop.2022.115245.

[12] 2023 U.S. Department of Agricultute, “US corn report.pdf.”

[13] R. Potumarthi, R. R. Baadhe, and A. Jetty, “Mixing of acid and base pretreated corncobs for improved production of reducing sugars and reduction in water use during neutralization,” *Bioresour. Technol.*, vol. 119, pp. 99–104, 2012, doi: 10.1016/j.biortech.2012.05.103.

[14] Ministry of Environment Forest and Climate Change (MoEF&CC), *India: First Biennial Update Report to the United Nations Framework Convention on Climate Change*, no. December. 2015. [Online]. Available: http://unfccc.int/resource/docs/natc/indbur1.pdf

[15] S. Mittal, E. O. Ahlgren, and P. R. Shukla, “Future biogas resource potential in India: A bottom-up analysis,” *Renew. Energy*, vol. 141, pp. 379–389, 2019, doi: https://doi.org/10.1016/j.renene.2019.03.133.

[16] C. R. Carere, R. Sparling, N. Cicek, and D. B. Levin, “Third generation biofuels via direct cellulose fermentation,” *Int. J. Mol. Sci.*, vol. 9, no. 7, pp. 1342–1360, 2008, doi: 10.3390/ijms9071342.

[17] P. McKendry, “Energy production from biomass (part 1): overview of biomass,” *Bioresour. Technol*, vol. 83, no. 1, pp. 37–46, 2002, doi: 10.1016/S0960-8524(01)00118-3.

[18] B. Alberts, A. Johnson, and J. Lewis, *Molecular Biology of the Cell-The Plant Cell Wall*, vol. 4th editio. 2017. doi: https://www.ncbi.nlm.nih.gov/books/NBK26928/.

[19] H. Rabemanolontsoa and S. Saka, “Comparative study on chemical composition of various biomass species,” *RSC Adv.*, vol. 3, no. 12, pp. 3946–3956, 2013, doi: 10.1039/c3ra22958k.

[20] NREL, “Biomass Compositional Analysis Laboratory Procedures | Bioenergy | NREL.” https://www.nrel.gov/bioenergy/biomass-compositional-analysis.html (accessed Oct. 02, 2021).

[21] L. Dai *et al.*, “Bridging the relationship between hydrothermal pretreatment and co-pyrolysis: Effect of hydrothermal pretreatment on aromatic production,” *Energy Convers. Manag.*, vol. 180, no. September 2018, pp. 36–43, 2019, doi: 10.1016/j.enconman.2018.10.079.

[22] K. Thangavelu, R. Desikan, O. P. Taran, and S. Uthandi, “Delignification of corncob via combined hydrodynamic cavitation and enzymatic pretreatment: Process optimization by response surface methodology,” *Biotechnol. Biofuels*, vol. 11, no. 1, pp. 1–13, 2018, doi: 10.1186/s13068-018-1204-y.

[23] X. Li, L. Yang, X. Gu, C. Lai, C. Huang, and Q. Yong, “A combined process for production of fumaric acid and xylooligosaccharides from corncob,” *BioResources*, vol. 13, no. 1, pp. 399–411, 2018, doi: 10.15376/biores.13.1.399-411.

[24] M. A. Medina-Morales *et al.*, “Biohydrogen production from thermochemically pretreated corncob using a mixed culture bioaugmented with Clostridium acetobutylicum,” *Int. J. Hydrogen Energy*, no. xxxx, 2021, doi: 10.1016/j.ijhydene.2021.04.046.

[25] C. Y. Bu, Y. X. Yan, L. H. Zou, S. P. Ouyang, Z. J. Zheng, and J. Ouyang, “Comprehensive utilization of corncob for furfuryl alcohol production by chemo-enzymatic sequential catalysis in a biphasic system,” *Bioresour. Technol.*, vol. 319, no. September 2020, p. 124156, 2021, doi: 10.1016/j.biortech.2020.124156.

[26] D. Dasgupta *et al.*, “Energy and life cycle impact assessment for xylitol production from corncob,” *J. Clean. Prod.*, vol. 278, no. 2021, p. 123217, 2021, doi: 10.1016/j.jclepro.2020.123217.

[27] M. A. Mengstie and N. G. Habtu, “Synthesis and Characterization of 5-Hydroxymethylfurfural from Corncob Using Solid Sulfonated Carbon Catalyst,” *Int. J. Chem. Eng.*, vol. 2020, 2020, doi: 10.1155/2020/8886361.

[28] M. Ioelovich, “Plant Biomass as a Renewable Source of Biofuels and Biochemicals,” no. October 2013, pp. 1–58, 2013.

[29] V. B. Agbor, N. Cicek, R. Sparling, A. Berlin, and D. B. Levin, “Biomass pretreatment: Fundamentals toward application,” *Biotechnol. Adv.*, vol. 29, no. 6, pp. 675–685, 2011, doi: 10.1016/j.biotechadv.2011.05.005.

[30] B. Yang and C. E. Wyman, “Pretreatment: the key to unlocking low-cost cellulosic ethanol,” *Biofuels, Bioprod. Biorefining*, vol. 2, no. 1, pp. 26–40, Jan. 2008, doi: https://doi.org/10.1002/bbb.49.

[31] P. K. Gandam *et al.*, “A New Insight into the Composition and Physical Characteristics of Corncob—Substantiating Its Potential for Tailored Biorefinery Objectives,” *Fermentation*, vol. 8, no. 12. 2022. doi: 10.3390/fermentation8120704.

[32] D. Araújo, M. Vilarinho, and A. Machado, “Effect of combined dilute-alkaline and green pretreatments on corncob fractionation: Pretreated biomass characterization and regenerated cellulose film production,” *Ind. Crops Prod.*, vol. 141, no. May, 2019, doi: 10.1016/j.indcrop.2019.111785.

[33] P. Sahare, R. Singh, R. S. Laxman, and M. Rao, “Effect of Alkali Pretreatment on the Structural Properties and Enzymatic Hydrolysis of Corn Cob,” *Appl. Biochem. Biotechnol.*, vol. 168, no. 7, pp. 1806–1819, 2012, doi: 10.1007/s12010-012-9898-y.

[34] A. Boonsombuti, A. Luengnaruemitchai, and S. Wongkasemjit, “Enhancement of enzymatic hydrolysis of corncob by microwave-assisted alkali pretreatment and its effect in morphology,” *Cellulose*, vol. 20, no. 4, pp. 1957–1966, 2013, doi: 10.1007/s10570-013-9958-7.

[35] K. Gao and L. Rehmann, “ABE fermentation from enzymatic hydrolysate of NaOH-pretreated corncobs,” *Biomass and Bioenergy*, vol. 66, pp. 110–115, 2014, doi: 10.1016/j.biombioe.2014.03.002.

[36] D. Chapla, J. Divecha, D. Madamwar, and A. Shah, “Utilization of agro-industrial waste for xylanase production by Aspergillus foetidus MTCC 4898 under solid state fermentation and its application in saccharification,” *Biochem. Eng. J.*, vol. 49, no. 3, pp. 361–369, 2010, doi: 10.1016/j.bej.2010.01.012.

[37] W. Luo *et al.*, “A facile and efficient pretreatment of corncob for bioproduction of butanol,” *Bioresour. Technol.*, vol. 140, pp. 86–89, 2013, doi: 10.1016/j.biortech.2013.04.063.

[38] H. Z. Ling, K. K. Cheng, J. P. Ge, and W. X. Ping, “Corncob Mild Alkaline Pretreatment for High 2,3-Butanediol Production by Spent Liquor Recycle Process,” *Bioenergy Res.*, vol. 10, no. 2, pp. 566–574, 2017, doi: 10.1007/s12155-017-9822-y.

[39] X. Peng, C. Zhang, Y. Tian, X. Guo, Y. Liu, and D. Xiao, “Corncob Residue Pretreatment for 2,3-Butanediol Production by Simultaneous Saccharification and Fermentation,” *Lect. Notes Electr. Eng.*, vol. 251, pp. 1469–1479, Nov. 2014, doi: 10.1007/978-3-642-37925-3_156.

[40] Z. Zhang *et al.*, “Comparison of high-titer lactic acid fermentation from NaOH-and NH3-H2O2-pretreated corncob by Bacillus coagulans using simultaneous saccharification and fermentation,” *Sci. Rep.*, vol. 6, no. November, pp. 1–10, 2016, doi: 10.1038/srep37245.

[41] A. Zheng *et al.*, “Quantitative comparison of different chemical pretreatment methods on chemical structure and pyrolysis characteristics of corncobs,” *J. Energy Inst.*, vol. 91, no. 5, pp. 676–682, 2018, doi: 10.1016/j.joei.2017.06.002.

[42] L. Jiang, Y. Wu, Z. Zhao, H. Li, K. Zhao, and F. Zhang, “Selectively biorefining levoglucosan from NaOH pretreated corncobs via fast pyrolysis,” *Cellulose*, vol. 26, no. 13–14, pp. 7877–7887, 2019, doi: 10.1007/s10570-019-02625-4.

[43] H. K. Tewari, L. Singh, S. S. Marwaha, and J. F. Kennedy, “Role of pretreatments on enzymatic hydrolysis of agricultural residues for reducing sugar production,” *J. Chem. Technol. Biotechnol.*, vol. 38, no. 3, pp. 153–165, 1987, doi: 10.1002/jctb.280380303.

[44] A. Sharma *et al.*, “Simultaneous saccharification and fermentation of alkali-pretreated corncob under optimized conditions using cold-tolerant indigenous holocellulase,” *Korean J. Chem. Eng.*, vol. 34, no. 3, pp. 773–780, 2017, doi: 10.1007/s11814-016-0334-9.

[45] N. Pérez-Rodríguez, F. Oliveira, B. Pérez-Bibbins, I. Belo, A. Torrado Agrasar, and J. M. Domínguez, “Optimization of xylanase production by filamentous fungi in solid-state fermentation and scale-up to horizontal tube bioreactor,” *Appl. Biochem. Biotechnol.*, vol.

173, no. 3, pp. 803–825, 2014, doi: 10.1007/s12010-014-0895-1.

[46] T. Robinson, B. Chandran, and P. Nigam, “Effect of pretreatments of three waste residues, wheat straw, corncobs and barley husks on dye adsorption,” *Bioresour. Technol.*, vol. 85, no. 2, pp. 119–124, 2002, doi: 10.1016/S0960-8524(02)00099-8.

[47] L. Feng *et al.*, “Comparison of nitrogen removal and microbial properties in solid-phase denitrification systems for water purification with various pretreated lignocellulosic carriers,” *Bioresour. Technol.*, vol. 224, pp. 236–245, 2017, doi: 10.1016/j.biortech.2016.11.002.

[48] A. Stachowiak-Wencek, M. Zborowska, H. Waliszewska, and B. Waliszewska, “Chemical changes in Lignocellulosic Biomass (Corncob) influenced by pretreatment and Anaerobic Digestion (AD),” *BioResources*, vol. 14, no. 4, pp. 8082–8099, 2019, doi: 10.15376/biores.14.4.8082-8099.

[49] M. Zhang, F. Wang, R. Su, W. Qi, and Z. He, “Ethanol production from high dry matter corncob using fed-batch simultaneous saccharification and fermentation after combined pretreatment,” *Bioresour. Technol.*, vol. 101, no. 13, pp. 4959–4964, Jul. 2010, doi: 10.1016/j.biortech.2009.11.010.

[50] M. Li, Y. L. Cheng, N. Fu, D. Li, B. Adhikari, and X. D. Chen, “Isolation and characterization of corncob cellulose fibers using microwave-assisted chemical treatments,” *Int. J. Food Eng.*, vol. 10, no. 3, pp. 427–436, 2014, doi: 10.1515/ijfe-2014-0052.

[51] X. Ouyang, L. Chen, S. Zhang, Q. Yuan, W. Wang, and R. J. Linhardt, “Effect of Simultaneous steam explosion and alkaline depolymerization on corncob lignin and cellulose structure,” *Chem. Biochem. Eng. Q.*, vol. 32, no. 2, pp. 177–189, 2018, doi: 10.15255/CABEQ.2017.1251.

[52] D. Araújo, M. C. R. Castro, A. Figueiredo, M. Vilarinho, and A. Machado, “Green synthesis of cellulose acetate from corncob: Physicochemical properties and assessment of environmental impacts,” *J. Clean. Prod.*, vol. 260, 2020, doi: 10.1016/j.jclepro.2020.120865.

[53] L. Ma *et al.*, “Optimization of sodium percarbonate pretreatment for improving 2,3-butanediol production from corncob,” *Prep. Biochem. Biotechnol.*, vol. 48, no. 3, pp. 218–225, 2018, doi: 10.1080/10826068.2017.1387563.

[54] Y. Chen, B. Dong, W. Qin, and D. Xiao, “Xylose and cellulose fractionation from corncob with three different strategies and separate fermentation of them to bioethanol,” *Bioresour. Technol.*, vol. 101, no. 18, pp. 6994–6999, 2010, doi: 10.1016/j.biortech.2010.03.132.

[55] R. Gupta, Y. P. Khasa, and R. C. Kuhad, “Evaluation of pretreatment methods in

improving the enzymatic saccharification of cellulosic materials," *Carbohydr. Polym.*, vol. 84, no. 3, pp. 1103–1109, 2011, doi: 10.1016/j.carbpol.2010.12.074.

[56] H. Chen *et al.*, "Improving enzymatic hydrolysis efficiency of corncob residue through sodium sulfite pretreatment," *Appl. Microbiol. Biotechnol.*, vol. 103, no. 18, pp. 7795–7804, 2019, doi: 10.1007/s00253-019-10050-7.

[57] R. Du, R. Su, W. Qi, and Z. He, "Enhanced enzymatic hydrolysis of corncob by ultrasound-assisted soaking in aqueous ammonia pretreatment," *3 Biotech*, vol. 8, no. 3, 2018, doi: 10.1007/s13205-018-1186-2.

[58] X. Chi *et al.*, "A clean and effective potassium hydroxide pretreatment of corncob residue for the enhancement of enzymatic hydrolysis at high solids loading," *RSC Adv.*, vol. 9, no. 20, pp. 11558–11566, 2019, doi: 10.1039/C9RA01555H.

[59] M. Idrees, A. Adnan, and F. A. Qureshi, "Optimization of sulfide/sulfite pretreatment of lignocellulosic biomass for lactic acid production," *Biomed Res. Int.*, vol. 2013, 2013, doi: 10.1155/2013/934171.

[60] Y. Sheng, X. Tan, Y. Gu, X. Zhou, M. Tu, and Y. Xu, "Effect of ascorbic acid assisted dilute acid pretreatment on lignin removal and enzyme digestibility of agricultural residues," *Renew. Energy*, vol. 163, pp. 732–739, 2021, doi: 10.1016/j.renene.2020.08.135.

[61] S. Wang, X. Ouyang, W. Wang, Q. Yuan, and A. Yan, "Comparison of ultrasound-assisted Fenton reaction and dilute acid-catalysed steam explosion pretreatment of corncobs: Cellulose characteristics and enzymatic saccharification," *RSC Adv.*, vol. 6, no. 80, pp. 76848–76854, 2016, doi: 10.1039/c6ra13125e.

[62] R. Koppram *et al.*, "Simultaneous saccharification and co-fermentation for bioethanol production using corncobs at lab, PDU and demo scales," *Biotechnol. Biofuels*, vol. 6, no. 1, pp. 2–11, 2013, doi: 10.1186/1754-6834-6-2.

[63] W. S. Lim and J. W. Lee, "Enzymatic hydrolysis condition of pretreated corncob by oxalic acid to improve ethanol production," *J. Korean Wood Sci. Technol.*, vol. 40, no. 4, pp. 294–301, 2012, doi: 10.5658/WOOD.2012.40.4.294.

[64] Q. Lin *et al.*, "Production of Xylooligosaccharide, Nanolignin, and Nanocellulose through a Fractionation Strategy of Corncob for Biomass Valorization," *Ind. Eng. Chem. Res.*, vol. 59, no. 39, pp. 17429–17439, 2020, doi: 10.1021/acs.iecr.0c02161.

[65] M. Yang, X. Gao, M. Lan, Y. Dou, and X. Zhang, "Rapid Fractionation of Lignocellulosic Biomass by p-TsOH Pretreatment," *Energy and Fuels*, vol. 33, no. 3, pp. 2258–2264, 2019, doi: 10.1021/acs.energyfuels.8b03770.

[66] J. Hu *et al.*, "Synthesis of a Stable Solid Acid Catalyst from Chloromethyl Polystyrene

through a Simple Sulfonation for Pretreatment of Lignocellulose in Aqueous Solution," *ChemSusChem*, vol. 14, no. 3, pp. 979–989, 2021, doi: 10.1002/cssc.202002599.

[67] R. Q. Zhang *et al.*, "Enhanced Biosynthesis of Furoic Acid via the Effective Pretreatment of Corncob into Furfural in the Biphasic Media," *Catal. Letters*, no. 0123456789, 2020, doi: 10.1007/s10562-020-03152-9.

[68] F. Yao, F. Shen, X. Wan, and C. Hu, "High yield and high concentration glucose production from corncob residues after tetrahydrofuran + H2O co-solvent pretreatment and followed by enzymatic hydrolysis," *Renew. Sustain. Energy Rev.*, vol. 132, no. July, p. 110107, 2020, doi: 10.1016/j.rser.2020.110107.

[69] L. Jiang *et al.*, "Effect of glycerol pretreatment on levoglucosan production from corncobs by fast pyrolysis," *Polymers (Basel).*, vol. 9, no. 11, 2017, doi: 10.3390/polym9110599.

[70] C. W. Zhang, S. Q. Xia, and P. S. Ma, "Facile pretreatment of lignocellulosic biomass using deep eutectic solvents," *Bioresour. Technol.*, vol. 219, no. July, pp. 1–5, 2016, doi: 10.1016/j.biortech.2016.07.026.

[71] P. Weerachanchai and J. M. Lee, "Effect of organic solvent in ionic liquid on biomass pretreatment," *ACS Sustain. Chem. Eng.*, vol. 1, no. 8, pp. 894–902, 2013, doi: 10.1021/sc300147f.

[72] Y. Su *et al.*, "Fractional pretreatment of lignocellulose by alkaline hydrogen peroxide: Characterization of its major components," *Food Bioprod. Process.*, vol. 94, no. March 2013, pp. 322–330, 2015, doi: 10.1016/j.fbp.2014.04.001.

[73] S. Upajak, N. Laosiripojana, V. Champreda, T. Kreethachart, and S. Imman, "Effect of combination of liquid hot water system and hydrogen peroxide pretreatment on enzymatic saccharification of corn cob," *Int. J. GEOMATE*, vol. 15, no. 51, pp. 31–38, 2018, doi: 10.21660/2018.51.24851.

[74] L. Ma, Y. Cui, R. Cai, X. Liu, C. Zhang, and D. Xiao, "Optimization and evaluation of alkaline potassium permanganate pretreatment of corncob," *Bioresour. Technol.*, vol. 180, no. 2015, pp. 1–6, 2015, doi: 10.1016/j.biortech.2014.12.078.

[75] X. Peng, W. Qiao, S. Mi, X. Jia, H. Su, and Y. Han, "Characterization of hemicellulase and cellulase from the extremely thermophilic bacterium Caldicellulosiruptor owensensis and their potential application for bioconversion of lignocellulosic biomass without pretreatment," *Biotechnol. Biofuels*, vol. 8, no. 1, pp. 1–14, 2015, doi: 10.1186/s13068-015-0313-0.

[76] A. Zheng *et al.*, "Comparison of the effect of wet and dry torrefaction on chemical structure and pyrolysis behavior of corncobs," *Bioresour. Technol.*, vol. 176, pp. 15–22, 2015, doi: 10.1016/j.biortech.2014.10.157.

[77] P. Seesuriyachan, A. Kawee-ai, and T. Chaiyaso, “Green and chemical-free process of enzymatic xylooligosaccharide production from corncob: Enhancement of the yields using a strategy of lignocellulosic destructuration by ultra-high pressure pretreatment,” *Bioresour. Technol.*, vol. 241, pp. 537–544, 2017, doi: 10.1016/j.biortech.2017.05.193.

[78] H. Li *et al.*, “An efficient pretreatment for the selectively hydrothermal conversion of corncob into furfural: The combined mixed ball milling and ultrasonic pretreatments,” *Ind. Crops Prod.*, vol. 94, pp. 721–728, 2016, doi: 10.1016/j.indcrop.2016.09.052.

[79] M. García-Torreiro, M. López-Abelairas, T. A. Lu-Chau, and J. M. Lema, “Fungal pretreatment of agricultural residues for bioethanol production,” *Ind. Crops Prod.*, vol. 89, pp. 486–492, 2016, doi: 10.1016/j.indcrop.2016.05.036.

[80] J. Luo, Y. Su, J. Chen, X. Wang, and J. Liu, “Pretreatment of lignin-containing cellulose micro/nano-fibrils (LCMNF) from corncob residues,” *Cellulose*, vol. 28, no. 8, pp. 4671–4684, 2021, doi: 10.1007/s10570-021-03798-7.

[81] R. Marchal, M. Ropars, J. Pourquié, F. Fayolle, and J. P. Vandecasteele, “Large-scale enzymatic hydrolysis of agricultural lignocellulosic biomass. Part 2: Conversion into acetone-butanol,” *Bioresour. Technol.*, vol. 42, no. 3, pp. 205–217, 1992, doi: 10.1016/0960-8524(92)90024-R.

[82] Z. Liu, C. Ma, C. Gao, and P. Xu, “Efficient utilization of hemicellulose hydrolysate for propionic acid production using Propionibacterium acidipropionici,” *Bioresour. Technol.*, vol. 114, pp. 711–714, 2012, doi: 10.1016/j.biortech.2012.02.118.

[83] C. Wang *et al.*, “A kinetic study on the hydrolysis of corncob residues to levulinic acid in the FeCl3–NaCl system,” *Cellulose*, vol. 26, no. 15, pp. 8313–8323, 2019, doi: 10.1007/s10570-019-02711-7.

[84] W. Guo, W. Jia, Y. Li, and S. Chen, “Performances of Lactobacillus brevis for producing lactic acid from hydrolysate of lignocellulosics,” *Appl. Biochem. Biotechnol.*, vol. 161, no. 1–8, pp. 124–136, 2010, doi: 10.1007/s12010-009-8857-8.

[85] W. Zheng, X. Liu, L. Zhu, H. Huang, T. Wang, and L. Jiang, “Pretreatment with γ-Valerolactone/[Mmim]DMP and Enzymatic Hydrolysis on Corncob and Its Application in Immobilized Butyric Acid Fermentation,” *J. Agric. Food Chem.*, vol. 66, no. 44, pp. 11709–11717, 2018, doi: 10.1021/acs.jafc.8b04323.

[86] D. Zhou *et al.*, “Activated carbons prepared via reflux-microwave-assisted activation approach with high adsorption capability for methylene blue,” *J. Environ. Chem. Eng.*, vol. 9, no. 1, p. 104671, 2021, doi: https://doi.org/10.1016/j.jece.2020.104671.

[87] F. Mureed, R. Nadeem, A. Mehmood, M. Siddique, and M. Bukhari, “Biosorption of zinc by chemically modified biomass of corncob (Zea mays L.),” *Middle East J. Sci. Res.*, vol.

11, pp. 1226–1231, Jan. 2012, doi: 10.5829/idosi.mejsr.2012.11.09.63246.

[88] G. K. Gupta, M. Ram, R. Bala, M. Kapur, and M. K. Mondal, “Pyrolysis of chemically treated corncob for biochar production and its application in Cr(VI) removal,” *Environ. Prog. Sustain. Energy*, vol. 37, no. 5, pp. 1606–1617, 2018, doi: 10.1002/ep.12838.

[89] M. Tao, Z. Jing, Z. Tao, H. Luo, and S. Zuo, “Improvements of nitrogen removal and electricity generation in microbial fuel cell-constructed wetland with extra corncob for carbon-limited wastewater treatment,” *J. Clean. Prod.*, vol. 297, p. 126639, 2021, doi: https://doi.org/10.1016/j.jclepro.2021.126639.

[90] N. Pérez-Rodríguez, D. García-Bernet, and J. M. Domínguez, “Extrusion and enzymatic hydrolysis as pretreatments on corn cob for biogas production,” *Renew. Energy*, vol. 107, pp. 597–603, 2017, doi: 10.1016/j.renene.2017.02.030.

[91] A. Zheng *et al.*, “Effect of torrefaction on structure and fast pyrolysis behavior of corncobs,” *Bioresour. Technol.*, vol. 128, pp. 370–377, 2013, doi: 10.1016/j.biortech.2012.10.067.

[92] H. Yang, L. Guo, and F. Liu, “Enhanced bio-hydrogen production from corncob by a two-step process: Dark- and photo-fermentation,” *Bioresour. Technol.*, vol. 101, no. 6, pp. 2049–2052, 2010, doi: 10.1016/j.biortech.2009.10.078.

[93] A. A. O. S. Prado *et al.*, “Evaluation of a new strategy in the elaboration of culture media to produce surfactin from hemicellulosic corncob liquor,” *Biotechnol. Reports*, vol. 24, p. e00364, 2019, doi: 10.1016/j.btre.2019.e00364.

[94] A. Zheng *et al.*, “Catalytic fast pyrolysis of biomass pretreated by torrefaction with varying severity,” *Energy and Fuels*, vol. 28, no. 9, pp. 5804–5811, 2014, doi: 10.1021/ef500892k.

[95] J. Ai *et al.*, “Corncob cellulose-derived hierarchical porous carbon for high performance supercapacitors,” *J. Power Sources*, vol. 484, no. August 2020, p. 229221, 2021, doi: 10.1016/j.jpowsour.2020.229221.

[96] B. Chen *et al.*, “Corncob residual reinforced polyethylene composites considering the biorefinery process and the enhancement of performance,” *J. Clean. Prod.*, vol. 198, pp. 452–462, 2018, doi: 10.1016/j.jclepro.2018.07.080.

[97] L. qun Jiang *et al.*, “Crude glycerol pretreatment for selective saccharification of lignocellulose via fast pyrolysis and enzyme hydrolysis,” *Energy Convers. Manag.*, vol. 199, no. August, p. 111894, 2019, doi: 10.1016/j.enconman.2019.111894.

[98] A. R. Shah and D. Madamwar, “Xylanase production under solid-state fermentation and its characterization by an isolated strain of Aspergillus foetidus in India,” *World J. Microbiol. Biotechnol.*, vol. 21, no. 3, pp. 233–243, 2005, doi: 10.1007/s11274-004-3622-1.

[99] K. K. Brar, S. Kaur, and B. S. Chadha, “A novel staggered hybrid SSF approach for efficient conversion of cellulose/hemicellulosic fractions of corncob into ethanol,” *Renew. Energy*, vol. 98, pp. 16–22, 2016, doi: 10.1016/j.renene.2016.03.082.

[100] S. Dechakhumwat, P. Hongmanorom, C. Thunyaratchatanon, S. M. Smith, S. Boonyuen, and A. Luengnaruemitchai, “Catalytic activity of heterogeneous acid catalysts derived from corncob in the esterification of oleic acid with methanol,” *Renew. Energy*, vol. 148, pp. 897–906, 2020, doi: 10.1016/j.renene.2019.10.174.

[101] P. H. Hoang, T. D. Cuong, and L. Q. Dien, “Ultrasound Assisted Conversion of Corncob-Derived Xylan to Furfural Under HSO3-ZSM-5 Zeolite Catalyst,” *Waste and Biomass Valorization*, no. 1, 2020, doi: 10.1007/s12649-020-01152-9.

[102] P. Zhang, X. Liao, C. Ma, Q. Li, A. Li, and Y. He, “Chemoenzymatic Conversion of Corncob to Furfurylamine via Tandem Catalysis with Tin-Based Solid Acid and Transaminase Biocatalyst,” *ACS Sustain. Chem. Eng.*, vol. 7, no. 21, pp. 17636–17642, 2019, doi: 10.1021/acssuschemeng.9b03510.

[103] Z. ye Mo, M. hui Zhang, D. feng Zheng, R. jing Dong, and X. qing Qiu, “Pretreatment of the corncob enzymatic residue with p-toluenesulfonic acid and valorization,” *Colloids Surfaces A Physicochem. Eng. Asp.*, vol. 577, no. May, pp. 296–305, 2019, doi: 10.1016/j.colsurfa.2019.05.093.

[104] X. Zhang, J. Zhu, L. Sun, Q. Yuan, G. Cheng, and D. S. Argyropoulos, “Extraction and characterization of lignin from corncob residue after acid-catalyzed steam explosion pretreatment,” *Ind. Crops Prod.*, vol. 133, no. March, pp. 241–249, 2019, doi: 10.1016/j.indcrop.2019.03.027.

[105] X. Zou, Y. Wang, G. Tu, Z. Zan, and X. Wu, “Adaptation and transcriptome analysis of Aureobasidium pullulans in corncob hydrolysate for increased inhibitor tolerance to malic acid production,” *PLoS One*, vol. 10, no. 3, pp. 1–17, 2015, doi: 10.1371/journal.pone.0121416.

[106] L. Jiang *et al.*, “Comprehensive Utilization of Hemicellulose and Cellulose to Release Fermentable Sugars from Corncobs via Acid Hydrolysis and Fast Pyrolysis,” *ACS Sustain. Chem. Eng.*, vol. 5, no. 6, pp. 5208–5213, 2017, doi: 10.1021/acssuschemeng.7b00561.

[107] M. Konishi, Y. Yoshida, and J. ichi Horiuchi, “Efficient production of sophorolipids by Starmerella bombicola using a corncob hydrolysate medium,” *J. Biosci. Bioeng.*, vol. 119, no. 3, pp. 317–322, 2015, doi: 10.1016/j.jbiosc.2014.08.007.

[108] S. You *et al.*, “Recycling Strategy and Repression Elimination for Lignocellulosic-Based Farnesene Production with an Engineered Escherichia coli,” *J. Agric. Food Chem.*, vol. 67, no. 35, pp. 9858–9867, 2019, doi: 10.1021/acs.jafc.9b03907.

[109] M. Ganesan, R. Mathivani Vinayakamoorthy, S. Thankappan, I. Muniraj, and S. Uthandi, "Thermotolerant glycosyl hydrolases-producing Bacillus aerius CMCPS1 and its saccharification efficiency on HCR-laccase (LccH)-pretreated corncob biomass," *Biotechnol. Biofuels*, vol. 13, no. 1, p. 124, 2020, doi: 10.1186/s13068-020-01764-2.

[110] A. Deng *et al.*, "Production of xylo-sugars from corncob by oxalic acid-assisted ball milling and microwave-induced hydrothermal treatments," *Ind. Crops Prod.*, vol. 79, pp. 137–145, 2016, doi: 10.1016/j.indcrop.2015.11.032.

[111] K. K. Cheng *et al.*, "Optimization of pH and acetic acid concentration for bioconversion of hemicellulose from corncobs to xylitol by Candida tropicalis," *Biochem. Eng. J.*, vol. 43, no. 2, pp. 203–207, 2009, doi: 10.1016/j.bej.2008.09.012.

[112] M. Zhang, F. Wang, R. Su, W. Qi, and Z. He, "Ethanol production from high dry matter corncob using fed-batch simultaneous saccharification and fermentation after combined pretreatment," *Bioresour. Technol.*, vol. 101, no. 13, pp. 4959–4964, 2010, doi: 10.1016/j.biortech.2009.11.010.

[113] M. C. T. Damaso, A. M. De Castro, R. M. Castro, C. M. M. C. Andrade, and N. Pereira, "Application of xylanase from Thermomyces lanuginosus IOC-4145 for enzymatic hydrolysis of corncob and sugarcane bagasse," *Appl. Biochem. Biotechnol. - Part A Enzym. Eng. Biotechnol.*, vol. 115, no. 1–3, pp. 1003–1012, 2004, doi: 10.1385/ABAB:115:1-3:1003.

[114] D. Araújo, M. C. R. Castro, A. Figueiredo, M. Vilarinho, and A. Machado, "Green synthesis of cellulose acetate from corncob: Physicochemical properties and assessment of environmental impacts," *J. Clean. Prod.*, vol. 260, p. 120865, 2020, doi: 10.1016/j.jclepro.2020.120865.

[115] G. Sun, J. Wan, Y. Sun, H. Li, C. Chang, and Y. Wang, "Enhanced removal of nitrate and refractory organic pollutants from bio-treated coking wastewater using corncobs as carbon sources and biofilm carriers," *Chemosphere*, vol. 237, p. 124520, 2019, doi: 10.1016/j.chemosphere.2019.124520.

[116] Y. Zhang, X. Mu, H. Wang, B. Li, and H. Peng, "Combined deacetylation and PFI refining pretreatment of corn cob for the improvement of a two-stage enzymatic hydrolysis," *J. Agric. Food Chem.*, vol. 62, no. 20, pp. 4661–4667, 2014, doi: 10.1021/jf500189a.

[117] S. Y. Leu and J. Y. Zhu, "Substrate-Related Factors Affecting Enzymatic Saccharification of Lignocelluloses: Our Recent Understanding," *Bioenergy Res.*, vol. 6, no. 2, pp. 405–415, 2013, doi: 10.1007/s12155-012-9276-1.

[118] L. Yang *et al.*, "Effects of sodium carbonate pretreatment on the chemical compositions and enzymatic saccharification of rice straw," *Bioresour. Technol.*, vol. 124, pp. 283–291, 2012, doi: 10.1016/j.biortech.2012.08.041.

[119] H. Xu, B. Li, and X. Mu, “Review of Alkali-Based Pretreatment to Enhance Enzymatic Saccharification for Lignocellulosic Biomass Conversion,” *Ind. Eng. Chem. Res.*, vol. 55, no. 32, pp. 8691–8705, 2016, doi: 10.1021/acs.iecr.6b01907.

[120] I. KUSAKABE, T. YASUI, and T. KOBAYASHI, “Enzymatic Hydrolysis-extraction of Xylan from Xylan-containing Natural Materials,” *Nippon Nōgeikagaku Kaishi*, vol. 50, no. 5, pp. 199–208, 1976, doi: 10.1271/nogeikagaku1924.50.5_199.

[121] C. Falco *et al.*, “Hydrothermal carbons from hemicellulose-derived aqueous hydrolysis products as electrode materials for supercapacitors,” *ChemSusChem*, vol. 6, no. 2, pp. 374–382, 2013, doi: 10.1002/cssc.201200817.

[122] O. Asmarani, A. D. Pertiwi, and N. N. Tri Puspaningsih, “Application of enzyme cocktails from Indonesian isolates to corncob (Zea mays) waste saccharification,” *Biocatal. Agric. Biotechnol.*, vol. 24, no. February, p. 101537, 2020, doi: 10.1016/j.bcab.2020.101537.

[123] K. K. Cheng, W. Wang, J. A. Zhang, Q. Zhao, J. P. Li, and J. W. Xue, “Statistical optimization of sulfite pretreatment of corncob residues for high concentration ethanol production,” *Bioresour. Technol.*, vol. 102, no. 3, pp. 3014–3019, Feb. 2011, doi: 10.1016/j.biortech.2010.09.117.

[124] A. Boonsombuti, K. Tangmanasakul, J. Nantapipat, K. Komolpis, A. Luengnaruemitchai, and S. Wongkasemjit, “Production of biobutanol from acid-pretreated corncob using Clostridium beijerinckii TISTR 1461: Process optimization studies,” *Prep. Biochem. Biotechnol.*, vol. 46, no. 2, pp. 141–149, 2016, doi: 10.1080/10826068.2014.995810.

[125] B. Y. Cai, J. P. Ge, H. Z. Ling, K. K. Cheng, and W. X. Ping, “Statistical optimization of dilute sulfuric acid pretreatment of corncob for xylose recovery and ethanol production,” *Biomass and Bioenergy*, vol. 36, pp. 250–257, 2012, doi: 10.1016/j.biombioe.2011.10.023.

[126] A. Boonsombuti, A. Luengnaruemitchai, and S. Wongkasemjit, “Effect of phosphoric acid pretreatment of corncobs on the fermentability of clostridium beijerinckii TISTR 1461 for biobutanol production,” *Prep. Biochem. Biotechnol.*, vol. 45, no. 2, pp. 173–191, 2015, doi: 10.1080/10826068.2014.907179.

[127] Y. Wang, Y. Hu, P. Qi, and L. Guo, “A new approach for economical pretreatment of corncobs,” *Appl. Sci.*, vol. 9, no. 3, 2019, doi: 10.3390/app9030504.

[128] S. Wang, X. Ouyang, W. Wang, Q. Yuan, and A. Yan, “Comparison of ultrasound-assisted Fenton reaction and dilute acid-catalysed steam explosion pretreatment of corncobs: cellulose characteristics and enzymatic saccharification,” *RSC Adv.*, vol. 6, no. 80, pp. 76848–76854, 2016, doi: 10.1039/C6RA13125E.

[129] X. Fan, G. Cheng, H. Zhang, M. Li, S. Wang, and Q. Yuan, “Effects of acid impregnated steam explosion process on xylose recovery and enzymatic conversion of cellulose in

corncob," *Carbohydr. Polym.*, vol. 114, pp. 21–26, 2014, doi: 10.1016/j.carbpol.2014.07.051.

[130] H. Qiao, L. Liu, J. Ouyang, and S. Ouyang, "Pretreatment of Corncob by Dilute Acetic Acid," *Chem. Ind. For. Prod.*, vol. 39, no. 1, pp. 81–87, 2019, [Online]. Available: http://www.cifp.ac.cn

[131] J. Han, R. Cao, X. Zhou, and Y. Xu, "An integrated biorefinery process for adding values to corncob in co-production of xylooligosaccharides and glucose starting from pretreatment with gluconic acid," *Bioresour. Technol.*, vol. 307, no. 159, p. 123200, 2020, doi: 10.1016/j.biortech.2020.123200.

[132] J. W. Lee, R. C. L. B. Rodrigues, and T. W. Jeffries, "Simultaneous saccharification and ethanol fermentation of oxalic acid pretreated corncob assessed with response surface methodology," *Bioresour. Technol.*, vol. 100, no. 24, pp. 6307–6311, 2009, doi: 10.1016/j.biortech.2009.06.088.

[133] Q. Qing *et al.*, "Catalytic conversion of corncob and corncob pretreatment hydrolysate to furfural in a biphasic system with addition of sodium chloride," *Bioresour. Technol.*, vol. 226, pp. 247–254, 2017, doi: 10.1016/j.biortech.2016.11.118.

[134] J. W. Lee, C. J. Houtman, H. Y. Kim, I. G. Choi, and T. W. Jeffries, "Scale-up study of oxalic acid pretreatment of agricultural lignocellulosic biomass for the production of bioethanol," *Bioresour. Technol.*, vol. 102, no. 16, pp. 7451–7456, 2011, doi: 10.1016/j.biortech.2011.05.022.

[135] C. Pan, S. Zhang, Y. Fan, and H. Hou, "Bioconversion of corncob to hydrogen using anaerobic mixed microflora," *Int. J. Hydrogen Energy*, vol. 35, no. 7, pp. 2663–2669, 2010, doi: 10.1016/j.ijhydene.2009.04.023.

[136] J. C. Contreras-Esquivel *et al.*, "Gluconic Acid as a New Green Solvent for Recovery of Polysaccharides by Clean Technologies," pp. 237–251, 2014, doi: 10.1007/978-3-662-43628-8_11.

[137] N. J. Cao *et al.*, "Ethanol production from corn cob pretreated by the ammonia steeping process using genetically engineered yeast," *Biotechnol. Lett.*, vol. 18, no. 9, pp. 1013–1018, 1996, doi: 10.1007/BF00129723.

[138] G. Wang *et al.*, "Comparison of process configurations for ethanol production from acid- and alkali-pretreated corncob by Saccharomyces cerevisiae strains with and without β-glucosidase expression," *Bioresour. Technol.*, vol. 142, pp. 154–161, 2013, doi: 10.1016/j.biortech.2013.05.033.

[139] K. Liu *et al.*, "High concentration ethanol production from corncob residues by fed-batch strategy," *Bioresour. Technol.*, vol. 101, no. 13, pp. 4952–4958, 2010, doi:

10.1016/j.biortech.2009.11.013.

[140] M. Narra *et al.*, “A bio-refinery concept for production of bio-methane and bio-ethanol from nitric acid pre-treated corncob and recovery of a high value fuel from a waste stream,” *Renew. Energy*, vol. 127, pp. 1–10, Nov. 2018, doi: 10.1016/j.renene.2018.04.044.

[141] P. Sukchum, W. Chulalaksananukul, and O. Chavalparit, “Effect of thermo-chemical pretreatment on bioethanol production from corncobs,” *Adv. Mater. Res.*, vol. 347–353, pp. 2532–2535, 2012, doi: 10.4028/www.scientific.net/AMR.347-353.2532.

[142] M. Yang, M. Lan, X. Gao, Y. Dou, and X. Zhang, “Sequential dilute acid/alkali pretreatment of corncobs for ethanol production,” *Energy Sources, Part A Recover. Util. Environ. Eff.*, vol. 43, no. 14, pp. 1769–1778, 2021, doi: 10.1080/15567036.2019.1648596.

[143] Y. Wang, L. Zhou, and Y. Sun, “Fuel ethanol production from corncob using dilute acid pretreatment and separated saccharification and fermentation by fed-batch strategy,” *ICMREE 2013 - Proc. 2013 Int. Conf. Mater. Renew. Energy Environ.*, vol. 1, pp. 232–235, 2013, doi: 10.1109/ICMREE.2013.6893655.

[144] M. Yang, M. Lan, X. Gao, Y. Dou, and X. Zhang, “Sequential dilute acid/alkali pretreatment of corncobs for ethanol production,” *Energy Sources, Part A Recover. Util. Environ. Eff.*, vol. 0, no. 0, pp. 1–10, 2019, doi: 10.1080/15567036.2019.1648596.

[145] H. Hattori and Y. Ono, *Solid Acid Catalysis*. 2015. doi: 10.1201/b15665.

[146] W. Qi *et al.*, “Carbon-Based Solid Acid Pretreatment in Corncob Saccharification: Specific Xylose Production and Efficient Enzymatic Hydrolysis,” *ACS Sustain. Chem. Eng.*, vol. 6, no. 3, pp. 3640–3648, 2018, doi: 10.1021/acssuschemeng.7b03959.

[147] S. Wang, W. Gao, H. Li, L. P. Xiao, R. C. Sun, and G. Song, “Selective fragmentation of biorefinery corncob lignin into p-hydroxycinnamic esters with a supported zinc molybdate catalyst,” *ChemSusChem*, vol. 11, no. 13, pp. 2114–2123, 2018, doi: 10.1002/cssc.201800455.

[148] M.-Q. Zhu *et al.*, “The effects of autohydrolysis pretreatment on the structural characteristics, adsorptive and catalytic properties of the activated carbon prepared from Eucommia ulmoides Oliver based on a biorefinery process,” *Bioresour. Technol.*, vol. 232, pp. 159–167, 2017, doi: https://doi.org/10.1016/j.biortech.2017.02.033.

[149] S. Zhang, J. Lu, M. Li, and Q. Cai, “Efficient production of furfural from corncob by an integrated mineral-organic-lewis acid catalytic process,” *BioResources*, vol. 12, no. 2, pp. 2965–2981, 2017, doi: 10.15376/biores.12.2.2965-2981.

[150] R. W. Thring, E. Chornet, and R. P. Overend, “Recovery of a solvolytic lignin: Effects of spent liquor/acid volume ratio, acid concentration and temperature,” *Biomass*, vol. 23, no.

4, pp. 289–305, 1990, doi: https://doi.org/10.1016/0144-4565(90)90038-L.

[151] A. Zheng *et al.*, “Overcoming biomass recalcitrance for enhancing sugar production from fast pyrolysis of biomass by microwave pretreatment in glycerol,” *Green Chem.*, vol. 17, no. 2, pp. 1167–1175, 2015, doi: 10.1039/c4gc01724b.

[152] L. qun Jiang *et al.*, “Selective saccharification of microwave-assisted glycerol pretreated corncobs via fast pyrolysis and enzymatic hydrolysis,” *Fuel*, vol. 265, no. November 2019, p. 116965, 2020, doi: 10.1016/j.fuel.2019.116965.

[153] J. M. Lopes, M. D. Bermejo, Á. Martín, and M. J. Cocero, “Ionic liquid as reaction media for the production of cellulose-derived polymers from cellulosic biomass,” *ChemEngineering*, vol. 1, no. 2, pp. 1–28, 2017, doi: 10.3390/chemengineering1020010.

[154] S. N. Sun, M. F. Li, T. Q. Yuan, F. Xu, and R. C. Sun, “Effect of ionic liquid/organic solvent pretreatment on the enzymatic hydrolysis of corncob for bioethanol production. Part 1: Structural characterization of the lignins,” *Ind. Crops Prod.*, vol. 43, no. 1, pp. 570–577, 2013, doi: 10.1016/j.indcrop.2012.07.074.

[155] Z. Guo, Q. Zhang, T. You, X. Zhang, F. Xu, and Y. Wu, “Short-time deep eutectic solvent pretreatment for enhanced enzymatic saccharification and lignin valorization,” *Green Chem.*, vol. 21, no. 11, pp. 3099–3108, 2019, doi: 10.1039/c9gc00704k.

[156] A. Procentese *et al.*, “Deep eutectic solvent pretreatment and subsequent saccharification of corncob,” *Bioresour. Technol.*, vol. 192, pp. 31–36, 2015, doi: 10.1016/j.biortech.2015.05.053.

[157] L. Ma *et al.*, “Isolation and structural analysis of hemicellulose from corncobs after a delignification pretreatment,” *Anal. Methods*, vol. 8, no. 41, pp. 7500–7506, 2016, doi: 10.1039/c6ay01863g.

[158] X. Bernata, A. Fortuny, F. Stüber, C. Bengoa, A. Fabregat, and J. Font, “Recovery of iron (III) from aqueous streams by ultrafiltration,” *Desalination*, vol. 221, no. 1, pp. 413–418, 2008, doi: https://doi.org/10.1016/j.desal.2007.01.100.

[159] V. Arantes, J. Jellison, and B. Goodell, “Peculiarities of brown-rot fungi and biochemical Fenton reaction with regard to their potential as a model for bioprocessing biomass,” *Appl. Microbiol. Biotechnol.*, vol. 94, no. 2, pp. 323–338, 2012, doi: 10.1007/s00253-012-3954-y.

[160] R. Sun and J. Ren, “Corncob Biorefinery for Platform Chemicals and Lignin Coproduction: Metal Chlorides as Catalysts,” *ACS Sustain. Chem. Eng.*, vol. 7, pp. 5309–5317, 2019, doi: 10.1021/acssuschemeng.8b06337.

[161] A. Kawee-Ai *et al.*, “Eco-friendly processing in enzymatic xylooligosaccharides production from corncob: Influence of pretreatment with sonocatalytic-synergistic Fenton

reaction and its antioxidant potentials," *Ultrason. Sonochem.*, vol. 31, pp. 184–192, 2016, doi: 10.1016/j.ultsonch.2015.12.018.

[162] H. T. Yu, B. Y. Chen, B. Y. Li, M. C. Tseng, C. C. Han, and S. G. Shyu, "Efficient pretreatment of lignocellulosic biomass with high recovery of solid lignin and fermentable sugars using Fenton reaction in a mixed solvent," *Biotechnol. Biofuels*, vol. 11, no. 1, pp. 1–11, 2018, doi: 10.1186/s13068-018-1288-4.

[163] Y. Sun and J. Cheng, "Hydrolysis of lignocellulosic materials for ethanol production: a review," *Bioresour. Technol.*, vol. 83, no. 1, pp. 1–11, 2002, doi: https://doi.org/10.1016/S0960-8524(01)00212-7.

[164] S. Imman, J. Arnthong, V. Burapatana, N. Laosiripojana, and V. Champreda, "Autohydrolysis of Tropical Agricultural Residues by Compressed Liquid Hot Water Pretreatment," *Appl. Biochem. Biotechnol.*, vol. 170, no. 8, pp. 1982–1995, 2013, doi: 10.1007/s12010-013-0320-1.

[165] Q. Yu *et al.*, "Structural characteristics of corncob and eucalyptus contributed to sugar release during hydrothermal pretreatment and enzymatic hydrolysis," *Cellulose*, vol. 24, no. 11, pp. 4899–4909, 2017, doi: 10.1007/s10570-017-1485-5.

[166] X. Li *et al.*, "Enhancing the production of renewable petrochemicals by co-feeding of biomass with plastics in catalytic fast pyrolysis with ZSM-5 zeolites," *Appl. Catal. A Gen.*, vol. 481, pp. 173–182, 2014, doi: https://doi.org/10.1016/j.apcata.2014.05.015.

[167] M. Michelin, H. A. Ruiz, M. de L. T. M. Polizeli, and J. A. Teixeira, "Multi-step approach to add value to corncob: Production of biomass-degrading enzymes, lignin and fermentable sugars," *Bioresour. Technol.*, vol. 247, no. July 2017, pp. 582–590, 2018, doi: 10.1016/j.biortech.2017.09.128.

[168] C. Teng, Q. Yan, Z. Jiang, G. Fan, and B. Shi, "Production of xylooligosaccharides from the steam explosion liquor of corncobs coupled with enzymatic hydrolysis using a thermostable xylanase," *Bioresour. Technol.*, vol. 101, no. 19, pp. 7679–7682, 2010, doi: 10.1016/j.biortech.2010.05.004.

[169] H. Li, X. Chen, J. Ren, H. Deng, F. Peng, and R. Sun, "Functional relationship of furfural yields and the hemicellulose-derived sugars in the hydrolysates from corncob by microwave-assisted hydrothermal pretreatment," *Biotechnol. Biofuels*, vol. 8, no. 1, pp. 1–12, 2015, doi: 10.1186/s13068-015-0314-z.

[170] A. Deng, J. Ren, H. Li, F. Peng, and R. Sun, "Corncob lignocellulose for the production of furfural by hydrothermal pretreatment and heterogeneous catalytic process," *RSC Adv.*, vol. 5, no. 74, pp. 60264–60272, 2015, doi: 10.1039/c5ra10472f.

[171] P. Alvira, E. Tomás-Pejó, M. Ballesteros, and M. J. Negro, "Pretreatment technologies for

an efficient bioethanol production process based on enzymatic hydrolysis: A review," *Bioresour. Technol.*, vol. 101, no. 13, pp. 4851–4861, 2010, doi: https://doi.org/10.1016/j.biortech.2009.11.093.

[172] N. Mosier *et al.*, "Features of promising technologies for pretreatment of lignocellulosic biomass," *Bioresour. Technol.*, vol. 96, no. 6, pp. 673–686, 2005, doi: https://doi.org/10.1016/j.biortech.2004.06.025.

[173] K. Merklein, S. S. Fong, and Y. Deng, *Biomass Utilization*. Elsevier B.V., 2016. doi: 10.1016/B978-0-444-63475-7.00011-X.

[174] T. H. Kim, F. Taylor, and K. B. Hicks, "Bioethanol production from barley hull using SAA (soaking in aqueous ammonia) pretreatment.," *Bioresour. Technol.*, vol. 99, no. 13, pp. 5694–5702, Sep. 2008, doi: 10.1016/j.biortech.2007.10.055.

[175] T. H. Kim and Y. Y. Lee, "Pretreatment and fractionation of corn stover by ammonia recycle percolation process," *Bioresour. Technol.*, vol. 96, no. 18, pp. 2007–2013, 2005, doi: https://doi.org/10.1016/j.biortech.2005.01.015.

[176] E. (Newton) Sendich *et al.*, "Recent process improvements for the ammonia fiber expansion (AFEX) process and resulting reductions in minimum ethanol selling price," *Bioresour. Technol.*, vol. 99, no. 17, pp. 8429–8435, 2008, doi: https://doi.org/10.1016/j.biortech.2008.02.059.

[177] W.-H. Chen, J. Peng, and X. T. Bi, "A state-of-the-art review of biomass torrefaction, densification and applications," *Renew. Sustain. Energy Rev.*, vol. 44, pp. 847–866, 2015, doi: https://doi.org/10.1016/j.rser.2014.12.039.

[178] P. Kumar, D. M. Barrett, M. J. Delwiche, and P. Stroeve, "Methods for pretreatment of lignocellulosic biomass for efficient hydrolysis and biofuel production," *Ind. Eng. Chem. Res.*, vol. 48, no. 8, pp. 3713–3729, 2009, doi: 10.1021/ie801542g.

[179] X. Tian *et al.*, "Influence of torrefaction pretreatment on corncobs: A study on fundamental characteristics, thermal behavior, and kinetic," *Bioresour. Technol.*, vol. 297, p. 122490, 2020, doi: 10.1016/j.biortech.2019.122490.

[180] Z. M. A. Bundhoo, "Effects of microwave and ultrasound irradiations on dark fermentative bio-hydrogen production from food and yard wastes," *Int. J. Hydrogen Energy*, vol. 42, no. 7, pp. 4040–4050, 2017, doi: https://doi.org/10.1016/j.ijhydene.2016.10.149.

[181] M. M. de S. Moretti *et al.*, "Pretreatment of sugarcane bagasse with microwaves irradiation and its effects on the structure and on enzymatic hydrolysis," *Appl. Energy*, vol. 122, pp. 189–195, 2014, doi: https://doi.org/10.1016/j.apenergy.2014.02.020.

[182] J. Luo, Z. Fang, and R. L. Smith, "Ultrasound-enhanced conversion of biomass to biofuels," *Prog. Energy Combust. Sci.*, vol. 41, pp. 56–93, 2014, doi:

https://doi.org/10.1016/j.pecs.2013.11.001.

[183] G. Ramadoss and K. Muthukumar, “Mechanistic study on ultrasound assisted pretreatment of sugarcane bagasse using metal salt with hydrogen peroxide for bioethanol production,” *Ultrason. Sonochem.*, vol. 28, pp. 207–217, 2016, doi: https://doi.org/10.1016/j.ultsonch.2015.07.006.

[184] M. Imai, K. Ikari, and I. Suzuki, “High-performance hydrolysis of cellulose using mixed cellulase species and ultrasonication pretreatment,” *Biochem. Eng. J.*, vol. 17, no. 2, pp. 79–83, 2004, doi: https://doi.org/10.1016/S1369-703X(03)00141-4.

[185] V. M. B. Balasubramaniam, S. I. Martínez-Monteagudo, and R. Gupta, “Principles and application of high pressure-based technologies in the food industry.,” *Annu. Rev. Food Sci. Technol.*, vol. 6, pp. 435–462, 2015, doi: 10.1146/annurev-food-022814-015539.

[186] A. R. F. C. Ferreira, A. B. Figueiredo, D. V Evtuguin, and J. A. Saraiva, “High pressure pre-treatments promote higher rate and degree of enzymatic hydrolysis of cellulose,” *Green Chem.*, vol. 13, no. 10, pp. 2764–2767, 2011, doi: 10.1039/C1GC15500H.

[187] S. C. T. Oliveira, A. B. Figueiredo, D. V Evtuguin, and J. A. Saraiva, “High pressure treatment as a tool for engineering of enzymatic reactions in cellulosic fibres,” *Bioresour. Technol.*, vol. 107, pp. 530–534, 2012, doi: https://doi.org/10.1016/j.biortech.2011.12.093.

[188] S. Du, X. Zhu, H. Wang, D. Zhou, W. Yang, and H. Xu, “High pressure assist-alkali pretreatment of cotton stalk and physiochemical characterization of biomass,” *Bioresour. Technol.*, vol. 148, pp. 494–500, 2013, doi: https://doi.org/10.1016/j.biortech.2013.09.020.

[189] J. F. Castañón-Rodríguez *et al.*, “Influence of high pressure processing and alkaline treatment on sugarcane bagasse hydrolysis,” *CyTA - J. Food*, vol. 13, no. 4, pp. 613–620, Oct. 2015, doi: 10.1080/19476337.2015.1029523.

[190] Wang Yuxin, 刘炳泗 B., 时志强 Z., and 刘凤丹 F., “Application of corncob-Based activated carbon as electrode material for electric double-Layer capacitors,” *Trans. Tianjin Univ.*, vol. 18, Jun. 2012, doi: 10.1007/s12209-012-1799-1.

[191] Y. R. Huang, Q. Q. Liu, Y. Z. Fan, and H. Z. Li, “A comparative study on the use of palm bark as a supplementary carbon source in partially saturated vertical constructed wetland: Organic matter characterization, release-adsorption kinetics, and pilot-scale performance,” *Chemosphere*, vol. 253, p. 126663, 2020, doi: 10.1016/j.chemosphere.2020.126663.

[192] S. Hyun Hong *et al.*, “Improved enzymatic hydrolysis of wheat straw by combined use of gamma ray and dilute acid for bioethanol production,” *Radiat. Phys. Chem.*, vol. 94, pp. 231–235, 2014, doi: https://doi.org/10.1016/j.radphyschem.2013.05.056.

[193] A. B. Diaz *et al.*, “Evaluation of microwave-assisted pretreatment of lignocellulosic

biomass immersed in alkaline glycerol for fermentable sugars production.," *Bioresour. Technol.*, vol. 185, pp. 316–323, Jun. 2015, doi: 10.1016/j.biortech.2015.02.112.

[194] J. Gao, L. Chen, J. Zhang, and Z. Yan, "Improved enzymatic hydrolysis of lignocellulosic biomass through pretreatment with plasma electrolysis," *Bioresour. Technol.*, vol. 171, p. 469—471, Nov. 2014, doi: 10.1016/j.biortech.2014.07.118.

[195] M. T. García-Cubero, L. G. Palacín, G. González-Benito, S. Bolado, S. Lucas, and M. Coca, "An analysis of lignin removal in a fixed bed reactor by reaction of cereal straws with ozone," *Bioresour. Technol.*, vol. 107, pp. 229–234, 2012, doi: https://doi.org/10.1016/j.biortech.2011.12.010.

[196] S. Zanini *et al.*, "Radical formation on CTMP fibers by argon plasma treatments and related lignin chemical changes," *BioResources*, vol. 3, Nov. 2008.

[197] C. Song, Z. Zhang, W. Chen, and C. Liu, "Converting Cornstalk Into Simple Sugars With High-Pressure Nonequilibrium Plasma," *IEEE Trans. Plasma Sci.*, vol. 37, no. 9, pp. 1817–1824, 2009, doi: 10.1109/TPS.2009.2025950.

[198] J. A. Souza-Corrêa *et al.*, "Atmospheric Pressure Plasma Pretreatment of Sugarcane Bagasse: the Influence of Biomass Particle Size in the Ozonation Process," *Appl. Biochem. Biotechnol.*, vol. 172, no. 3, pp. 1663–1672, 2014, doi: 10.1007/s12010-013-0609-0.

[199] M. Benoit *et al.*, "Depolymerization of Cellulose Assisted by a Nonthermal Atmospheric Plasma," *Angew. Chemie Int. Ed.*, vol. 50, no. 38, pp. 8964–8967, Sep. 2011, doi: https://doi.org/10.1002/anie.201104123.

[200] J. A. Souza-Corrêa, M. A. Ridenti, C. Oliveira, S. R. Araújo, and J. Amorim, "Decomposition of Lignin from Sugar Cane Bagasse during Ozonation Process Monitored by Optical and Mass Spectrometries," *J. Phys. Chem. B*, vol. 117, no. 11, pp. 3110–3119, Mar. 2013, doi: 10.1021/jp3121879.

[201] M. Liu *et al.*, "Cleavage of Covalent Bonds in the Pyrolysis of Lignin, Cellulose, and Hemicellulose," *Energy & Fuels*, vol. 29, no. 9, pp. 5773–5780, Sep. 2015, doi: 10.1021/acs.energyfuels.5b00983.

[202] J.-M. Hardy, O. Levasseur, M. Vlad, L. Stafford, and B. Riedl, "Surface free radicals detection using molecular scavenging method on black spruce wood treated with cold, atmospheric-pressure plasmas," *Appl. Surf. Sci.*, vol. 359, pp. 137–142, 2015, doi: https://doi.org/10.1016/j.apsusc.2015.10.062.

[203] Y. Cao *et al.*, "Atmospheric Low-Temperature Plasma-Induced Changes in the Structure of the Lignin Macromolecule: An Experimental and Theoretical Investigation," *J. Agric. Food Chem.*, vol. 68, no. 2, pp. 451–460, 2020, doi: 10.1021/acs.jafc.9b05604.

[204] C. Dumas, G. Silva Ghizzi Damasceno, A. Barakat, H. Carrère, J.-P. Steyer, and X. Rouau,

"Effects of grinding processes on anaerobic digestion of wheat straw," *Ind. Crops Prod.*, vol. 74, pp. 450–456, 2015, doi: https://doi.org/10.1016/j.indcrop.2015.03.043.

[205] A. Singh and D. Rathore, *Biohydrogen production: Sustainability of current technology and future perspective*. 2016. doi: 10.1007/978-81-322-3577-4.

[206] H. Xu *et al.*, "Quantitative characterization of the impact of pulp refining on enzymatic saccharification of the alkaline pretreated corn stover," *Bioresour. Technol.*, vol. 169C, pp. 19–26, Jun. 2014, doi: 10.1016/j.biortech.2014.06.068.

[207] Z. Zhang, N. Tahir, Y. Li, T. Zhang, S. Zhu, and Q. Zhang, "Tailoring of structural and optical parameters of corncobs through ball milling pretreatment," *Renew. Energy*, vol. 141, pp. 298–304, 2019, doi: 10.1016/j.renene.2019.03.152.

[208] J. Zhang *et al.*, "Efficient Acetone-Butanol-Ethanol Production from Corncob with a New Pretreatment Technology-Wet Disk Milling," *Bioenergy Res.*, vol. 6, no. 1, pp. 35–43, 2013, doi: 10.1007/s12155-012-9226-y.

[209] W. Liu *et al.*, "Comparative study on different pretreatment on enzymatic hydrolysis of corncob residues," *Bioresour. Technol.*, vol. 295, p. 122244, 2020, doi: 10.1016/j.biortech.2019.122244.

[210] G. Ji, C. Gao, W. Xiao, and L. Han, "Mechanical fragmentation of corncob at different plant scales: Impact and mechanism on microstructure features and enzymatic hydrolysis," *Bioresour. Technol.*, vol. 205, pp. 159–165, 2016, doi: 10.1016/j.biortech.2016.01.029.

[211] A. Barakat, C. Mayer-Laigle, A. Solhy, R. A. D. Arancon, H. De Vries, and R. Luque, "Mechanical pretreatments of lignocellulosic biomass: Towards facile and environmentally sound technologies for biofuels production," *RSC Adv.*, vol. 4, no. 89, pp. 48109–48127, 2014, doi: 10.1039/c4ra07568d.

[212] J. Zheng, K. Choo, C. Bradt, R. Lehoux, and L. Rehmann, "Enzymatic hydrolysis of steam exploded corncob residues after pretreatment in a twin-screw extruder," *Biotechnol. Reports*, vol. 3, pp. 99–107, 2014, doi: 10.1016/j.btre.2014.06.008.

[213] J. Zheng, K. Choo, and L. Rehmann, "The effects of screw elements on enzymatic digestibility of corncobs after pretreatment in a twin-screw extruder," *Biomass and Bioenergy*, vol. 74, pp. 224–232, 2015, doi: 10.1016/j.biombioe.2015.01.022.

[214] H. T. Song *et al.*, "Synergistic effect of cellulase and xylanase during hydrolysis of natural lignocellulosic substrates," *Bioresour. Technol.*, vol. 219, pp. 710–715, 2016, doi: 10.1016/j.biortech.2016.08.035.

[215] T. You, X. Li, R. Wang, X. Zhang, and F. Xu, "Effects of synergistic fungal pretreatment on structure and thermal properties of lignin from corncob," *Bioresour. Technol.*, vol. 272, pp. 123–129, 2019, doi: 10.1016/j.biortech.2018.09.145.

[216] T. You, X. Li, R. Wang, X. Zhang, and F. Xu, “Effects of synergistic fungal pretreatment on structure and thermal properties of lignin from corncob,” *Bioresour. Technol.*, vol. 272, no. August 2018, pp. 123–129, 2019, doi: 10.1016/j.biortech.2018.09.145.

[217] V. Kumar, S. K. Yadav, J. Kumar, and V. Ahluwalia, “A critical review on current strategies and trends employed for removal of inhibitors and toxic materials generated during biomass pretreatment,” *Bioresour. Technol.*, vol. 299, no. December 2019, p. 122633, 2020, doi: 10.1016/j.biortech.2019.122633.

[218] T. A. Clark and K. L. Mackie, “Fermentation Inhibitors in Wood Hydrolysates Derived From the Softwood Pinus Radiata.,” *J. Chem. Technol. Biotechnol. Biotechnol.*, vol. 34 B, no. 2, pp. 101–110, 1984, doi: 10.1002/jctb.280340206.

[219] S. R. Parekh, S. Yu, and M. Wayman, “Adaptation of Candida shehatae and Pichia stipitis to wood hydrolysates for increased ethanol production,” *Appl. Microbiol. Biotechnol.*, vol. 25, no. 3, pp. 300–304, 1986, doi: 10.1007/BF00253667.

[220] D.-J. Seo, H. Fujita, and A. Sakoda, “Effects of a non-ionic surfactant, Tween 20, on adsorption/desorption of saccharification enzymes onto/from lignocelluloses and saccharification rate,” *Adsorption*, vol. 17, no. 5, pp. 813–822, 2011, doi: 10.1007/s10450-011-9340-8.

[221] Q. Qing, B. Yang, and C. E. Wyman, “Impact of surfactants on pretreatment of corn stover,” *Bioresour. Technol.*, vol. 101, no. 15, pp. 5941–5951, 2010, doi: https://doi.org/10.1016/j.biortech.2010.03.003.

[222] A. Eckard, K. Muthukumarappan, and W. Gibbons, “A Review of the Role of Amphiphiles in Biomass to Ethanol Conversion,” *Appl. Sci.*, vol. 3, no. 2, pp. 396–419, 2013, doi: 10.3390/app3020396.

[223] E. K. Kleingesinds, Á. H. M. José, L. P. Brumano, T. Silva-Fernandes, D. Rodrigues, and R. C. L. B. Rodrigues, “Intensification of bioethanol production by using Tween 80 to enhance dilute acid pretreatment and enzymatic saccharification of corncob,” *Ind. Crops Prod.*, vol. 124, no. April, pp. 166–176, 2018, doi: 10.1016/j.indcrop.2018.07.037.

[224] T. Zheng, F. Lei, P. Li, S. Liu, and J. Jiang, “Stimulatory effects of rhamnolipid on corncob residues ethanol production via high-solids simultaneous saccharification and fermentation,” *Fuel*, vol. 257, no. August, p. 116091, 2019, doi: 10.1016/j.fuel.2019.116091.

[225] H. Lou *et al.*, “Enhancement and Mechanism of a Lignin Amphoteric Surfactant on the Production of Cellulosic Ethanol from a High-Solid Corncob Residue,” *J. Agric. Food Chem.*, vol. 67, no. 22, pp. 6248–6256, 2019, doi: 10.1021/acs.jafc.9b01208.

[226] J. W. Lee, J. Y. Zhu, D. Scordia, and T. W. Jeffries, “Evaluation of ethanol production

from corncob using scheffersomyces (Pichia) stipitis CBS 6054 by volumetric scale-up," *Appl. Biochem. Biotechnol.*, vol. 165, no. 3–4, pp. 814–822, 2011, doi: 10.1007/s12010-011-9299-7.

[227] N. Eken-Saraçoğlu and Y. Arslan, "Comparison of different pretreatments in ethanol fermentation using corn cob hemicellulosic hydrolysate with Pichia stipitis and Candida shehatae," *Biotechnol. Lett.*, vol. 22, no. 10, pp. 855–858, 2000, doi: 10.1023/A:1005663313597.

[228] K. ichi Hatano, N. Aoyagi, T. Miyakawa, M. Tanokura, and K. Kubota, "Evaluation of nonionic adsorbent resins for removal of inhibitory compounds from corncob hydrolysate for ethanol fermentation," *Bioresour. Technol.*, vol. 149, pp. 541–545, 2013, doi: 10.1016/j.biortech.2013.08.166.

[229] R. Gupta, G. Mehta, and R. Chander Kuhad, "Fermentation of pentose and hexose sugars from corncob, a low cost feedstock into ethanol," *Biomass and Bioenergy*, vol. 47, pp. 334–341, 2012, doi: 10.1016/j.biombioe.2012.09.027.

[230] S. Liu, H. Liu, C. Shen, W. Fang, Y. Xiao, and Z. Fang, "Comparison of performances of different fungal laccases in delignification and detoxification of alkali-pretreated corncob for bioethanol production," *J. Ind. Microbiol. Biotechnol.*, vol. 48, no. 1–2, 2021, doi: 10.1093/jimb/kuab013.

[231] H. Gu, J. Zhang, and J. Bao, "Inhibitor analysis and adaptive evolution of Saccharomyces cerevisiae for simultaneous saccharification and ethanol fermentation from industrial waste corncob residues," *Bioresour. Technol.*, vol. 157, pp. 6–13, 2014, doi: 10.1016/j.biortech.2014.01.060.

[232] H. Gu, J. Zhang, and J. Bao, "High tolerance and physiological mechanism of Zymomonas mobilis to phenolic inhibitors in ethanol fermentation of corncob residue," *Biotechnol. Bioeng.*, vol. 112, no. 9, pp. 1770–1782, 2015, doi: 10.1002/bit.25603.

[233] L. Pedraza *et al.*, "Sequential Thermochemical Hydrolysis of Corncobs and Enzymatic Saccharification of the Whole Slurry Followed by Fermentation of Solubilized Sugars to Ethanol with the Ethanologenic Strain Escherichia coli MS04," *Bioenergy Res.*, vol. 9, no. 4, pp. 1046–1052, 2016, doi: 10.1007/s12155-016-9756-9.

[234] Q. Lan *et al.*, "Coordinately express hemicellulolytic enzymes in Kluyveromyces marxianus to improve the saccharification and ethanol production from corncobs," *Biotechnol. Biofuels*, vol. 14, no. 1, pp. 1–14, 2021, doi: 10.1186/s13068-021-02070-1.

[235] K. Valta, C. Papadaskalopoulou, M. Dimarogona, and E. Topakas, "Bioethanol from waste - Prospects and challenges of current and emerging technologies," *Byprod. from Agric. Fish. Adding Value Food, Feed. Pharma Fuels*, pp. 421–456, 2019, doi: 10.1002/9781119383956.ch18.

[236] G. Wang *et al.*, "Comparison of process configurations for ethanol production from acid- and alkali-pretreated corncob by Saccharomyces cerevisiae strains with and without β-glucosidase expression," *Bioresour. Technol.*, vol. 142, pp. 154–161, 2013, doi: 10.1016/j.biortech.2013.05.033.

[237] C. Feng *et al.*, "Ethanol production from acid- and alkali-pretreated corncob by endoglucanase and β-glucosidase co-expressing Saccharomyces cerevisiae subject to the expression of heterologous genes and nutrition added," *World Journal of Microbiology and Biotechnology*, vol. 32, no. 5. 2016. doi: 10.1007/s11274-016-2043-2.

[238] S. Imman, N. Laosiripojana, and V. Champreda, "Effects of Liquid Hot Water Pretreatment on Enzymatic Hydrolysis and Physicochemical Changes of Corncobs," *Appl. Biochem. Biotechnol.*, pp. 1–12, 2017, doi: 10.1007/s12010-017-2541-1.

[239] M. Michelin and J. A. Teixeira, "Liquid hot water pretreatment of multi feedstocks and enzymatic hydrolysis of solids obtained thereof," *Bioresour. Technol.*, vol. 216, pp. 862–869, 2016, doi: 10.1016/j.biortech.2016.06.018.

[240] Y. Hu, B. Wang, W. Liu, R. Wu, and Q. Hou, "Effects of mechanical pretreatments on enzymatic hydrolysis of mixed lignocellulosic substrates for biorefineries," *BioResources*, vol. 14, no. 2, pp. 4639–4652, 2019, doi: 10.15376/biores.14.2.4639-4652.

[241] P. Pocan, E. Bahcegul, M. H. Oztop, and H. Hamamci, "Enzymatic Hydrolysis of Fruit Peels and Other Lignocellulosic Biomass as a Source of Sugar," *Waste and Biomass Valorization*, vol. 9, no. 6, pp. 929–937, 2018, doi: 10.1007/s12649-017-9875-3.

[242] G. S. Wang, J. W. Lee, J. Y. Zhu, and T. W. Jeffries, "Dilute acid pretreatment of corncob for efficient sugar production," *Appl. Biochem. Biotechnol.*, vol. 163, no. 5, pp. 658–668, 2011, doi: 10.1007/s12010-010-9071-4.

[243] Q. Xu *et al.*, "Enhanced Enzymatic Hydrolysis of Corncob by Synthesized Enzyme-Mimetic Magnetic Solid Acid Pretreatment in an Aqueous Phase," *ACS Omega*, vol. 4, no. 18, pp. 17864–17873, 2019, doi: 10.1021/acsomega.9b02699.

[244] J. Zhang, C. Lei, G. Liu, Y. Bao, V. Balan, and J. Bao, "In-Situ Vacuum Distillation of Ethanol Helps to Recycle Cellulase and Yeast during SSF of Delignified Corncob Residues," *ACS Sustain. Chem. Eng.*, vol. 5, no. 12, pp. 11676–11685, 2017, doi: 10.1021/acssuschemeng.7b03084.

[245] P. Sahare, R. Singh, R. S. Laxman, and M. Rao, "Effect of Alkali Pretreatment on the Structural Properties and Enzymatic Hydrolysis of Corn Cob," *Appl. Biochem. Biotechnol.*, vol. 168, no. 7, pp. 1806–1819, 2012, doi: 10.1007/s12010-012-9898-y.

[246] DuPont, "Accellerase® 1500," *DuPont Genencor Sci.*, pp. 1–4, 2013, [Online]. Available: http://accellerase.dupont.com/fileadmin/user_upload/live/accellerase/documents/DUP-

00413_ProdSheet_1500_web.pdf

[247] A. Patel and A. R. Shah, “Integrated lignocellulosic biorefinery: Gateway for production of second generation ethanol and value added products,” *J. Bioresour. Bioprod.*, vol. 6, no. 2, pp. 108–128, 2021, doi: 10.1016/j.jobab.2021.02.001.

[248] F. Liu, Z. Wang, R. R. Manglekar, and A. Geng, “Enhanced cellulase production through random mutagenesis of Talaromyces pinophilus OPC4-1 and fermentation optimization,” *Process Biochem.*, vol. 90, no. July, pp. 12–22, 2020, doi: 10.1016/j.procbio.2019.11.025.

[249] D. Cai *et al.*, “Biorefinery of corn cob for microbial lipid and bio-ethanol production: An environmental friendly process,” *Bioresour. Technol.*, vol. 211, pp. 677–684, 2016, doi: 10.1016/j.biortech.2016.03.159.

[250] H. Yu *et al.*, “Efficient utilization of hemicellulose and cellulose in alkali liquor-pretreated corncob for bioethanol production at high solid loading by Spathaspora passalidarum U1-58,” *Bioresour. Technol.*, vol. 232, pp. 168–175, 2017, doi: 10.1016/j.biortech.2017.01.077.

[251] M. Zhang, P. Shukla, M. Ayyachamy, K. Permaul, and S. Singh, “Improved bioethanol production through simultaneous saccharification and fermentation of lignocellulosic agricultural wastes by Kluyveromyces marxianus 6556,” *World J. Microbiol. Biotechnol.*, vol. 26, no. 6, pp. 1041–1046, 2010, doi: 10.1007/s11274-009-0267-0.

[252] B. Sunkar and B. Bhukya, “Bi-phasic hydrolysis of corncobs for the extraction of total sugars and ethanol production using inhibitor resistant and thermotolerant yeast, Pichia kudriavzevii,” *Biomass and Bioenergy*, vol. 153, no. August, p. 106230, 2021, doi: 10.1016/j.biombioe.2021.106230.

[253] C. Lei, J. Zhang, L. Xiao, and J. Bao, “An alternative feedstock of corn meal for industrial fuel ethanol production: Delignified corncob residue,” *Bioresour. Technol.*, vol. 167, pp. 555–559, 2014, doi: 10.1016/j.biortech.2014.06.005.

[254] J. W. Lee, J. Y. Zhu, D. Scordia, and T. W. Jeffries, “Evaluation of ethanol production from corncob using scheffersomyces (Pichia) stipitis CBS 6054 by volumetric scale-up,” *Appl. Biochem. Biotechnol.*, vol. 165, no. 3–4, pp. 814–822, Oct. 2011, doi: 10.1007/s12010-011-9299-7.

[255] D. Camargo, S. D. Gomes, and L. Sene, “Ethanol production from sunflower meal biomass by simultaneous saccharification and fermentation (SSF) with Kluyveromyces marxianus ATCC 36907,” *Bioprocess Biosyst. Eng.*, vol. 37, no. 11, pp. 2235–2242, 2014, doi: 10.1007/s00449-014-1201-x.

[256] N. P. P. Pabbathi, A. Velidandi, P. K. Gandam, P. Koringa, S. R. Parcha, and R. R. Baadhe, “Novel buffalo rumen metagenome derived acidic cellulase Cel-3.1 cloning,

characterization, and its application in saccharifying rice straw and corncob biomass," *Int. J. Biol. Macromol.*, vol. 170, p. 239, 2021, doi: 10.1016/j.ijbiomac.2020.12.041.

[257] M. Chen, L. Xia, and P. Xue, "Enzymatic hydrolysis of corncob and ethanol production from cellulosic hydrolysate," *Int. Biodeterior. Biodegrad.*, vol. 59, no. 2, pp. 85–89, 2007, doi: 10.1016/j.ibiod.2006.07.011.

[258] F. Latif and M. I. Rajoka, "Production of ethanol and xylitol from corn cobs by yeasts," *Bioresour. Technol.*, vol. 77, no. 1, pp. 57–63, 2001, doi: 10.1016/S0960-8524(00)00134-6.

[259] Z. Lewis Liu, S. A. Weber, M. A. Cotta, and S. Z. Li, "A new β-glucosidase producing yeast for lower-cost cellulosic ethanol production from xylose-extracted corncob residues by simultaneous saccharification and fermentation," *Bioresour. Technol.*, vol. 104, pp. 410–416, 2012, doi: 10.1016/j.biortech.2011.10.099.

[260] L. Liu *et al.*, "Engineered Polyploid Yeast Strains Enable Efficient Xylose Utilization and Ethanol Production in Corn Hydrolysates," *Front. Bioeng. Biotechnol.*, vol. 9, no. March, pp. 1–11, 2021, doi: 10.3389/fbioe.2021.655272.

[261] P. Boonchuay *et al.*, "An integrated process for xylooligosaccharide and bioethanol production from corncob," *Bioresour. Technol.*, vol. 256, pp. 399–407, May 2018, doi: 10.1016/j.biortech.2018.02.004.

[262] K. K. Cheng, J. Wu, Z. N. Lin, and J. A. Zhang, "Aerobic and sequential anaerobic fermentation to produce xylitol and ethanol using non-detoxified acid pretreated corncob," *Biotechnol. Biofuels*, vol. 7, no. 1, pp. 1–9, 2014, doi: 10.1186/s13068-014-0166-y.

[263] K. G. De Carvalho Lima, C. M. Takahashi, and F. Alterthum, "Ethanol production from corn cob hydrolysates by Escherichia coli KO11," *J. Ind. Microbiol. Biotechnol.*, vol. 29, no. 3, pp. 124–128, 2002, doi: 10.1038/sj.jim.7000287.

[264] C. Fan, K. Qi, X. X. Xia, and J. J. Zhong, "Efficient ethanol production from corncob residues by repeated fermentation of an adapted yeast," *Bioresour. Technol.*, vol. 136, pp. 309–315, 2013, doi: 10.1016/j.biortech.2013.03.028.

[265] B. Sunkar and B. Bhukya, "Bi-phasic hydrolysis of corncobs for the extraction of total sugars and ethanol production using inhibitor resistant and thermotolerant yeast, Pichia kudriavzevii," *Biomass and Bioenergy*, vol. 153, no. April, 2021, doi: 10.1016/j.biombioe.2021.106230.

[266] H. Ji, K. Xu, X. Dong, D. Sun, and L. Jin, "Sequential production of D-xylonate and ethanol from non-detoxified corncob at low-ph by Pichia Kudriavzevii via a two-stage fermentation strategy," *J. Fungi*, vol. 7, no. 12, 2021, doi: 10.3390/jof7121038.

[267] Y. H. Chang, K. S. Chang, C. W. Huang, C. L. Hsu, and H. Der Jang, "Comparison of

batch and fed-batch fermentations using corncob hydrolysate for bioethanol production," *Fuel*, vol. 97, pp. 166–173, 2012, doi: 10.1016/j.fuel.2012.02.006.

[268] J. T. Cunha *et al.*, "Cell surface engineering of Saccharomyces cerevisiae for simultaneous valorization of corn cob and cheese whey via ethanol production," *Energy Convers. Manag.*, vol. 243, no. March, Sep. 2021, doi: 10.1016/j.enconman.2021.114359.

[269] P. Kahar, K. Taku, and S. Tanaka, "Enzymatic digestion of corncobs pretreated with low strength of sulfuric acid for bioethanol production," *J. Biosci. Bioeng.*, vol. 110, no. 4, pp. 453–458, 2010, doi: 10.1016/j.jbiosc.2010.05.002.

[270] P. Boonchuay *et al.*, "Bioethanol production from cellulose-rich corncob residue by the thermotolerant saccharomyces cerevisiae TC-5," *J. Fungi*, vol. 7, no. 7, 2021, doi: 10.3390/jof7070547.

[271] H. Yu *et al.*, "Efficient utilization of hemicellulose and cellulose in alkali liquor-pretreated corncob for bioethanol production at high solid loading by Spathaspora passalidarum U1-58," *Bioresour. Technol.*, vol. 232, pp. 168–175, 2017, doi: 10.1016/j.biortech.2017.01.077.

[272] R. Su *et al.*, "Ethanol Production from High-Solid SSCF of Alkaline-Pretreated Corncob Using Recombinant Zymomonas mobilis CP4," *Bioenergy Res.*, vol. 6, no. 1, pp. 292–299, 2013, doi: 10.1007/s12155-012-9256-5.

[273] J.-W. Lee, R. C. L. B. Rodrigues, and T. W. Jeffries, "Simultaneous saccharification and ethanol fermentation of oxalic acid pretreated corncob assessed with response surface methodology," *Bioresour. Technol.*, vol. 100, no. 24, pp. 6307–6311, 2009, doi: https://doi.org/10.1016/j.biortech.2009.06.088.

[274] Y. H. Chang, K. S. Chang, C. W. Huang, C. L. Hsu, and H. Der Jang, "Comparison of batch and fed-batch fermentations using corncob hydrolysate for bioethanol production," *Fuel*, vol. 97, pp. 166–173, Jul. 2012, doi: 10.1016/j.fuel.2012.02.006.

[275] J. W. Lee, R. C. L. B. Rodrigues, H. J. Kim, I. G. Choi, and T. W. Jeffries, "The roles of xylan and lignin in oxalic acid pretreated corncob during separate enzymatic hydrolysis and ethanol fermentation," *Bioresour. Technol.*, vol. 101, no. 12, pp. 4379–4385, Jun. 2010, doi: 10.1016/j.biortech.2009.12.112.

[276] J. T. Cunha *et al.*, "Consolidated bioprocessing of corn cob-derived hemicellulose: Engineered industrial Saccharomyces cerevisiae as efficient whole cell biocatalysts," *Biotechnol. Biofuels*, vol. 13, no. 1, pp. 1–15, 2020, doi: 10.1186/s13068-020-01780-2.

[277] H. Song *et al.*, "Genetically modified Saccharomyces cerevisiae for one-step fermentation of bioalcohol using corncob as sole carbon source," *Ann. Microbiol.*, vol. 64, no. 2, pp. 781–785, 2014, doi: 10.1007/s13213-013-0714-x.

[278] B. G. Schuster and M. S. Chinn, “Consolidated Bioprocessing of Lignocellulosic Feedstocks for Ethanol Fuel Production,” *Bioenergy Res.*, vol. 6, no. 2, pp. 416–435, 2013, doi: 10.1007/s12155-012-9278-z.

[279] Y. Tang, D. Zhao, C. Cristhian, and J. Jiang, “Simultaneous saccharification and cofermentation of lignocellulosic residues from commercial furfural production and corn kernels using different nutrient media,” *Biotechnol. Biofuels*, vol. 4, p. 22, Jul. 2011, doi: 10.1186/1754-6834-4-22.

[280] T. Zheng, H. Yu, S. Liu, J. Jiang, and K. Wang, “Achieving high ethanol yield by co-feeding corncob residues and tea-seed cake at high-solids simultaneous saccharification and fermentation,” *Renew. Energy*, vol. 145, pp. 858–866, 2020, doi: 10.1016/j.renene.2019.06.083.

[281] L. Xie *et al.*, “Efficient hydrolysis of corncob residue through cellulolytic enzymes from Trichoderma strain G26 and L-lactic acid preparation with the hydrolysate.,” *Bioresour. Technol.*, vol. 193, pp. 331–336, Oct. 2015, doi: 10.1016/j.biortech.2015.06.101.

[282] Z. Bai, Z. Gao, J. Sun, B. Wu, and B. He, “D-Lactic acid production by Sporolactobacillus inulinus YBS1-5 with simultaneous utilization of cottonseed meal and corncob residue,” *Bioresour. Technol.*, vol. 207, pp. 346–352, 2016, doi: 10.1016/j.biortech.2016.02.007.

[283] W. L. Zhang, Z. Y. Liu, Z. Liu, and F. L. Li, “Butanol production from corncob residue using Clostridium beijerinckii NCIMB 8052,” *Lett. Appl. Microbiol.*, vol. 55, no. 3, pp. 240–246, 2012, doi: 10.1111/j.1472-765X.2012.03283.x.

[284] Y. Wang, W. Liu, L. Zhang, and Q. Hou, “Characterization and comparison of lignin derived from corncob residues to better understand its potential applications,” *Int. J. Biol. Macromol.*, vol. 134, pp. 20–27, 2019, doi: 10.1016/j.ijbiomac.2019.05.013.

[285] S. Wijitkosum and P. Jiwnok, “Elemental composition of biochar obtained from agriculturalwaste for soil amendment and carbon sequestration,” *Appl. Sci.*, vol. 9, no. 19, 2019, doi: 10.3390/app9193980.

[286] G. V. Subhash and S. V. Mohan, “Sustainable biodiesel production through bioconversion of lignocellulosic wastewater by oleaginous fungi,” *Biomass Convers. Biorefinery*, vol. 5, no. 2, pp. 215–226, 2015, doi: 10.1007/s13399-014-0128-4.

[287] R. Mahmud, S. M. Moni, K. High, and M. Carbajales-Dale, “Integration of techno-economic analysis and life cycle assessment for sustainable process design – A review,” *J. Clean. Prod.*, vol. 317, no. December 2020, p. 128247, 2021, doi: 10.1016/j.jclepro.2021.128247.

[288] P. K. Gandam *et al.*, “Corncob based biorefinery: A comprehensive review of pretreatment methodologies, and biorefinery platforms,” *J. Energy Inst.*, no. December 2021, 2022, doi:

10.1016/j.joei.2022.01.004.

[289] ISO, “ISO 14040:2006,” 2006. https://www.iso.org/standard/37456.html (accessed Dec. 19, 2021).

[290] ISO, “ISO 14044:2006,” 2006. https://www.iso.org/standard/38498.html (accessed Dec. 19, 2021).

[291] A. Aui, Y. Wang, and M. Mba-Wright, “Evaluating the economic feasibility of cellulosic ethanol: A meta-analysis of techno-economic analysis studies,” *Renew. Sustain. Energy Rev.*, vol. 145, no. March, p. 111098, 2021, doi: 10.1016/j.rser.2021.111098.

[292] T. Jarunglumlert and C. Prommuak, “Net energy analysis and techno-economic assessment of co-production of bioethanol and biogas from cellulosic biomass,” *Fermentation*, vol. 7, no. 4, 2021, doi: 10.3390/fermentation7040229.

[293] B. Pang *et al.*, “Improved value and carbon footprint by complete utilization of corncob lignocellulose,” *Chem. Eng. J.*, vol. 419, no. March, p. 129565, 2021, doi: 10.1016/j.cej.2021.129565.

[294] F. Liu, X. Guo, Y. Wang, G. Chen, and L. Hou, “Process simulation and economic and environmental evaluation of a corncob-based biorefinery system,” *J. Clean. Prod.*, vol. 329, no. November, p. 129707, 2021, doi: 10.1016/j.jclepro.2021.129707.

[295] S. H. Duque, C. A. Cardona, and J. Moncada, “Techno-economic and environmental analysis of ethanol production from 10 agroindustrial residues in Colombia,” *Energy and Fuels*, vol. 29, no. 2, pp. 775–783, 2015, doi: 10.1021/ef5019274.

[296] F. Liu *et al.*, “Environmental life cycle assessment of lignocellulosic ethanol-blended fuels: A case study,” *J. Clean. Prod.*, vol. 245, no. xxxx, p. 118933, 2020, doi: 10.1016/j.jclepro.2019.118933.

[297] Y. Huang, C. Chen, and H. Huang, “Analyzing life-cycle water footprint for advanced bio-liquid fuel: Crop residues and non-grain biofuels in China,” *J. Clean. Prod.*, vol. 293, p. 126151, 2021, doi: 10.1016/j.jclepro.2021.126151.

[298] Y. Wang, M. H. Cheng, and M. M. Wright, “Lifecycle energy consumption and greenhouse gas emissions from corncob ethanol in China,” *Biofuels, Bioprod. Biorefining*, vol. 12, no. 6, pp. 1037–1046, Nov. 2018, doi: 10.1002/bbb.1920.

[299] F. Liu, G. Chen, B. Yan, W. Ma, and Z. Cheng, “Exergy analysis of a new lignocellulosic biomass-based polygeneration system,” *Energy*, vol. 140, pp. 1087–1095, 2017, doi: 10.1016/j.energy.2017.09.040.

[300] B. Pang *et al.*, “Improved value and carbon footprint by complete utilization of corncob lignocellulose,” *Chem. Eng. J.*, vol. 419, no. February, p. 129565, 2021, doi:

10.1016/j.cej.2021.129565.

[301] Y. Wang, M. H. Cheng, and M. M. Wright, “Lifecycle energy consumption and greenhouse gas emissions from corncob ethanol in China,” *Biofuels, Bioprod. Biorefining*, vol. 12, no. 6, pp. 1037–1046, 2018, doi: 10.1002/bbb.1920.

[302] A. Sluiter *et al.*, “Determination of total solids in biomass and total dissolved solids in liquid process samples,” *Natl. Renew. Energy Lab.*, no. March, p. 9, 2008, doi: NREL/TP-510-42621.

[303] B. Hames, R. Ruiz, C. Scarlata, a Sluiter, J. Sluiter, and D. Templeton, “Preparation of Samples for Compositional Analysis Laboratory Analytical Procedure (LAP) Issue Date : 8 / 06 / 2008 Preparation of Samples for Compositional Analysis Laboratory Analytical Procedure (LAP),” *Natl. Renew. Energy Lab.*, no. August, pp. 1–9, 2008.

[304] P. J. Van Soest, J. B. Robertson, and B. A. Lewis, “Methods for Dietary Fiber, Neutral Detergent Fiber, and Nonstarch Polysaccharides in Relation to Animal Nutrition,” *J. Dairy Sci.*, vol. 74, no. 10, pp. 3583–3597, 1991, doi: 10.3168/jds.S0022-0302(91)78551-2.

[305] X. Li, C. Sun, B. Zhou, and Y. He, “Determination of Hemicellulose, Cellulose and Lignin in Moso Bamboo by Near Infrared Spectroscopy,” *Sci. Rep.*, vol. 5, no. October, pp. 1–11, 2015, doi: 10.1038/srep17210.

[306] ASTM E1131, “Standard Test Method for Compositional Analysis by Thermogravimetry,” *ASTM Int.*, vol. 08, no. Reapproved 2014, p. 6, 2015, [Online]. Available: https://compass.astm.org/EDIT/html_annot.cgi?E1131+20

[307] D. Díez, A. Urueña, R. Piñero, A. Barrio, and T. Tamminen, “and Lignin Content in Di ff erent Types of Biomasses by Thermogravimetric Analysis and Pseudocomponent Kinetic Model,” *Processes*, vol. 8, no. 1048, pp. 1–21, 2020.

[308] F. Rego, A. P. Soares Dias, M. Casquilho, F. C. Rosa, and A. Rodrigues, “Fast determination of lignocellulosic composition of poplar biomass by thermogravimetry,” *Biomass and Bioenergy*, vol. 122, no. January, pp. 375–380, 2019, doi: 10.1016/j.biombioe.2019.01.037.

[309] R. M. Gendreau and R. Burton, “The KBr Pellet: A Useful Technique for Obtaining Infrared Spectra of Inorganic Species,” *Appl. Spectrosc.*, vol. 33, no. 6, pp. 581–584, 1979, [Online]. Available: http://opg.optica.org/as/abstract.cfm?URI=as-33-6-581

[310] O. Faix, “Classification of Lignins from Different Botanical Origins by FT-IR Spectroscopy,” *Holzforschung*, vol. 45, no. s1, pp. 21–28, 1991, doi: 10.1515/hfsg.1991.45.s1.21.

[311] M. L. Nelson and R. T. O’Connor, “Relation of certain infrared bands to cellulose crystallinity and crystal lattice type. Part II. A new infrared ratio for estimation of

crystallinity in celluloses I and II," *J. Appl. Polym. Sci.*, vol. 8, no. 3, pp. 1325–1341, 1964, doi: 10.1002/app.1964.070080323.

[312] G. Fernand, "Classification of Fine Structural Characteristics in Cellulose by Infrared Spectroscopy," vol. 32, no. 2, pp. 177–181, 1960.

[313] H. Struszczyk, "Modification of Lignins. 111. Reaction of Lignosulfonates with Chlorophosphazenes," *J. Macromol. Sci. Part A - Chem.*, vol. 23, no. 8, pp. 973–992, 1986, doi: 10.1080/00222338608081105.

[314] A. O. Balogun, O. A. Lasode, H. Li, and A. G. McDonald, "Fourier Transform Infrared (FTIR) Study and Thermal Decomposition Kinetics of Sorghum bicolour Glume and Albizia pedicellaris Residues," *Waste and Biomass Valorization*, vol. 6, no. 1, pp. 109–116, 2015, doi: 10.1007/s12649-014-9318-3.

[315] Y. Huang *et al.*, "Analysis of lignin aromatic structure in wood based on the IR spectrum," *J. Wood Chem. Technol.*, vol. 32, no. 4, pp. 294–303, 2012, doi: 10.1080/02773813.2012.666316.

[316] R. R. N. Mvondo, P. Meukam, J. Jeong, D. D. S. Meneses, and E. G. Nkeng, "Influence of water content on the mechanical and chemical properties of tropical wood species," *Results Phys.*, vol. 7, pp. 2096–2103, 2017, doi: 10.1016/j.rinp.2017.06.025.

[317] L. Segal, J. J. Creely, A. E. Martin, and C. M. Conrad, "An Empirical Method for Estimating the Degree of Crystallinity of Native Cellulose Using the X-Ray Diffractometer," *Text. Res. J.*, vol. 29, no. 10, pp. 786–794, 1959, doi: 10.1177/004051755902901003.

[318] R. Rotaru *et al.*, "Ferromagnetic iron oxide-cellulose nanocomposites prepared by ultrasonication," *Polym. Chem.*, vol. 9, no. 7, pp. 860–868, 2018, doi: 10.1039/c7py01587a.

[319] W. Ruland, "X-ray determination of crystallinity and diffuse disorder scattering," *Acta Crystallogr.*, vol. 14, no. 11, pp. 1180–1185, 1961, doi: 10.1107/s0365110x61003429.

[320] P. Scherrer, "Bestimmung der Grosse und der inneren Struktur von Kolloidterilchen mittels Rontgestrahlen," *Nachrichten von der Gesellschaft der Wissenschaften zu Göttingen, Math. Klasse*, no. 26, pp. 98–100, 1918.

[321] W. H. Bragg and W. L. Bragg, "The reflection of X-rays by crystals," *Proc. R. Soc. London. Ser. A, Contain. Pap. a Math. Phys. Character*, vol. 88, no. 605, pp. 428–438, 1913, doi: 10.1098/rspa.1913.0040.

[322] T. K. Ghose, "Measurement of cellulase activities," vol. 59, no. 2, pp. 257–268, 1987, doi: doi:10.1351/pac198759020257.

[323] M. Mandels and D. Sternberg, “Recent advances in cellulase technology,” *Hakko Kogaku Zasshi; (Japan), Conf. Annu. Meet. Soc. Ferment. Technol. Osaka, Japan, 30 Oct 1975*, vol. 54, no. 4, pp. 267–286, 1976.

[324] S. A. Alrumman, “Enzymatic saccharification and fermentation of cellulosic date palm wastes to glucose and lactic acid,” *Brazilian J. Microbiol.*, vol. 47, no. 1, pp. 110–119, 2016, doi: 10.1016/j.bjm.2015.11.015.

[325] H. Hu *et al.*, “Multipurpose Use of a Corncob Biomass for the Production of Polysaccharides and the Fabrication of a Biosorbent,” *ACS Sustain. Chem. Eng.*, vol. 6, no. 3, pp. 3830–3839, 2018, doi: 10.1021/acssuschemeng.7b04179.

[326] X. Fan *et al.*, “Surfactant assisted microwave irradiation pretreatment of corncob: Effect on hydrogen production capacity, energy consumption and physiochemical structure,” *Bioresour. Technol.*, vol. 357, p. 127302, 2022, doi: https://doi.org/10.1016/j.biortech.2022.127302.

[327] P. Selvakumar *et al.*, “Optimization of binary acids pretreatment of corncob biomass for enhanced recovery of cellulose to produce bioethanol,” *Fuel*, vol. 321, no. April, p. 124060, 2022, doi: 10.1016/j.fuel.2022.124060.

[328] J. Anioła, J. Gawęcki, J. Czarnocińska, and G. Galiński, “Corncobs as a source of dietary fiber,” *Polish J. Food Nutr. Sci.*, vol. 59, no. 3, pp. 247–249, 2009.

[329] X. Li, C. Sun, B. Zhou, and Y. He, “Determination of Hemicellulose, Cellulose and Lignin in Moso Bamboo by Near Infrared Spectroscopy,” *Sci. Rep.*, vol. 5, no. October, pp. 1–11, 2015, doi: 10.1038/srep17210.

[330] X. Yao, K. Xu, and Y. Liang, “Research on the thermo-physical properties of corncob residues as gasification feedstock and assessment for characterization of corncob ash from gasification,” *BioResources*, vol. 11, no. 4, pp. 9823–9841, 2016, doi: 10.15376/biores.11.4.9823-9841.

[331] W. Kemp, “Organic spectroscopy,” *J. Chem. Educ.*, vol. 79, no. SUPPL., p. 26, 2002, doi: 10.1042/bst0040394.

[332] D. Ciolacu, J. Kovac, and V. Kokol, “The effect of the cellulose-binding domain from Clostridium cellulovorans on the supramolecular structure of cellulose fibers,” *Carbohydr. Res.*, vol. 345, no. 5, pp. 621–630, 2010, doi: 10.1016/j.carres.2009.12.023.

[333] J. Shi, L. Lu, W. Guo, M. Liu, and Y. Cao, “On preparation, structure and performance of high porosity bulk cellulose aerogel,” *Plast. Rubber Compos.*, vol. 44, no. 1, pp. 26–32, 2015, doi: 10.1179/1743289814Y.0000000107.

[334] D. L. Pavia, G. M. Lampman, G. S. Kriz, and J. A. Vyvyan, *Introduction to Spectroscopy*. Cengage Learning, 2008. [Online]. Available:

https://books.google.co.in/books?id=FkaNOdwk0FQC

[335] Z. Ling *et al.*, "Effects of ball milling on the structure of cotton cellulose," *Cellulose*, vol. 26, no. 1, pp. 305–328, 2019, doi: 10.1007/s10570-018-02230-x.

[336] N. M. Stark, D. J. Yelle, and U. P. Agarwal, "Techniques for Characterizing Lignin," *Lignin Polym. Compos.*, pp. 49–66, 2016, doi: 10.1016/B978-0-323-35565-0.00004-7.

[337] T. Virtanen *et al.*, "Analysis of membrane fouling by Brunauer-Emmet-Teller nitrogen adsorption/desorption technique," *Sci. Rep.*, vol. 10, no. 1, pp. 1–10, 2020, doi: 10.1038/s41598-020-59994-1.

[338] R. J. Sammons, D. P. Harper, N. Labbé, J. J. Bozell, T. Elder, and T. G. Rials, "Characterization of organosolv lignins using thermal and FT-IR spectroscopic analysis," *BioResources*, vol. 8, no. 2, pp. 2752–2767, 2013, doi: 10.15376/biores.8.2.2752-2767.

[339] P. K. Adapa, L. G. Tabil, G. J. Schoenau, T. Canam, and T. Dumonceaux, "Quantitative Analysis of Lignocellulosic Components of Non-Treated and Steam Exploded Barley, Canola, Oat and Wheat Straw Using Fourier Transform Infrared Spectroscopy," *J. Agric. Sci. Technol. B*, vol. 1, no. January, pp. 177–188, 2011.

[340] F. Xu and D. Wang, "Analysis of Lignocellulosic Biomass Using Infrared Methodology," *Pretreat. Biomass Process. Technol.*, no. December 2015, pp. 7–25, 2015, doi: 10.1016/B978-0-12-800080-9.00002-5.

[341] A. Maceda, M. Soto-Hernández, C. B. Peña-Valdivia, C. Trejo, and T. Terrazas, "Characterization of lignocellulose of Opuntia (Cactaceae) species using FTIR spectroscopy: possible candidates for renewable raw material," *Biomass Convers. Biorefinery*, 2020, doi: 10.1007/s13399-020-00948-y.

[342] Z. Deng, A. Xia, Q. Liao, X. Zhu, Y. Huang, and Q. Fu, "Laccase pretreatment of wheat straw: Effects of the physicochemical characteristics and the kinetics of enzymatic hydrolysis," *Biotechnol. Biofuels*, vol. 12, no. 1, pp. 1–12, 2019, doi: 10.1186/s13068-019-1499-3.

[343] T. He, Z. Jiang, P. Wu, J. Yi, J. Li, and C. Hu, "Fractionation for further conversion: From raw corn stover to lactic acid," *Sci. Rep.*, vol. 6, no. November, pp. 1–11, 2016, doi: 10.1038/srep38623.

[344] R. Md Salim, J. Asik, and M. S. Sarjadi, "Chemical functional groups of extractives, cellulose and lignin extracted from native Leucaena leucocephala bark," *Wood Sci. Technol.*, vol. 55, no. 2, pp. 295–313, 2021, doi: 10.1007/s00226-020-01258-2.

[345] L. Vandsburger and P. Blanchet, "Modification of hardwood samples in the flowing afterglow of N2 – O2 dielectric barrier discharges open to ambient air Determination of active species in the modification of hardwood samples in the flowing afterglow of N 2

dielectric barrier discharges op," no. February, 2014, doi: 10.1007/s10570-014-0496-8.

[346] A. Casas, M. Oliet, M. V Alonso, and F. Rodríguez, "Dissolution of Pinus radiata and Eucalyptus globulus woods in ionic liquids under microwave radiation : Lignin regeneration and characterization," *Sep. Purif. Technol.*, vol. 97, pp. 115–122, 2012, doi: 10.1016/j.seppur.2011.12.032.

[347] M. Traoré, J. Kaal, and A. Martínez Cortizas, "Differentiation between pine woods according to species and growing location using FTIR-ATR," *Wood Sci. Technol.*, vol. 52, no. 2, pp. 487–504, 2018, doi: 10.1007/s00226-017-0967-9.

[348] S. Rongpipi, D. Ye, E. D. Gomez, and E. W. Gomez, "Progress and opportunities in the characterization of cellulose – an important regulator of cell wall growth and mechanics," *Front. Plant Sci.*, vol. 9, no. March, pp. 1–28, 2019, doi: 10.3389/fpls.2018.01894.

[349] M. Fan, D. Dai, and B. Huang, "Fourier Transform Infrared Spectroscopy for Natural Fibres," *Fourier Transform - Mater. Anal.*, 2012, doi: 10.5772/35482.

[350] S. M. Moosavinejad, M. Madhoushi, M. Vakili, and D. Rasouli, "Evaluation of degradation in chemical compounds of wood in historical buildings using Ft-Ir And Ft-Raman vibrational spectroscopy," *Maderas Cienc. y Tecnol.*, vol. 21, no. 3, pp. 381–392, 2019, doi: 10.4067/S0718-221X2019005000310.

[351] E. J. Foster *et al.*, "Current characterization methods for cellulose nanomaterials," *Chem. Soc. Rev.*, vol. 47, no. 8, pp. 2609–2679, 2018, doi: 10.1039/c6cs00895j.

[352] K. Kafle, H. Shin, C. M. Lee, S. Park, and S. H. Kim, "Progressive structural changes of Avicel, bleached softwood, and bacterial cellulose during enzymatic hydrolysis," *Sci. Rep.*, vol. 5, no. May, pp. 1–10, 2015, doi: 10.1038/srep15102.

[353] M. Ioelovich, "Characterization of Various Kinds of Nanocellulose," *Handb. Nanocellulose Cellul. Nanocomposites*, pp. 51–100, 2017, doi: 10.1002/9783527689972.ch2.

[354] S. Park, J. O. Baker, M. E. Himmel, P. A. Parilla, and D. K. Johnson, "Cellulose crystallinity index: Measurement techniques and their impact on interpreting cellulase performance," *Biotechnol. Biofuels*, vol. 3, pp. 1–10, 2010, doi: 10.1186/1754-6834-3-10.

[355] Q. Qing, M. Huang, Y. He, L. Wang, and Y. Zhang, "Dilute Oxalic Acid Pretreatment for High Total Sugar Recovery in Pretreatment and Subsequent Enzymatic Hydrolysis," *Appl. Biochem. Biotechnol.*, vol. 177, no. 7, pp. 1493–1507, 2015, doi: 10.1007/s12010-015-1829-2.

[356] W. Liu *et al.*, "Comparative study on different pretreatment on enzymatic hydrolysis of corncob residues," *Bioresour. Technol.*, vol. 295, no. October 2019, p. 122244, 2020, doi: 10.1016/j.biortech.2019.122244.

[357] Y. Zhu, T. H. Kim, Y. Y. Lee, R. Chen, and R. T. Elander, “Enzymatic production of xylooligosaccharides from corn stover and corn cobs treated with aqueous ammonia.,” *Appl. Biochem. Biotechnol.*, vol. 129–132, pp. 586–598, 2006, doi: 10.1385/abab:130:1:586.

[358] E. Mardawati, S. M. Pratiwi, R. Andoyo, T. Rialita, and M. Djali, “Ozonation Pre-treatment Evaluation for Xylanase Crude Extract Production from Corncob under Solid-State Fermentation,” vol. 1, no. 2, pp. 27–34, 2017.

[359] a. Sluiter *et al.*, “NREL/TP-510-42618 analytical procedure - Determination of structural carbohydrates and lignin in Biomass,” *Lab. Anal. Proced.*, no. April 2008, p. 17, 2012, doi: NREL/TP-510-42618.

[360] R. E. Araujo Piraine, D. G. Nickens, D. J. Sun, F. P. Leivas Leite, and M. L. Bochman, “Isolation of wild yeasts from Olympic National Park and Moniliella megachiliensis ONP131 physiological characterization for beer fermentation,” *Food Microbiol.*, vol. 104, no. November 2021, 2022, doi: 10.1016/j.fm.2021.103974.

[361] L. J. Wickerham, *Taxonomy of Yeasts*. U.S. Department of Agriculture, 1951. [Online]. Available: https://books.google.co.in/books?id=ihi-FxcLqJkC

[362] C. Kurtzman, J. W. Fell, and T. Boekhout, *The Yeasts: A Taxonomic Study*. Elsevier Science, 2011. [Online]. Available: https://books.google.co.in/books?id=yfg79rlIFIkC

[363] J. McFARLAND, “THE NEPHELOMETER:AN INSTRUMENT FOR ESTIMATING THE NUMBER OF BACTERIA IN SUSPENSIONS USED FOR CALCULATING THE OPSONIC INDEX AND FOR VACCINES.,” *J. Am. Med. Assoc.*, vol. XLIX, no. 14, pp. 1176–1178, Oct. 1907, doi: 10.1001/jama.1907.25320140022001f.

Journal Publications (from this work)

1. Gandam, P.K., Chinta, M.L., Gandham, A.P., Pabbathi, N.P.P., Velidandi, A., Prabhu, A.A., Baadhe, R.R*., 2024. Integrated multi-objective optimization of sodium bicarbonate pretreatment for the outer anatomical portion of corncob using central composite design, artificial neural networks, and metaheuristic algorithms. Ind. Crops Prod. 207, 117717. https://doi.org/https://doi.org/10.1016/j.indcrop.2023.117717 (Impact factor 5.9)

2. Gandam, Pradeep K, Chinta, M.L., Gandham, A.P., Pabbathi, N.P., Konakanchi, S., Bhavanam, A., Atchuta, S.R., Baadhe, R.R*., Bhatia, R.K., 2022. A New Insight into the Composition and Physical Characteristics of Corncob— Substantiating Its Potential for Tailored Biorefinery Objectives. Fermentation. https://doi.org/10.3390/fermentation8120704 (Impact factor: 3.7)

3. P.K. Gandam, M.L. Chinta, N.P. Prashanth, A. Velidandi, M. Sharma, R.C. Kuhad, M. Tabatabaei, M. Aghbashlo, R.R. Baadhe*, V.K. Gupta, Corncob based biorefinery: A comprehensive review of pretreatment methodologies, and biorefinery platforms, J. Energy Inst. (2022). https://doi.org/10.1016/j.joei.2022.01.004 (Impact factor 5.7)

4. P.K. Gandam, M.L. Chinta, N.P.P. Pabbathi, R.R. Baadhe*, M. Sharma, V.K. Thakur, G.D. Sharma, J. Ranjitha, V.K. Gupta, Second-generation bioethanol production from corncob – A comprehensive review on pretreatment and bioconversion strategies, including techno-economic and lifecycle perspective, Ind. Crops Prod. 186 (2022) 115245. https://doi.org/10.1016/j.indcrop.2022.115245 (Impact factor 5.9)

(* Correspondig author)

Journal Publications (from collaborative works):

1. Velidandi, A., Kumar Gandam, P., Latha Chinta, M., Konakanchi, S., reddy Bhavanam, A., Raju Baadhe*, R., Sharma, M., Gaffey, J., Nguyen, Q.D., Gupta, V.K., 2023a. State-of-the-art and future directions of machine learning for biomass characterization and for sustainable biorefinery. J. Energy Chem. 81, 42–63. https://doi.org/10.1016/j.jechem.2023.02.020 (Impact factor: 13.1)
2. Pabbathi, N.P.P., Velidandi, A., Gandam, P.K., Koringa, P., Parcha, S.R., Baadhe*, R.R., 2021a. Novel buffalo rumen metagenome derived acidic cellulase Cel-3.1 cloning, characterization, and its application in saccharifying rice straw and corncob biomass. Int. J. Biol. Macromol. 170, 239. https://doi.org/10.1016/j.ijbiomac.2020.12.041 (Impact factor: 8.2)
3. Pabbathi, N.P.P., Velidandi, A., Pogula, S., Gandam, P.K., Baadhe, R.R*., Sharma, M., Sirohi, R., Thakur, V.K., Gupta, V.K., 2022. Brewer's spent grains-based biorefineries: A critical review. Fuel 317, 123435. https://doi.org/https://doi.org/10.1016/j.fuel.2022.123435 (Impact factor: 7.4)
4. Pabbathi, N.P.P., Velidandi, A., Tavarna, T., Gupta, S., Raj, R.S., Gandam, P.K., Baadhe, R.R*., 2021b. Role of metagenomics in prospecting novel endoglucanases, accentuating functional metagenomics approach in second-generation biofuel production: a review. Biomass Convers. Biorefinery. https://doi.org/10.1007/s13399-020-01186-y (Impact factor: 4.1)
5. Velidandi, A., Sarvepalli, M., Gandam, P.K., Prashanth Pabbathi, N.P., Baadhe, R.R*., 2023b. Characterization, catalytic, and recyclability studies of nano-sized spherical palladium particles synthesized using aqueous poly-extract (turmeric, neem, and tulasi). Environ. Res. 228, 115821. https://doi.org/10.1016/j.envres.2023.115821 (Impact factor: 8.3

(* Correspondig author)

Book chapters (from collaborative work)

1. Chinta, M.L., Gandam, P.K., Parcha, S.R., 2022. Chapter 6 - Natural polymer based hydrogel systems for wound management, in: Sah, M.K., Kasoju, N., Mano, J.F.B.T.-N.P. in W.H. and R. (Eds.), . Elsevier, pp. 129–165. https://doi.org/https://doi.org/10.1016/B978-0-323-90514-5.00006-7 (book chapter)